UNIVERSITY OF MISSOURI-ROLLA

CENTER FOR INFRASTRUCTURE ENGINEERING STUDIES

Strengthening of Rural Bridges Using Rapid-Installation FRP Technology

By

A. Rizzo

N. Galati

A. Nanni

University Transportation Center Program at the University of Missouri-Rolla

Disclaimer

Technical Report Documentation Page

1. Report No.	2. Government Accession No.	3. Recipient's Catalog No.
UTC R135		

4. Title and Subtitle	5. Report Date
Strengthening of Rural Bridges Using Rapid-Installation FRP Technology	January 2007
	6. Performing Organization Code
7. Author/s A. Rizzo, N. Galati, and A. Nanni	8. Performing Organization Report No. 00001406/0008404
9. Performing Organization Name and Address Center for Infrastructure Engineering Studies/UTC program University of Missouri - Rolla 223 Engineering Research Lab Rolla, MO 65409	10. Work Unit No. (TRAIS) 11. Contract or Grant No. DTRS98-G-0021
12. Sponsoring Organization Name and Address U.S. Department of Transportation Research and Special Programs Administration 400 7th Street, SW Washington, DC 20590-0001	13. Type of Report and Period Covered Final 14. Sponsoring Agency Code
15. Supplementary Notes	

16. Abstract

Three bridges were strengthened using an innovative method developed at University of Missouri – Rolla. It consists of strengthening reinforced concrete members using Fiber Reinforced Polymer (FRP) laminates, having high bearing and longitudinal strengths, mechanically fastened to concrete elements using wedge anchors spaced in a proper pattern. It results rapid and uses conventional typically available hand-tools, lightweight materials and unskilled labor.

The three bridges are No. 1330005, No. 3855006 and No. 2210010. Bridge No. 3855006 was originally constructed in 1976 while the year built is not known for the other two bridges.

17. Key Words	18. Distribution Statement
infrastructure, rural bridges, flexural capacity, carbon fibers, abutment, concrete deck, FEM, GRP, in-situ load test, load rating, mechanically fastened FRP pre-cured laminates, non destructive test, static load test, reinforced concrete, strengthening, structural evaluation, RC girder, strain	No restrictions. This document is available to the public through the National Technical Information Service, Springfield, Virginia 22161.

19. Security Classification (of this report)	20. Security Classification (of this page)	21. No. Of Pages	22. Price
unclassified	unclassified	308	

Form DOT F 1700.7 (8-72)

RESEARCH INVESTIGATION

DESIGN AND IN-SITU LOAD TESTING OF BRIDGE No. 1330005

ROUTE 3560 – PHELPS COUNTY, MO

PREPARED FOR THE
MISSOURI DEPARTMENT OF TRANSPORTATION

IN COOPERATION WITH THE
UNIVERSITY TRANSPORTATION CENTER

Written By:

Andrea Rizzo, MS Candidate

Nestore Galati, Research Engineer

Antonio Nanni, V. & M. Jones Professor of Civil Engineering

CENTER FOR INFRASTRUCTURE ENGINEERING STUDIES

UNIVERSITY OF MISSOURI – ROLLA

Submitted
January 2005

DESIGN AND IN-SITU LOAD TESTING OF BRIDGE No. 1330005

ROUTE 3560 – PHELPS COUNTY, MO

Executive Summary

This report presents the use of Mechanically Fastened - Fiber Reinforced Polymers (MF-FRP) pre-cured laminates for the flexural strengthening of a concrete bridge. The system consists of pre-cured FRP laminates bolted onto the concrete surface in order to provide the necessary flexural reinforcement to girders and deck. The advantage of the technique is in the fact that it does not require any surface preparation prior to the installation of the FRP.

The bridge selected for this project consists of four Reinforced Concrete (RC) girders monolithically cast with the deck. It can be assumed as simply-supported by the abutments. The bridge is load posted and located on Route 3560 in Phelps County, MO. The bridge analysis was performed for maximum loads determined in accordance to AASHTO Design specification, 17th edition. The strengthening scheme was designed in compliance with the ACI 440.2R-02 design guide and on previous research work on MF-FRP system.

The retrofitting of the structure was executed in Spring 2004. The MF-FRP strengthening technique was easily implemented and showed satisfactory performances. Two load tests, one prior to and another after the strengthening, were performed. A Finite Element Method (FEM) analysis was undertaken. The numerical model was able to represent the behavior of the bridge and demonstrated the safety of the proposed posting limit.

ACKNOWLEDGMENTS

The project was made possible with the financial support received from the UMR - University Transportation Center on Advanced Materials, Center for Infrastructure Engineering Studies at the University of Missouri-Rolla and Meramec Regional Planning Commission (MRPC). Master Contractors installed the FRP systems. Strongwell provided the FRP materials.

The authors would like to acknowledge Rick Pilcher, District Liaison Engineer at MoDOT, and Lesley Bennish, Community Development Specialist from Meramec Regional Planning Commission, for their assistance in this project.

TABLE OF CONTENTS

Page

LIST OF ILLUSTRATIONS

LIST OF TABLES

NOMENCLATURE

ADT	Annual Daily Traffic
A_g	Gross Area of a Section
A_s	Area of the Generic Tensile Non-prestressed Steel Reinforcement
$A_{s,slab\ long.}$	Area of the Longitudinal Tensile Non-prestressed Steel Reinforcement of the Deck
$A_{s,slab\ transv.}$	Area of the Transverse Tensile Non-prestressed Steel Reinforcement of the Deck
$A_{s,web}$	Area of the Longitudinal Tensile Non-prestressed Steel Reinforcement of the Girders Web
A_{tire}	Area of the Print of a Wheel according to AASHTO (2002): $A_{tire} = l_{tire} w_{tire}$
A_1	Factor for Dead Loads
A_2	Factor for Live Loads
b_0	Perimeter of Critical Section
b_w	Web Width
B	Design Flange Width for a Girder according to AASHTO (2002) Section 4.6.2.6.1
B^{Ext}	Design Flange Width for an Interior Girder according to AASHTO (2002) Section 4.6.2.6.1
B^{Int}	Design Flange Width for an Exterior Girder according to AASHTO (2002) Section 4.6.2.6.1
$c.o.v._c$	Coefficient of Variation for the Compressive Strength $f_c^{'}$ of Concrete: $c.o.v._c = \frac{f_c^{'}}{SD_c}$
$c.o.v._y$	Coefficient of Variation for the Specified Yield Strength f_y of Non-

prestressed Steel Reinforcement: $c.o.v._y = \frac{f_y}{SD_y}$

C	Capacity of the Member
C_E	Environmental Reduction Factor according to ACI 440 Table 7.1: for Carbon Plate Exposed in Exterior Aggressive Ambient $C_E = 0.85$
d	Effective Depth of the Steel Reinforcement for a Generic Section
d_c	Length of the Cantilever Deck
d_g	Spacing between Girders on Center
$d_{slab\ long.}$	Effective Depth of the Longitudinal Tensile Non-prestressed Steel Reinforcement of the Deck
$d_{slab\ transv.}$	Effective Depth of the Transverse Tensile Non-prestressed Steel Reinforcement of the Deck
d_{web}	Effective Depth of the Longitudinal Tensile Non-prestressed Steel Reinforcement of the Girders Web
D	Dead Load of the Bridge
D_i	Part of Deck between the Girders No. i and $i+1$ with $i = 1,2,3$
D_L	Distribution Length of the Lane Lad in the Transverse Direction
D_P	Distance between Two Wheels of the Truck in the Transverse Direction
E_c	Modulus of Elasticity of Concrete according ACI 318-02 Section 8.5.1: $E_c = 57000\sqrt{f_c^{'}}\ psi$ with $\left[f_c^{'}\right] = [psi]$
E_f	Modulus of Elasticity of the Pre-cured FRP Laminate
E_s	Modulus of Elasticity of Non-prestressed Steel Reinforcement
$f_c^{'}$	Specified Compressive Strength of Concrete
f_{fu}	Design Tensile Strength of the Pre-cured FRP Laminate: $f_{fu} = C_E f_{fu}^*$
f_{fu}^*	Guaranteed Tensile Strength of the Pre-cured FRP Laminate as Reported by the Manufacturer

f_y	Specified Yield Strength of Non-prestressed Steel Reinforcement
F_{FRP}	Maximum Axial Load that the Pre-cured FRP Laminate Experiences at Ultimate Conditions
G_i	Girder No. i with $i = 1, 2..4$
h	Overall Thickness of Member
h_b	Embedment Depth of the Anchor
h_c	Vertical Distance between Supports of the Wall
H_d	Height of the Deck
H_g	Height of the Girders Web
H_o	Height of the Deck Overlay
I	Live Load Impact Factor: $I = \dfrac{50}{l_d + 125} \leq 0.30$ where $[l_d] = [ft]$
$I_{experimental,\, i}$	Live Load Impact Factor Measured during the Load Test after Strengthening in the Pass No. i with $i = Pass\ \#1, Pass\ \#2..Pass\ \#5$
k	Effective Length Factor according to ACI 318-02 Section 14.5.2: $k = 2.0$ for Walls Not Braced against Lateral Translation
K_a	Generalized Stiffness of the Bridge after Strengthening
K_p	Generalized Stiffness of the Bridge Prior to Strengthening
l_c	Clear Span of the Bridge
l_d	Design Length of the Bridge
l_{tire}	Size of the Print of a Wheel in the Longitudinal Direction according to AASHTO (2002)
L	Live Load Applied on the Bridge. The Same Symbol is Used in Some Figures to Indicate the Design Span of the Bridge
M_n	Nominal Moment Strength at Section
M_s	Unfactored Moment due to the Most Demanding Load Condition for a Structural Element

M_u	Ultimate (Factored) Moment due to the Most Demanding Load Condition for a Structural Element
$n_{b,\min}$	Minimum Number of Fastener to Anchor a Pre-cured FRP laminate so that Failure in Tension Controls: $n_{b,\min} = \dfrac{F_{FRP}}{R_b}$
P	Generic Concentrated Load Applied to a Structure
$P_{front-axle}$	Total Load corresponding to the Truck Front Axle
$P_{rear-axle}$	Total Load corresponding to the Truck Rear Axles
P_{H15-44}	Weight of a Rear Axle Wheel of the $H15-44$ Truck
P_n	Nominal Axial Capacity of the Concrete Walls for Unit of Length
q	Generic Uniform Distributed Load Applied to the Structure
q_{DL}	Uniform Distributed Load due to Dead Loads
q_{LL}	Uniform Distributed Load due to Live Loads
R_{ab}	Ultimate (Factored) Axial Load due to the Most Demanding Load Condition for the Two Walls
R_b	Design Shear Capacity of the Connection
R_i	Reaction of the Girder G_i. The Same Symbol is Used to Indicate the LVDT No. i with $i = 1,2..13$
RF	Rating Factor
RT	Rating of the Bridge: $RT = RF \cdot W$
SD_c	Standard Deviation for the Specified Compressive Strength $f_c^{'}$ of Concrete
SD_y	Standard Deviation for the Specified Yield Strength f_y of Non-prestressed Steel Reinforcement
SG_i	Strain Gauge No. i with $i = 1,2..5$
t_f	Thickness of the Pre-cured FRP Laminate
T_b	Shear Capacity of the Connection

T_c	Shear Capacity of the Anchor Embedded in Concrete
V_c	Concrete Contribution to the Shear Capacity
V_n	Nominal Shear Strength at Section
$V_{c,i}$	Nominal Shear Strength at Section for Punching Shear Check: $i = 1, 2, 3$
V_s	Unfactored Shear due to the Most Demanding Load Condition for a Structural Element
V_u	Ultimate (Factored) Shear due to the Most Demanding Load Condition for a Structural Element
w_f	Width of the Pre-cured FRP Laminate
w_{tire}	Size of the Print of a Wheel in the Transverse Direction according to AASHTO (2002)
W	Weight of the Nominal Truck Used to Determine the Live Load Effect
W_g	Width of the Girders Web
W_r	Width of the Roadway
W_{rc}	Width of the Roadway between Curbs
x	Generic Position of the Truck in the Transverse Direction of the Bridge
a_s	Coefficient Used in the Punching Shear Check according to ACI 318-02: $a_s = 40$ for Interior Load; $a_s = 30$ for Edge Load; $a_s = 20$ for Corner Load
b_c	Ratio of Long Side to Short Side of the Area over Which the Load is Distributed for Punching Shear Check
b_d	Coefficient as per AASHTO (2002) Table 3.22.1A: $b_d = 1.0$ for Ultimate Conditions and $b_d = 1.0$ for Service Conditions
b_L	Coefficient as per AASHTO (2002) Table 3.22.1A: $b_L = 1.67$ for Ultimate Conditions and $b_L = 1.00$ for Service Conditions
g	Coefficient as per AASHTO (2002) Table 3.22.1A: $g = 1.3$ for Ultimate Conditions and $g = 1.0$ for Service Conditions

$d_{\max}$	Maximum Displacement Experienced during Load Tests
e_{fu}	Design Tensile Strain of the Pre-cured FRP Laminate: $e_{fu} = C_E e^*_{fu}$
e^*_{fu}	Guaranteed Tensile Strain of the Pre-cured FRP Laminate as Reported by the Manufacturer
f	Strength Reduction Factor according to ACI 318-02 Section 9.3: $f = 0.70$ for Axial Load and Axial Load with Flexure for Member without Spiral Reinforcement conforming to ACI 318-02 Section 10.9.3. The Same Symbol is Applied to Indicate the Factors Used to Convert Nominal Values to Design Capacities of Member
f_{punch}	Strength Reduction Factor for Punching Shear Check according to ACI 318-02 Section 9.3: $f_{punch} = 0.85$
r_w	Ratio of Tensile Non-prestressed Steel Reinforcement: $r_w = \dfrac{A_s}{b_w d}$
w_u	Ultimate Value of Stresses due to Moments and Shear Forces

CONVERSION OF UNITS

1 Inch (in) = $8.333 \cdot 10^{-2}$ Feet (ft)

1 Inch (in) = $2.54 \cdot 10^{-2}$ Meters (m)

1 Foot (ft) = 12 Inches (in)

1 Foot (ft) = $3.048 \cdot 10^{-1}$ Meters (m)

1 Kip (kip) = 4.448222 Kilonewton (kN)

1 Kip (kip) = $4.448222 \cdot 10^{3}$ Newton (N)

1 Kip (kip) = 10^{3} Pounds-Force (lbf)

1 Kip per Square Inch (ksi) = 6.894757 Mega Pascal (MPa)

1 Kip per Square Inch (ksi) = $6.894757 \cdot 10^{6}$ Pascal (Pa)

1 Mile per Hour (MPH) = 4.470 Meter per Second (m/s)

1 Pound-Force (lbf) = 4.448222 Newton (N)

1 Pound-Force (lbf) = $4.448222 \cdot 10^{-3}$ Newton (kN)

1 Pound-Force per Square Inch (psi) = $6.894757 \cdot 10^{-3}$ Megapascal (MPa)

1 Pound-Force per Square Inch (psi) = $6.894757 \cdot 10^{3}$ Pascal (Pa)

1 Ton-Force (ton) = $2 \cdot 10^{3}$ Pounds-Force (lbf)

1 Ton-Force (ton) = 2 Kips (kip)

1. BACKGROUND

1.1. Delta Regional Authority Program Project

In December 2002, as a result of its partnership with University of Missouri, Rolla – University Transportation Center (UMR-UTC), the Meramec Regional Planning Commission (MRPC) received a $193895 grant award from the Delta Regional Authority for bridge improvement projects in Crawford, Dent, Phelps, and Washington Counties.

1.2. Need for the Proposed Project

Transportation infrastructure is one of the major economic development needs for the Meramec Region. Local roads and bridges affect the economic welfare of the region by providing links to the major routes. Local roads and bridges are the collector systems into the larger state highway system for the transport of manufactured products and agricultural goods, accessing employment centers, and bringing travelers and tourists to the region. While many residents are engaged in agriculture and use the roads for farm-to-market routes, a growing number of people are working in cities and living in unincorporated areas relying on rural roads to commute to work. Aging bridges prohibit growth in much of the region because they severely limit access to many communities.

According to the National Bridge Inventory in 1995, 29 percent of county bridges do not meet minimum tolerable conditions to be left as-is. Nationwide, 40 percent of rural bridges are posted as to weight or other travel restrictions. Load postings are defined as the safe loads to cross a bridge. Loads over the posted limit cause damage to the structure and shorten the life of the bridge. Examples of vehicles affected would be school buses, fire trucks and ambulances, commercial truck traffic and large farm equipment. Dump trucks are affected by all load postings according to the Missouri Department of Transportation (MoDOT) and emergency vehicles are affected by most postings. The Federal Highway Administration (FHWA) classifies 32 percent of rural bridges as structurally deficient. Over one-third of the rural bridges in Crawford, Dent, Phelps and Washington counties are considered deficient by MoDOT standards. Much of the problems with local bridges are due to age and obsolete design.

The high cost associated with bridge replacement keeps communities from addressing many bridges. Even the cost to repair bridges is high when using conventional technologies. Maintaining and upgrading transportation infrastructure is a challenge for rural regions because of the sparse density of residents and number of roads and bridges running throughout the area. The low Average Daily Traffic (ADT) on most rural bridges seems to make the cost for bridge replacement ineffective. Low-volume bridges make it difficult for rural areas to compete for grant funding to assist with bridge replacements because rural areas are in competition with larger metropolitan areas. Rural areas are at a disadvantage because more populated areas can incorporate additional aspects of transportation, such as public transit and major economic impact, in grant proposals.

1.3. Description of the Project

Fiber-reinforced polymer (FRP) materials have recently emerged as a practical alternative for construction and renovation of bridges. Advantages of FRP materials are that they resist corrosion, long outlive conventional materials, and have high strength-to-weight ratio. Placement of FRP material is in two forms, near-surface mounted bars and externally-bonded laminates, and the materials are applied on the underside of bridges. UMR has been working with FRP technology on projects around the state and in the Meramec Region. Projects have included strengthening of bridges in Boone County, Phelps County, and St. Louis. Bridges constructed with FRP materials were installed in the city of St. James, MO. FRP strengthening of bridges has had significant cost and time savings over conventional methods.

MRPC is working with local elected officials, UMR and MoDOT to identify and develop 31 bridge strengthening projects in the four-county area of Crawford, Dent, Phelps and Washington. Counties provide MRPC a list of bridge needs and MRPC staff reviews the list with UMR and MoDOT representatives to determine bridges that would be prime candidates for FRP strengthening technology. MoDOT will also review the bridges to determine those that have previously been inspected and found to be structurally deficient or require a load posting. MoDOT will also help determine if projects can help the counties earn soft-match credit towards larger projects using Bridge Replacement Off-system (BRO) funds. MRPC will then determine the economic development impact each bridge has on the region and prioritize projects based on this ranking. The University will prepare design specifications for applying FRP material to each bridge. Contractors will be competitively procured to install the FRP material and those contractors will be required to have or receive certification from UMR for FRP technology training. The University will monitor the application of FRP material to each bridge. Each county may use a third party engineering firm to seal the design and monitor the contractor's activity to ensure that the results of the FRP technology are accurate and valid. Bridges may be tested for load posting before and after the strengthening process to determine the effect of the activity on the strength of each bridge. It is anticipated that strengthening will allow for the load postings to be removed or significantly raised for the structures subjected to such limitations.

1.4. Complementing Existing Regional Plans

Through MRPC, each county completed a Strategic Plan in 2000-2001 to identify current needs and develop a plan of action. This information became part of the region's Comprehensive Economic Development Strategy. Transportation infrastructure was a common need found in all counties. A top priority for economic development was determined to be the need for a better transportation system. Each county identified an objective to improve existing infrastructure. Activities proposed to address the transportation system included encouraging transportation development to enhance economic growth. Most counties found that tourism is directly related to the transportation system and if the tourism industry is to be promoted in the region, the transportation system must be addressed. Counties determined that activities must include improvements to local roads and bridges as well as state routes.

Each community will be required to cover 30 percent of the cost to reinforce each bridge addressed in their jurisdiction. Communities are also responsible for using a third party engineering firm to seal the University's design work and inspect the work of contractor(s) hired to apply the FRP reinforcement. The bridges to be addressed are not deficient due to poor maintenance, but to age and structural obsolescence. Once strengthened, the bridges will have an increased life by removing or upgrading the current load postings. Each community budgets for road and bridge maintenance and this will not change with the proposed project. Strengthening is the only alternative to replacement, and should not require additional maintenance from the community's road crews.

An improved transportation system is a severe need all across the state, including these four Delta counties of the Meramec Region. The transportation system, bridges in particular, was found to be a top priority in the strategic plans for each county as part of the Comprehensive Economic Development Strategy developed for the region. Transportation was directly related to economic development in each county and for the region. The transportation infrastructure of the region has a direct impact on economic development by providing the means necessary to transport raw materials and products, employees to/from work and consumers to/from business centers.

1.5. Impact of the Project

Strengthening bridges will allow for communities to open bridges to more traffic and facilitate the movement of freight, farm equipment and products, and commuter traffic. Counties will add new strength to bridges that otherwise would need to be replaced or closed due to posting limits. Major employment centers are located in each of the four counties. The industries are dependent upon moving their goods and, in the Meramec Region, goods move only via the road system. Major employment centers rely on the local transportation system to allow access for employees and connecting with larger transportation systems for moving materials and products. Such industries include Doe Run Inc., Salem Memorial District Hospital and US Food Service in Dent County, Dana Brake Parts Inc., Meramec Industries Inc., and Missouri Baptist Hospital in Crawford County, Briggs & Stratton Corp., Boys & Girls Town of Missouri and Wal-Mart Distribution Center in Phelps County and Red Wing Shoe Co., Georgian Gardens Nursing Home and YMCA of the Ozarks in Washington County.

Up to 31 county bridges may be strengthened using the FRP technology. Strengthening will remove load postings or significantly increase postings so that bridges will be open to more traffic. These bridges will allow for more access from county roads to major routes running through the area, directly impacting the economic development potential of the region.

2. INTRODUCTION

This report summarizes the procedures used for the upgrade of the bridge No. 1330005 (see Figure 2.1), located in Phelps County (Route 3560), MO. The bridge is actually load posted to a maximum weight of 10 *ton*.

Figure 2.1. Bridge No. 1330005

The total length of the bridge is $7925\ mm\ (26\ ft)$ and the total width of the deck is $6680\ mm\ (21\ ft\ 11\ in)$. The span of the bridge consists of four reinforced concrete (RC) girders monolithically cast with a $152\ mm\ (6\ in)$ deep deck. It can be assumed as simply-supported by the abutments.

2.1. Objectives

The primary objectives of this document are to analyze the bridge superstructure and to provide the design calculations for its strengthening using a Mechanically Fastened Fiber-Reinforced Polymer system (MF-FRP). The advantage system consists of pre-cured FRP laminates bolted onto the concrete surface in order to provide the necessary flexural reinforcement to girders and deck. The strength of the technique is in the fact that it does not require any surface preparation prior to the installation of the FRP.

2.2. Bridge Conditions

Prior to the strengthening of the bridge, a detailed investigation was required to determine the initial conditions of the bridge and the properties of the constituent materials.

From visual observations, some concrete spalling along the longitudinal edges of the bridge was observed. The girders and deck showed traces of steel rebar corrosion (see Figure 2.2-a). As a consequence of the insufficient amount of longitudinal reinforcement, all the girders were visibly cracked at mid-span (see Figure 2.2-b). In addition, due to the inadequate transversal reinforcement, the deck also presented a longitudinal crack halfway between adjacent girders (see Figure 2.3-a). The abutments appeared to be in good condition except for some vertical cracks running down from the edges of the girders across the entire height of the abutment (see Figure 2.3-b).

The details of the bridge reinforcement and material properties were unknown due to the unavailability of the bridge plans. As a consequence, at the onset of the project, these properties were determined in-situ, based on visual and Non Destructive Testing (NDT) evaluation.

In particular, three concrete cores were drilled from the deck (see Figure 2.4-a), and they were tested in compliance with ASTM C39/C39M-1 and ASTM C42/C42M-99 (see Figure 2.4-b). The following results were found:

§ Average Compression Strength: $f_c^{'} = 46.6\ MPa\ (6760\ psi)$;

§ Standard Deviation: $SD_c = 3.9\ MPa\ (560\ psi)$;

§ Variance: $c.o.v._c = 100\frac{SD_c}{f_c^{'}} = 8.3\%$.

Concrete cover and size of longitudinal and transverse steel bars in the deck were determined from the concrete cores (see Figure 2.5-a) as follows:

Ø Transverse Direction

$\#4$ (12.7 mm $(0.5\ in)$ diameter) steel bars

average spacing: $432\ mm\ (17\ in)$ on center clear concrete cover: $63.5\ mm\ (2\frac{1}{2}\ in)$;

- Longitudinal Direction

  $\#4$ ($12.7\ mm\ (0.5\ in)$ diameter) steel bars

  average spacing: $330\ mm\ (13\ in)$ on center

  clear concrete cover: $50.4\ mm\ (2\ in)$.

a) Girders and Deck b) Bending Cracks in the Girders

Figure 2.2. Condition of the Superstructure

a) Longitudinal Crack in the Deck b) Vertical Crack in the Abutment

Figure 2.3. Condition of Deck and Abutments

a) Coring b) Compression Tests

Figure 2.4. Material Characterization of the Concrete

Concrete cover, number and size of flexural and shear reinforcement for the girders were determined by chipping off concrete at different locations (see Figure 2.5-b). The reinforcement consisted of:

- Flexural Reinforcement

  $3\ \#6$ (19 mm $\left(\frac{6}{8}\ in\right)$ diameter) steel bars

  clear concrete cover: $76.2\ mm\ (3\ in)$;

- Shear Reinforcement

  $1\ \#4$ (12.7 mm $(0.5\ in)$ diameter) steel bars $@355\ mm\ (14\ in)$ on center at the mid-span

  $2\ \#4$ (12.7 mm $(0.5\ in)$ diameter) steel bars $@355\ mm\ (14\ in)$ on center (close to the abutments)

  clear concrete cover: $57\ mm\ \left(2\frac{1}{4}\ in\right)$.

The location of the steel reinforcement for the deck and girders was accurately detected with a rebar locator. Using the same equipment it was also possible to determine that all girders were reinforced with the same amount of steel.

The mechanical properties of the steel reinforcement were determinate by testing three specimens cut from an exposed bar found in one of the abutments. They were tested according to ASTM A615 and ASTM A955 (see Figure 2.5-c). The following results were found:

- Average Yield Strength: $f_y = 377.1\, MPa\ (54690\, psi)$;
- Standard Deviation: $SD_y = 28.7\, MPa\ (4170\, psi)$;
- Variance: $c.o.v._y = 100\dfrac{SD_y}{f_y} = 7.6\%$.

Based on the experimental results, a Grade 50 steel was assumed for design.

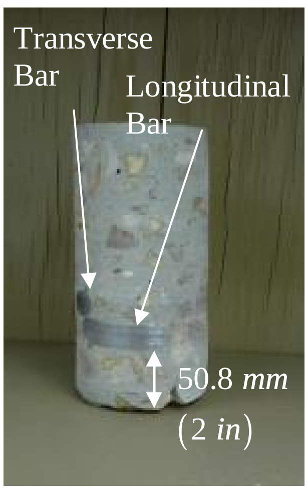

a) Pieces of Bars in a Core

b) Broken Section of a Girder

c) Tension Test

Figure 2.5. Material Characterization of the Steel Bars

The geometry of the bridge is summarized in Table 2.1. Figure 2.6 and Figure 2.7 show the longitudinal and plan view of the bridge. Figure 2.7 also draws the position from where the concrete cores where extracted and the longitudinal and transverse steel reinforcement of the deck.

Cross section and steel reinforcement for the girders are summarized in Figure 2.8, Figure 2.9 and Figure 2.10. In particular, Figure 2.8 summarizes cross-section and longitudinal reinforcement for all the girders while Figure 2.9 and Figure 2.10 show the shear reinforcement for the outer and the inner girders respectively.

Table 2.1. Geometry of the Bridge

Clear Span	$l_c = 7315\ mm\ (24\ ft)$
Design Length	$l_d = 7620\ mm\ (25\ ft)$
Deck Height	$H_d = 152\ mm\ (6\ in)$
Girder Web Height	$H_g = 406\ mm\ (16\ in)$
Girder Width	$W_g = 366\ mm\ (14\ in)$
Spacing between Girders On Center	$d_g = 1803\ mm\ (5\ ft\ 11\ in)$
Cantilever Deck	$d_c = 457\ mm\ (1\ ft\ 6\ in)$
Roadway Width	$W_r = 6680\ mm\ (21\ ft\ 11\ in)$
Curb to Curb Roadway Width	$W_{rc} = 6172\ mm\ (20\ ft\ 3\ in)$
Overlay Height (Compact Gravel)	$H_o = 152\ mm\ (6\ in)$

The analysis and design of the bridge was performed according to the MoDOT Bridge Manual, to the experimental results attained at the University of Wisconsin-Madison (Bank et al., 2002) and at the University of Missouri-Rolla. The assumed load configurations were consistent with the AASHTO Specifications (AASHTO, 2002).

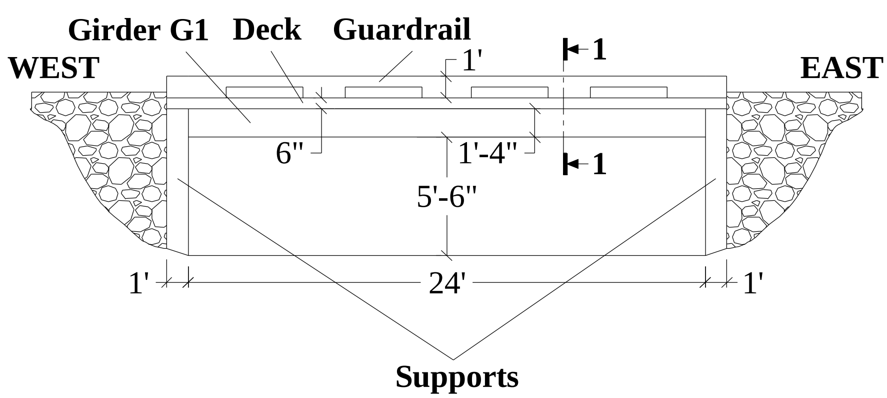

Figure 2.6. Longitudinal View of the Bridge

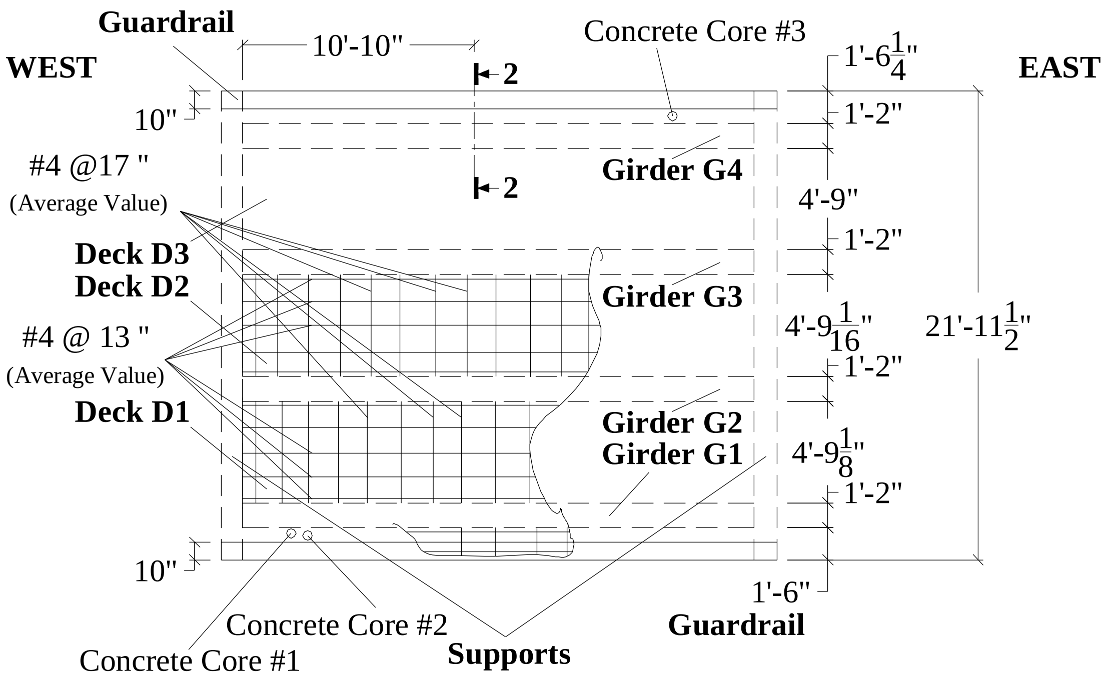

Figure 2.7. Plan View of the Bridge

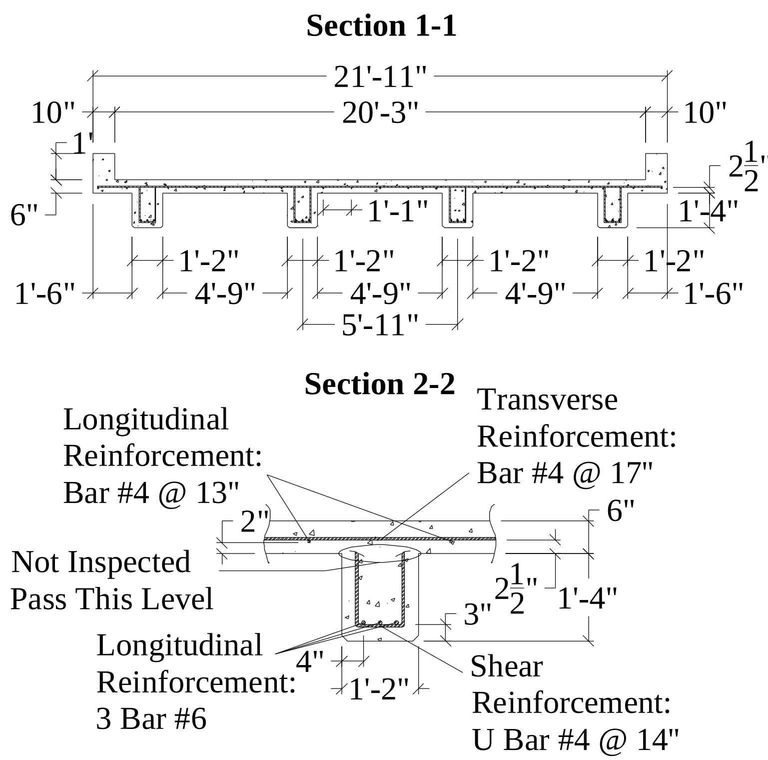

Figure 2.8. Details of the Inspected Sections

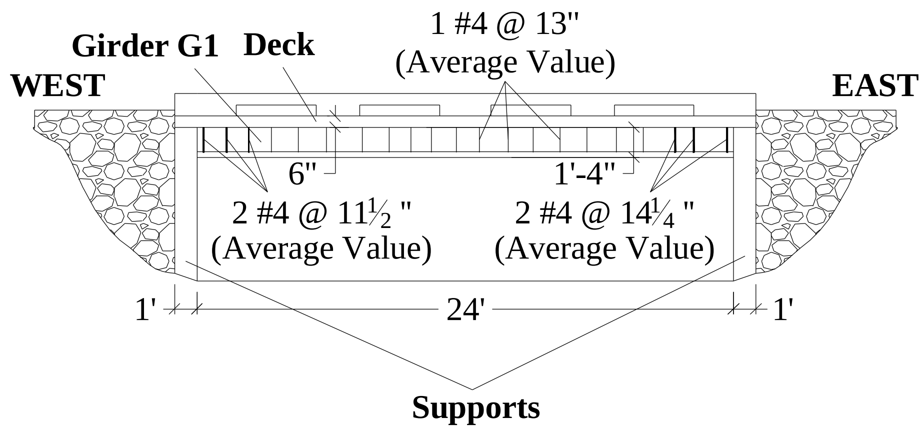

Figure 2.9. Shear Reinforcement in the Outer Girders (G1 and G4)

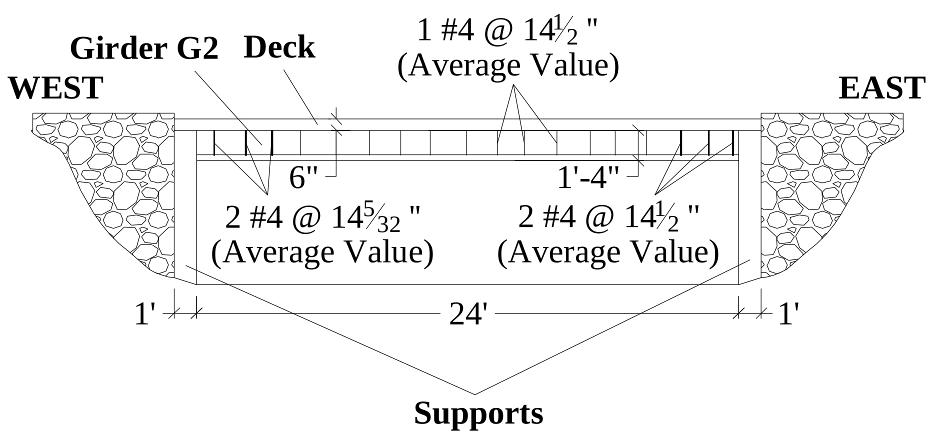

Figure 2.10. Shear Reinforcement in the Inner Girders (G2 and G3)

3. STRUCTURAL ANALYSIS

3.1. Load Combinations

For the structural analysis of the bridge, the definitions of design truck and design lane are necessary. This will be addressed in the next section.

Ultimate values of bending moments and shear forces are obtained by multiplying their nominal values with the dead and live load factors and by the impact factor according to AASHTO (2002) as shown in equation (3.1):

$$w_u = g\left[b_d D + b_L (1+I) L\right] \tag{3.1}$$

where

D	is the dead load;
L	is the live load;
g , b_d , b_L	are coefficients as per AASHTO (2002) Table 3.22.1A:
	ultimate conditions $\Rightarrow g = 1.3$, $b_d = 1.0$, $b_L = 1.67$;
	service conditions $\Rightarrow g = 1.0$, $b_d = 1.0$, $b_L = 1.00$;
I	is the live load impact calculated as follows:

$$I = \frac{50}{l_d + 125} = \frac{50}{25.0 + 125} = 0.33 \le 0.30 \tag{3.2}$$

and $l_d = 25\ ft\ (7620\ mm)$ represents the span length from center to center of support. The impact factor should not be larger than 0.30, and therefore the latter value is assumed for the design.

3.2. Design Truck and Design Lanes

Prior to the design of the strengthening, the analysis of the bridge was conducted by considering a H15-44 truck load (which represents the design truck load as per AASHTO, 2002 Section 3.7.4) having geometrical characteristics and weight properties shown in Figure 3.1.

According to AASHTO Section 3.6.3 (2002), roadway widths between 6096 and $7315\ mm$ $(20 \text{ and } 24\ ft)$ shall have two design lanes, each one equal to one-half of the roadway width. However, in this case, the low value of the Annual Daily Traffic ($ADT = 35$) of the bridge allows to deal just with one design lane. To be noted that the centerline of the wheels of the rear axle shown in Figure 3.1 is located $305.0\ mm$ $(1.0\ ft)$ away from the curb as specified in AASHTO (2002) for slab design.

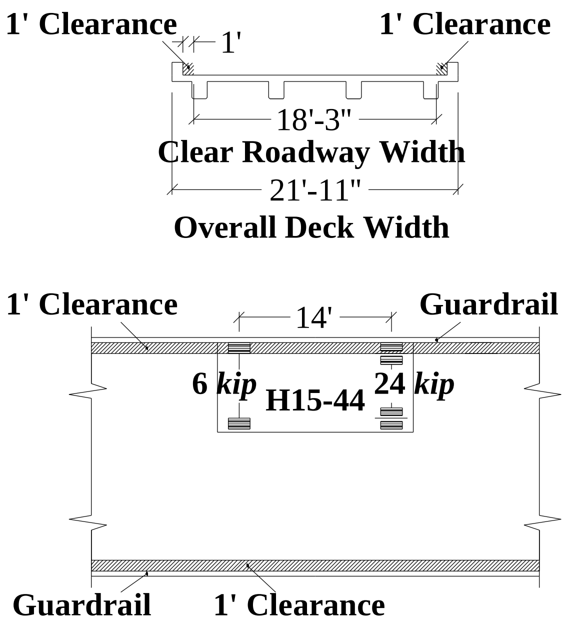

Figure 3.1. Truck Load and Truck Lanes

Two loading conditions are required to be checked as laid out in Figure 3.2.

The H15-44 design truck load (Figure 3.2-a) has a front axle load of $26.7\ kN$ $(6.0\ kip)$ and rear axle load located $356\ mm$ $(14\ ft)$ behind the drive axle.

The design lane loading condition consists of a load of $2.1\,kN$ $(0.48\,kip)$ per linear foot, uniformly distributed in the longitudinal direction with a single concentrated load so placed on the span as to produce maximum stress. The concentrated load and uniform load are considered to be uniformly distributed over a $3048\,mm$ $(10.0\,ft)$ width on a line normal to the center of the lane. The intensity of the concentrated load is represented in Figure 3.2-b for both bending moments and shear forces. This load shall be placed in such positions within the design lane as to produce the maximum stress in the member.

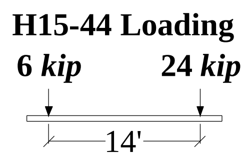

a) Design Truck (H15-44)

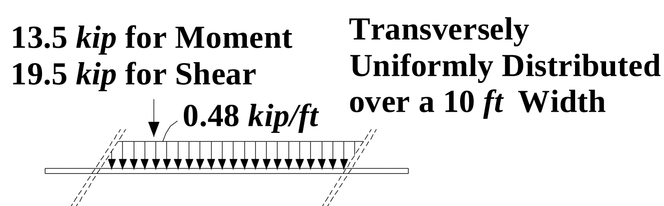

b) Design Lane

Figure 3.2. Loading Conditions

3.3. Slab Analysis

Since it was not possible to detect the presence of longitudinal reinforcement in the negative moment regions, the continuity of the deck over the girders was conservatively neglected. This led to model the deck as a slab simply-supported between two girders (see Figure 3.3).

Figure 3.3 shows the worst loading condition for the slab between girders G2 and G3. The design value was determined from the truck design condition when the wheel is in the middle of the slab. The load of the wheel was spread over a surface $508 \times 254\,mm$ $(20 \times 10\,in)$ as prescribed in the AASHTO (2002) Section 4.3.30. A commercial finite elements program (SAP 2000) was used to analyze the structure. The ultimate moment found from this analysis was (see Figure 3.4):

$$M_u = 37.4 \frac{kN \cdot m}{m} \left(8.4 \frac{kip \cdot ft}{ft} \right).$$

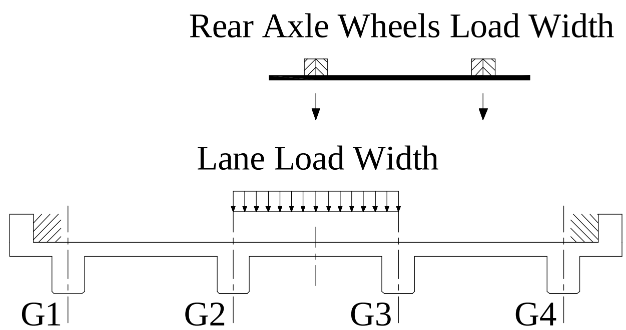

Figure 3.3. Slab Load Conditions

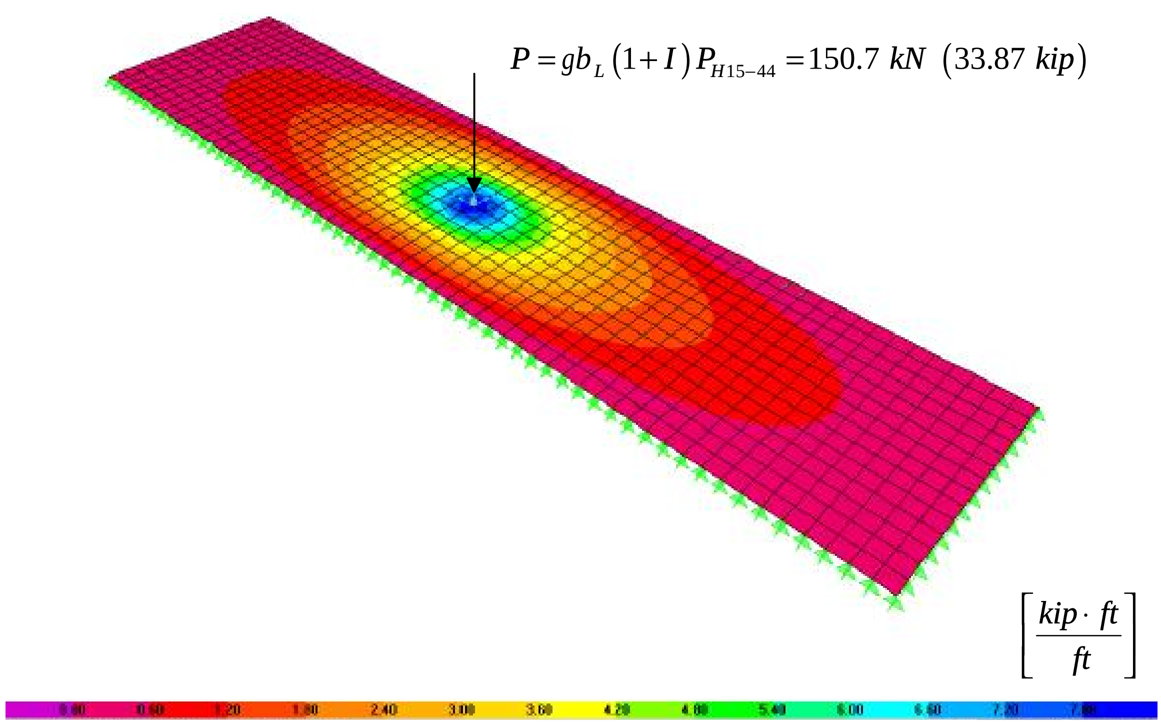

Figure 3.4. Slab Transversal Bending Moment Distribution

3.4. Girders Analysis

The transverse load distribution was found by analyzing the structure represented in Figure 3.5, where a generic axle of unit weight $P = 1\,kN\ (0.225\,kip)$ and a unitary uniform distributed load $q = 1\frac{kN}{m}\left(0.068\frac{kip}{ft}\right)$ have been assumed. As mentioned, the continuity of the slab was neglected and therefore the scheme to be considered for the structural analysis is the one shown in Figure 3.5. From Figure 3.5 it can be observed that by increasing the value of x the design lanes move from the left to the right portion of the bridge slab.

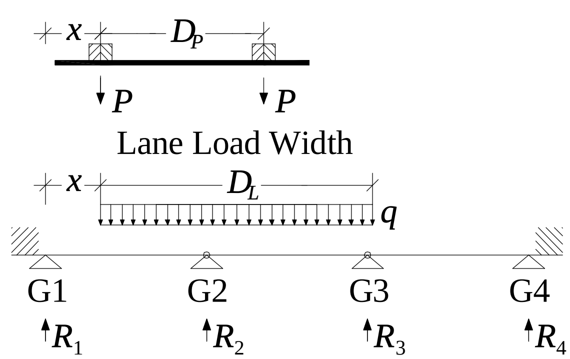

Figure 3.5. Girders Load Conditions for Analysis and Design

Table 3.1 summarizes the results of the analysis, where q_{DL} is related to a uniform distributed load over all the spans (like the dead load), q_{LL} to a uniform distributed load over the two spans next to the support (like the lane design load) and P to the truck design load.

Table 3.2 summarizes the results in terms of unfactored and factored bending moments (M_s and M_u) and shear forces (V_s and V_u). The maximum values, found considering the positions of the load that produces the worst condition for the structure (i.e., varying the position of the truck along the length of the bridge), are adopted for design.

Figure 3.6 and Figure 3.7 show respectively the bending moment M_u and the shear V_u envelopes due to the load obtained, taking for each section (at the distance x from the left support) the maximum value given by the two loading conditions: the worst load condition is that one related to the truck load design.

Table 3.1. Distribution Coefficient for the Girders

Load Combination \ *Girder Reaction*	R_1 $[kN]$ $([kip])$	R_2 $[kN]$ $([kip])$	R_3 $[kN]$ $([kip])$	R_4 $[kN]$ $([kip])$
q_{DL} over all the spans in kN/m (kip/ft)	78.92 (5.408)	81.00 (5.550)	81.00 (5.550)	78.92 (5.408)
q_{LL} over the two spans next to the support in kN/m (kip/ft)	46.90 (3.214)	86.26 (5.911)	86.26 (5.911)	46.90 (3.214)
P in kN (kip)	15.61 (1.070)	14.55 (0.997)	14.55 (0.997)	15.61 (1.070)

Table 3.2. Interior Girder Bending Moments and Shear Forces

Loading Condition	*Unfactored Moment*[a)] M_s $[kN \cdot m]$ $([kip \cdot ft])$	*Factored Moment*[a)] M_u $[kN \cdot m]$ $([kip \cdot ft])$	*Unfactored Shear*[b)] V_s $[kN]$ $([kip])$	*Factored Shear*[b)] V_u $[kN]$ $([kip])$
Dead Load	103.0 (76.0)	134.1 (98.9)	16.5 (12.2)	21.4 (15.8)
H15-44 Load Design Condition *Number of Lanes* = 1				
Truck Design	101.4 (74.8)	286.1 (211.0)	18.0 (13.3)	50.84 (37.5)
Total	204.5 (150.8)	*420.2* (*309.9*)	34.4 (25.4)	*72.3* (*53.3*)
Lane Design	97.8 (72.1)	275.9 (203.5)	20.5 (15.1)	57.8 (42.6)
Total	201.0 (148.2)	346.2 (*255.3*)	37.0 (27.3)	*79.2* (*58.4*)

a) Computed at a cross-section in the middle of the span.
b) Computed at a cross-section in the middle of the support.

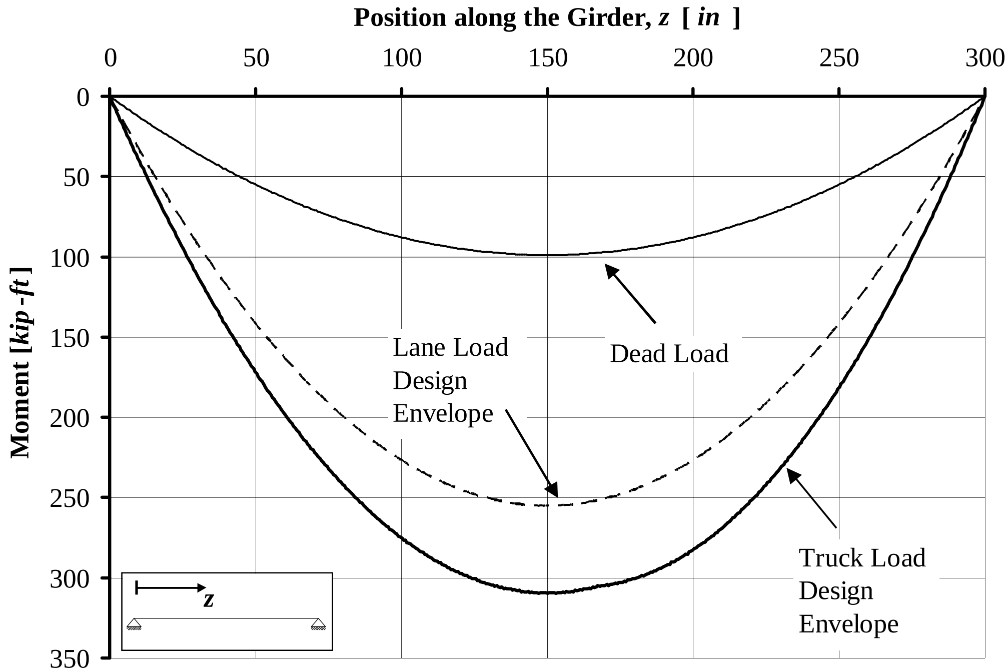

Figure 3.6. Interior Girder Bending Moment Diagrams Envelopes

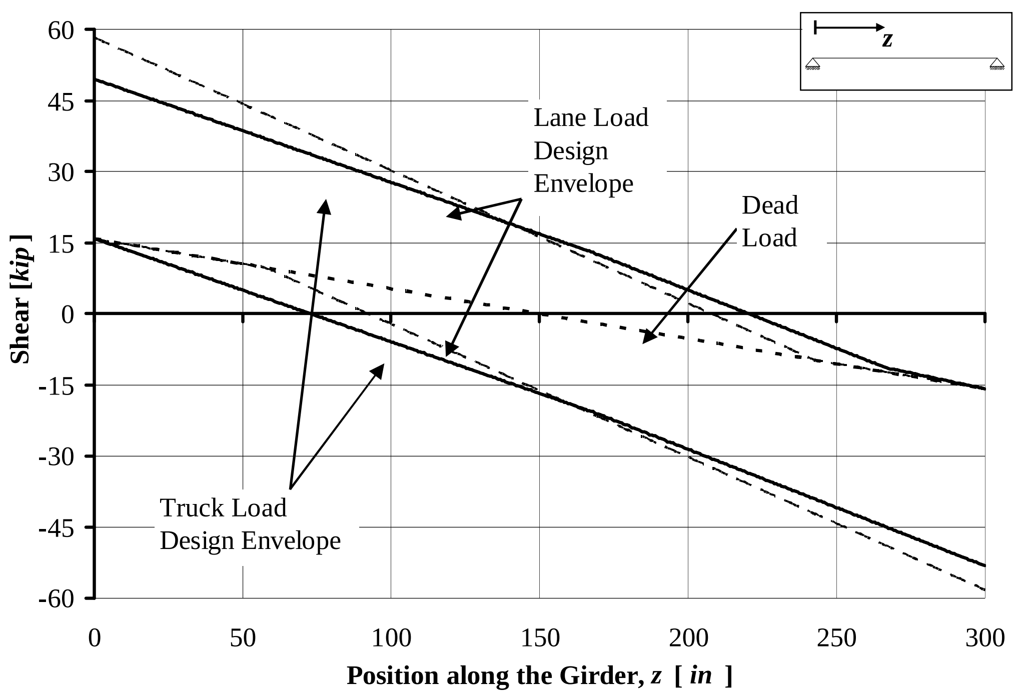

Figure 3.7. Interior Girder Shear Diagrams Envelopes

3.5. Analysis of the Abutments

The abutment can be analyzed as a wall loaded in its plane. According to ACI 318-02 Section 14.5.2, design axial load strength $f P_n$ for a wall of solid rectangular cross section with resultant of all factored loads located within the middle third of the overall thickness of the wall is given by

$$f P_n = 0.55 f\, f_c^{'} A_g \left[1 - \left(\frac{k h_c}{32 h} \right)^2 \right] \cong 1713\ kN\ \ (385\ kip) \qquad (3.3)$$

where

$f = 0.70$	is the strength reduction factor;
A_g	is the gross area of the section;
k	is the effective length factor ($k = 2.0$ for walls not braced against lateral translation;
h_c	is the vertical distance between supports;
h	is the overall thickness of member.

The worst loading condition comes out by considering the maximum shear demand of the girders:

$$R_{ab} = V_u = 58.4\ kip\,.$$

Since $R_{ab} < f P_n$, the supports do not need further analysis.

4. DESIGN

4.1. Assumptions

Mechanically-Fastened FRP laminate design is carried out according to the principles of ACI 440.2R-02 (ACI 440 in the following). The properties of concrete, steel and FRP laminates used in the design are summarized in Table 4.1. The concrete and steel properties are obtained by testing of samples while the FRP properties are guaranteed values.

The f factors used to convert nominal values to design capacities are obtained as specified in AASHTO (2002) for the as-built and from ACI 440 for the strengthened members.

Table 4.1. Material Properties

Concrete	*Steel*		*FRP - SAFSTRIP*			
Compressive Strength $f_c^{'}$ $[MPa]$ $([psi])$	Yield Strength f_y $[MPa]$ $([ksi])$	Modulus of Elasticity E_s $[GPa]$ $([ksi])$	Tensile Strength f_{fu}^{*} $[MPa]$ $([ksi])$	Modulus of Elasticity E_f $[GPa]$ $([ksi])$	Thickness t_f $[mm]$ $([in])$	Width w_f $[mm]$ $([in])$
46.6 (6760)	344.7 (50)	200.0 (29000)	588.8 (85.4)	60.7 (8800)	3.175 (0.125)	101.6 (4.00)

Material properties of the FRP reinforcement reported by manufacturers, such as the ultimate tensile strength, typically do not consider long-term exposure to environmental conditions, and should be considered as initial properties. FRP properties to be used in all design equations are given as follows (ACI 440):

$$\begin{aligned} f_{fu} &= C_E f_{fu}^{*} \\ e_{fu} &= C_E e_{fu}^{*} \end{aligned} \tag{4.1}$$

where f_{fu} and e_{fu} are the FRP design tensile strength and ultimate strain considering the environmental reduction factor C_E as given in Table 7.1 (ACI 440), and f_{fu}^* and e_{fu}^* represent the FRP guaranteed tensile strength and ultimate strain as reported by the manufacturer (see Table 4.1).

The maximum strength that the MF-FRP strengthening can develop depends on the capacity of the connection bolt-strip and, therefore, on the number of fasteners used.

In order to mechanically fasten the FRP laminate to the concrete, the optimal solution in terms of mechanical behavior of the connection was found as a result of an experimental program conducted at UMR. The chosen fastening system consisted of:

- Concrete wedge anchor (diameter $9.525\ mm\ \left(3/8\ in\right)$ and total length $57.15\ mm\ \left(2\,1/4\ in\right)$ - Figure 4.1). The shear capacity T_c of the anchor embedded in the concrete depends upon the embedment depth h_b and the strength of the concrete $f_c^{'}$. The shear strength of the anchor, T_b, becomes equal to T_c with a value of $26.7\ kN\ \left(6.0\ kip\right)$ when $f_c^{'} = 41.4 MPa\ \left(6000\ psi\right)$ and $h_b = 38.1\ mm$ $\left(1\,1/2\ in\right)$;

- Steel washer (inner diameter $11.112\ mm\ \left(7/16\ in\right)$, outer diameter $25.4\ mm\ \left(1\ in\right)$ and thickness $1.587\ mm\ \left(1/16\ in\right)$ - Figure 4.1);

- Epoxy between the washer and the FRP and throughout the hole on the FRP.

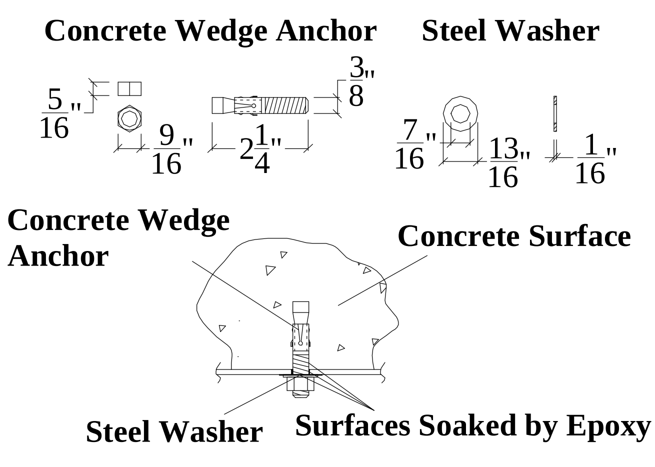

Figure 4.1. Details of the Connection Concrete-FRP

Bond tests on the connection FRP-fastener showed that at the ultimate conditions, the applied load is uniformly distributed between all the fasteners. In addition, it was observed that for concrete having an $f_c^{'} \geq 27.6\ MPa\ \left(4000\ psi\right)$, the failure mode of the connection is due to the bearing of the FRP. The experimental ultimate load supported by this connection was found to be $14.0\ kN\ \left(3.15\ kip\right)$. For design purposes a safety factor equal to 1.25 was assumed and therefore the design capacity of the connection is $R_b = 11.1\ kN\ \left(2.5\ kip\right)$.

Under these assumptions, the minimum number of fasteners $n_{b,\min}$ to anchor each FRP strip so that failure of the FRP controls, is given by:

$$n_{b,\min} = \frac{F_{FRP}}{R_b} \tag{4.2}$$

where F_{FRP} is the maximum load that the FRP strip experiences at ultimate conditions. Assuming $C_E = 0.85$ (i.e., carbon plate exposed in exterior aggressive ambient) and taking into account the net area of the strip (i.e., subtraction of the area lost to insert the bolt), from equation (4.2) the minimum number of bolts to reach the ultimate capacity of the FRP strip is 26. If fewer bolts are used, the failure would occur at the connection (i.e. bearing of the FRP strip).

4.2. Superstructure Design

4.2.1. Assumptions

The geometrical properties and the internal steel flexural reinforcement of the design cross section are summarized in Figure 2.8 and Table 4.2. The expression for the flange width B, is given by the equation (4.3), according to AASHTO (2002) Section 4.6.2.6.1 for interior and exterior girders, respectively:

$$\begin{cases} B^{Int} = \min\left(\frac{l_d}{4}, 12H_s + W_g, d_g\right) \\ B^{Ext} = \min\left(\frac{l_d}{4}, 12h_s + W_g, \frac{d_g + W_g}{2} + d_c\right) \end{cases} \tag{4.3}$$

where l_d, H_s, W_g, d_g and d_c are defined in Table 2.1. It results:

$$\begin{aligned} B^{Int} &\cong 1803\ mm\ (71\ in) \\ B^{Est} &\cong 1549\ mm\ (61\ in) \end{aligned}.$$

Table 4.2. Geometrical Properties and Internal Steel Reinforcement

Slab Thickness	Web Width	Flange Width	Slab Longitudinal Tensile Steel Area	Effective Depth	Slab Transverse Tensile Steel Area	Effective Depth	Web Tensile Steel Area	Effective Depth
H_d $[mm]$ $([in])$	W_g $[mm]$ $([in])$	B $[mm]$ $([in])$	$A_{s,slab\ long.}$ $[mm^2]$ $([in^2])$	$d_{slab\ long.}$ $[mm]$ $([in])$	$A_{s,slab\ transv.}$ $[mm^2/m]$ $([in^2/ft])$	$d_{slab\ transv.}$ $[mm]$ $([in])$	$A_{s,web}$ $[mm^2]$ $([in^2])$	d_{web} $[mm]$ $([in])$
152.4 (6.0)	355.6 (14)	1803.4 (71)	506.4 (0.785)	95.2 $(3\frac{3}{4})$	292.1 (0.138)	108.0 $(4\frac{1}{4})$	854.2 (1.324)	473.1 $(18\frac{5}{8})$

4.2.2. Flexural Strengthening

Table 4.3 summarizes the strengthening recommendations for the superstructure of the bridge. It can be observed that for the longitudinal direction the new moment capacity is slightly smaller than the demand. The value can be accepted because of the high safety factors used for design.

Figure 4.2 details the longitudinal flexural strengthening, while Figure 4.3 shows the transverse one. Finally, the pattern of the bolts for longitudinal and transversal reinforcement is shown in Figure 4.4.

The bolt pattern was verified at the ultimate condition in order to avoid having any section in which the moment demand is greater than the moment capacity. During this step, the position of the bolts is optimized. Figure 4.5 details the moment capacity of the beam along its length for the chosen bolt pattern. Appendix E contains some pictures of the FRP strengthening installation.

Table 4.3. Strengthening Summary

Section	*Strengthening Scheme*	*Design Capacity* fM_n $[kN \cdot m]$ $([kip \cdot ft])$		*Moment Demand* M_u $[kN \cdot m]$ $([kip \cdot ft])$
		Un-strengthened	*Strengthened*	
Longitudinal Direction	*Bottom of each girder:* 3 Plates *Sides of each girder:* 2 Plates	158.0 (116.5)	408.1 (301.0)	420.2 (309.9)
Transversal Direction	*Each span of the deck*: 15 Plates @ $457.2\ mm\ (18\ in)$ o/c	3.4[a)] (2.5)[a)]	17.4[a)] (12.8)[a)]	17.1[a)] (12.6)[a)]

a) Value corresponding to a $457.2\ mm\ (18\ in)$ wide stripe of the deck.

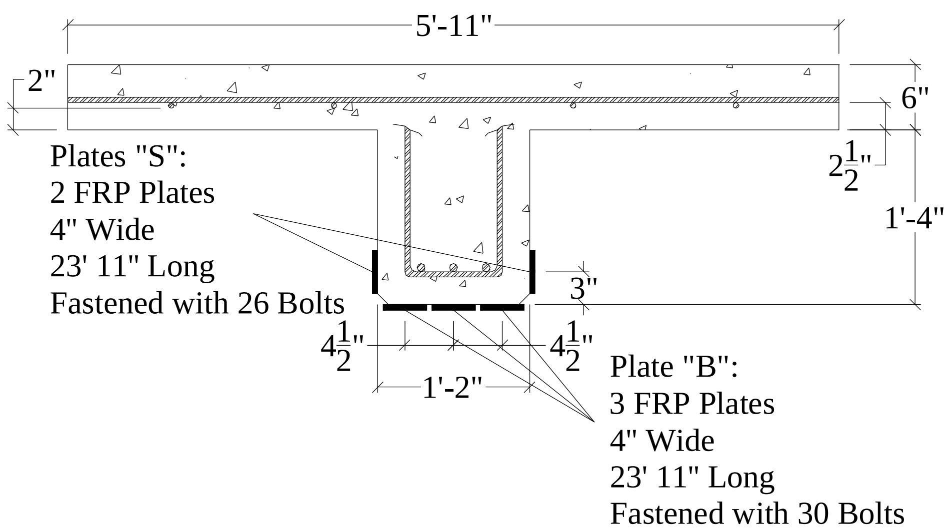

Figure 4.2. Girder Strengthened Section

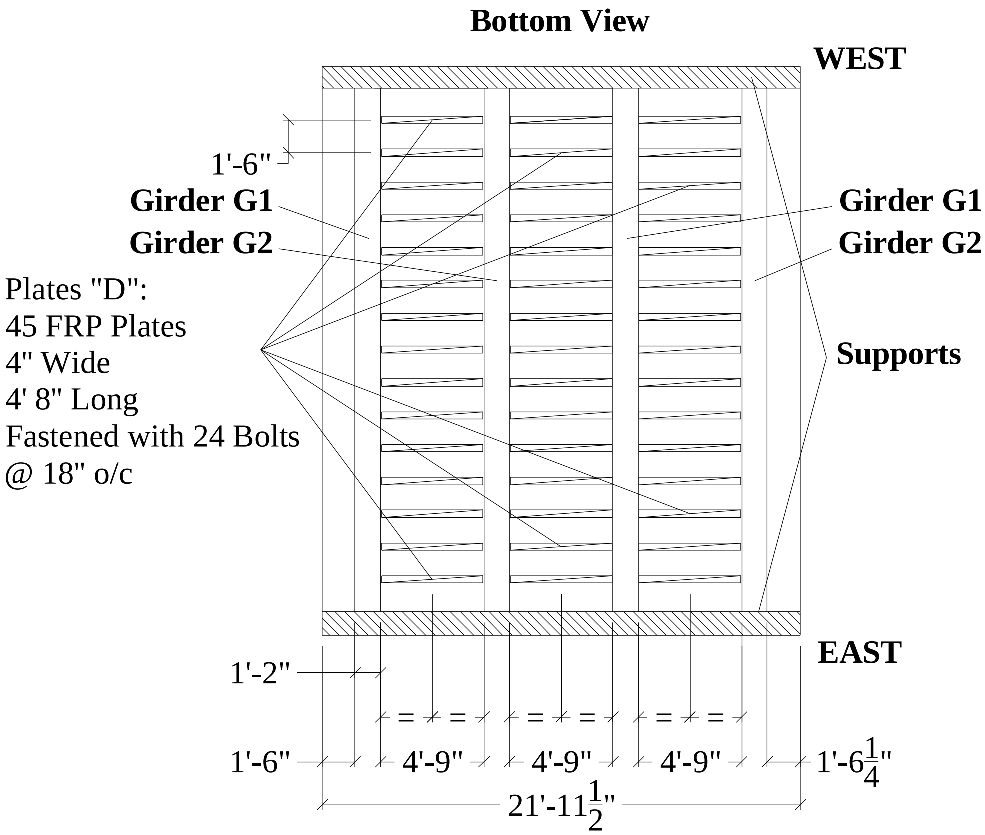

Figure 4.3. Strengthening of the Deck

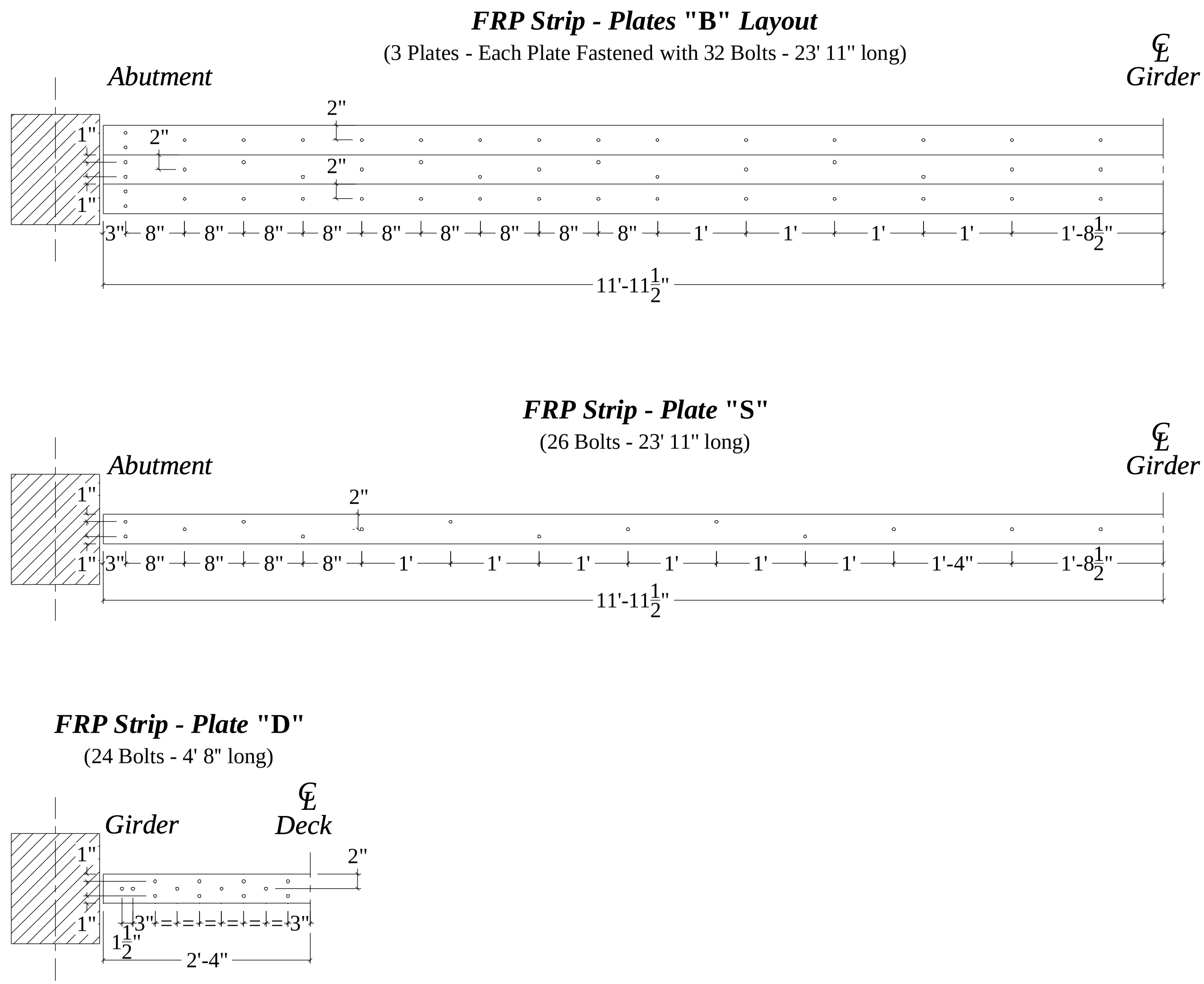

Figure 4.4. Pattern of the Bolts

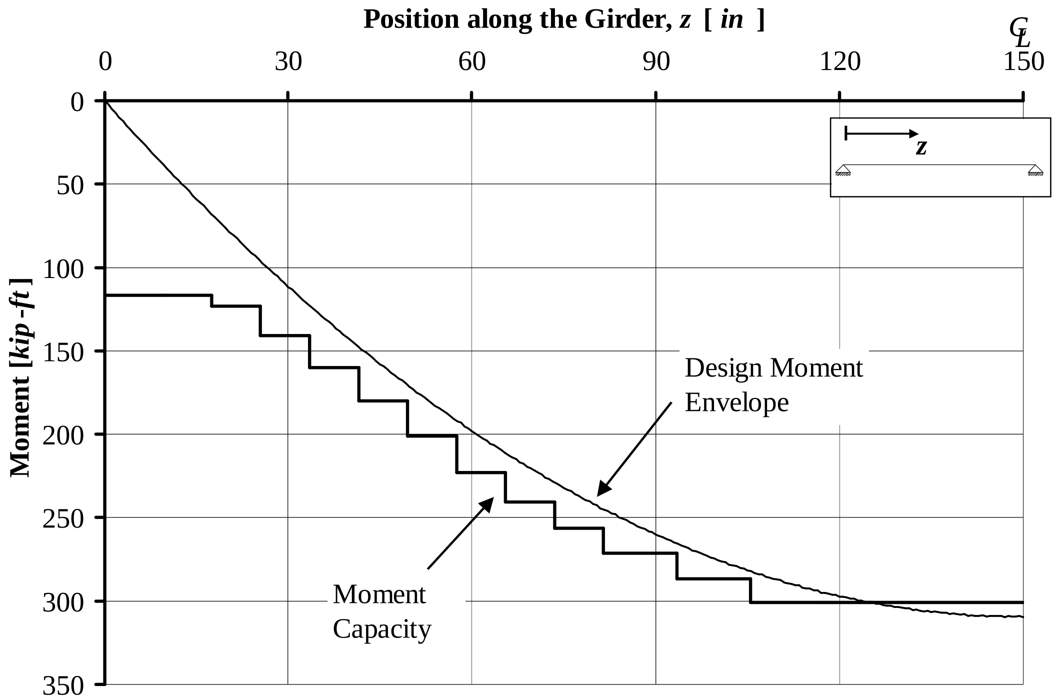

Figure 4.5. Diagram of the Capacity of the Beam at the Ultimate Load Conditions

4.2.3. Shear Check

The concrete contribution to the shear capacity was calculated based on equation (11-5) of ACI 318-02 as follows:

$$\begin{cases} V_c = \left(1.9\sqrt{f_c^{'}} + 2500\, r_w \dfrac{V_u d}{M_u}\right) b_w d \leq 3.5\sqrt{f_c^{'}}\, b_w d \\ \left[\, f_c^{'} \right] = [\, psi\,] \end{cases} \tag{4.4}$$

The as-built shear capacity is then computed by adding the concrete contribution to the one due to the shear reinforcement. Table 4.4 summarizes the findings for the superstructure. Since the capacity is higher than the demand, it can be concluded that no shear reinforcement is required.

Table 4.4. Superstructure Shear Capacity

Element	*Shear Capacity* fV_n	*Shear Demand* V_u
Slab $\left[\frac{kN}{m}\right]\left(\left[\frac{kip}{ft}\right]\right)$	87.6 (6.0)	51.1 (3.5)
Interior Girder		
Close to the Supports $[kN]$ $([kip])$ Stirrups $2\#4@356$ mm $(14$ $in)$	381.7 (85.8)	260.0 (58.4)
914 mm $(3$ $ft)$ from the Abutments $[kN]$ $([kip])$ Stirrups $1\#4@356$ mm $(14$ $in)$	245.5 (55.2)	209.1 (47.0)

4.2.4. Punching Shear Check

The deck must also be checked for punching shear. This check was based on ACI 318-02 requirements. ACI 318-02 Sec. 11.12.2.1 prescribes that for non-prestressed slabs and footings, V_c shall be the smallest of the following expressions:

$$\begin{cases} V_{c,1} = \left(2 + \frac{4}{b_c}\right)\sqrt{f_c^{'}}b_0 d \\ V_{c,2} = \left(\frac{a_s d}{b_0} + 2\right)\sqrt{f_c^{'}}b_0 d \qquad \text{with } \left[f_c^{'}\right] = [psi] \\ V_{c,3} = 4\sqrt{f_c^{'}}b_0 d \end{cases} \tag{4.5}$$

where:

- b_c is the ratio of long side to short side of the area over which the load is distributed;
- a_s is 40 for interior load, 30 for edge load and 20 for corner load;
- b_0 is the perimeter of critical section;
- d is the distance from the extreme compression fiber to centroid of tension reinforcement.

By using a tire contact area as given by AASHTO (2002):

$$\begin{cases} l_{tire} = 254\ mm\ \ (10\ in) \\ w_{tire} = 508\ mm\ \ (20\ in) \\ A_{tire} = l_{tire} w_{tire} = 129032\ mm^2\ \ (200\ in^2) \end{cases} \tag{4.6}$$

the following shear capacity can be found:

$$f_{punch} V_c = f_{punch} \min\left(V_{c,01}, V_{c,02}, V_{c,03}\right) \cong 0.85\left(307\ kN\right) \cong 258\ kN\ \ \left(58.0\ kip\right)$$

which is smaller than the ultimate punching shear capacity given by:

$$g b_L \left(1 + I\right) P_{H15-44} \cong 151.2\ kN\ \ \left(34.0\ kip\right).$$

5. FIELD EVALUATION

5.1. Introduction

Although in-situ bridge load testing is recommended by the AASHTO (2002) Specification as an “effective means of evaluating the structural performance of a bridge”, no guidelines currently exist for bridge load test protocols. In each case, the load test objectives, load configuration, instrumentation type and placement, and analysis techniques are to be determined by the organization conducting the test.

In order to validate the behavior of the bridge prior to and after strengthening, static load tests were performed with H15 and H20 legal trucks, respectively, on bridge No.1330005 (see Figure 5.1): the first test was conducted in December 2003 while the second one was conducted in June 2004, one month after the installation of the strengthening. Figure 5.2 shows the distribution of the load between the axles of each truck and the loading configurations that maximize the stresses and deflections at mid-span of deck panels and girders under a total of five passes, one central and four laterals. For each pass, two and three stops were executed respectively for the load test prior to and after the strengthening. For each stop, the truck rear axle was centered over the marks on the deck. During each stop, the truck was stationary for at least two minutes before proceeding to the next location in order to allow stable readings.

Figure 5.1. Load Tests prior to and after Strengthening on Bridge No.1330005

Displacements in the longitudinal and transverse directions were measured using Linear Variable Differential Transducers (LVDTs). Strains in the strengthening material were monitored by means of strain gages. Figure 5.3 and Figure 5.4 show the details of the instrumentation whose layout was designed to gain the maximum amount of information about the structure. It was assumed that the bridge acted symmetrically, therefore the instrumentation was concentrated on one half of the bridge.

Figure 5.5 compares the results prior to and after strengthening relative to Pass #3 corresponding to the rear axle of the truck at the mid-span (Stop #2 and Stop #3 for the load test prior to and after strengthening, respectively). The experimental results were normalized by dividing displacements to the weight of the truck used for testing. The performance of the structure prior to and after the strengthening was determined by comparing the normalized experimental results prior to and after strengthening. In both cases, the bridge performed well in terms of overall deflection. In fact, the maximum deflection measured during the load test is below the allowable deflection prescribed by AASHTO, 2002 Section 8.9.3 ($d_{\max} \le L/800 = 9.525\ mm\ (0.375\ in)$).

As one can see from Figure 5.5, the strengthening provided a slight increase of the stiffness of the bridge while the slope of the deformation line remains unchanged. For these reasons, the ratio between the stiffness K_p and K_a, prior to and after the strengthening respectively, could be estimated as the ratio between the normalized displacements prior to and after the strengthening: on average, it results $K_a/K_p \cong 1.23$.

Figure 5.6 reports the reading of the strain gages applied to the FRP strengthening, relative to Pass #3 Stop #3. The strain readings (between 120 and 170 me) for the most loaded girders indicate a satisfactory performance of the FRP laminates. The distribution of the strain is not symmetric as one might expect from a symmetric load condition as that one shown in Figure 5.6. The difference between the strain readings in girders G2 and G3 can be attributed to the fact that the laminate on girder G3 was less engaged. This kind of behavior is typical of the non-bond critical strengthening systems where the strengthening needs relatively large deformations of the structure before being completely engaged.

Results for the other load configurations are summarized in Appendices A, B and C together with the theoretical values obtained with the Finite Element Method (FEM) model described in the next section.

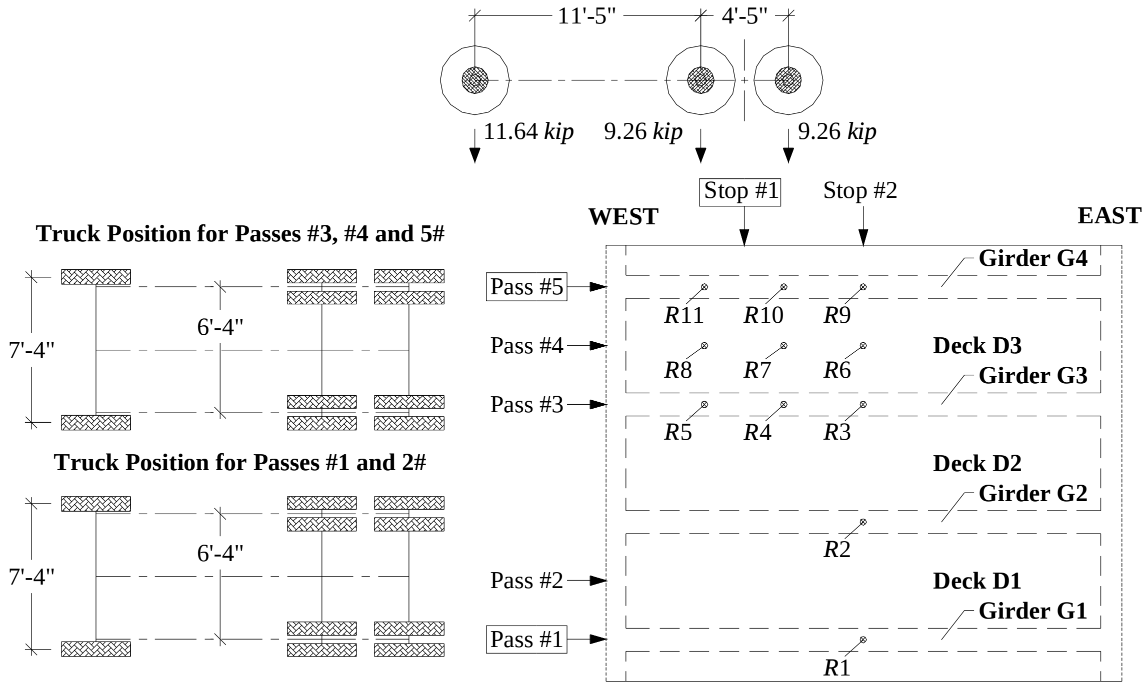

a) H15 Legal Truck Prior to Strengthening

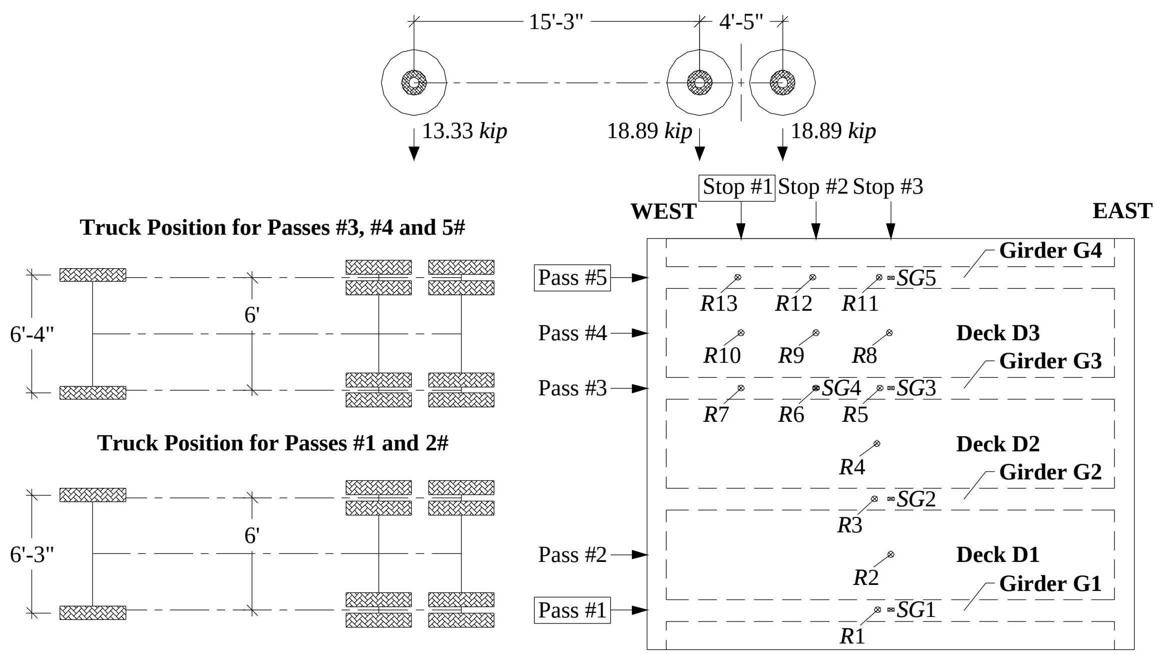

b) H20 Legal Truck after Strengthening

Figure 5.2. Legal Trucks Used in the Load Tests

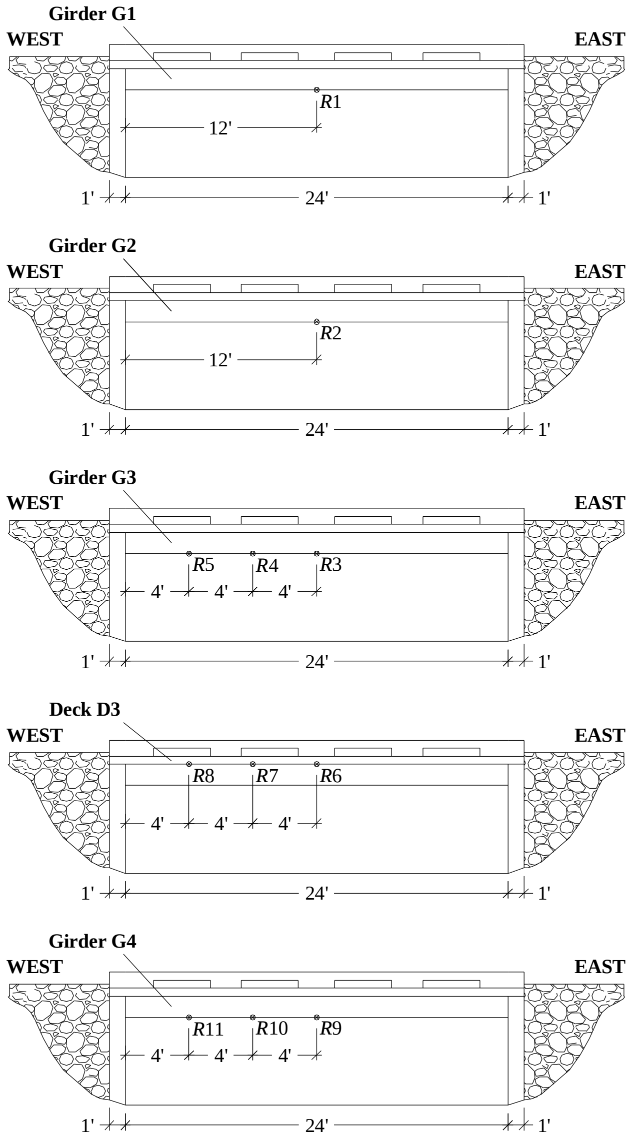

Figure 5.3. LVDT Positions in the Load Test Prior to Strengthening

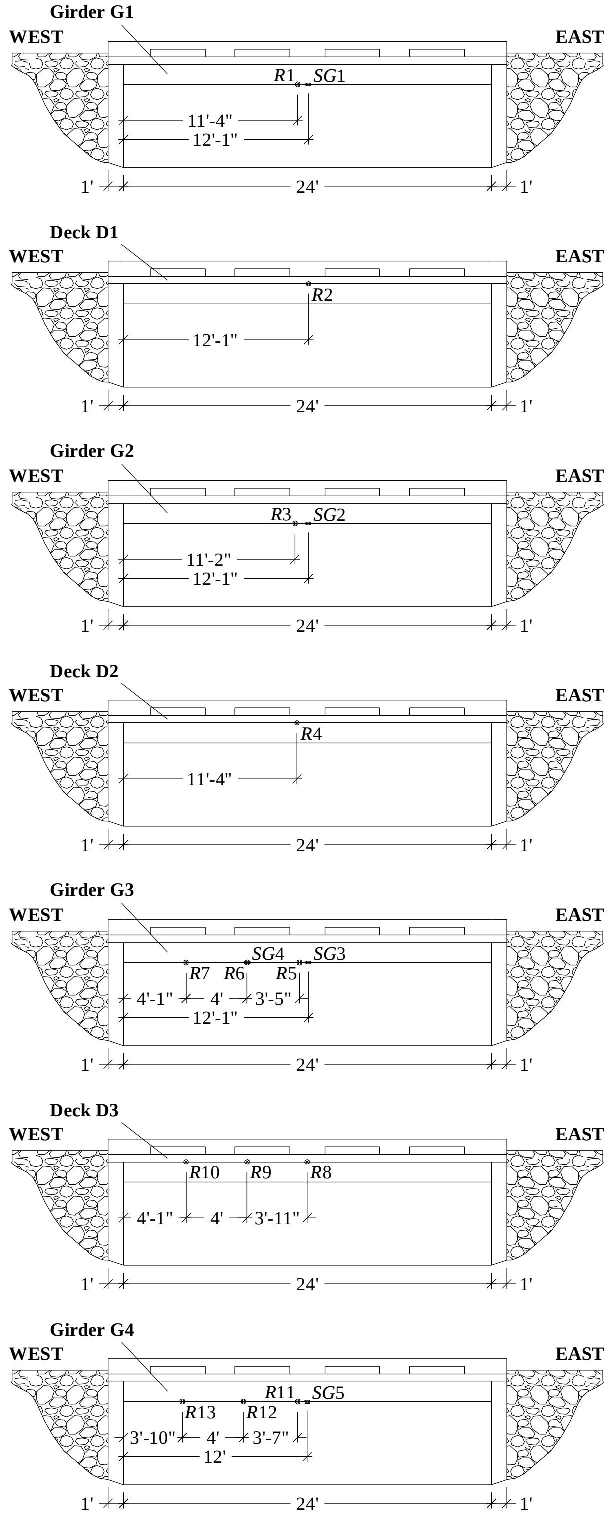

Figure 5.4. LVDT and Strain Gage Positions in the Load Test after Strengthening

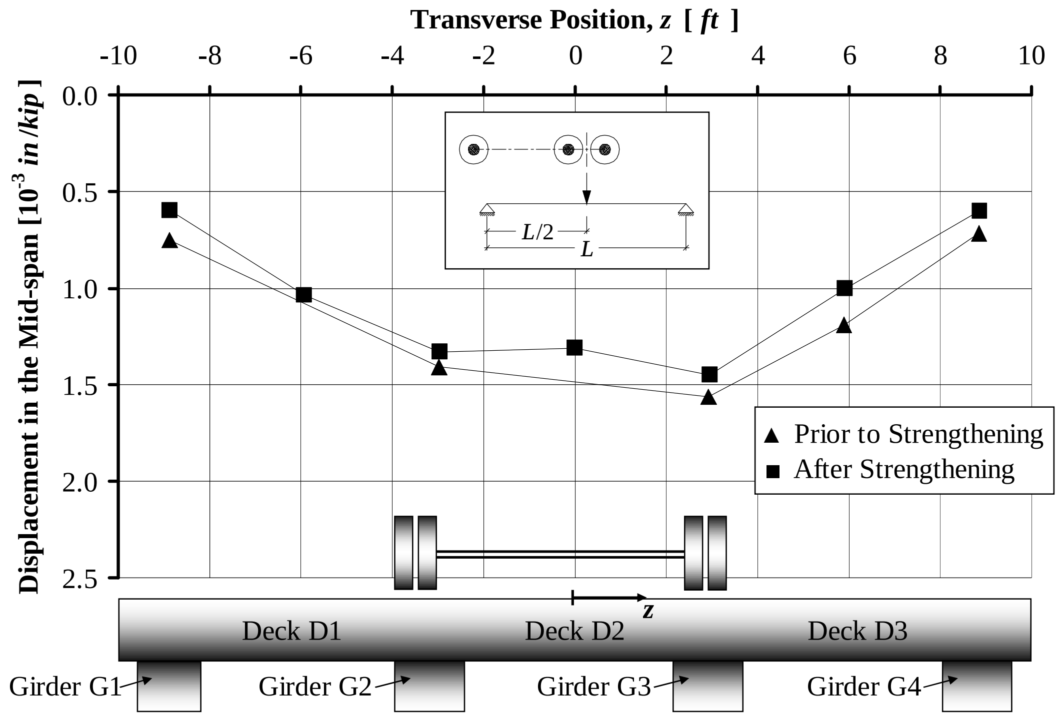

Figure 5.5. Mid-span Displacement, Pass #3 and Rear Axle in the Mid-span

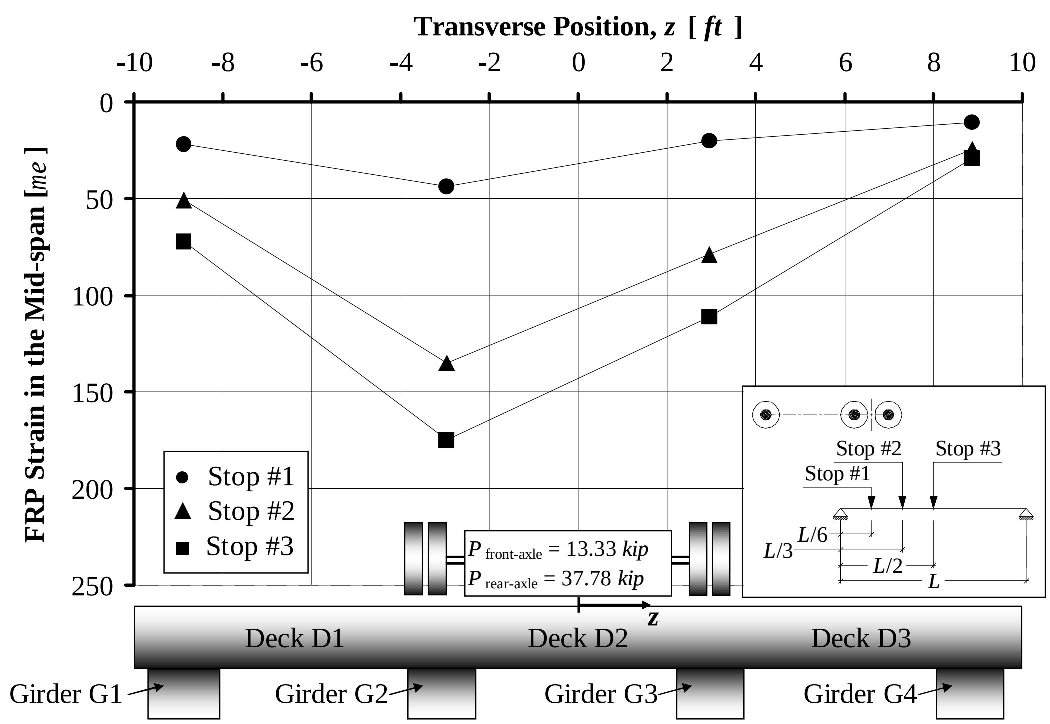

Figure 5.6. Mid-span Strain in the FRP Laminates, Pass #3 Stop #3

5.2. Additional Load Test

A dynamic test was conducted on the strengthened bridge in order to determine the impact factor by moving the truck on Pass #3 at speeds equal to 2.2, 4.5, 8.9 and 13.4 m/s (5, 10, 20 and 30 MPH). The dynamic test was performed acquiring the data at a frequency of $22\ Hz$. The live load impact factor I was computed as the ratio between the difference between the maximum dynamic and static displacements to the maximum static deflection (i.e. Pass #3 Stop #3). As an example, Figure 5.7 shows the dynamic deflections as a function of time at a 13.4 m/s (30 MPH) speed. Figure 5.8 plots the live load impact factor I for displacements and strains for different truck speeds. In most cases, it is possible to determine the truck speed above which the impact factor decreases. This is due to the fact that by increasing the speed, the time of application of the load on the bridge is reduced and, consequently, the corresponding deflection is reduced due to bridge hysteretic behavior. From Figure 5.8., it is possible to state that the maximum impact factor related to this test was $I_{experimental,\ Pass\ \#3} \cong 0.23$ which is smaller than that one used for design according to AASHTO (2002) ($I = 0.30$).

Appendix D reports all the results obtained at different truck speeds.

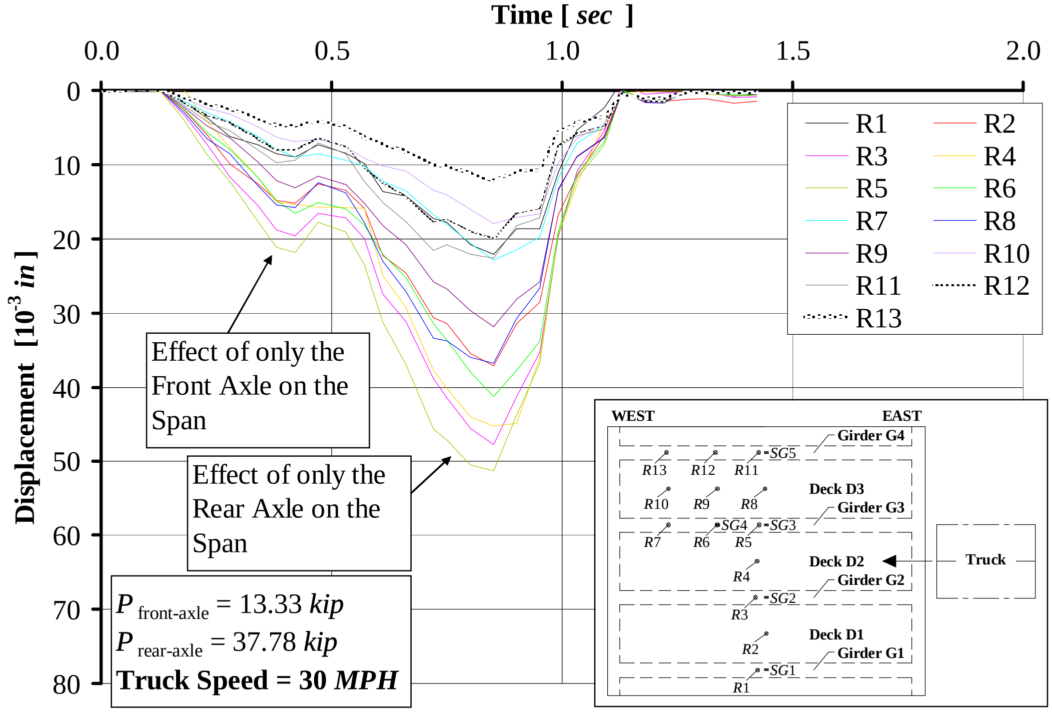

Figure 5.7. After Strengthening Displacements at 13.4 m/s (30 MPH)

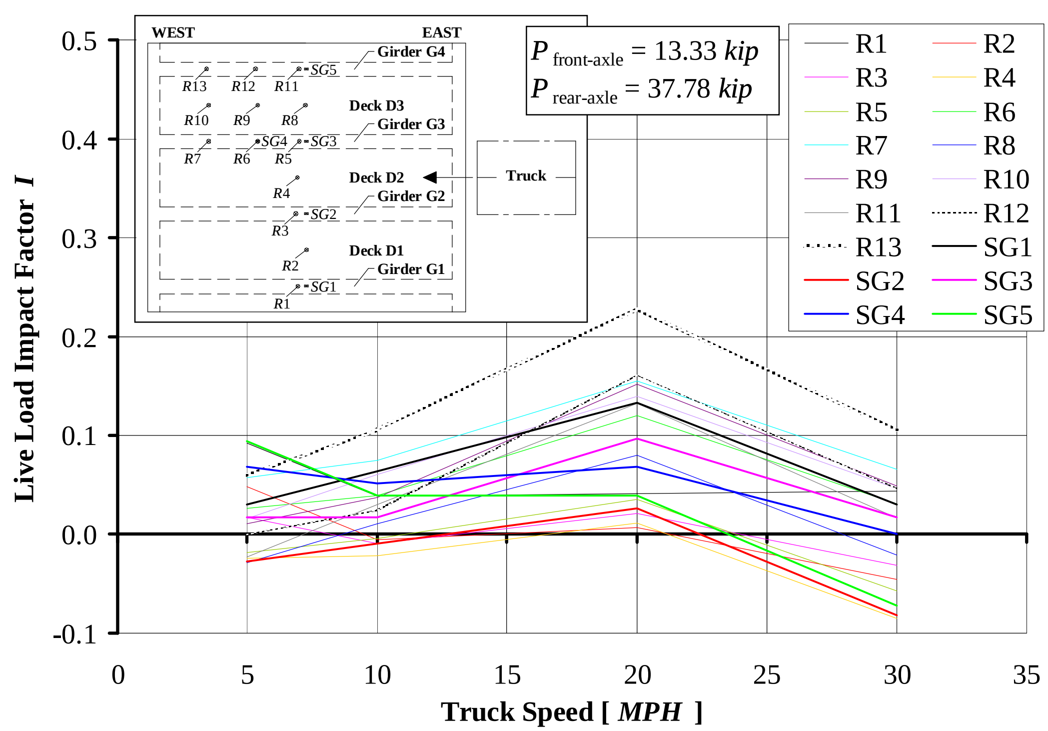

Figure 5.8. Live Load Impact Factor I versus Truck Speed

5.3. FEM Analysis

In this section, a FEM analysis model is described. This model was developed in order to interpret the experimental data prior to and after the strengthening. For this purpose, a commercially available finite element program ANSYS 7.1 was used. Details of the geometry can be found in Figure 5.9 and Figure 5.10.

The element SOLID65 was chosen to model the concrete and the FRP laminates. SOLID65 is used for the three-dimensional modeling of solids with or without reinforcing bars. The solid is capable of cracking in tension and crushing in compression. In addition, up to three different rebar specifications may be defined. The element is defined by eight nodes having three degrees of freedom at each node: translations in the nodal x, y and z directions. SOLID65 is subject to the following assumption and restrictions:

- cracking is permitted in three orthogonal directions at each integration point;
- if cracking occurs at an integration point, the cracking is modeled through an adjustment of material properties which effectively treats the cracking as a "smeared band" of cracks, rather than discrete cracks;
- the concrete material is assumed to be initially isotropic;
- whenever the reinforcement capability of the element is used, the reinforcement is assumed to be "smeared" throughout the element;
- in addition to cracking and crushing, the concrete may also undergo plasticity, with the Drucker-Prager failure surface being most commonly used. In this case, the plasticity is done before the cracking and crushing checks.

For this project, the material properties of concrete were assumed to be isotropic and linear elastic, since the applied load was relatively low with respect to the ultimate load condition. The modulus of elasticity of the concrete was based on the measured compressive strength of the cores obtained from the slab according to the standard equation ACI 318-02 Section 8.5.1: $E_c = 57000\sqrt{f_c^{'}}\ psi \approx$ 32.6 GPa $\left(4738\ ksi\right)$ with $\left[f_c^{'}\right] = \left[psi\right]$.

In order to take into account the presence of the cracks in the girders and in the deck, as a result of a parametric analysis, the modulus of elasticity was reduced to $16.3\ \mathit{GPa}\ (2369\ \mathit{ksi})$ in the elements corresponding to the cracks as shown in Figure 5.9b. The depth of the cracks was chosen according to the data collected during the in-situ inspection while the width was assumed to be equal to the elements dimensions. The concrete Poisson's ratio was set to 0.19. Different elements were used to optimize the model and decrease the computation time. The chosen shape and size in the longitudinal and transverse cross sections allowed to locate more accurately the steel rebars (see Figure 5.10a), to properly connect the FRP laminates to the surface of the concrete (see Figure 5.10b) and to reduce the number of the elements in the "secondary" parts of the model, such as the curbs (see Figure 5.10a). The modulus of the elasticity and the Poisson's ratio for the steel reinforcement were assumed as $200.0\ \mathit{GPa}\ (29000\ \mathit{ksi})$ and 0.3, respectively.

The connections between the FRP laminates and the concrete surface were modeled as rigid, neglecting any form of non-linearity due to a potential initial non-perfect engagement of the strengthening. Modulus of the elasticity and the Poisson's ratio for the FRP laminates were assumed to be $60.6\ \mathit{GPa}\ (8800\ \mathit{ksi})$ and 0.3, respectively.

The bridge was vertically restrained at both ends while the longitudinal displacement was fixed to zero at one end only (see Figure 5.10a). The loads were assumed as uniformly distributed over $508\times254\ \mathit{mm}\ (20\times10\ \mathit{in})$ areas as specified in AASHTO (2002) Section 4.3.30. Such loads were applied at the top of the deck simulating, in such way, the truck wheel prints (see Figure 5.9a). The uniform load was concentrated at the nodes corresponding to the truck wheel print and each force was determined by dividing the total load for the number of nodes.

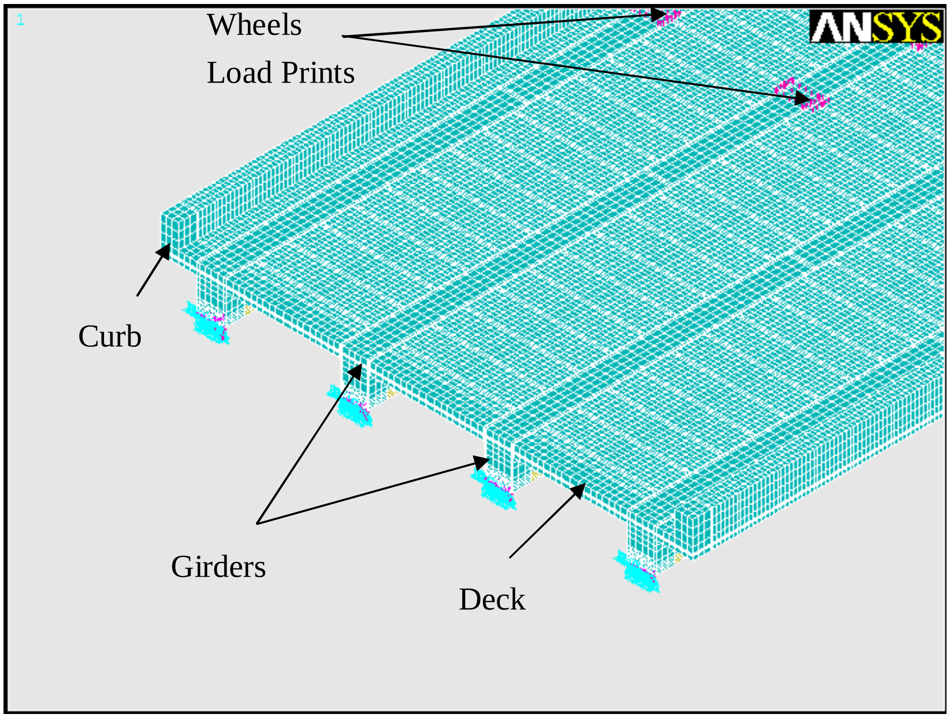

a) Global View of the Model

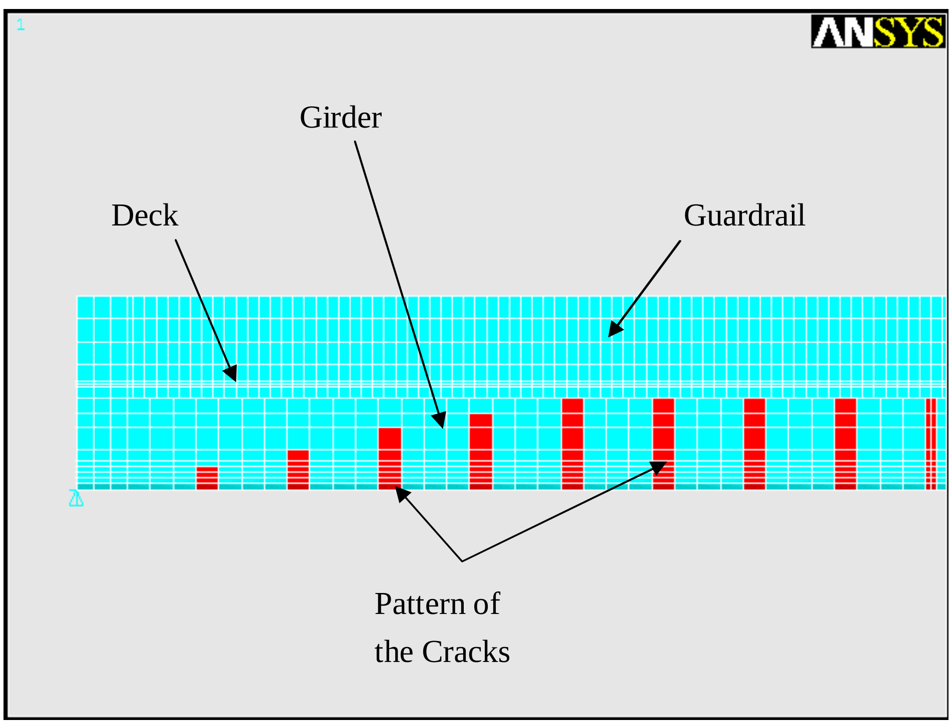

b) Details of the Cracks Modeling

Figure 5.9. FEM Model Geometry (I)

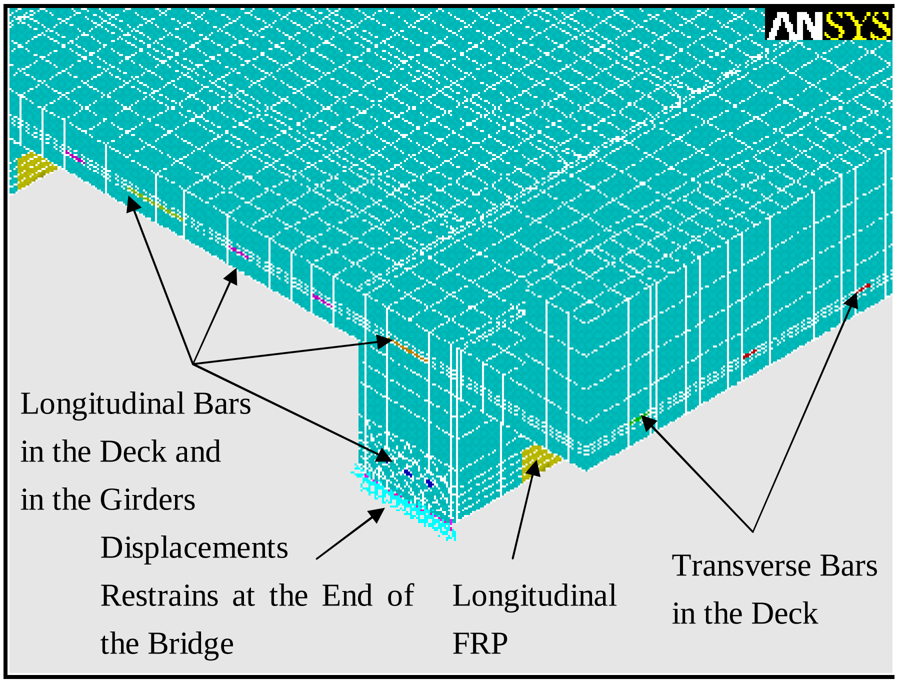

a) Details of the Steel Reinforcement and Boundary Conditions

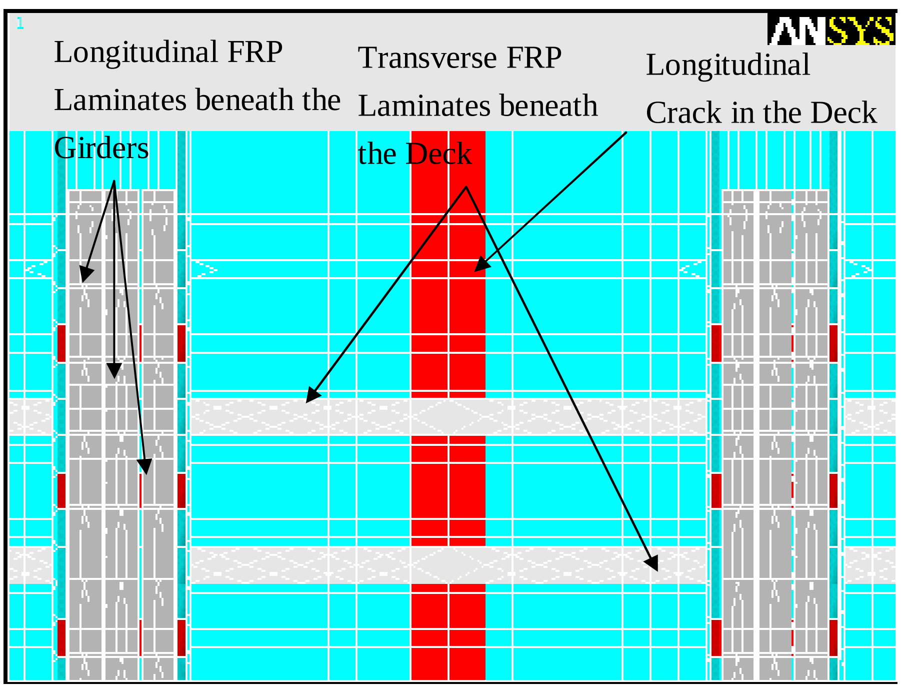

b) Details of the FRP Strenghtening (Bottom View)

Figure 5.10. FEM Model Geometry (II)

Figure 5.11 reports the experimental and analytical mid-span displacements, relative to Pass #3 when the rear axle of the truck is in the mid-span (Stop #2 and Stop #3 for the load test prior to and after strengthening, respectively). The graph shows a good match in deflections between experimental and analytical results.

Figure 5.12 compares experimental and analytical strains on the FRP, relative to the Pass #3 and Stops #1, #2 and #3. The graph shows a good match in strains between experimental and analytical results for girders G1 and G2. The mismatch for girders G3 and G4 can be explained with the incomplete engagement of the FRP laminates to the concrete.

Figure 5.13 plots the longitudinal distribution of the strain in the middle of the central laminates present in each girder. It is important to note that there is stress concentration in a small area of the laminates around each fastener. The peak in the mid-span is emphasized by the presence of the crack in the concrete.

Appendices A, B and C report all the analysis developed for the bridge prior to and after the strengthening.

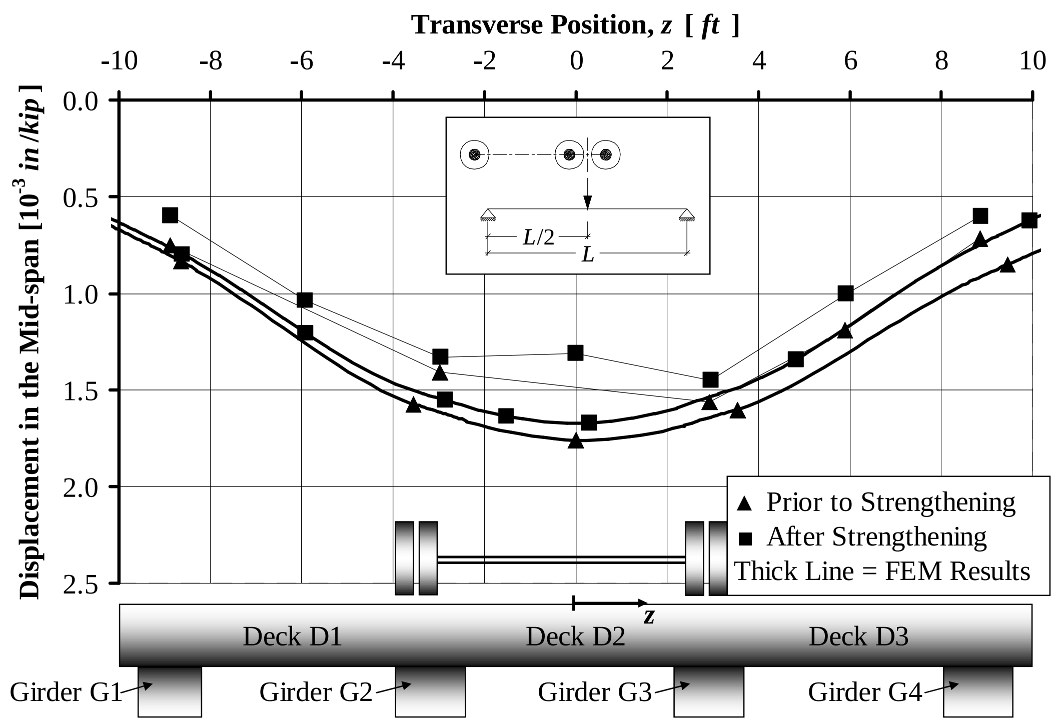

Figure 5.11. Comparison of Experimental and Analytical Results for Mid-span Displacement, Pass #3 and Rear Axle in the Mid-span

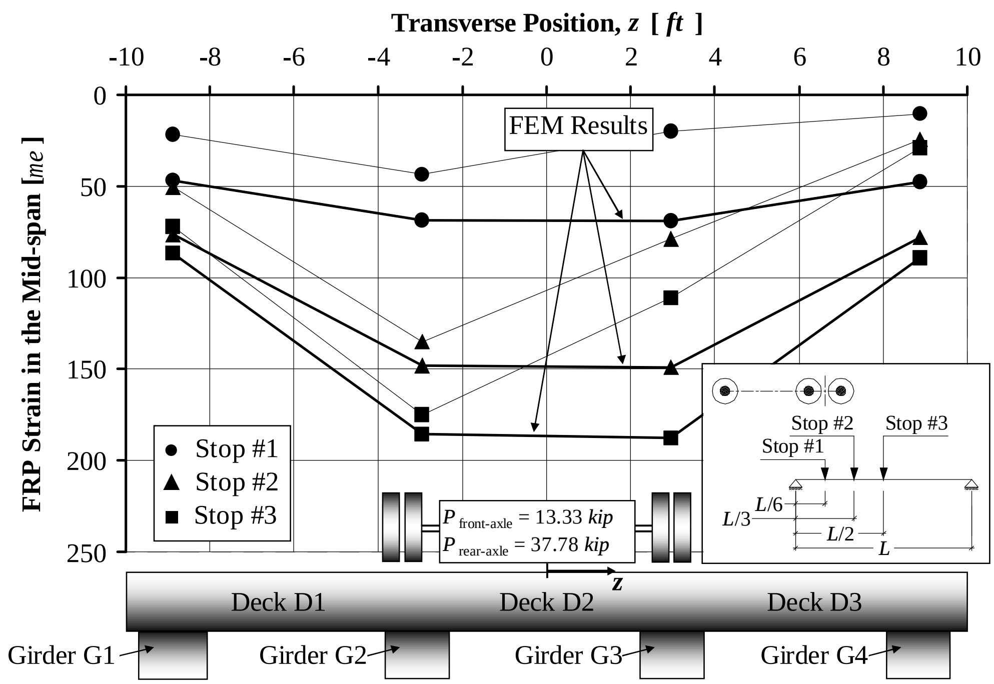

Figure 5.12. Comparison of Experimental and Analytical Results for Strain in the FRP Fastened on the Girders at Mid-span, Pass #3 and Stops #1, #2 and #3

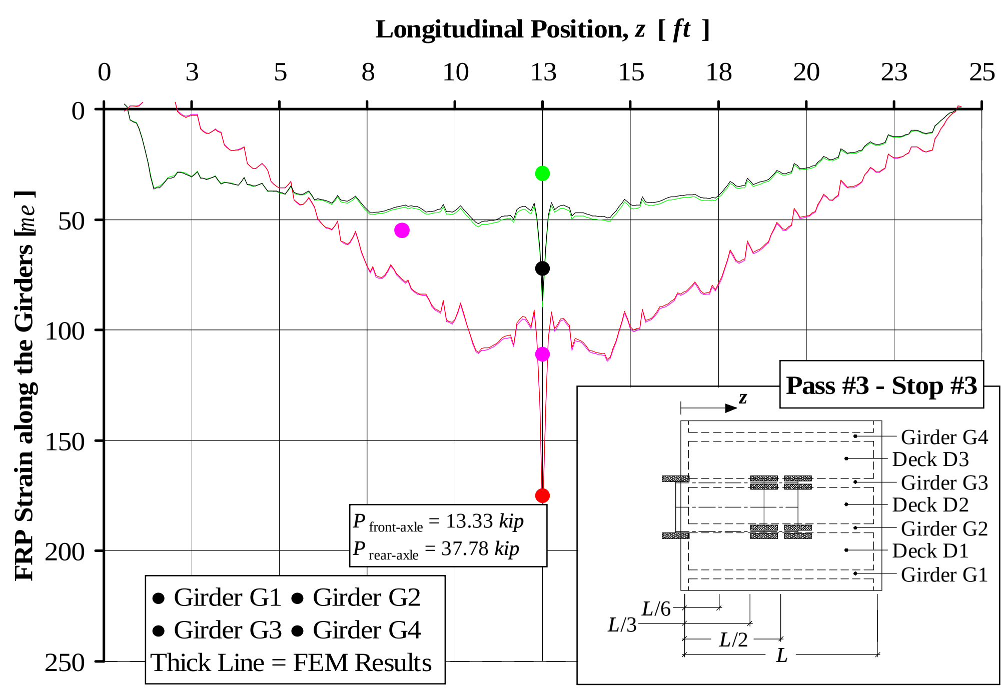

Figure 5.13. Comparison of Experimental and Analytical Results for Strain in the Longitudinal Direction in the FRP Fastened on the Girders, Pass #3 Stop #3

6. LOAD RATING

Bridge load rating calculations provide a basis for determining the safe load capacity of a bridge. According to the Missouri Department of Transportation (MoDOT), anytime a bridge is built, rehabilitated, or reevaluated for any reason, inventory and operating ratings are required using the Load Factor rating. All bridges should be rated at two load levels, the maximum load level called the Operating Rating and a lower load level called the Inventory Rating. The Operating Rating is the maximum permissible load that should be allowed on the bridge. Exceeding this level could damage the bridge. The Inventory Rating is the load level the bridge can carry on a daily basis without damaging the bridge.

In Missouri, for the Load Factor Method the Operating Rating is based on the appropriate ultimate capacity using current AASHTO specifications (AASHTO, 1996). The vehicle used for the live load calculations in the Load Factor Method is the HS20 truck. If the stress levels produced by this vehicle configuration are exceeded, load posting may be required.

The method for determining the rating factor is that outlined by AASHTO in the Manual for Condition Evaluation of Bridges (AASHTO, 2002). Equation (6.1) was used:

$$RF = \frac{C - A_1 D}{A_2 L (1 + I)} \tag{6.1}$$

where:

RF is the Rating Factor;

C is the capacity of the member;

D is the dead load effect on the member;

L is the live load effect on the member;

I is the impact factor to be used with the live load effect;

A_1 is the factor for dead loads;

A_2 is the factor for live loads.

Since the load factor method is being used, A_1 is taken as 1.3 and A_2 varies depending on the desired rating level. For Inventory Rating, $A_2 = 2.17$, and for Operating Rating, $A_2 = 1.3$.

To determine the rating RT of the bridge, equation (6.2) was used:

$$RT = RF \cdot W \tag{6.2}$$

where W is the weight of the nominal truck used to determine the live load effect.

For the bridge No. 1330005, the Load Rating was calculated for a number of different trucks, HS20, H20, 3S2 and MO5. Ratings are required at the inventory and operating levels by the load factor method on each bridge for the HS20 truck. The H20 legal vehicle is used to model the load for single unit vehicles. The 3S2 vehicle is used as a model for all other vehicles. The MO5 is used to model the commercial zone loadings.

For each of the different loading conditions, the maximum shear and maximum moment were calculated. Impact factors are also taken into account for Load Ratings. This value is 30% for the bridge No. 1330005. The shear and moment values for the deck and the girders are shown in Table 6.1 and Table 6.2.

Table 6.1. Maximum Shear and Moment due to Live Load for the Deck

Truck	Maximum Shear $[kN]$ $([kip])$	Maximum Moment $[kN \cdot m]$ $([kip \cdot ft])$	Maximum Shear with Impact $[kN]$ $([kip])$	Maximum Moment with Impact $[kN \cdot m]$ $([kip \cdot ft])$
HS20	5.83 (1.31)	4.38 (3.23)	7.56 (1.70)	5.69 (4.20)
MO5	3.07 (0.69)	2.39 (1.76)	4.00 (0.90)	3.10 (2.29)
H20	3.07 (0.69)	2.39 (1.76)	4.00 (0.90)	3.10 (2.29)
3S2	4.36 (0.98)	3.23 (2.38)	5.65 (1.27)	4.19 (3.09)

Table 6.2. Maximum Shear and Moment due to Live Load for the Girders

Truck	Maximum Shear $[kN]$ $([kip])$	Maximum Moment $[kN \cdot m]$ $([kip \cdot ft])$	Maximum Shear with Impact $[kN]$ $([kip])$	Maximum Moment with Impact $[kN \cdot m]$ $([kip \cdot ft])$
HS20	102.18 (22.97)	140.14 (103.36)	132.82 (29.86)	182.18 (134.37)
MO5	90.30 (20.30)	161.45 (119.08)	117.39 (26.39)	209.88 (154.80)
H20	72.02 (16.19)	115.82 (85.42)	93.63 (21.05)	150.55 (111.04)
3S2	72.37 (16.27)	116.64 (86.03)	94.12 (21.16)	151.62 (111.83)

Table 6.3 and Table 6.4 give the results of the Load Rating pertaining to moment and shear respectively for the deck.

Table 6.3. Rating Factor for the Deck (Bending Moment)

Truck	Rating Factor *RF*	Rating *RT* $[ton]$	Rating Type
HS20	2.140	69.9 (77.0)	Operating
HS20	1.282	41.9 (46.2)	Inventory
MO5	3.924	130.4 (143.8)	Operating
H20	3.375	61.2 (67.5)	Posting
3S2	2.500	83.1 (91.6)	Posting

Table 6.4. Rating Factor for the Deck (Shear)

Truck	Rating Factor *RF*	Rating *RT* $[ton]$	Rating Type
HS20	2.498	81.6 (89.9)	Operating
HS20	1.496	48.9 (53.9)	Inventory
MO5	4.725	157.1 (173.1)	Operating
H20	4.064	73.7 (81.3)	Posting
3S2	2.872	95.5 (105.2)	Posting

Table 6.5 and Table 6.6 give the results of the Load Rating pertaining to moment and shear respectively for the girders.

Table 6.5. Rating Factor for the Girders (Bending Moment)

Truck	Rating Factor RF	Rating RT $[ton]$	Rating Type
HS20	1.157	37.8 (41.7)	Operating
HS20	0.693	22.6 (25.0)	Inventory
MO5	1.004	33.4 (36.8)	Operating
H20	1.204	21.8 (24.1)	Posting
3S2	1.195	39.7 (43.8)	Posting
HS20	1.157	37.8 (41.7)	Operating

Table 6.6. Rating Factor for the Girders (Shear)

Truck	Rating Factor RF	Rating RT $[ton]$	Rating Type
HS20	1.803	58.9 (64.9)	Operating
HS20	1.080	35.3 (38.9)	Inventory
MO5	2.041	67.8 (74.8)	Operating
H20	2.200	39.9 (44.0)	Posting
3S2	2.189	72.8 (80.2)	Posting

In Missouri, load posting is established using the H20 and 3S2 vehicles. Therefore, according to Table 6.5, the bridge should be posted at $21.8\ ton_{SI}\ \ (24.1\ ton)$. But, since the legal loads established for Missouri are defined as $20.9\ ton_{SI}\ \ 23.0\ ton$ for single unit vehicles and $36.3\ ton_{SI}\ \ (40.0\ ton)$ for all others, the existing load posting can be removed.

7. Conclusions

Conclusions based on the retrofitting of the bridge utilizing FRP materials can be summarized as follows:

- The mechanically fastened (MF) FRP system showed to be a feasible solution for the strengthening of the bridge;
- In-situ load testing has proven to be useful and convincing;
- The FEM analysis has shown good match with experimental results demonstrating the effectiveness of the strengthening technique;
- As a result of FRP strengthening, the load posting of the bridge can be removed.

8. REFERENCES

AASHTO (1996). "LRFD bridge design specifications." Second Edition, Published by the American Association of State Highway and Transportation Officials, Washington D.C.

AASHTO (2002). "Standard specifications for highway bridges." 17th Edition, Published by the American Association of State Highway and Transportation Officials, Washington D.C.

ACI Committee 318 (1999). "Building code requirements for structural concrete and commentary." ACI 318R-99, Published by the American Concrete Institute, Farmington Hills, MI.

ACI Committee 318 (2002). "Building code requirements for structural concrete and commentary." ACI 318R-02, Published by the American Concrete Institute, Farmington Hills, MI.

ACI Committee 440 (1996). "State-of-the-art report on FRP for concrete structures." ACI 440R-96, Manual of Concrete Practice, ACI, Farmington Hills, MI, 68 pp.

ACI Committee 440 (2002). "Guide for the design and construction of externally bonded FRP systems for strengthening concrete structures." ACI 440.2R-02, Published by the American Concrete Institute, Farmington Hills, MI.

Alkhrdaji, T., Nanni, A., Chen, G., and Barker, M. (1999). "Upgrading the transportation infrastructure: solid RC decks strengthened with FRP." Concrete International, American Concrete Institute, Vol. 21, No. 10, October, pp. 37-41.

ANSYS User's Manual for Revision 6.1 (2000). Volume I Procedure and Volume III Elements, Swanson Analysis Systems, Inc.

Arora, D. (2003). "Rapid strengthening of reinforced concrete bridge with mechanically fastened fiber-reinforced polymer strips." M.Sc. Thesis, University of Wisconsin – Madison.

Bank, L. C., Lamanna A. J., Ray, J. C., and Velásquez G. I. (2002). "Rapid strengthening of reinforced concrete beams with mechanically fastened, fiber-reinforced polymeric composite materials.” US Army Corps of Engineers, Washington D.C.

Bank, L. C., Borowicz D. T., Lamanna A. J., Ray J. C., and Velásquez G. I. (2002). “Rapid strengthening of full-sized concrete beams with powder-actuated fastening systems and Fiber-Reinforced Polymer (FRP) composite materials.” US Army Corps of Engineers, Washington D.C.

Borowicz, D. T. (2002). “Rapid strengthening of concrete beams with powder-actuated fastening systems and Fiber-Reinforced Polymer (FRP) composite materials.” M.Sc. Thesis, University of Wisconsin – Madison.

Lamanna, A.J. (2002). “Flexural strengthening of reinforced concrete beams with mechanically fastened fiber reinforced polymer strips.” PhD Thesis, University of Wisconsin – Madison.

APPENDICES

APPENDIX

A. Prior to Strengthening Test Results

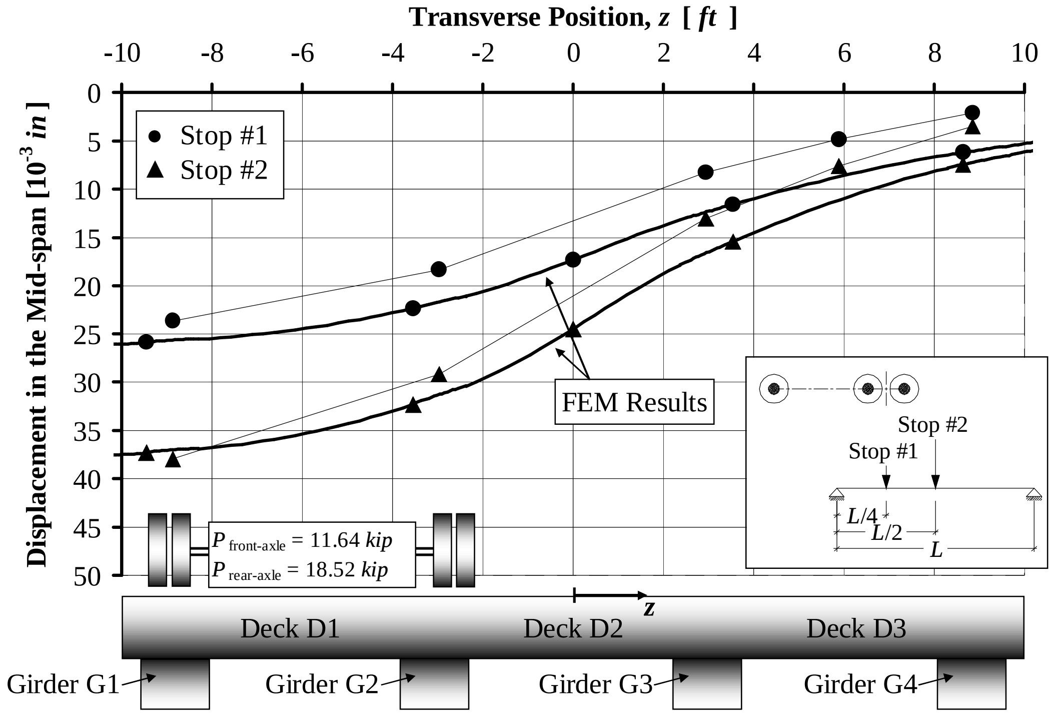

Figure A. 1. Prior to Strengthening Mid-span Displacement, Pass #1

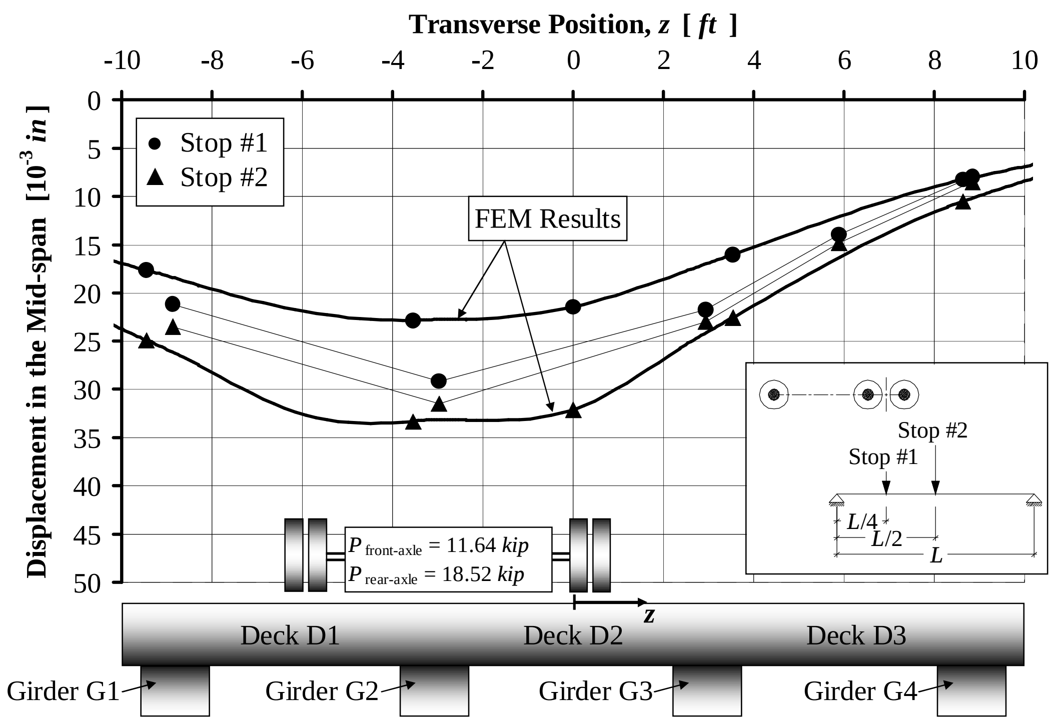

Figure A. 2. Prior to Strengthening Mid-span Displacement, Pass #2

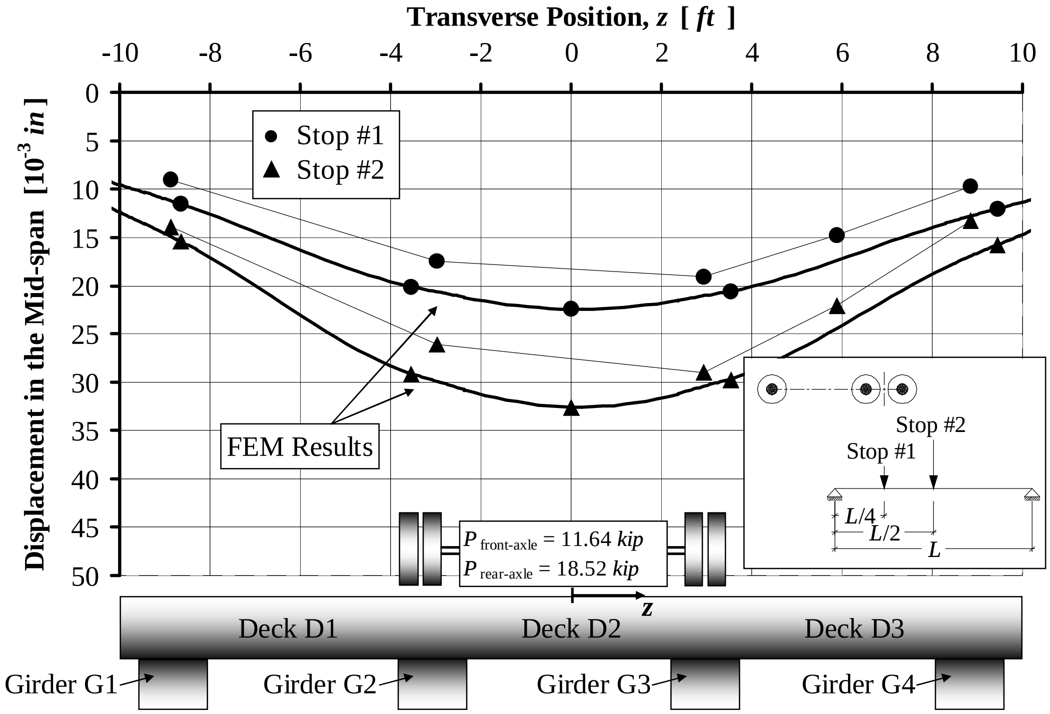

Figure A. 3. Prior to Strengthening Mid-span Displacement, Pass #3

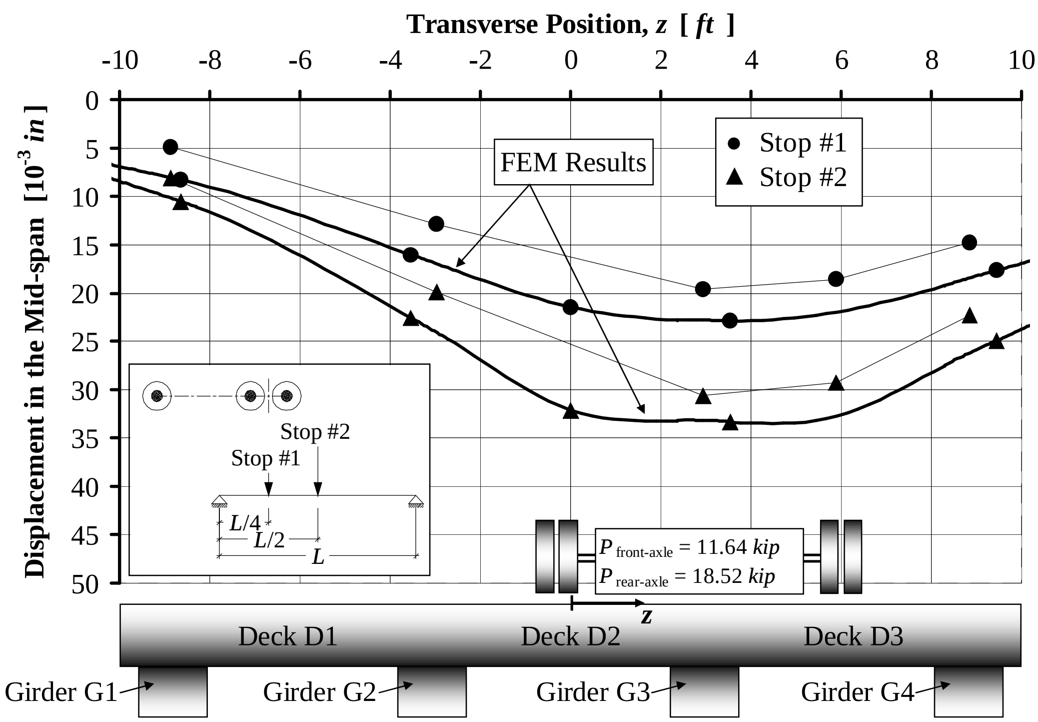

Figure A. 4. Prior to Strengthening Mid-span Displacement, Pass #4

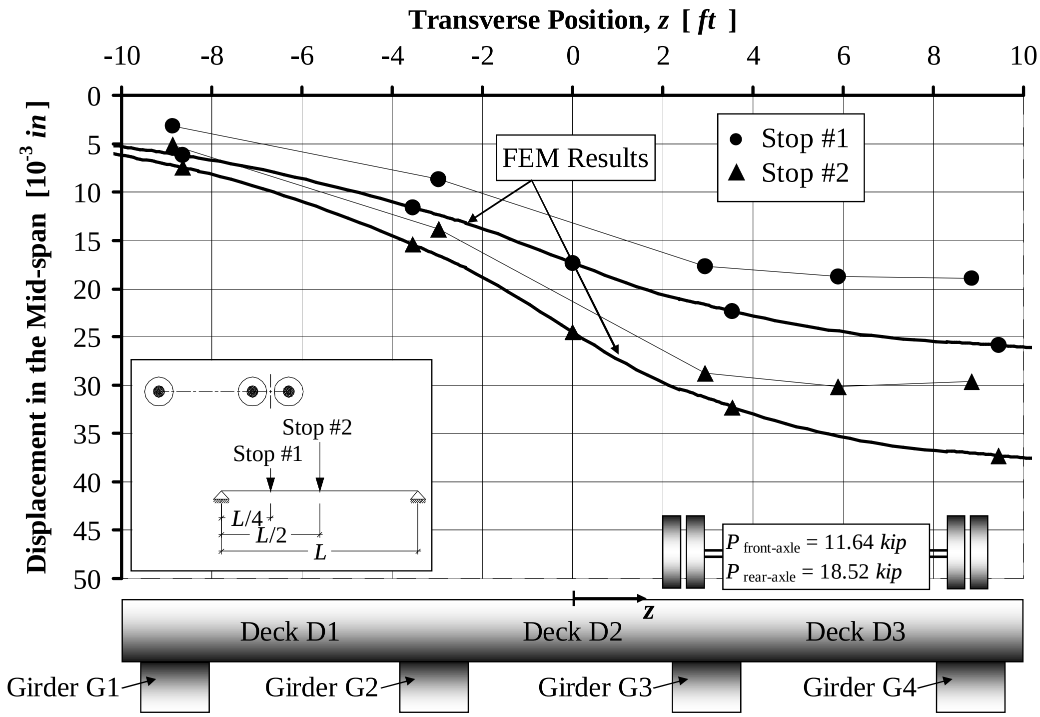

Figure A. 5. Prior to Strengthening Mid-span Displacement, Pass #5

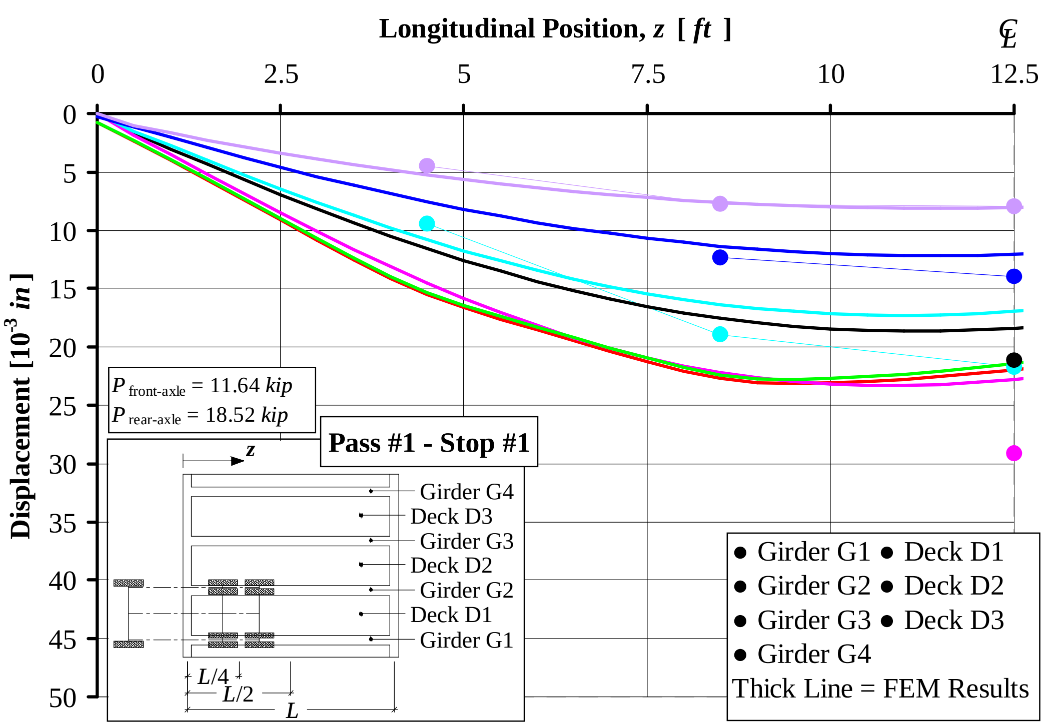

Figure A. 6. Prior to Strengthening Displacement Distribution, Pass #1 Stop #1

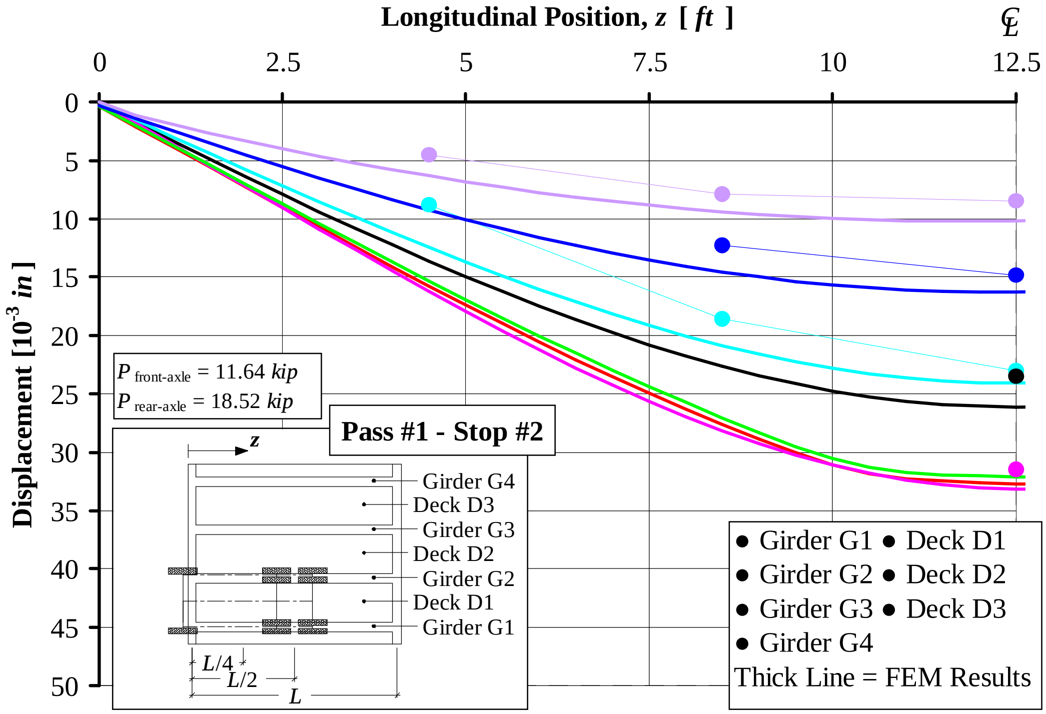

Figure A. 7. Prior to Strengthening Displacement Distribution, Pass #1 Stop #2

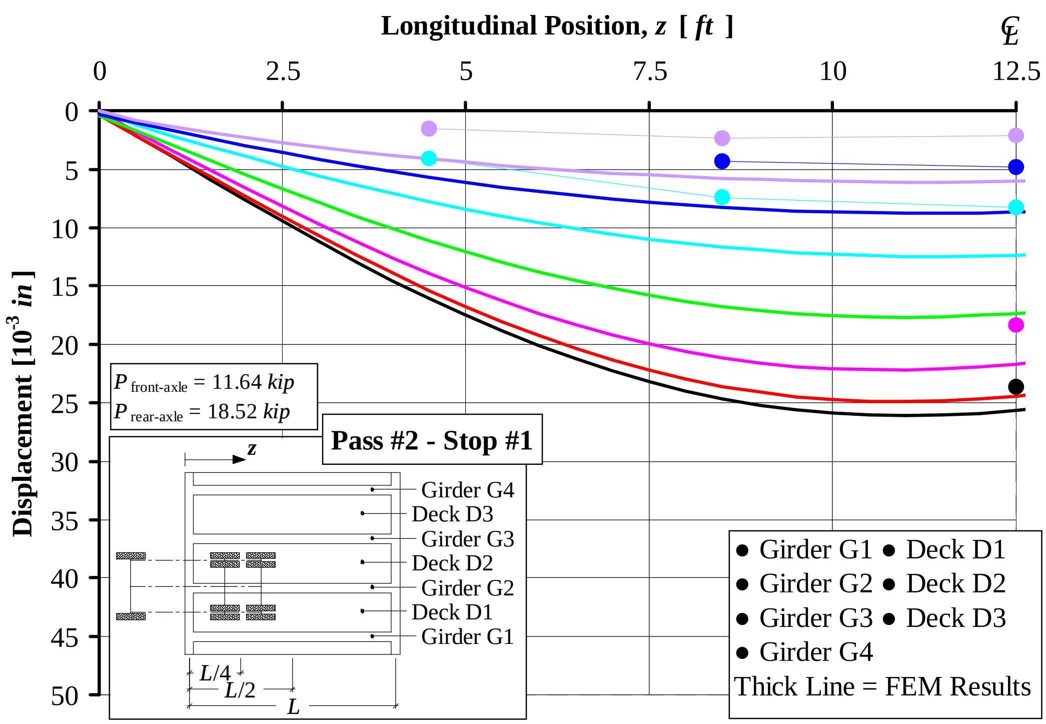

Figure A. 8. Prior to Strengthening Displacement Distribution, Pass #2 Stop #1

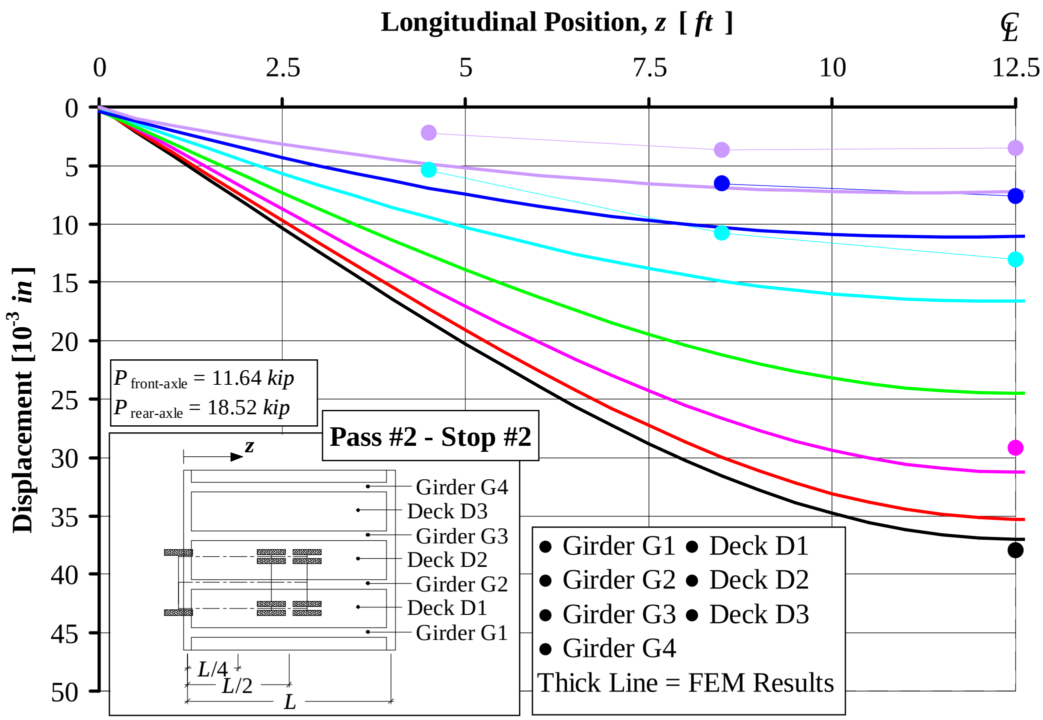

Figure A. 9. Prior to Strengthening Displacement Distribution, Pass #2 Stop #2

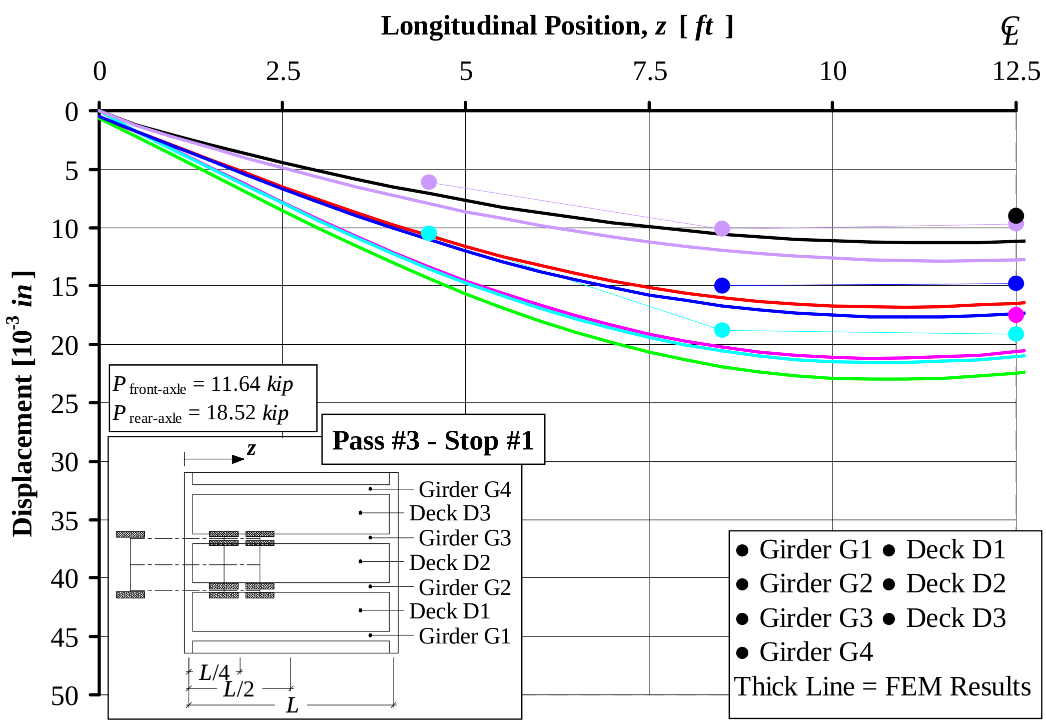

Figure A. 10. Prior to Strengthening Displacement Distribution, Pass #3 Stop #1

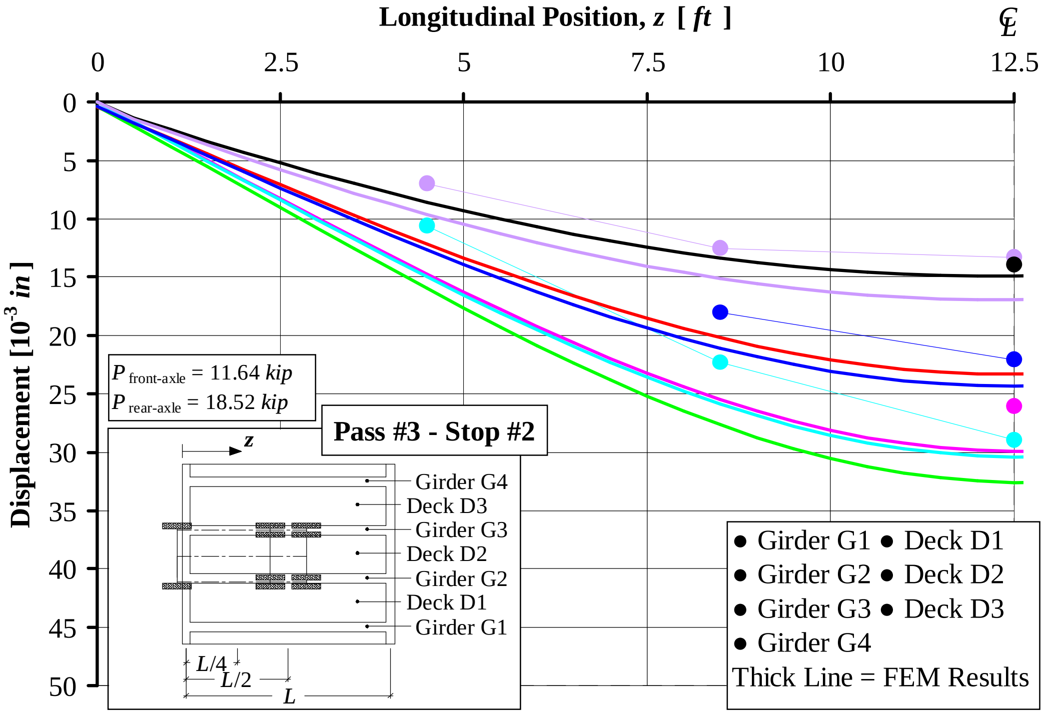

Figure A.11. Prior to Strengthening Displacement Distribution, Pass #3 Stop #2

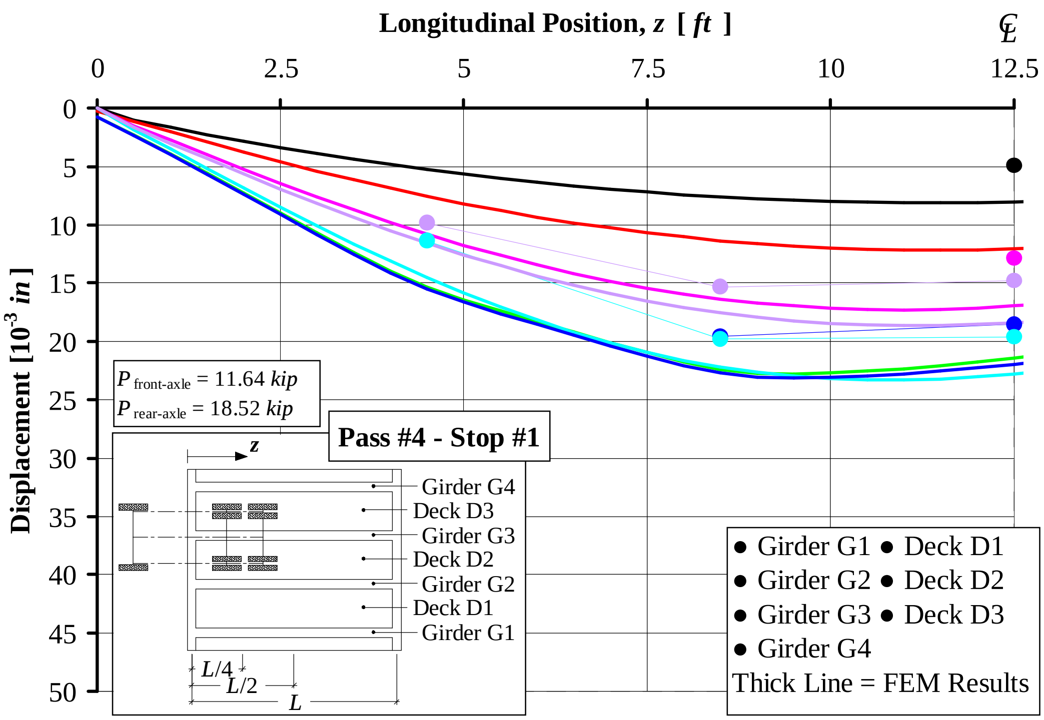

Figure A. 12. Prior to Strengthening Displacement Distribution, Pass #4 Stop #1

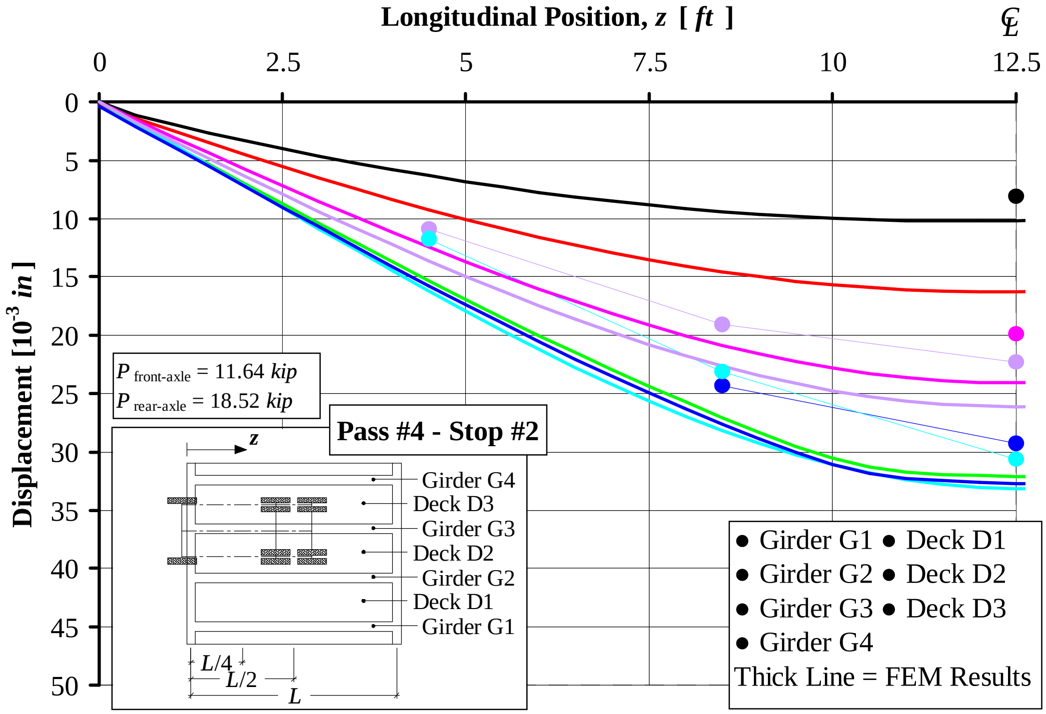

Figure A. 13. Prior to Strengthening Displacement Distribution, Pass #4 Stop #2

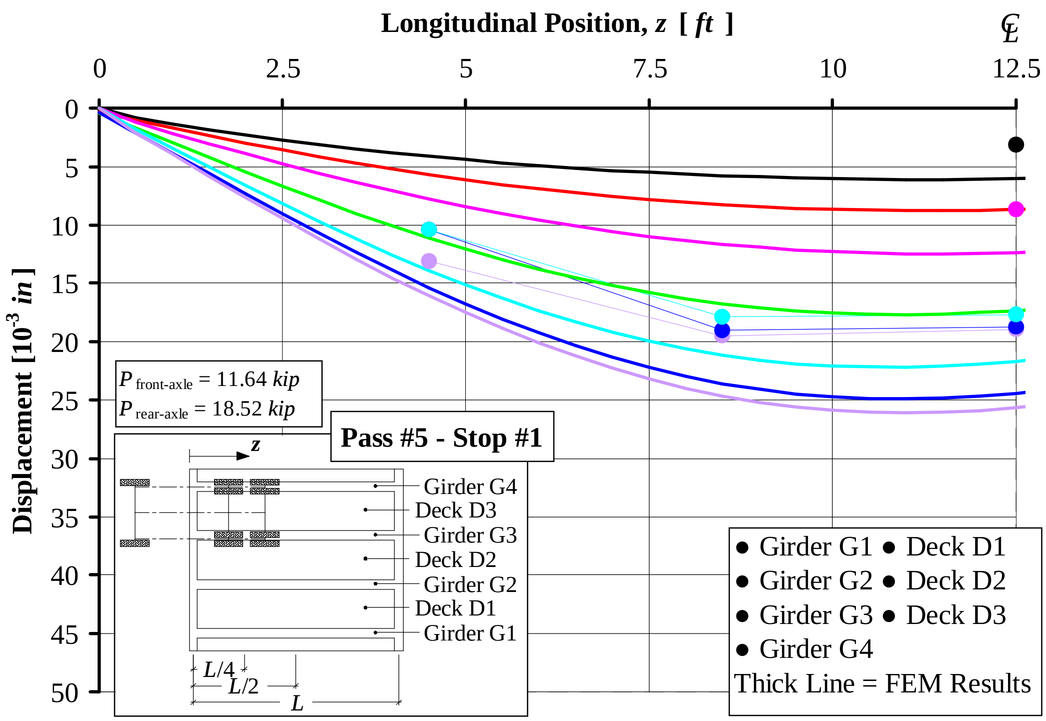

Figure A. 14. Prior to Strengthening Displacement Distribution, Pass #5 Stop #1

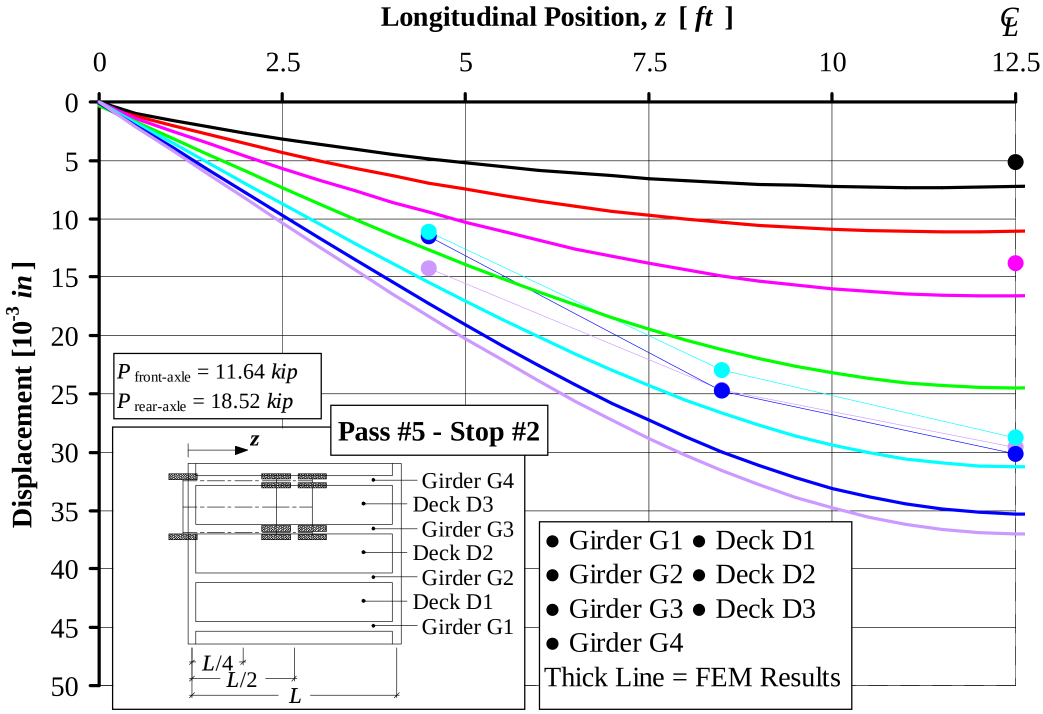

Figure A. 15. Prior to Strengthening Displacement Distribution, Pass #5 Stop #2

APPENDIX

B. After Strengthening Test Results

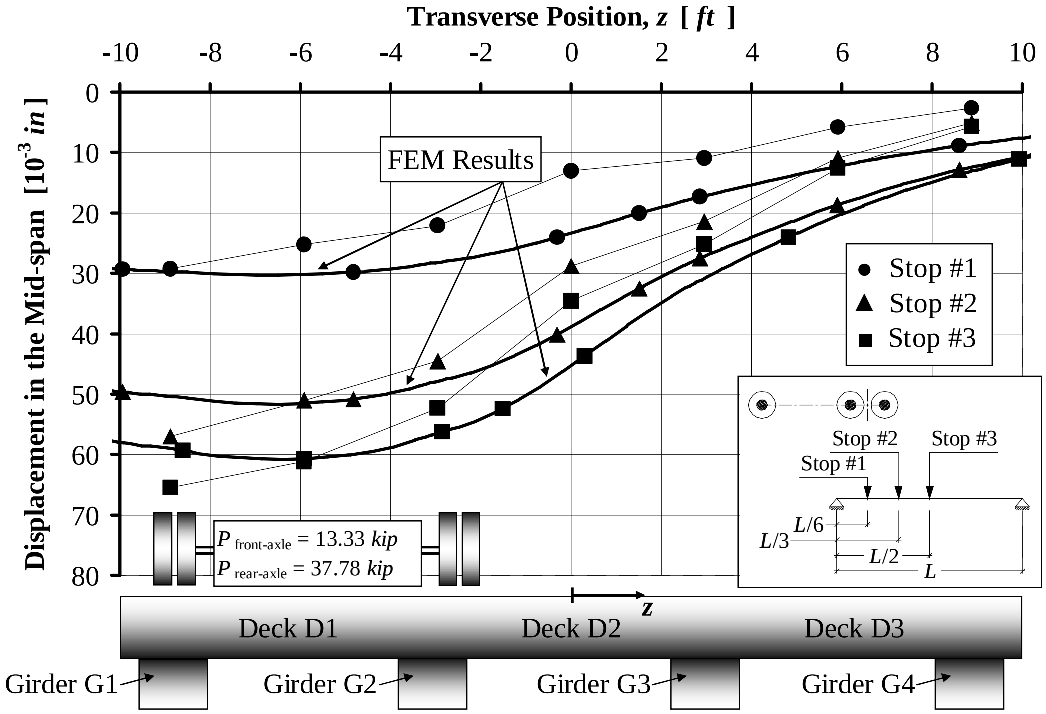

Figure B. 1. After Strengthening Mid-span Displacement, Pass #1

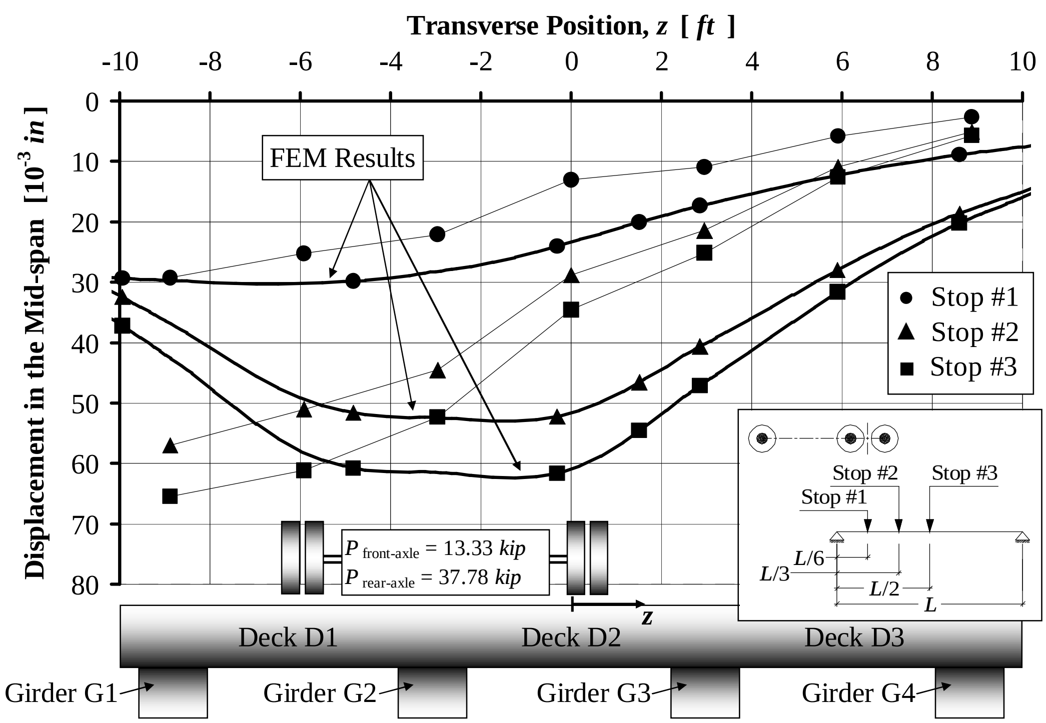

Figure B. 2. After Strengthening Mid-span Displacement, Pass #2

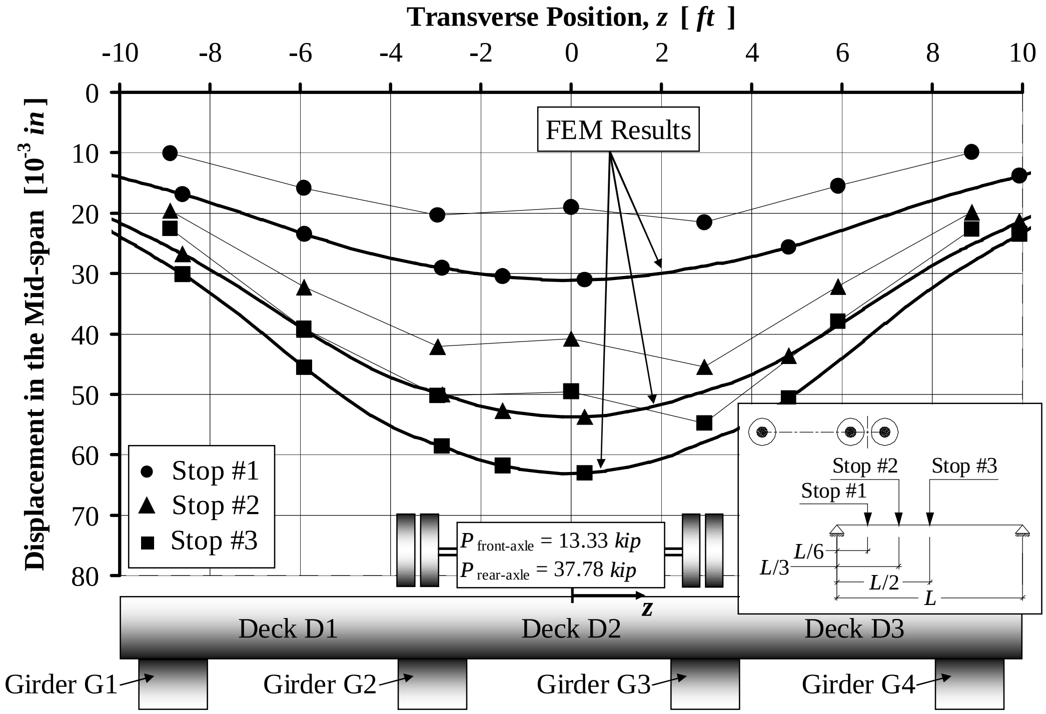

Figure B. 3. After Strengthening Mid-span Displacement, Pass #3

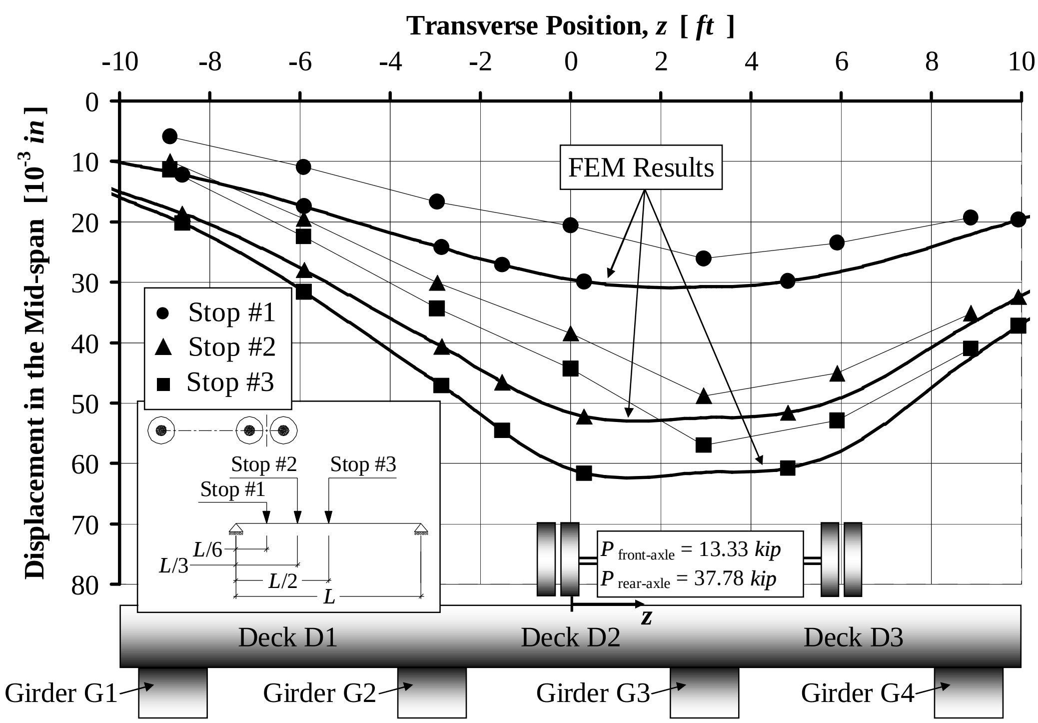

Figure B. 4. After Strengthening Mid-span Displacement, Pass #4

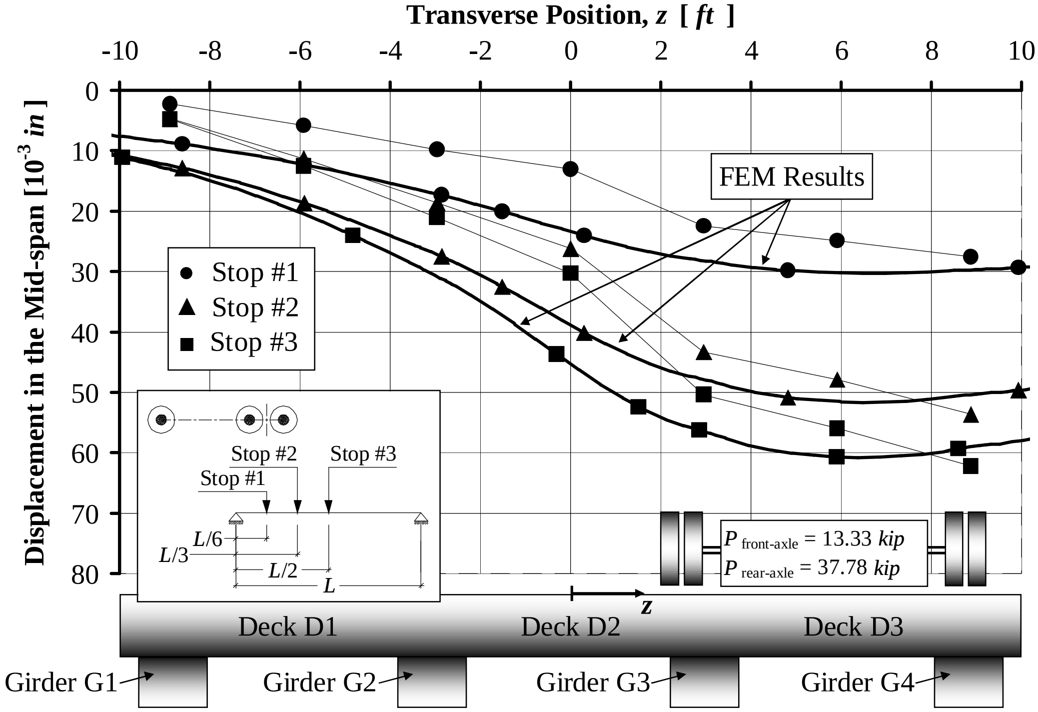

Figure B. 5. After Strengthening Mid-span Displacement, Pass #5

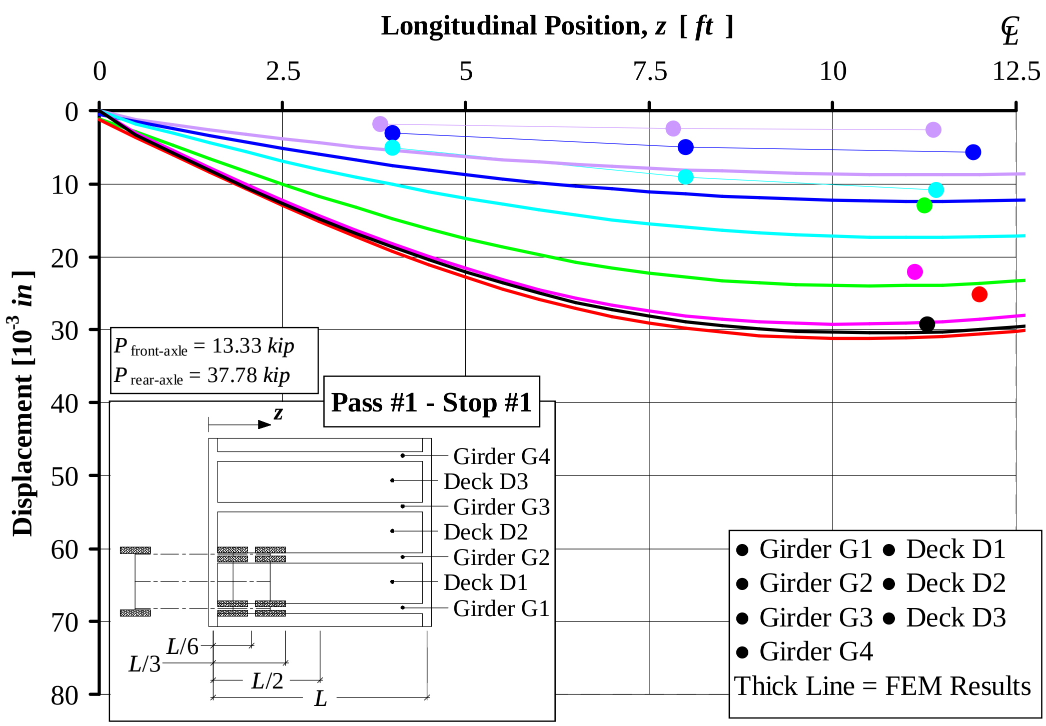

Figure B. 6. After Strengthening Displacement Distribution, Pass #1 Stop #1

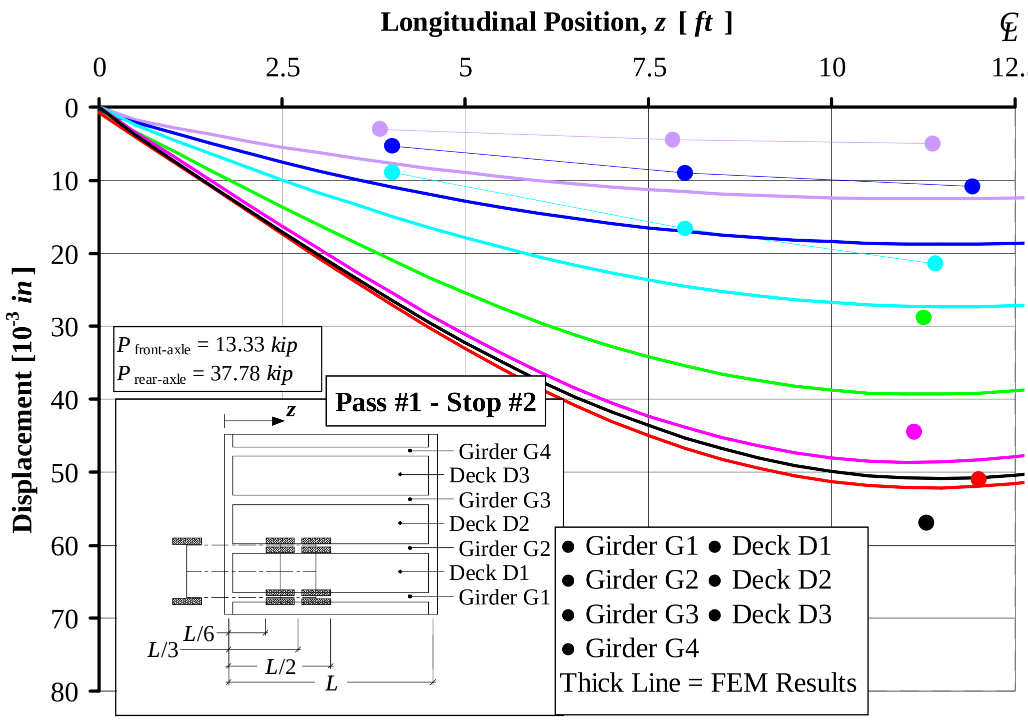

Figure B. 7. After Strengthening Displacement Distribution, Pass #1 Stop #2

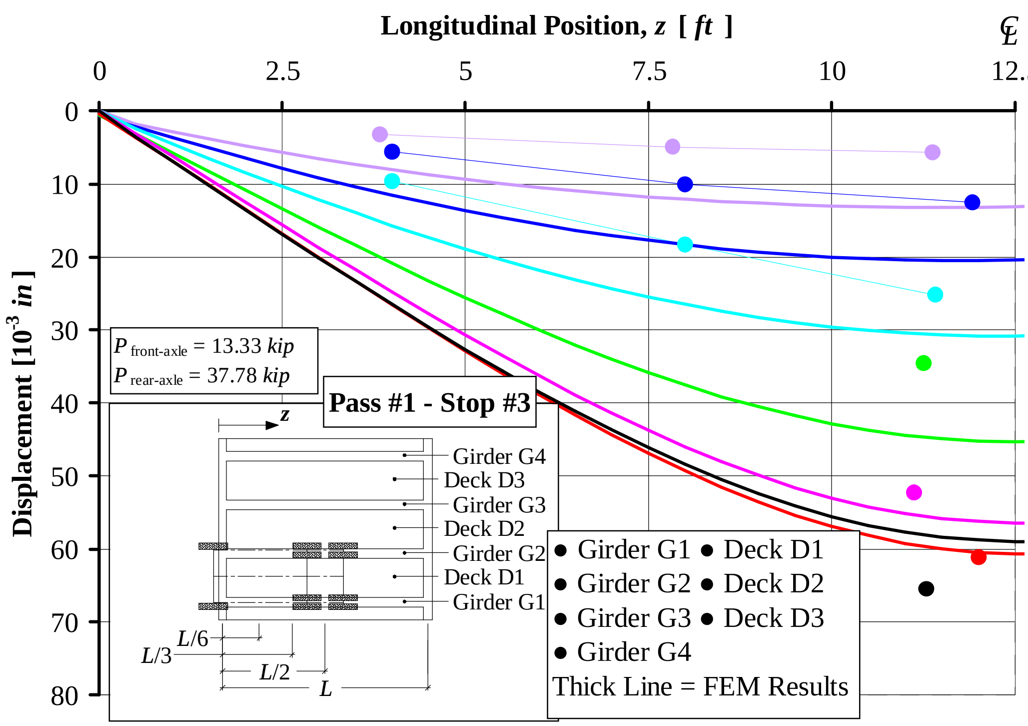

Figure B. 8. After Strengthening Displacement Distribution, Pass #1 Stop #3

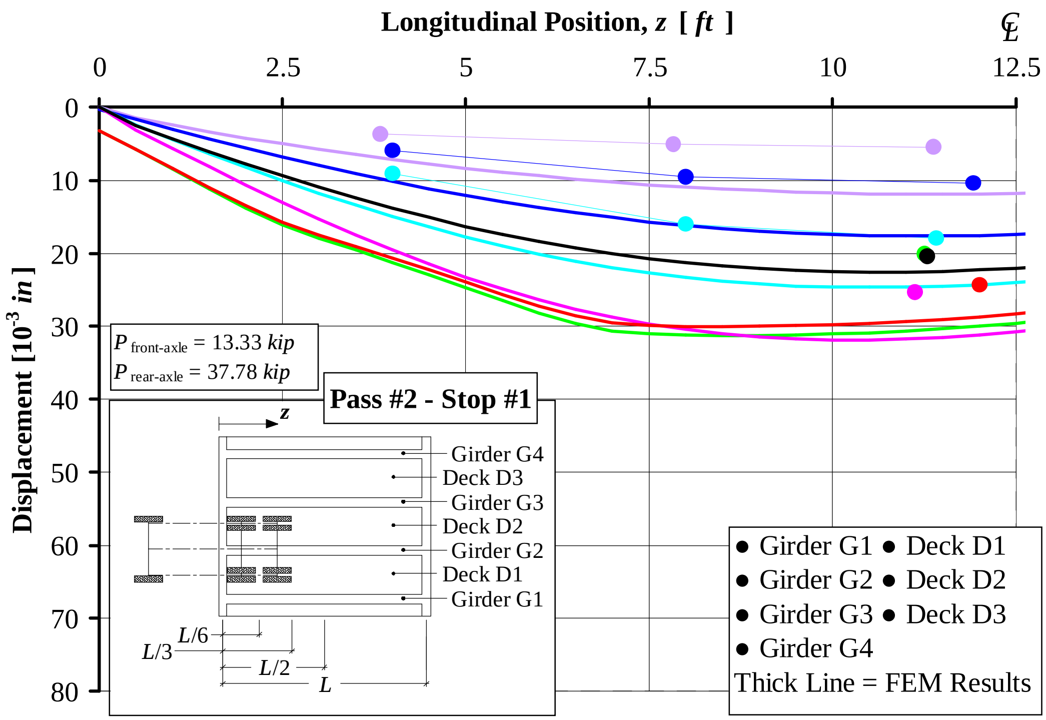

Figure B. 9. After Strengthening Displacement Distribution, Pass #2 Stop #1

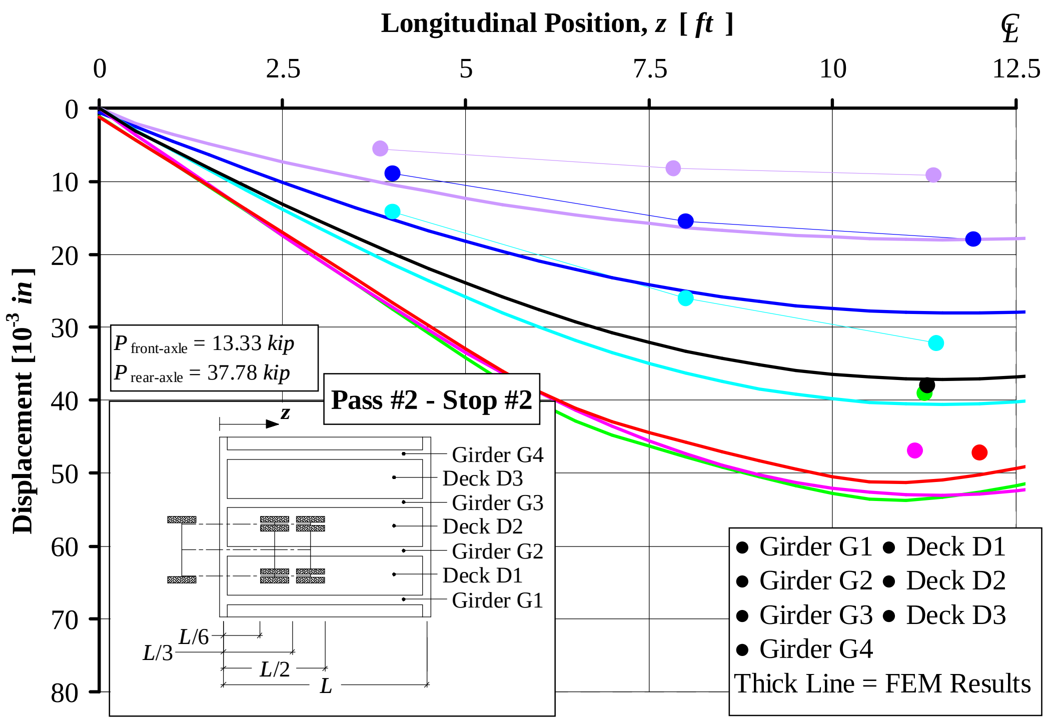

Figure B. 10. After Strengthening Displacement Distribution, Pass #2 Stop #2

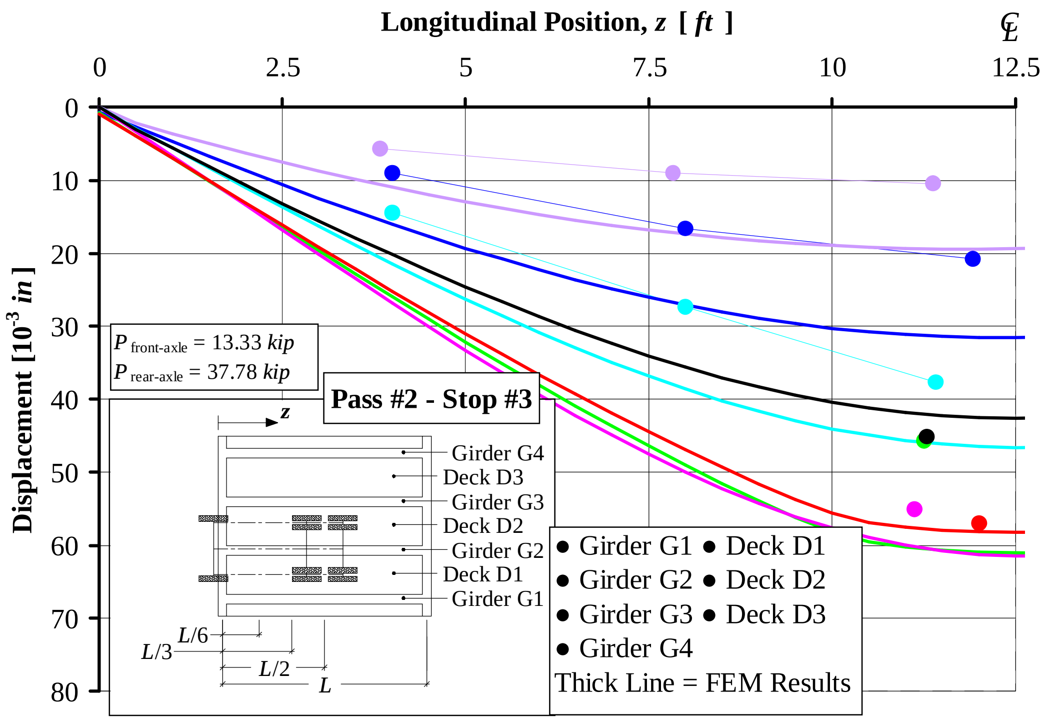

Figure B. 11. After Strengthening Displacement Distribution, Pass #2 Stop #3

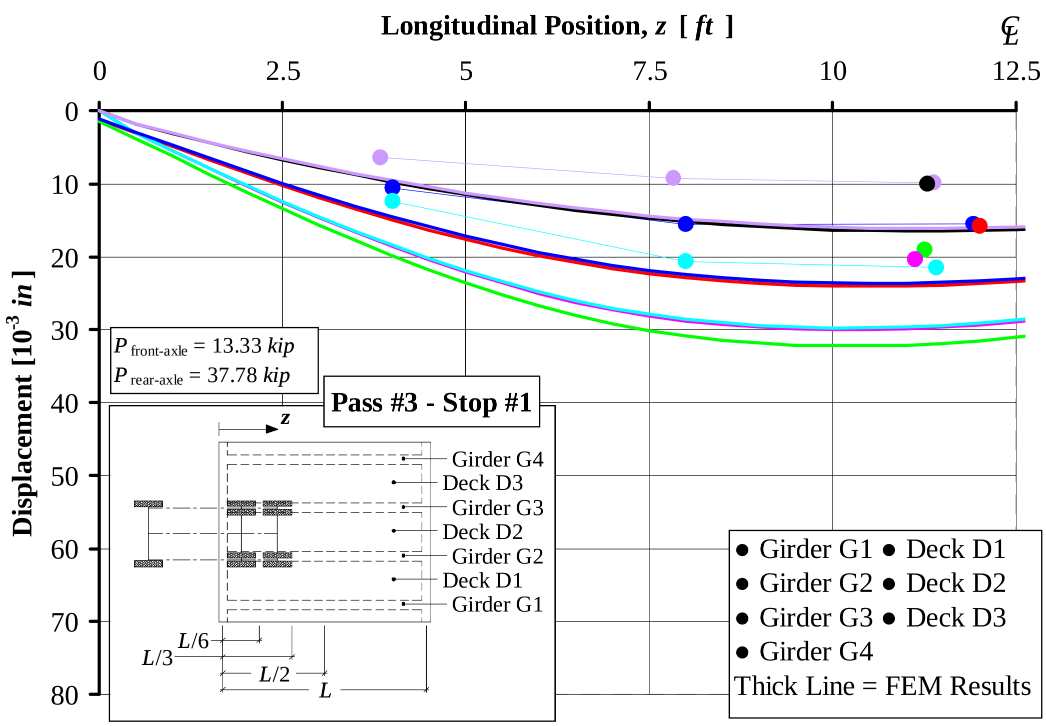

Figure B. 12. After Strengthening Displacement Distribution, Pass #3 Stop #1

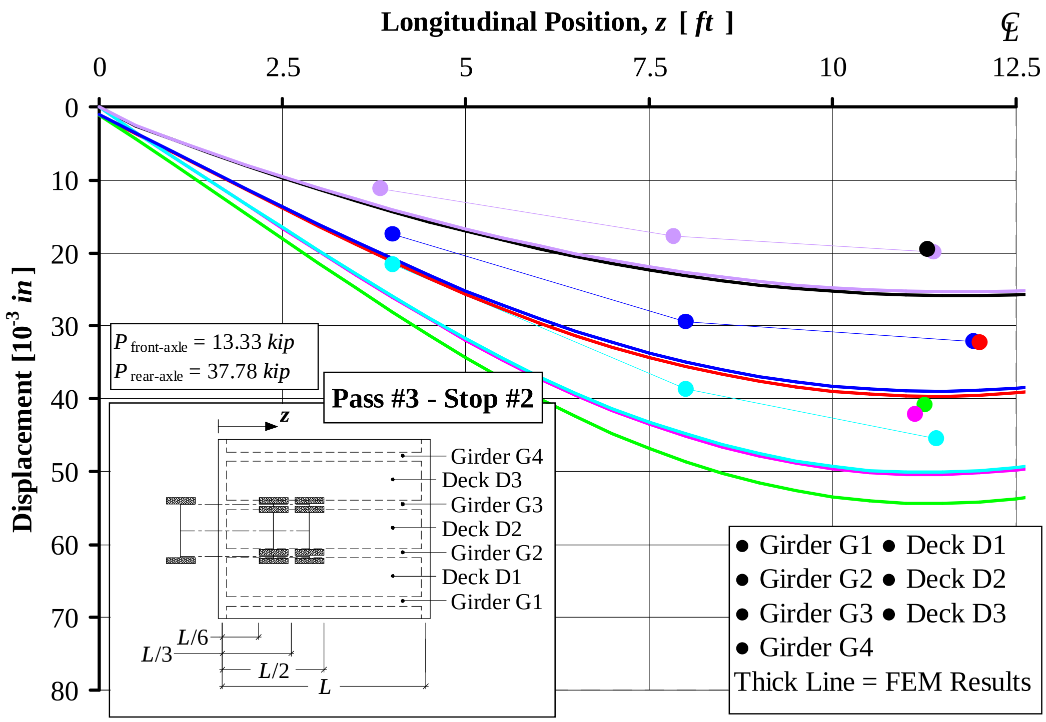

Figure B. 13. After Strengthening Displacement Distribution, Pass #3 Stop #2

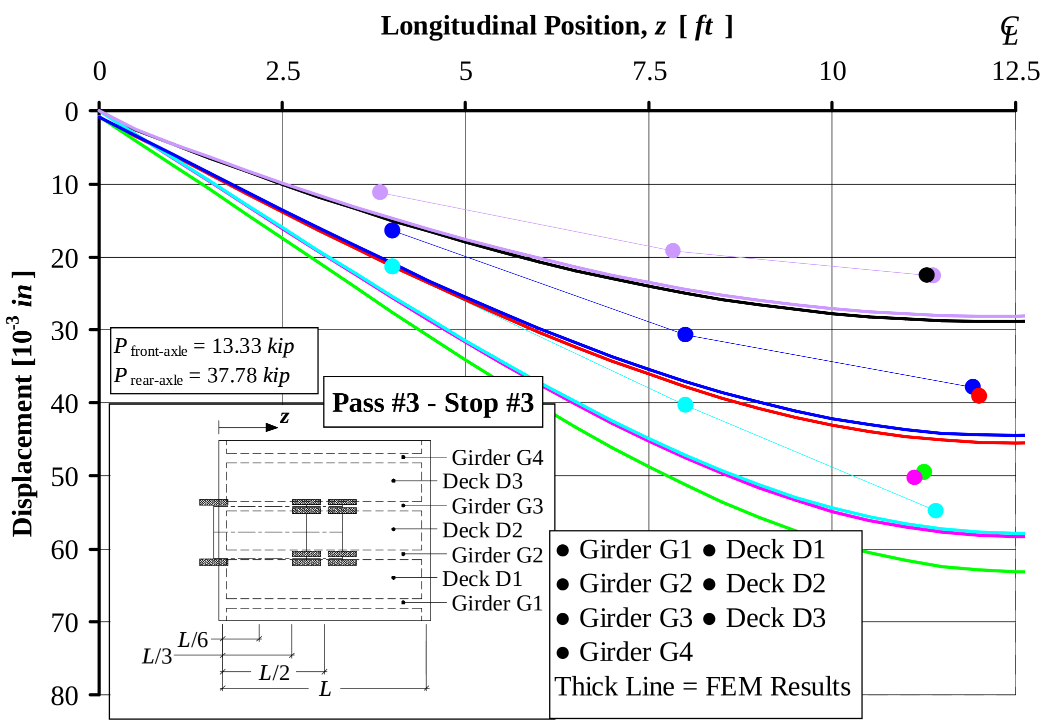

Figure B. 14. After Strengthening Displacement Distribution, Pass #3 Stop #3

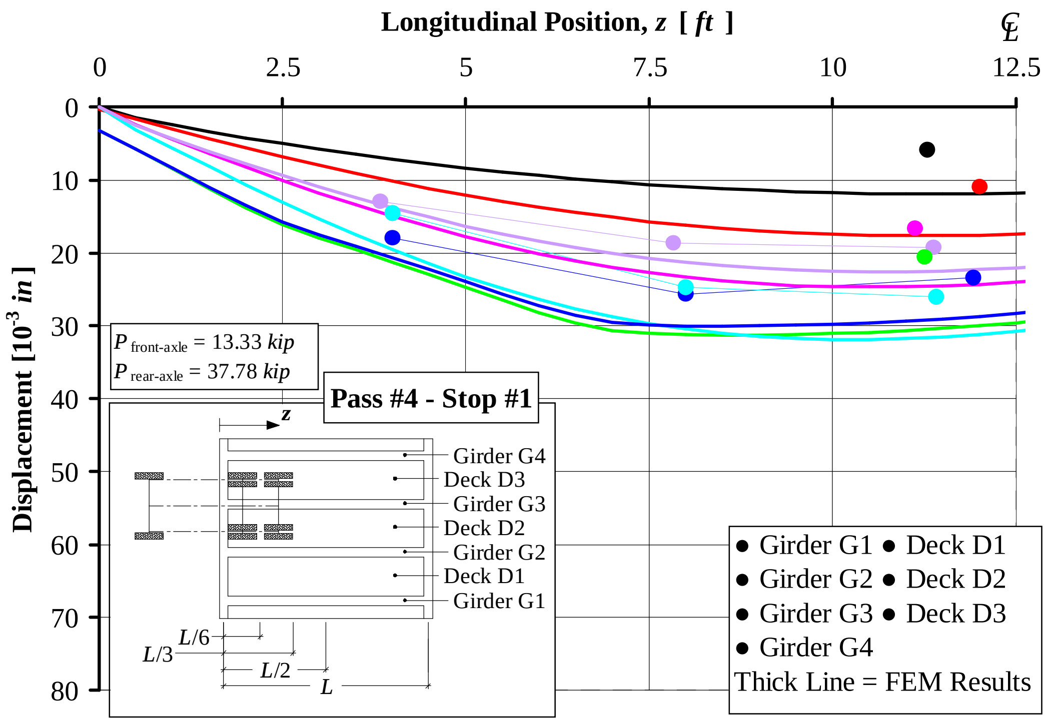

Figure B. 15. After Strengthening Displacement Distribution, Pass #4 Stop #1

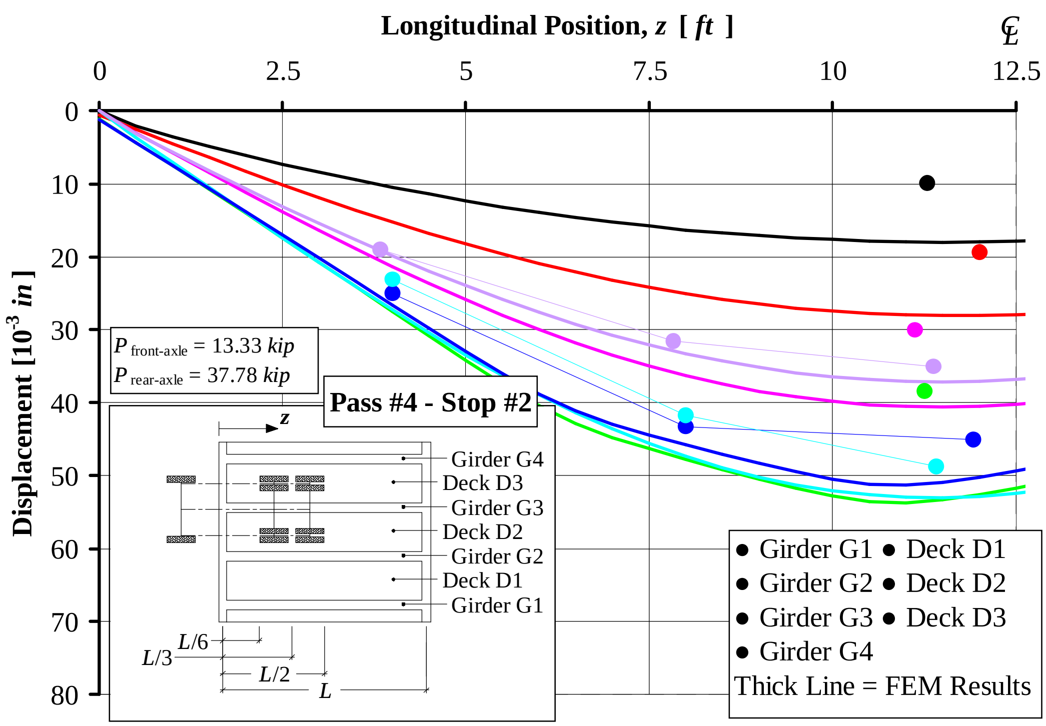

Figure B. 16. After Strengthening Displacement Distribution, Pass #4 Stop #2

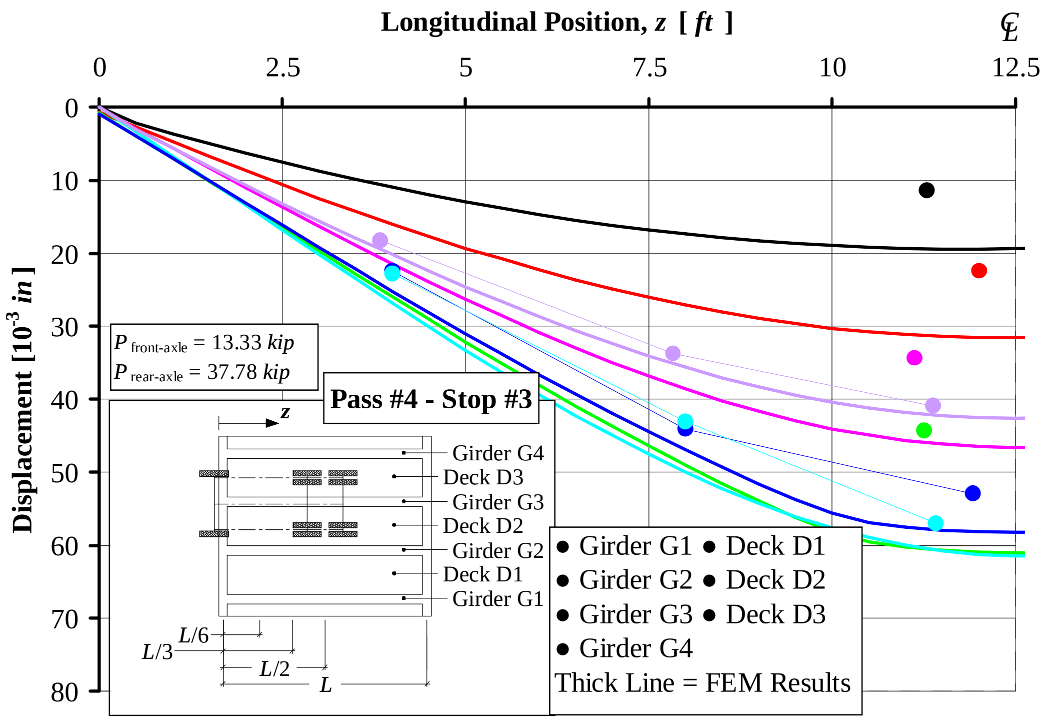

Figure B. 17. After Strengthening Displacement Distribution, Pass #4 Stop #3

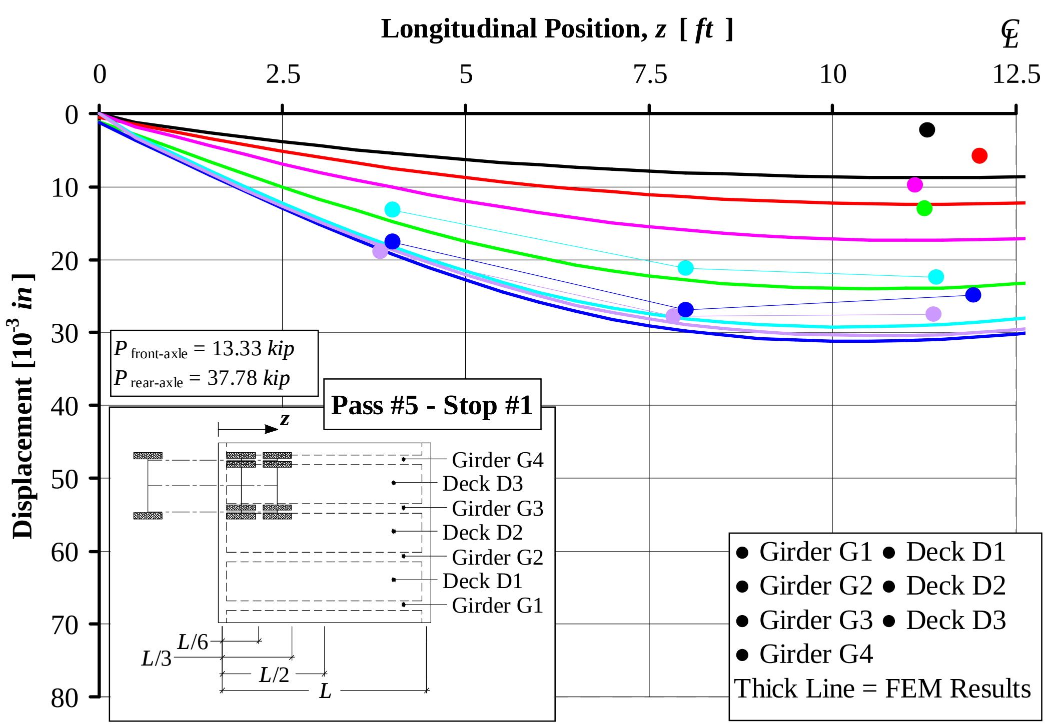

Figure B. 18. After Strengthening Displacement Distribution, Pass #5 Stop #1

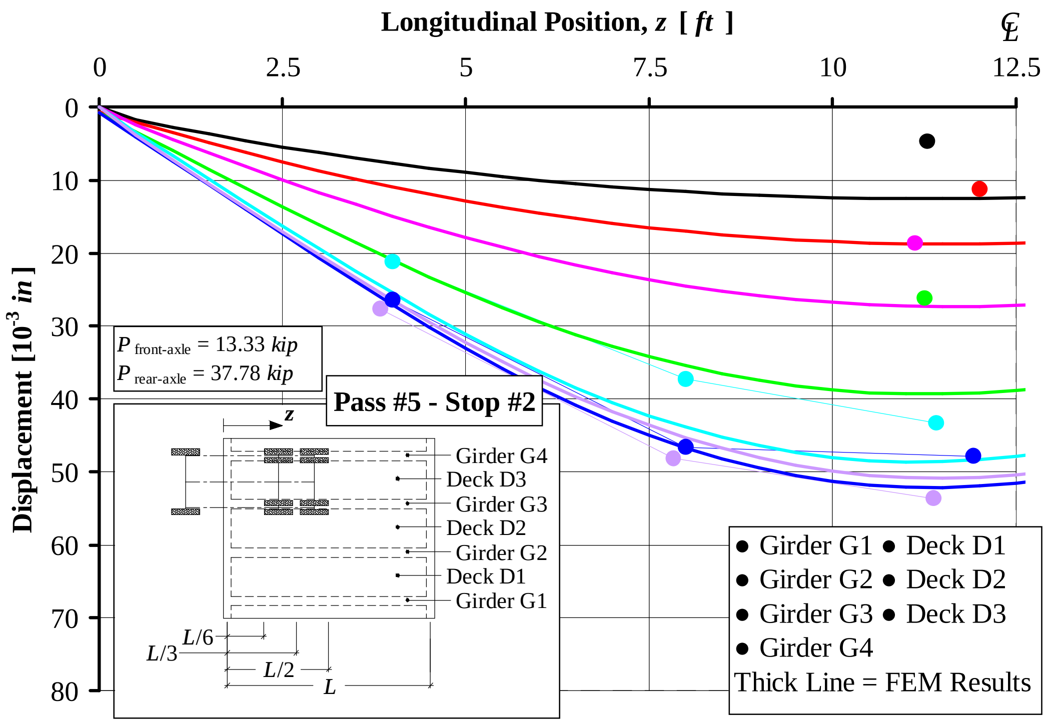

Figure B. 19. After Strengthening Displacement Distribution, Pass #5 Stop #2

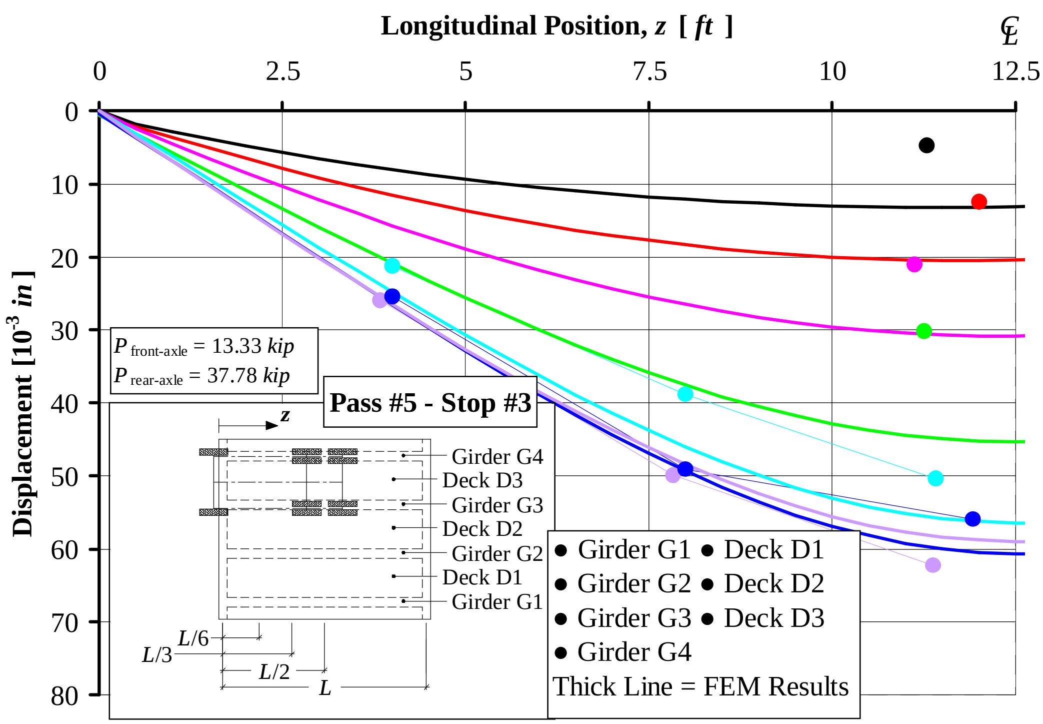

Figure B. 20. After Strengthening Displacement Distribution, Pass #5 Stop #3

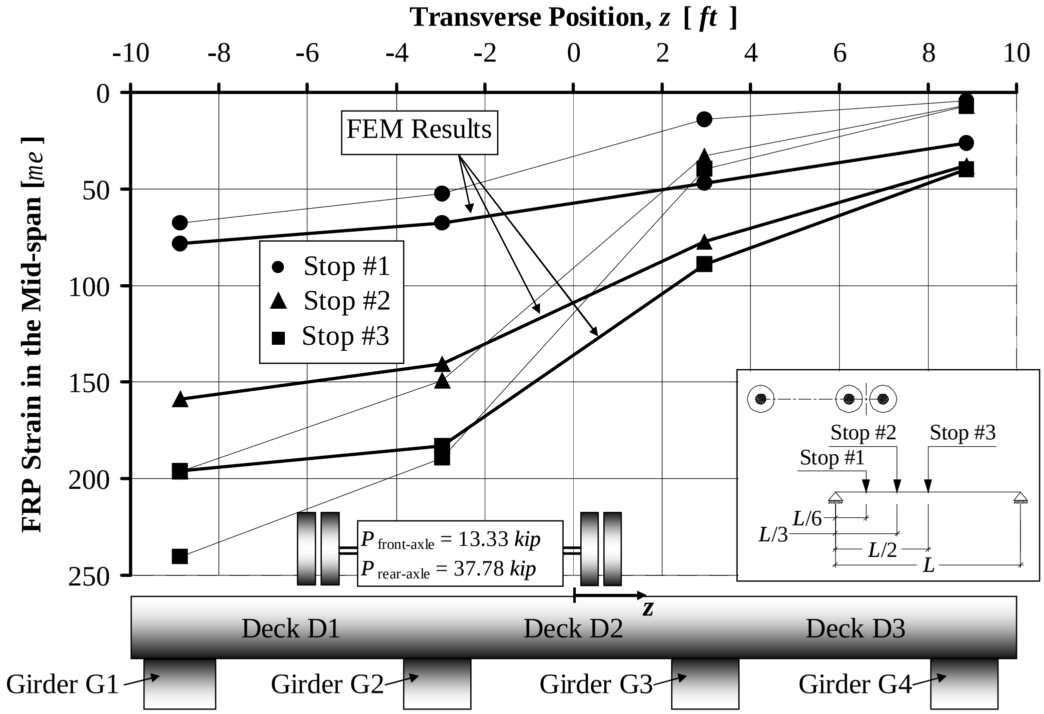

Figure B. 21. Strain in the FRP Strengthening on the Girders at Mid-span, Pass #1

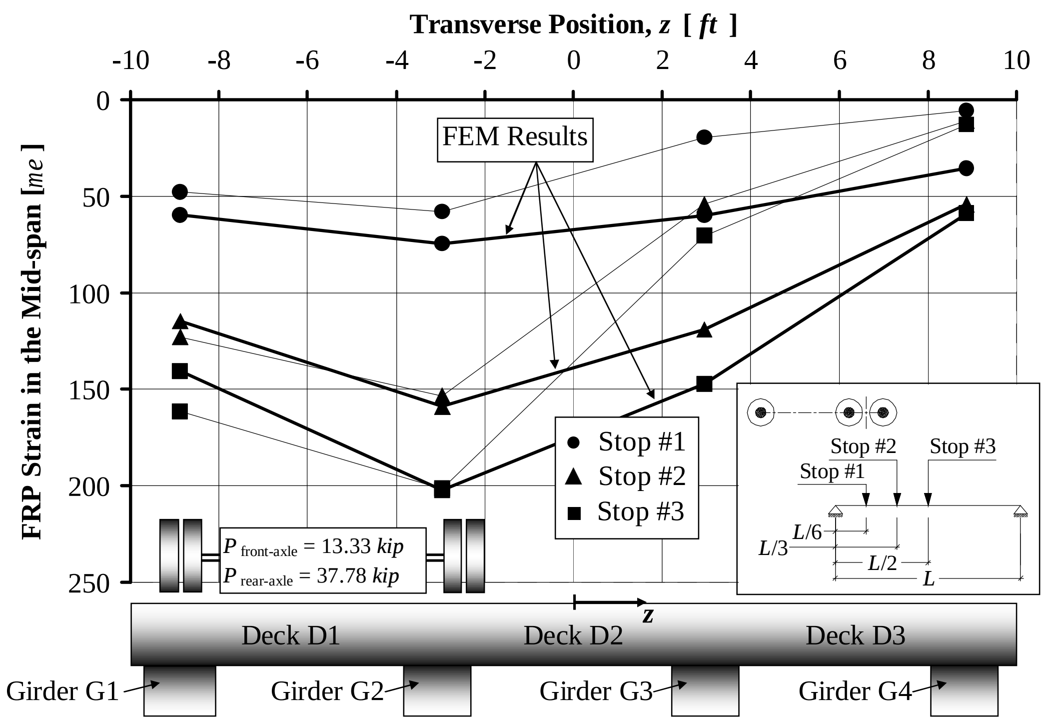

Figure B. 22. Strain in the FRP Strengthening on the Girders at Mid-span, Pass #2

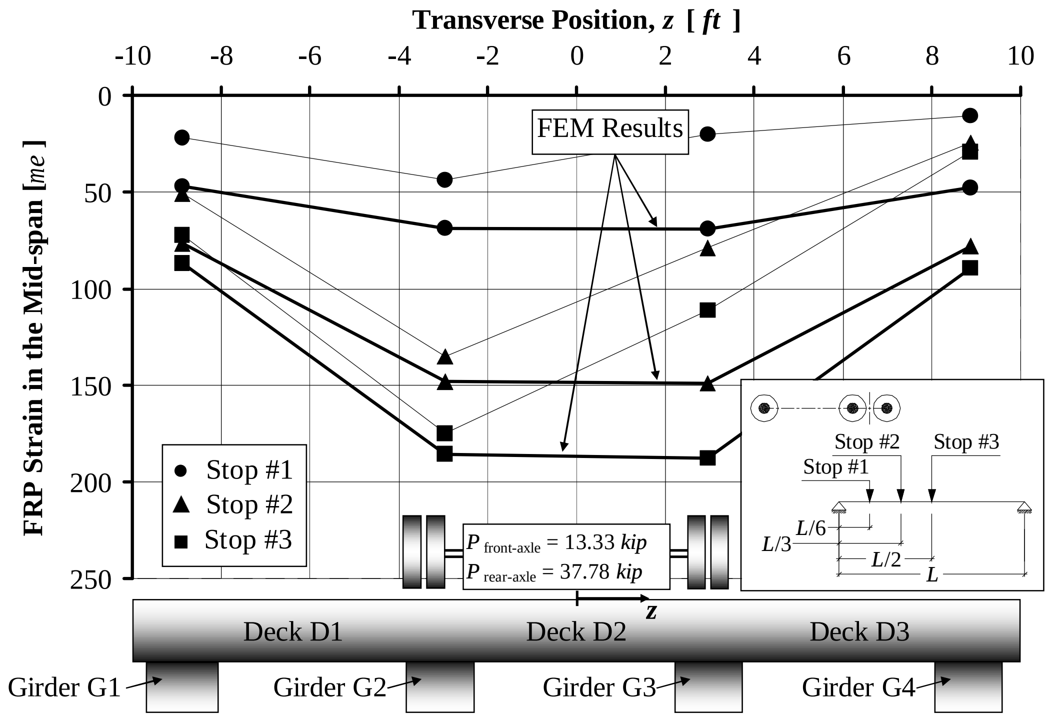

Figure B. 23. Strain in the FRP Strengthening on the Girders at Mid-span, Pass #3

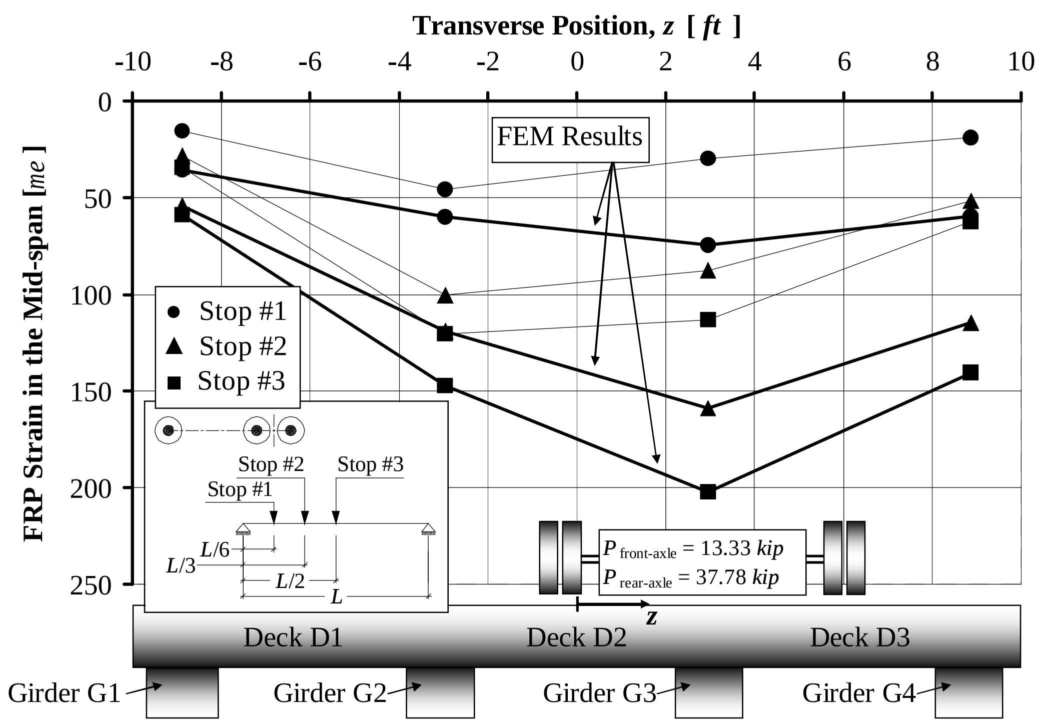

Figure B. 24. Strain in the FRP Strengthening on the Girders at Mid-span, Pass #4

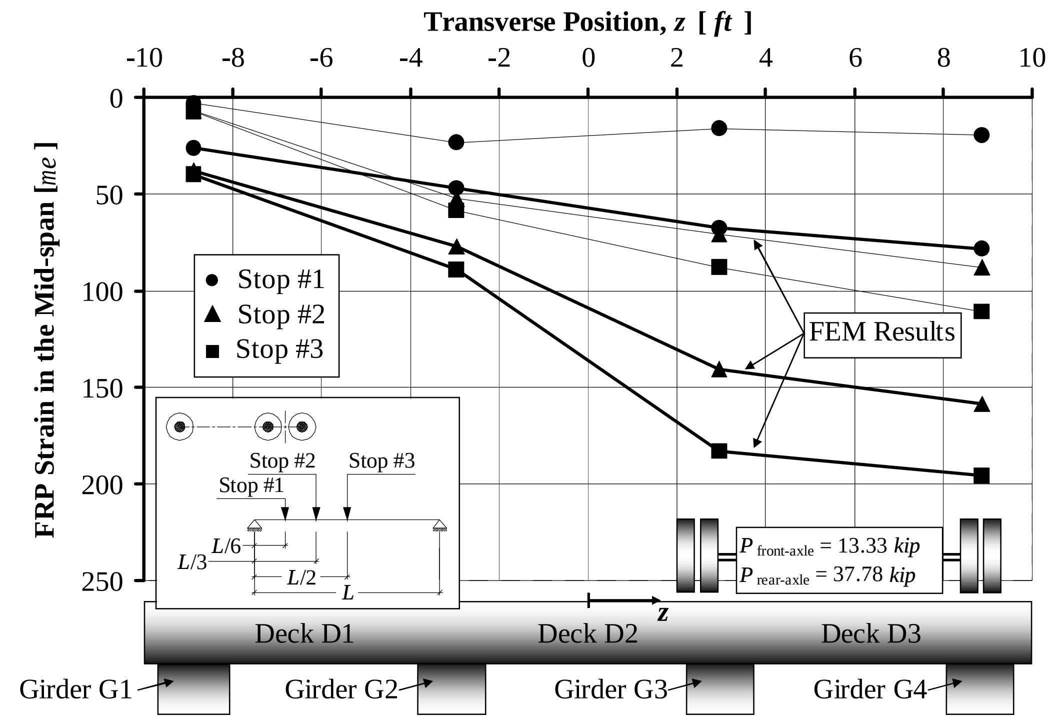

Figure B. 25. Strain in the FRP Strengthening on the Girders at Mid-span, Pass #5

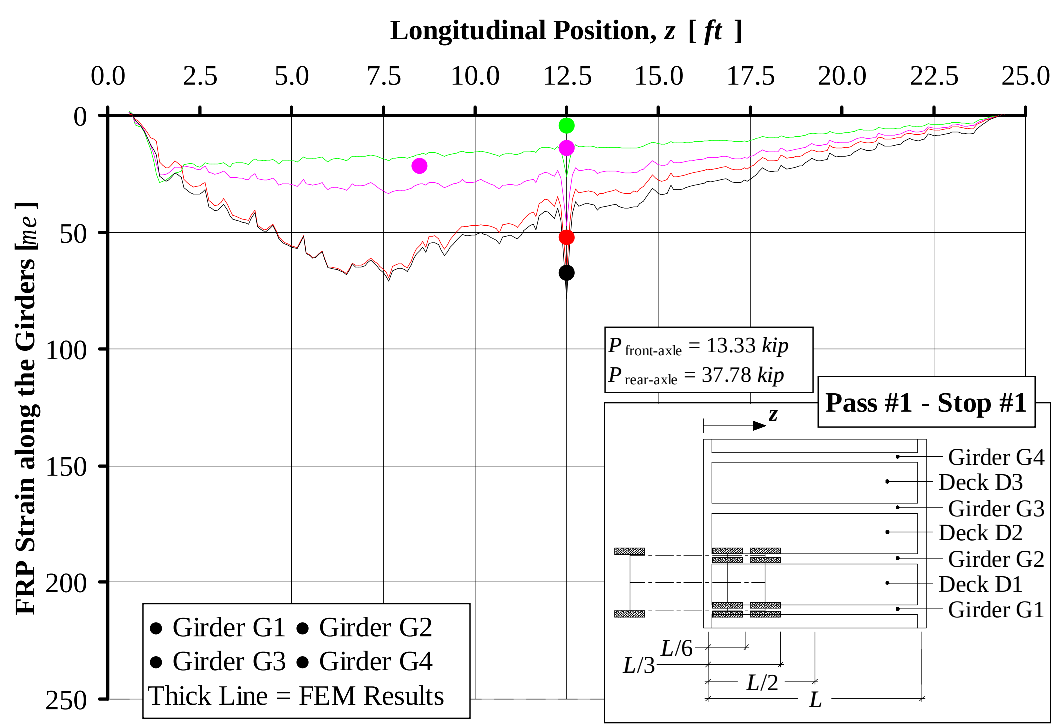

Figure B. 26. Strain Distribution in the FRP along the Girders, Pass #1 Stop #1

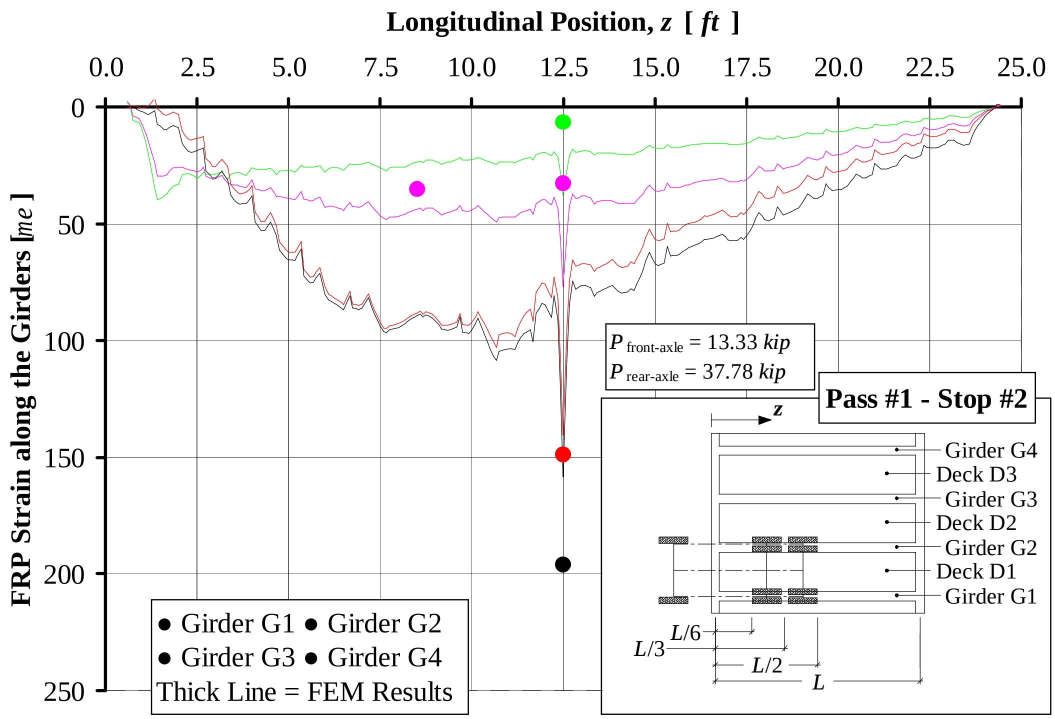

Figure B. 27. Strain Distribution in the FRP along the Girders, Pass #1 Stop #2

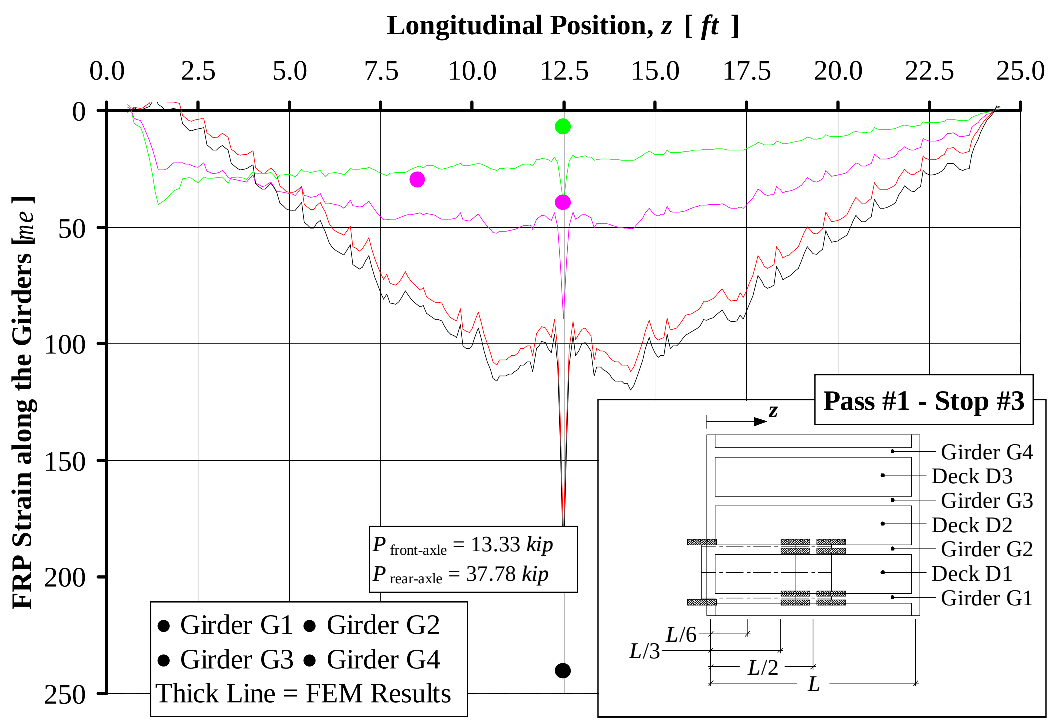

Figure B. 28. Strain Distribution in the FRP along the Girders, Pass #1 Stop #3

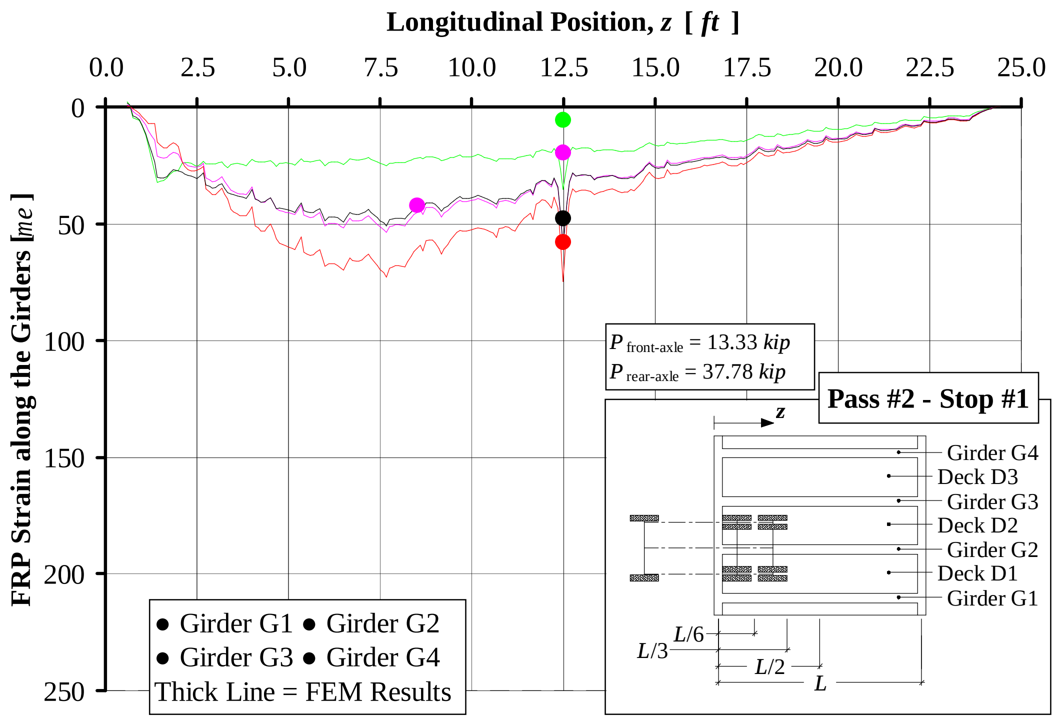

Figure B. 29. Strain Distribution in the FRP along the Girders, Pass #2 Stop #1

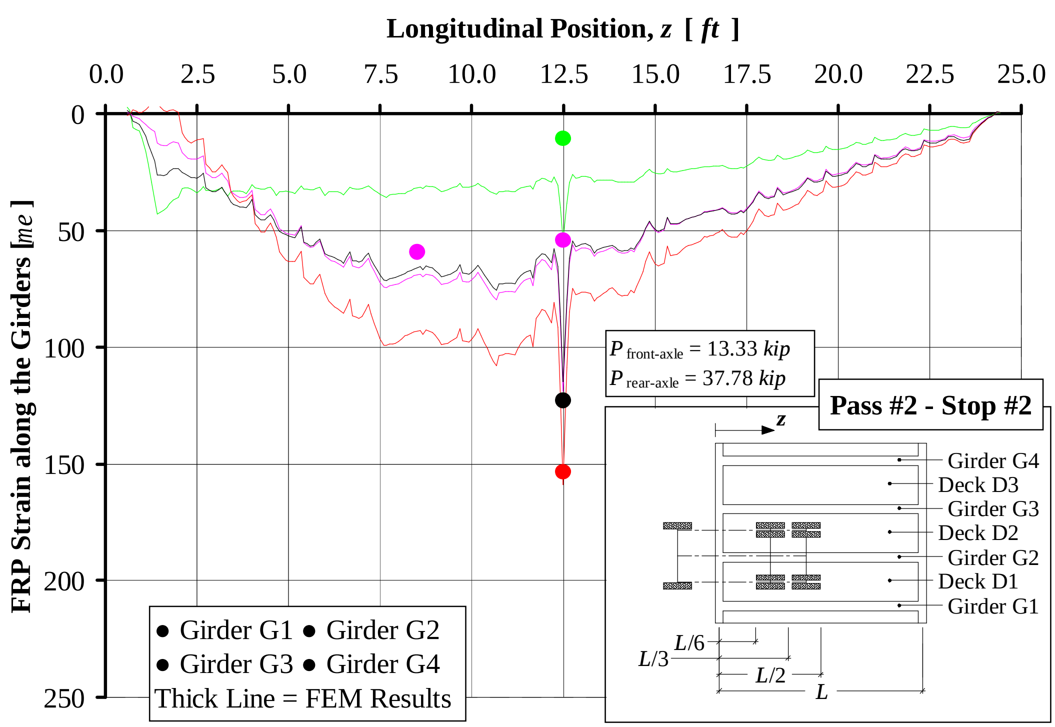

Figure B. 30. Strain Distribution in the FRP along the Girders, Pass #2 Stop #2

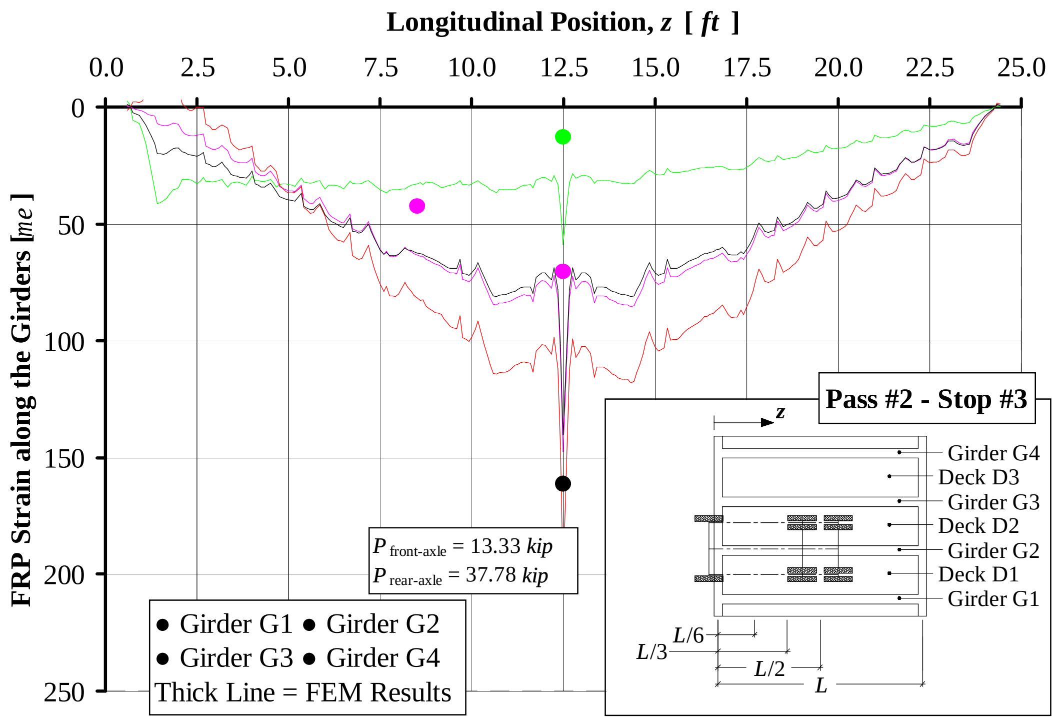

Figure B. 31. Strain Distribution in the FRP along the Girders, Pass #2 Stop #3

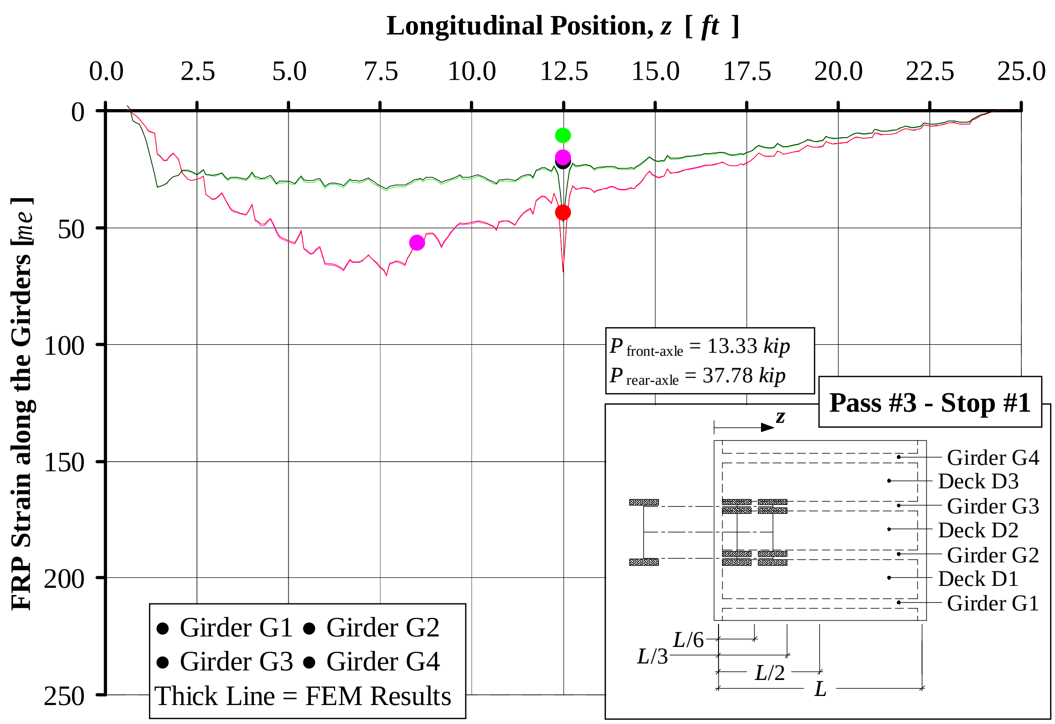

Figure B. 32. Strain Distribution in the FRP along the Girders, Pass #3 Stop #1

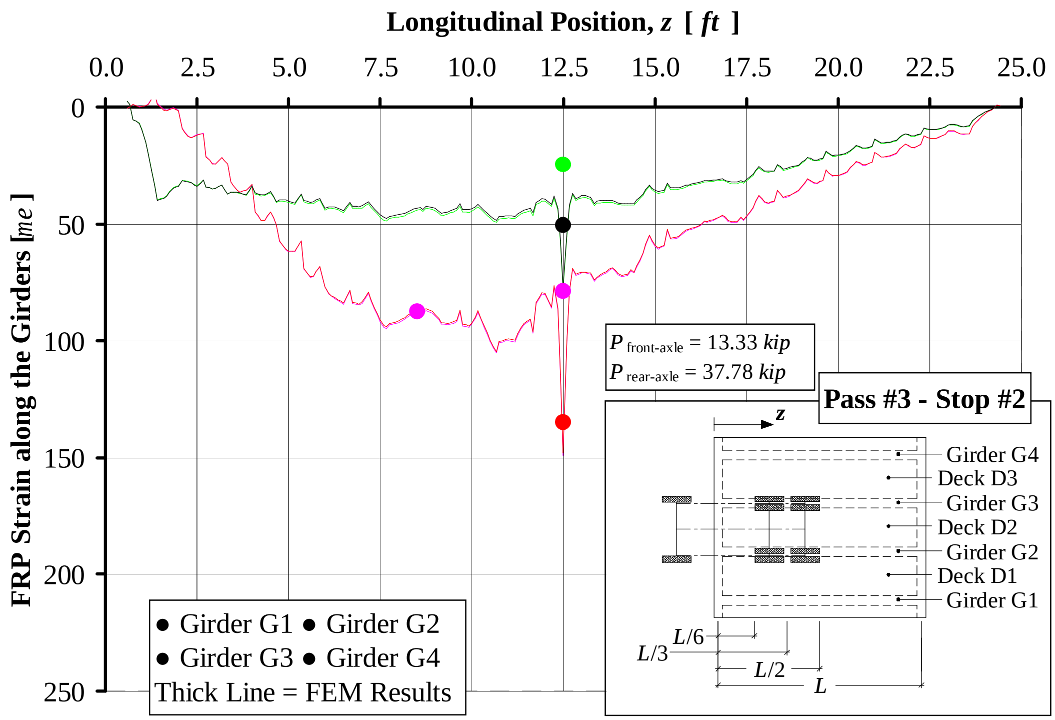

Figure B. 33. Strain Distribution in the FRP along the Girders, Pass #3 Stop #2

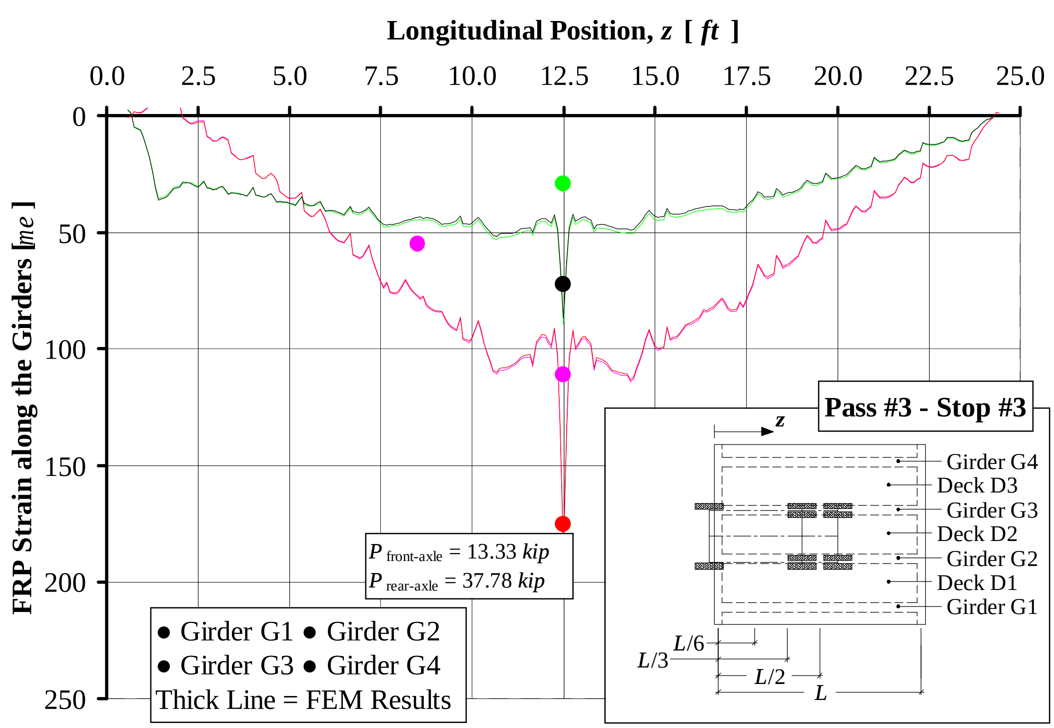

Figure B. 34. Strain Distribution in the FRP along the Girders, Pass #3 Stop #3

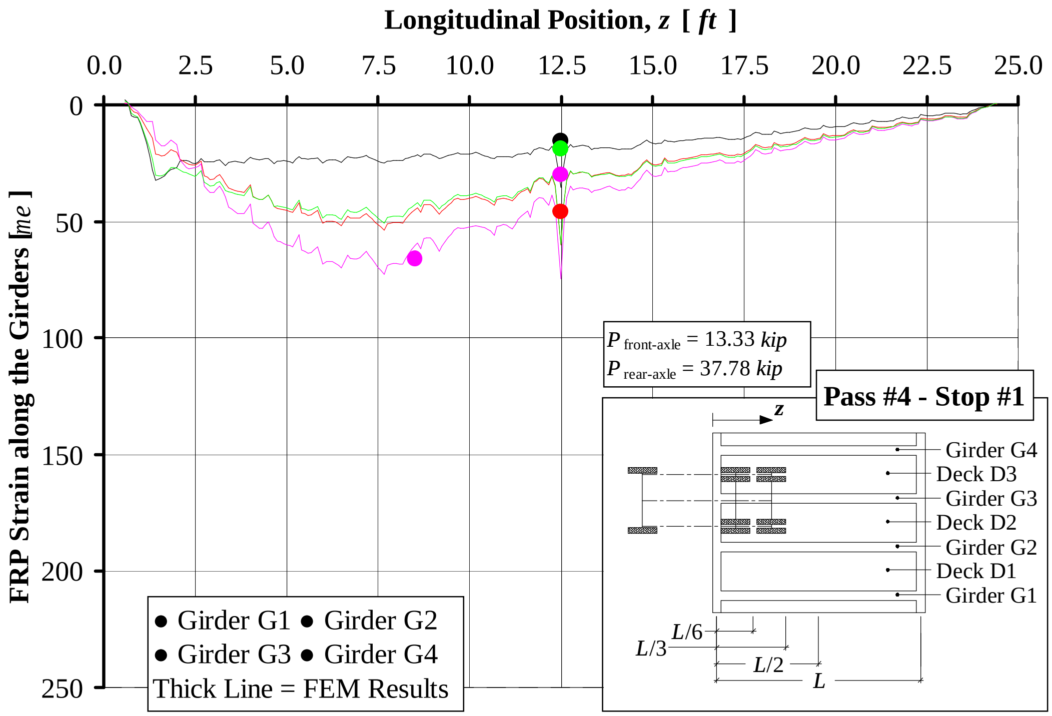

Figure B. 35. Strain Distribution in the FRP along the Girders, Pass #4 Stop #1

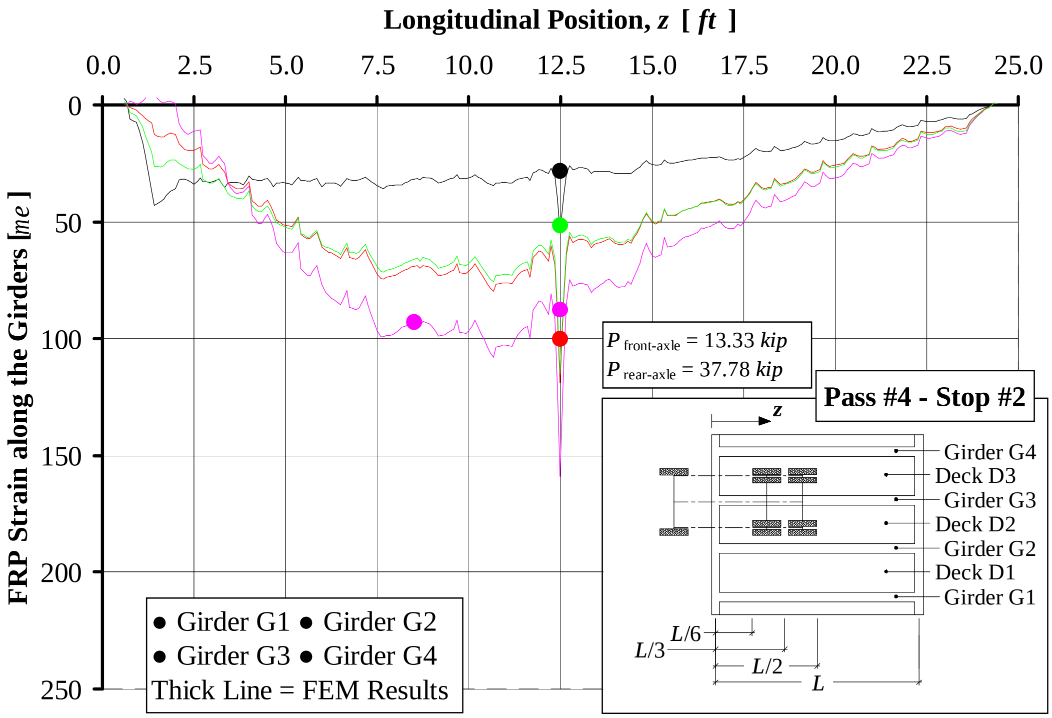

Figure B. 36. Strain Distribution in the FRP along the Girders, Pass #4 Stop #2

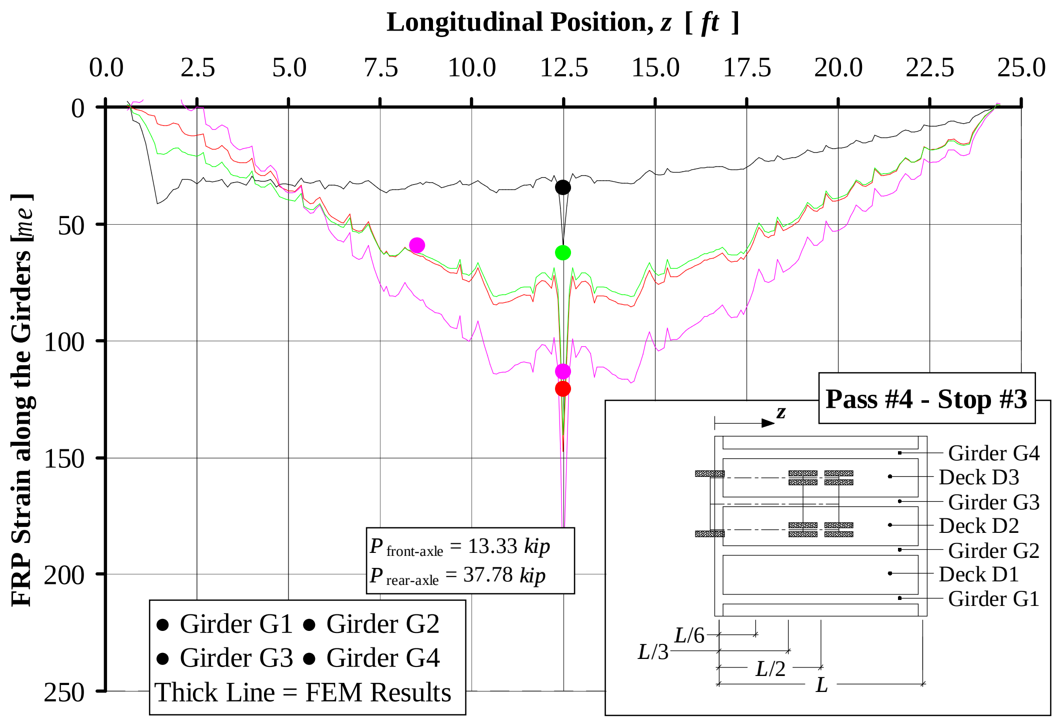

Figure B. 37. Strain Distribution in the FRP along the Girders, Pass #4 Stop #3

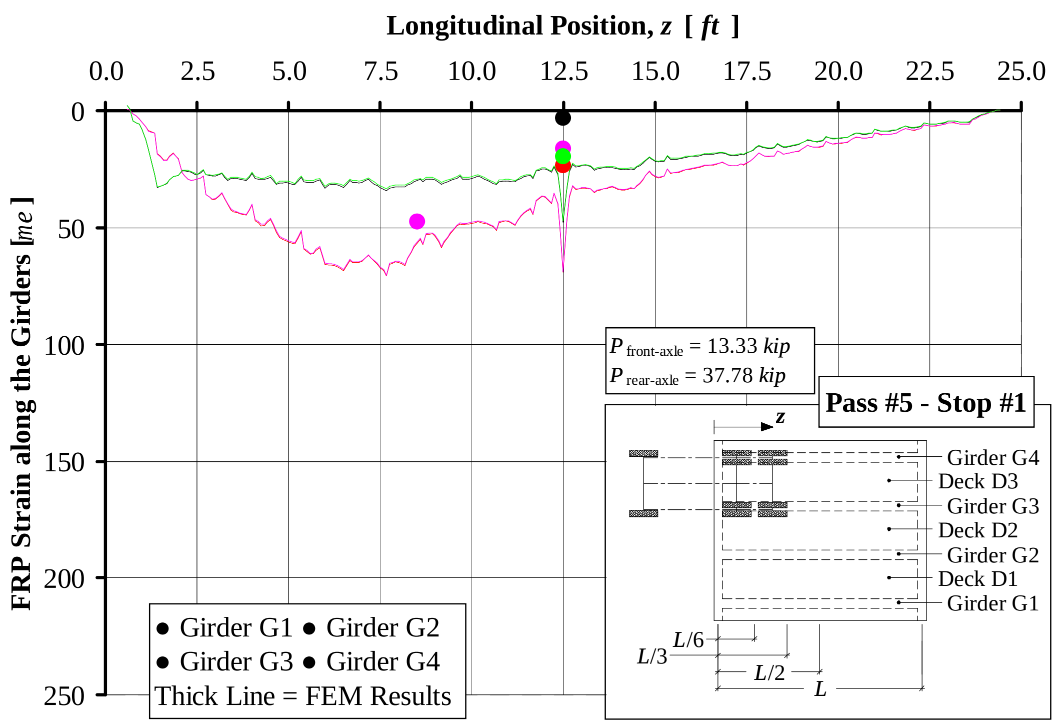

Figure B. 38. Strain Distribution in the FRP along the Girders, Pass #5 Stop #1

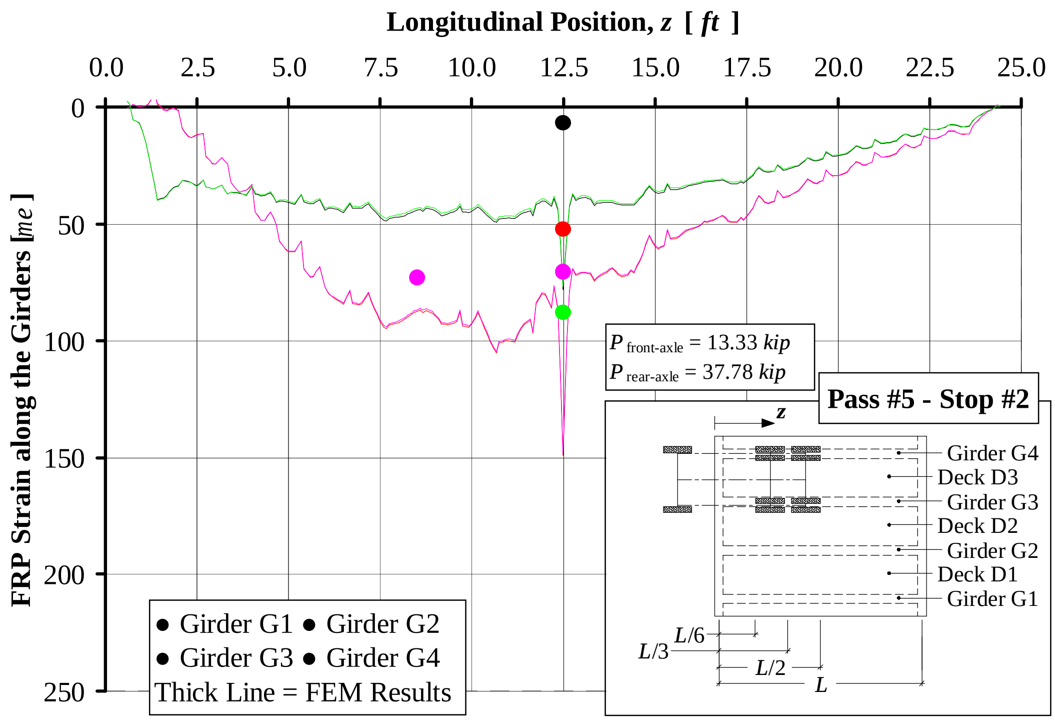

Figure B. 39. Strain Distribution in the FRP along the Girders, Pass #5 Stop #2

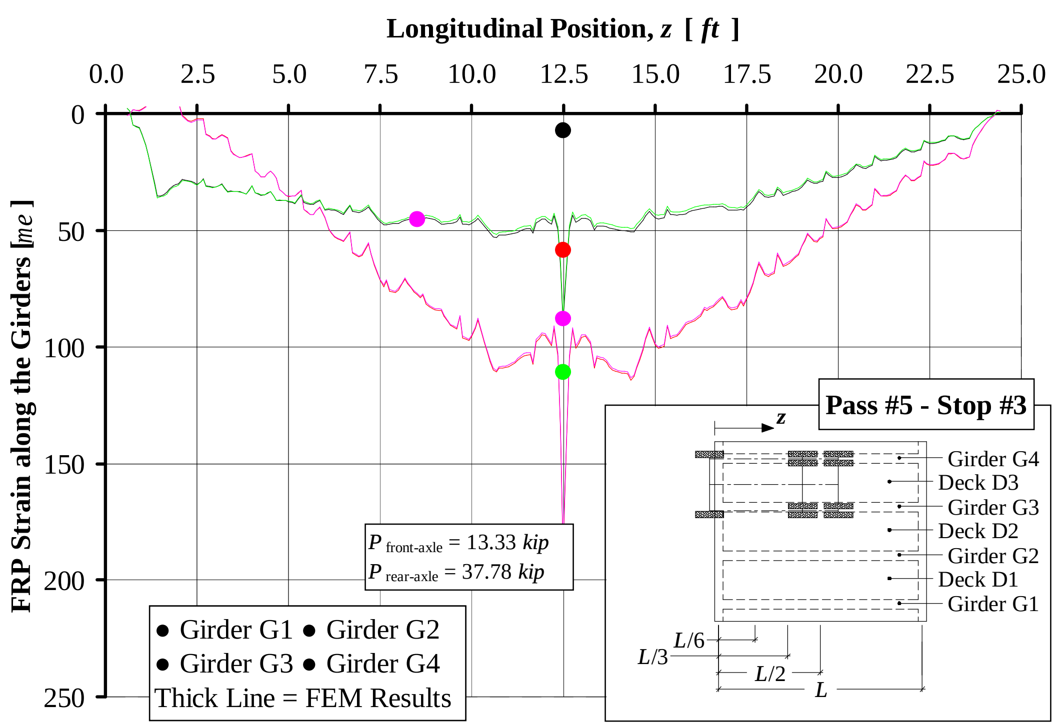

Figure B. 40. Strain Distribution in the FRP along the Girders, Pass #5 Stop #3

APPENDIX

C. Comparison between prior to and after Strengthening Normalized Results

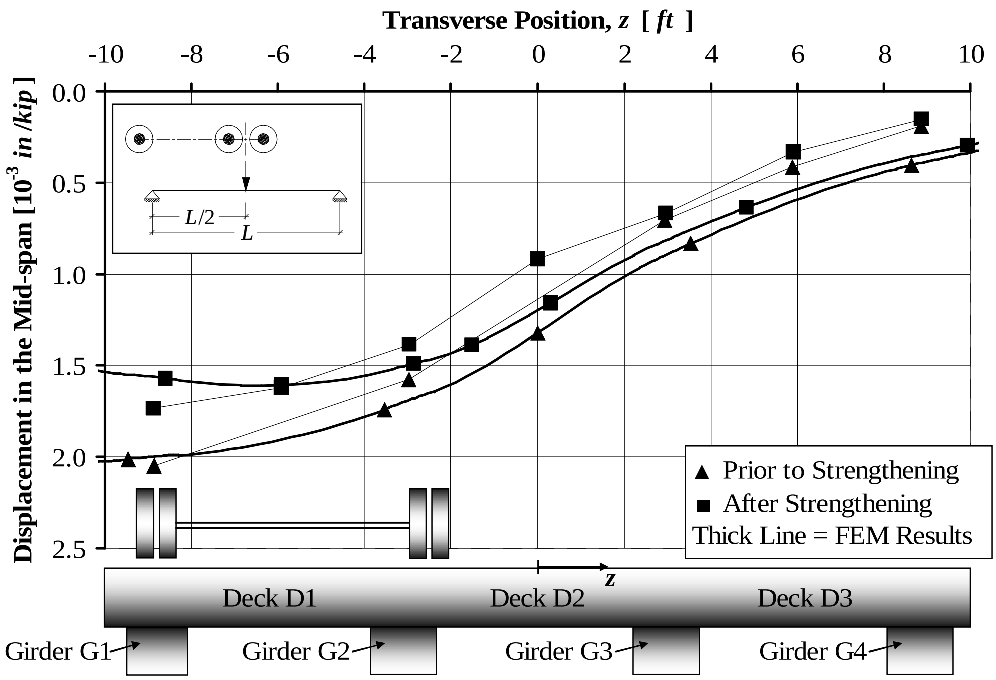

Figure C. 1. Mid-span Displacement prior to and after the Strengthening, Pass #1 and Rear Axle in the Mid-span

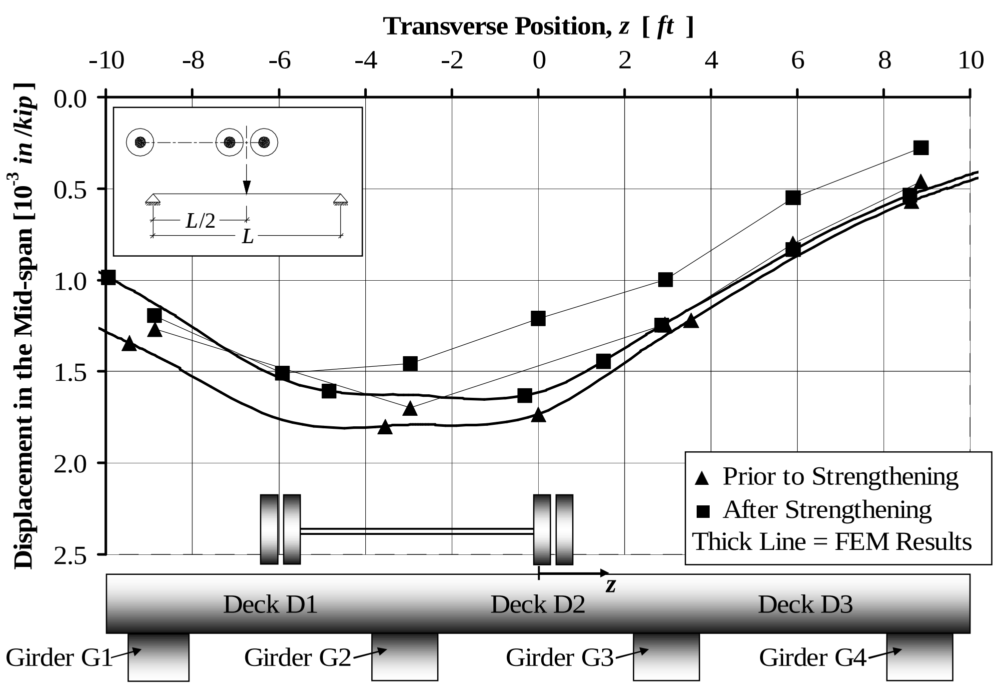

Figure C. 2. Mid-span Displacement prior to and after the Strengthening, Pass #2 and Rear Axle in the Mid-span

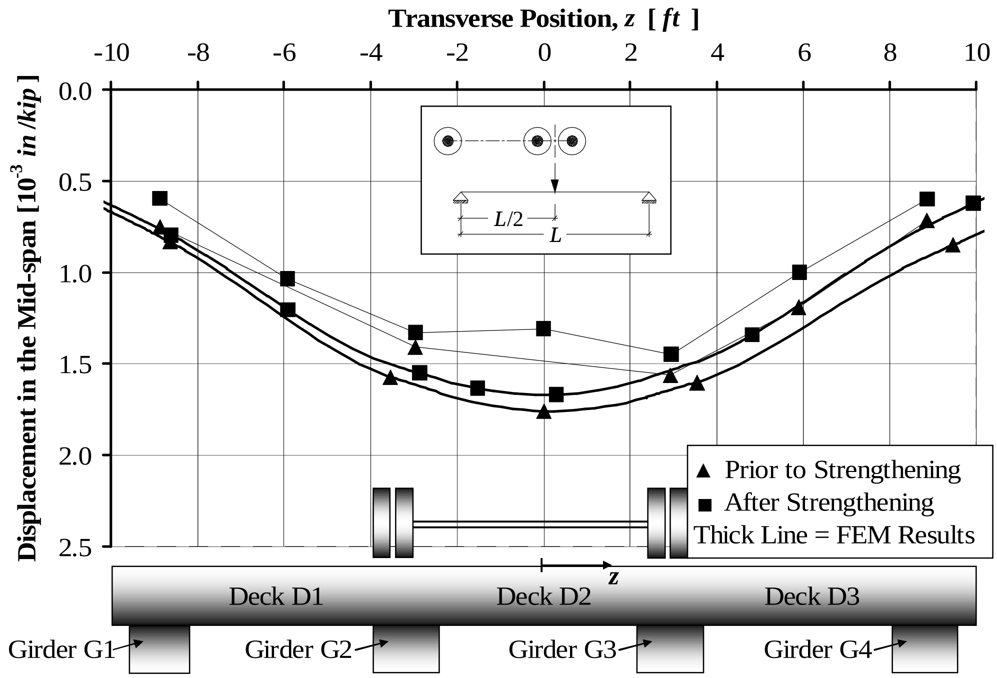

Figure C. 3. Mid-span Displacement prior to and after the Strengthening, Pass #3 and Rear Axle in the Mid-span

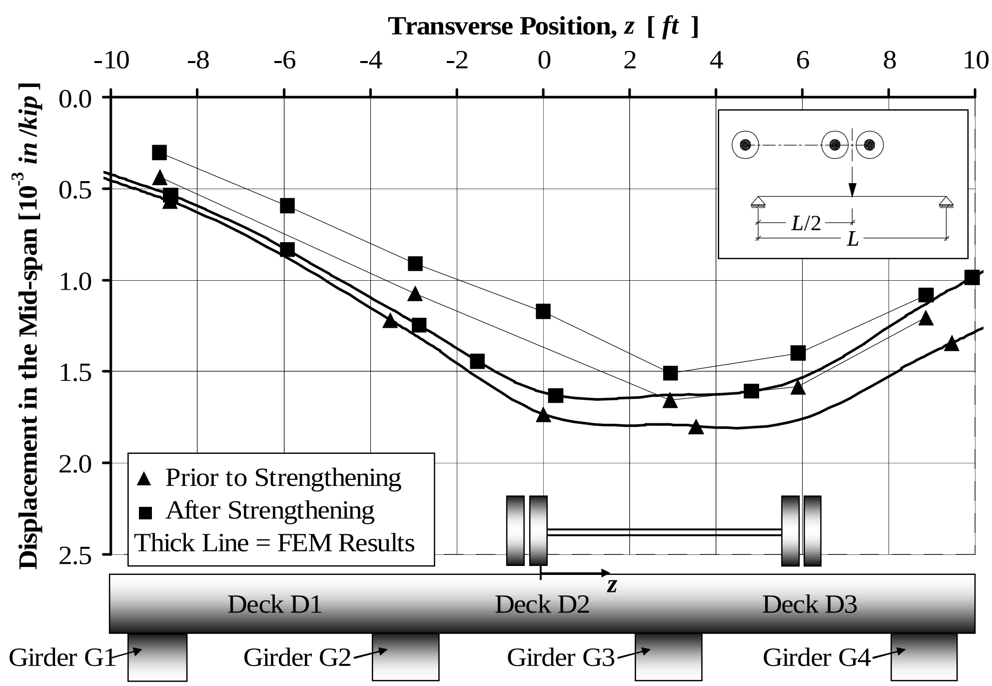

Figure C. 4. Mid-span Displacement prior to and after the Strengthening, Pass #4 and Rear Axle in the Mid-span

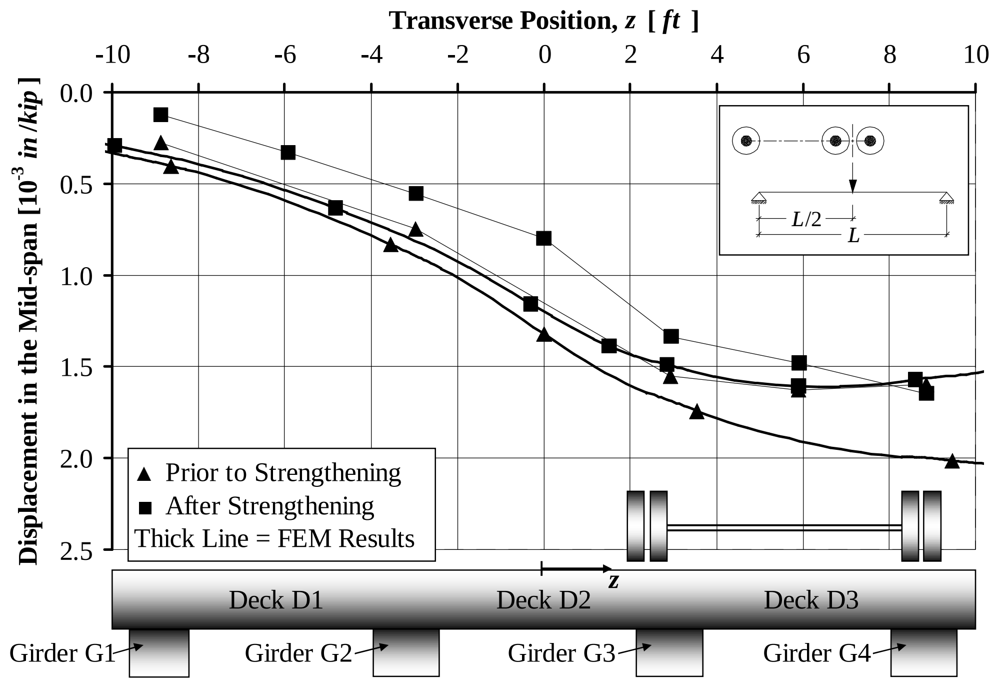

Figure C. 5. Mid-span Displacement prior to and after the Strengthening, Pass #5 and Rear Axle in the Mid-span

APPENDIX

D. Dynamic Test Results

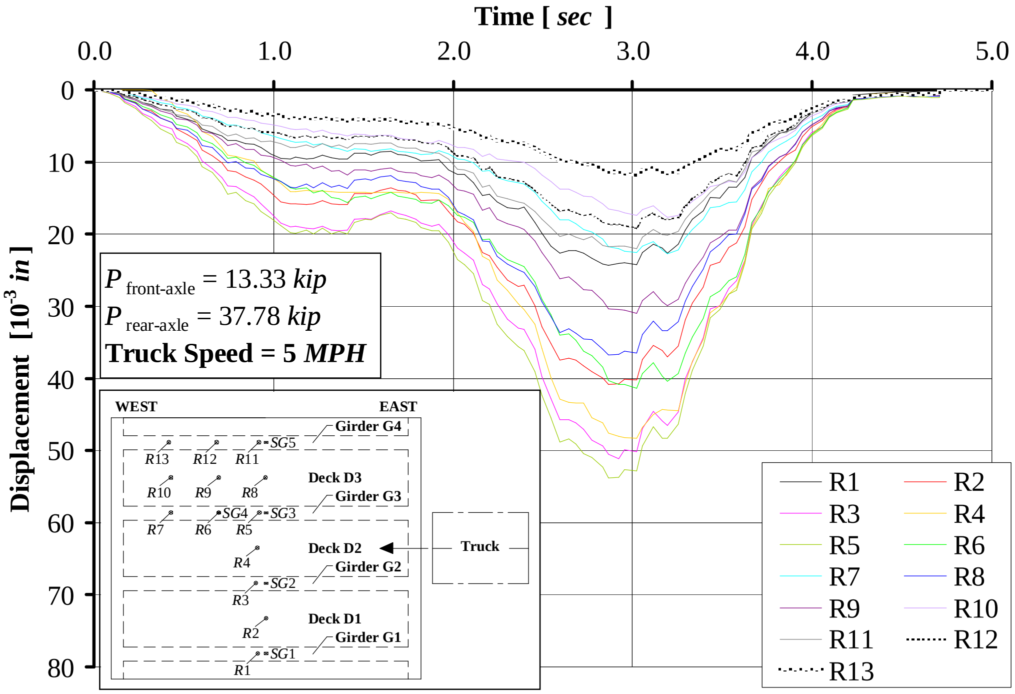

Figure D. 1. After Strengthening Displacements at $2.2\ m/s\ (5\ MPH)$

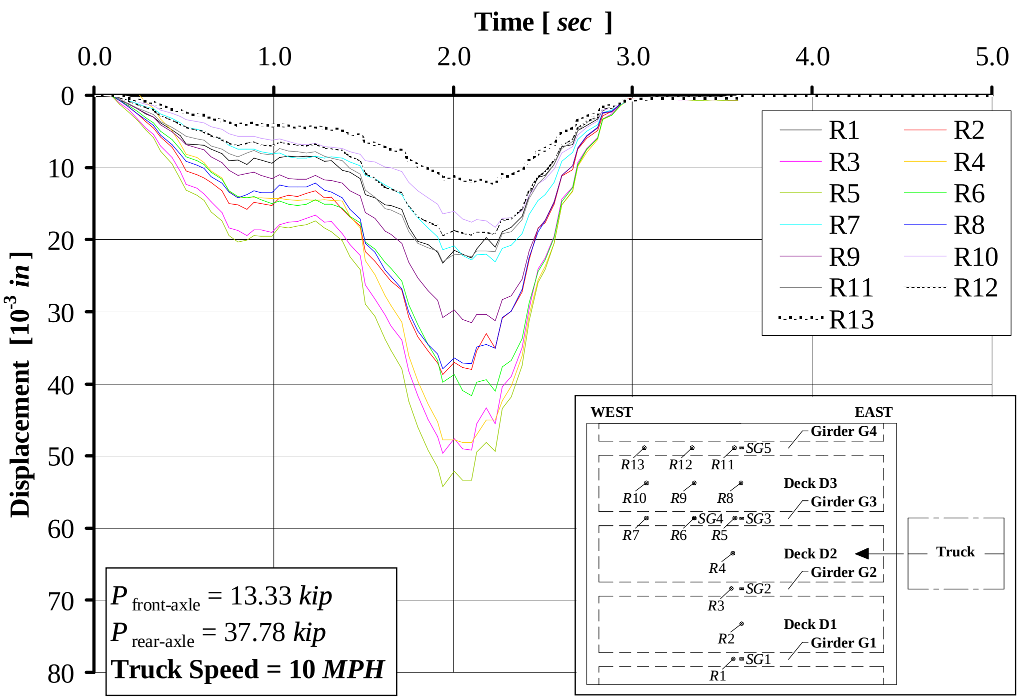

Figure D. 2. After Strengthening Displacements at $4.5\ m/s\ (10\ MPH)$

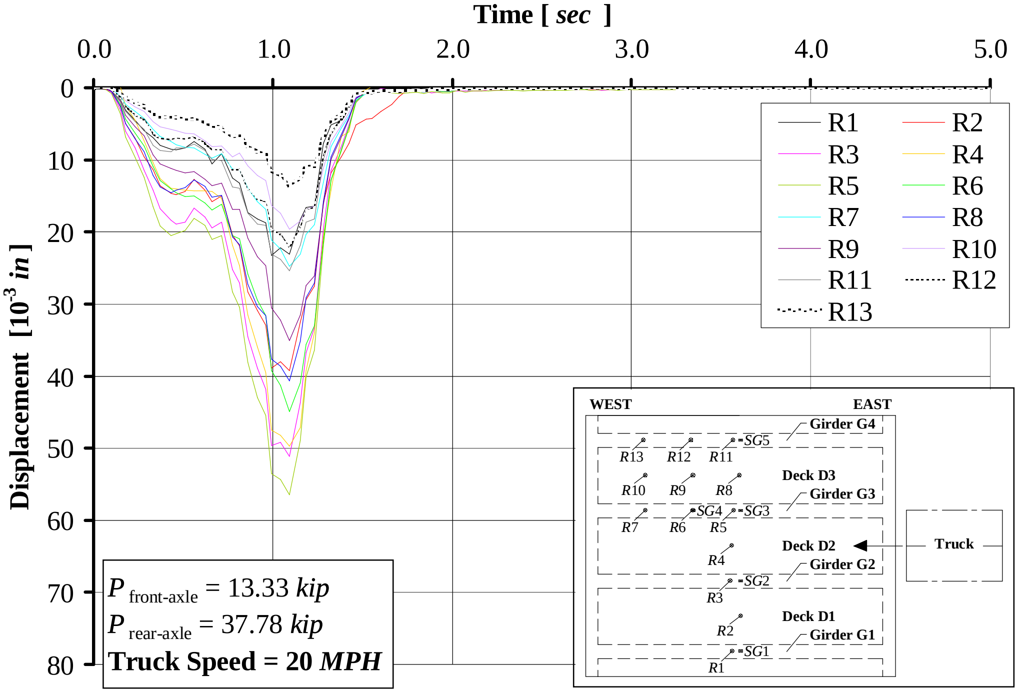

Figure D. 3. After Strengthening Displacements at 8.9 m/s $(20\ MPH)$

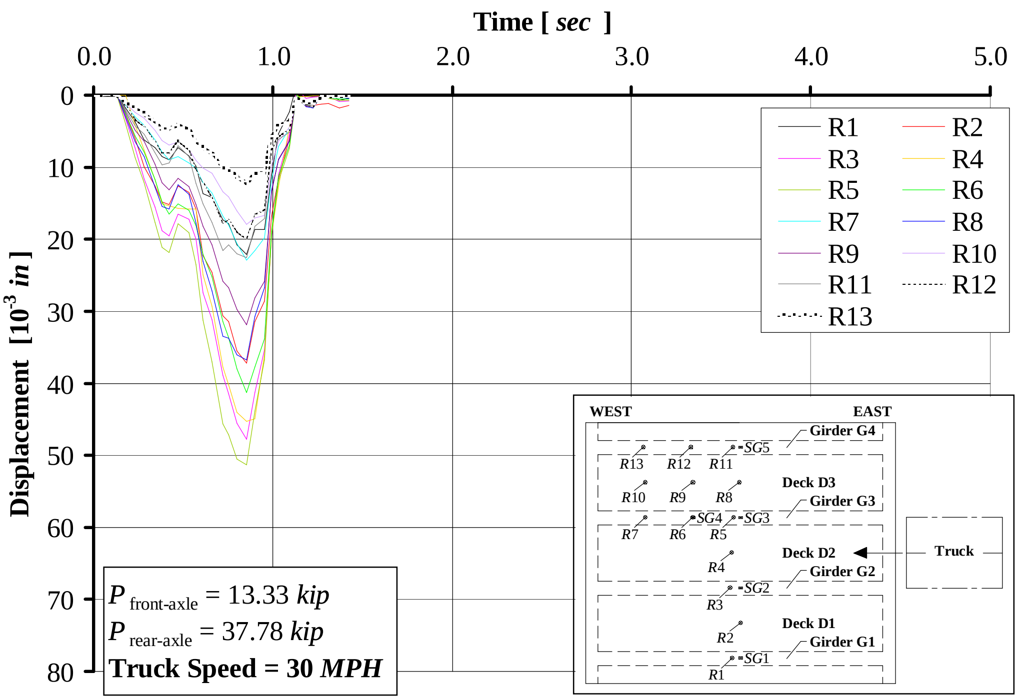

Figure D. 4. After Strengthening Displacements at 13.4 m/s $(30\ MPH)$

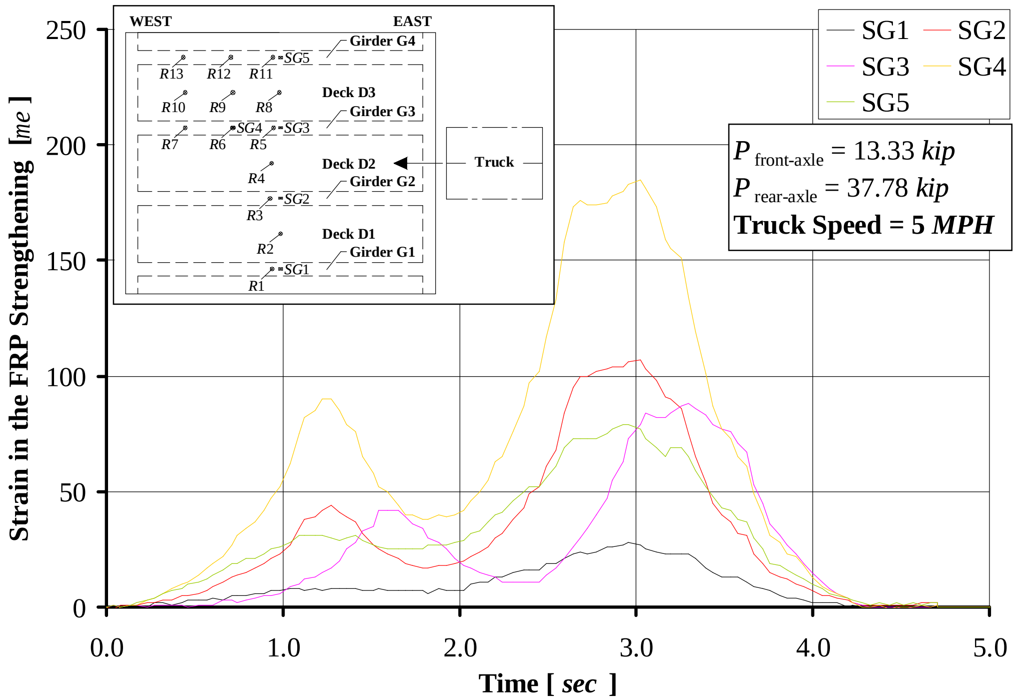

Figure D. 5. After Strengthening Strain in the FRP Laminates at 2.2 m/s $(5\ MPH)$

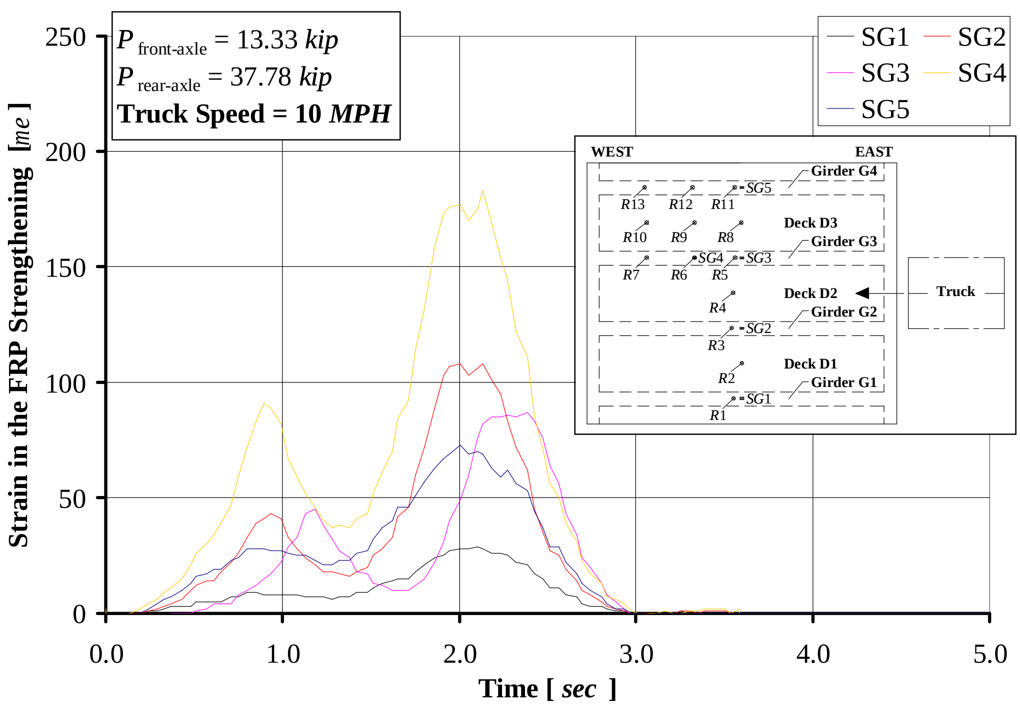

Figure D. 6. After Strengthening Strain in the FRP Laminates at 4.5 m/s $(10\ MPH)$

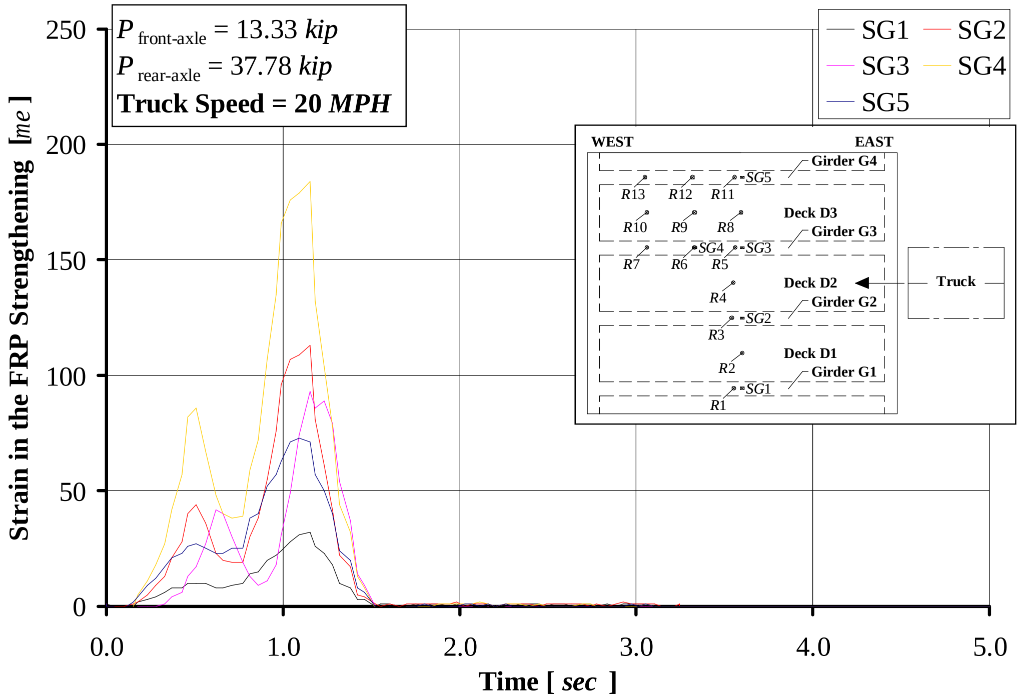

Figure D. 7. After Strengthening Strain in the FRP Laminates at 8.9 m/s $(20\ MPH)$

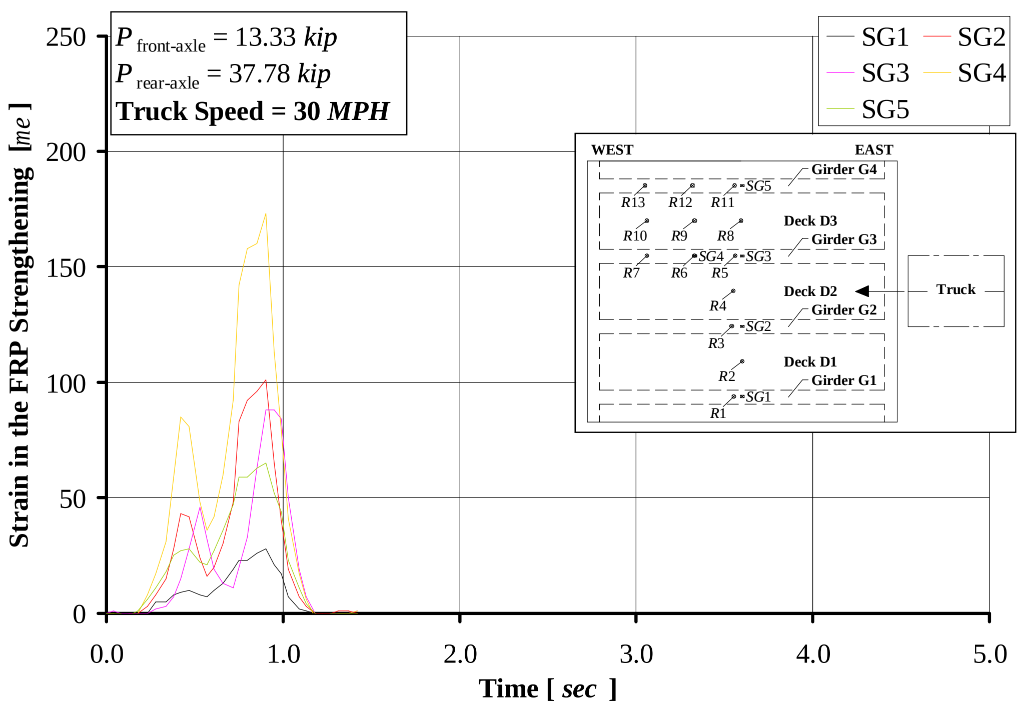

Figure D. 8. After Strengthening Strain in the FRP Laminates at 13.4 m/s $(30\ MPH)$

APPENDIX

E. Installation of the MF-FRP Strengthening System

Figure E. 1. Drilling of the Pre-cured FRP Laminates

Figure E. 2. Positioning of the Pre-cured FRP Laminates

Figure E. 3. Drilling of the Holes in the Concrete

a) Hole Filling with Epoxy b) Bolt Hammering c) Torque Control Clamping

Figure E. 4. Fastening Procedure

Figure E. 5. Bridge No. 1330005 after Strengthening

RESEARCH INVESTIGATION

DESIGN AND IN-SITU LOAD TESTING OF BRIDGE No. 3855006

ROUTE 3855 – PHELPS COUNTY, MO

PREPARED FOR THE
MISSOURI DEPARTMENT OF TRANSPORTATION

IN COOPERATION WITH THE
UNIVERSITY TRANSPORTATION CENTER

Written By:

Andrea Rizzo, MS Candidate

Nestore Galati, Research Engineer

Antonio Nanni, V. & M. Jones Professor of Civil Engineering

CENTER FOR INFRASTRUCTURE ENGINEERING STUDIES

UNIVERSITY OF MISSOURI – ROLLA

Submitted
January 2005

DESIGN AND IN-SITU LOAD TESTING OF BRIDGE No. 3855006

ROUTE 3855 – PHELPS COUNTY, MO

Executive Summary

This report presents the use of Mechanically Fastened - Fiber Reinforced Polymers (MF-FRP) pre-cured laminates for the flexural strengthening of a concrete bridge superstructure. The system consists of pre-cured FRP laminates bolted onto the concrete surface in order to provide the necessary flexural reinforcement to girders and deck. The advantage of the technique is in the fact that it does not require any surface preparation prior to the installation of the FRP.

The bridge selected for this project is a 2-span structure with each span consisting of three reinforced concrete (RC) girders monolithically cast with the deck. In the design, each span was assumed simply-supported by the central pier and abutments. The bridge is located on Route 3855 in Phelps County, MO. The bridge analysis was performed for maximum loads determined in accordance to AASHTO Design specification, 17th edition. The strengthening scheme was designed in compliance with the ACI 440.2R-02 design guide and on previous research work on MF-FRP system.

The retrofitting of the structure was executed in spring 2004. The MF-FRP strengthening technique was easily implemented and showed satisfactory performance. A load test after the strengthening was performed and a Finite Element Method (FEM) analysis was undertaken. The numerical model was able to represent the behavior of the bridge and demonstrated the safety of the proposed posting limit.

ACKNOWLEDGMENTS

The project was made possible with the financial support received from the UMR - University Transportation Center on Advanced Materials, Center for Infrastructure Engineering Studies at the University of Missouri-Rolla and Meramec Regional Planning Commission (MRPC). Master Contractors installed the FRP systems. Strongwell provided the FRP materials.

The authors would like to acknowledge Rick Pilcher, District Liaison Engineer at MoDOT, and Lesley Bennish, Community Development Specialist from Meramec Regional Planning Commission, for their assistance in this project.

TABLE OF CONTENTS

Page

LIST OF ILLUSTRATIONS

LIST OF TABLES

NOMENCLATURE

ADT	Annual Daily Traffic
A_g	Gross Area of a Section
A_s	Area of the Generic Tensile Non-prestressed Steel Reinforcement
$A_{s,slab\ long.}$	Area of the Longitudinal Tensile Non-prestressed Steel Reinforcement of the Deck
$A_{s,slab\ transv.}$	Area of the Transverse Tensile Non-prestressed Steel Reinforcement of the Deck
A_{tire}	Area of the Print of a Wheel according to AASHTO (2002): $A_{tire} = l_{tire} w_{tire}$
A_1	Factor for Dead Loads
A_2	Factor for Live Loads
b_0	Perimeter of Critical Section
b_w	Web Width
$c.o.v._c$	Coefficient of Variation for the Compressive Strength $f_c^{'}$ of Concrete: $c.o.v._c = \frac{f_c^{'}}{SD_c}$
$c.o.v._y$	Coefficient of Variation for the Specified Yield Strength f_y of Non-prestressed Steel Reinforcement: $c.o.v._y = \frac{f_y}{SD_y}$
C	Capacity of the Member
C_E	Environmental Reduction Factor according to ACI 440 Table 7.1: for Carbon Plate Exposed in Exterior Aggressive Ambient $C_E = 0.85$
d	Effective Depth of the Steel Reinforcement for a Generic Section
d_c	Length of the Cantilever Deck
d_g	Spacing between Girders on Center

$d_{slab\ long.}$	Effective Depth of the Longitudinal Tensile Non-prestressed Steel Reinforcement of the Deck
$d_{slab\ transv.}$	Effective Depth of the Transverse Tensile Non-prestressed Steel Reinforcement of the Deck
Di	Pre-cured FRP Laminate Designed for the Strengthening of the Span Si with $i = 1$ or 2
D	Dead Load of the Bridge
E_c	Modulus of Elasticity of Concrete according ACI 318-02 Section 8.5.1: $E_c = 57000\sqrt{f_c^{'}}\ psi$ with $\left[f_c^{'}\right] = \left[psi\right]$
E_f	Modulus of Elasticity of the Pre-cured FRP Laminate
E_s	Modulus of Elasticity of Non-prestressed Steel Reinforcement
E_{LL}	Lane Loads according to AASHTO Section 3.24.3.2 (2002): $E_{LL} = 2E_{WL}$
E_{WL}	Wheel Loads according to AASHTO Section 3.24.3.2 (2002): $E_{WL} = 4 + 0.06S \leq 7\ ft$
$f_c^{'}$	Specified Compressive Strength of Concrete
f_{fu}	Design Tensile Strength of the Pre-cured FRP Laminate: $f_{fu} = C_E f_{fu}^{*}$
f_{fu}^{*}	Guaranteed Tensile Strength of the Pre-cured FRP Laminate as Reported by the Manufacturer
f_y	Specified Yield Strength of Non-prestressed Steel Reinforcement
F_{FRP}	Maximum Axial Load that the Pre-cured FRP Laminate Experiences at Ultimate Conditions
G$i.j$	Girder No. $j = 1, 2..3$ in the Span Si with $i = 1$ or 2
h	Overall Thickness of Member
h_b	Embedment Depth of the Anchor
h_c	Vertical Distance between Supports of the Wall
H_d	Height of the Deck

H_g	Height of the Girders Web
H_o	Height of the Deck Overlay
I	Live Load Impact Factor: $I = \dfrac{50}{l_d + 125} \leq 0.30$ where $[l_d] = [ft]$
$I_{experimental,\, i}$	Live Load Impact Factor Measured during the Load Test after Strengthening in the Pass No. i with $i = Pass\ \#1, Pass\ \#2..Pass\ \#5$
k	Effective Length Factor according to ACI 318-02 Section 14.5.2: $k = 2.0$ for Walls Not Braced against Lateral Translation
l_c	Clear Span of the Slab
l_d	Design Length of the Slab
l_{tire}	Size of the Print of a Wheel in the Longitudinal Direction according to AASHTO (2002)
L	Live Load Applied on the Bridge. The Same Symbol is Used in Some Figures to Indicate the Design Span of the Bridge
M_n	Nominal Moment Strength at Section
M_s	Unfactored Moment due to the Most Demanding Load Condition for a Structural Element
M_u	Ultimate (Factored) Moment due to the Most Demanding Load Condition for a Structural Element
$n_{b,\min}$	Minimum Number of Fastener to Anchor a Pre-cured FRP laminate so that Failure in Tension Controls: $n_{b,\min} = \dfrac{F_{FRP}}{R_b}$
P	Generic Concentrated Load Applied to a Structure
$P_{front-axle}$	Total Load corresponding to the Truck Front Axle
$P_{rear-axle}$	Total Load corresponding to the Truck Rear Axles
P_{H15-44}	Weight of a Rear Axle Wheel of the $H15-44$ Truck
P_n	Nominal Axial Capacity of the Concrete Walls for Unit of Length

R_{ab}	Ultimate (Factored) Axial Load due to the Most Demanding Load Condition for the Two Walls
R_b	Design Shear Capacity of the Connection
Ri	LVDT No. i with $i = 1, 2..10$
RF	Rating Factor
RT	Rating of the Bridge: $RT = RF \cdot W$
S	Spacing of the Supports
Si	Span No. i with $i = 1$ or 2. The Same Symbol is Used to Indicate the Support No. i with $i = 1, 2..3$
SD_c	Standard Deviation for the Specified Compressive Strength $f_c^{'}$ of Concrete
SD_y	Standard Deviation for the Specified Yield Strength f_y of Non-prestressed Steel Reinforcement
SGi	Strain Gauge No. i with $i = 1, 2..8$
t_f	Thickness of the Pre-cured FRP Laminate
T_b	Shear Capacity of the Connection
T_c	Shear Capacity of the Anchor Embedded in Concrete
V_c	Concrete Contribution to the Shear Capacity
V_n	Nominal Shear Strength at Section
$V_{c,i}$	Nominal Shear Strength at Section for Punching Shear Check: $i = 1, 2, 3$
V_s	Unfactored Shear due to the Most Demanding Load Condition for a Structural Element
V_u	Ultimate (Factored) Shear due to the Most Demanding Load Condition for a Structural Element
w_f	Width of the Pre-cured FRP Laminate
w_{tire}	Size of the Print of a Wheel in the Transverse Direction according to

	AASHTO (2002)
W	Weight of the Nominal Truck Used to Determine the Live Load Effect
W_g	Width of the Girders Web
W_r	Width of the Roadway
W_{rc}	Width of the Roadway between Curbs
x	Generic Position of the Truck in the Transverse Direction of the Bridge
z	Distance from the Left Support of the Generic Section
a_s	Coefficient Used in the Punching Shear Check according to ACI 318-02: $a_s = 40$ for Interior Load; $a_s = 30$ for Edge Load; $a_s = 20$ for Corner Load
b_c	Ratio of Long Side to Short Side of the Area over Which the Load is Distributed for Punching Shear Check
b_d	Coefficient as per AASHTO (2002) Table 3.22.1A: $b_d = 1.0$ for Ultimate Conditions and $b_d = 1.0$ for Service Conditions
b_L	Coefficient as per AASHTO (2002) Table 3.22.1A: $b_L = 1.67$ for Ultimate Conditions and $b_L = 1.00$ for Service Conditions
g	Coefficient as per AASHTO (2002) Table 3.22.1A: $g = 1.3$ for Ultimate Conditions and $g = 1.0$ for Service Conditions
$d_{\max}$	Maximum Displacement Experienced during Load Tests
e_{fu}	Design Tensile Strain of the Pre-cured FRP Laminate: $e_{fu} = C_E e^*_{fu}$
e^*_{fu}	Guaranteed Tensile Strain of the Pre-cured FRP Laminate as Reported by the Manufacturer
f	Strength Reduction Factor according to ACI 318-02 Section 9.3: $f = 0.70$ for Axial Load and Axial Load with Flexure for Member without Spiral Reinforcement conforming to ACI 318-02 Section 10.9.3. The Same Symbol is Applied to Indicate the Factors Used to Convert Nominal Values to Design Capacities of Member

f_{punch} Strength Reduction Factor for Punching Shear Check according to ACI 318-02 Section 9.3: $f_{punch} = 0.85$

r_w Ratio of Tensile Non-prestressed Steel Reinforcement: $r_w = \frac{A_s}{b_w d}$

w_u Ultimate Value of Stresses due to Moments and Shear Forces

CONVERSION OF UNITS

1 Inch (in) = $8.333 \cdot 10^{-2}$ Feet (ft)

1 Inch (in) = $2.54 \cdot 10^{-2}$ Meters (m)

1 Foot (ft) = 12 Inches (in)

1 Foot (ft) = $3.048 \cdot 10^{-1}$ Meters (m)

1 Kip (kip) = 4.448222 Kilonewton (kN)

1 Kip (kip) = $4.448222 \cdot 10^{3}$ Newton (N)

1 Kip (kip) = 10^{3} Pounds-Force (lbf)

1 Kip per Square Inch (ksi) = 6.894757 Mega Pascal (MPa)

1 Kip per Square Inch (ksi) = $6.894757 \cdot 10^{6}$ Pascal (Pa)

1 Mile per Hour (MPH) = 4.470 Meter per Second (m/s)

1 Pound-Force (lbf) = 4.448222 Newton (N)

1 Pound-Force (lbf) = $4.448222 \cdot 10^{-3}$ Newton (kN)

1 Pound-Force per Square Inch (psi) = $6.894757 \cdot 10^{-3}$ Megapascal (MPa)

1 Pound-Force per Square Inch (psi) = $6.894757 \cdot 10^{3}$ Pascal (Pa)

1 Ton-Force (ton) = $2 \cdot 10^{3}$ Pounds-Force (lbf)

1 Ton-Force (ton) = 2 Kips (kip)

1. BACKGROUND

1.1. Delta Regional Authority Program Project

In December 2002, as a result of its partnership with University of Missouri, Rolla – University Transportation Center (UMR-UTC), the Meramec Regional Planning Commission (MRPC) received a $193895 grant award from the Delta Regional Authority for bridge improvement projects in Crawford, Dent, Phelps, and Washington Counties.

1.2. Need for the Proposed Project

Transportation infrastructure is one of the major economic development needs for the Meramec Region. Local roads and bridges affect the economic welfare of the region by providing links to the major routes. Local roads and bridges are the collector systems into the larger state highway system for the transport of manufactured products and agricultural goods, accessing employment centers, and bringing travelers and tourists to the region. While many residents are engaged in agriculture and use the roads for farm-to-market routes, a growing number of people are working in cities and living in unincorporated areas relying on rural roads to commute to work. Aging bridges prohibit growth in much of the region because they severely limit access to many communities.

According to the National Bridge Inventory in 1995, 29 percent of county bridges do not meet minimum tolerable conditions to be left as-is. Nationwide, 40 percent of rural bridges are posted as to weight or other travel restrictions. Load postings are defined as the safe loads to cross a bridge. Loads over the posted limit cause damage to the structure and shorten the life of the bridge. Examples of vehicles affected would be school buses, fire trucks and ambulances, commercial truck traffic and large farm equipment. Dump trucks are affected by all load postings according to the Missouri Department of Transportation (MoDOT) and emergency vehicles are affected by most postings. The Federal Highway Administration (FHWA) classifies 32 percent of rural bridges as structurally deficient. Over one-third of the rural bridges in Crawford, Dent, Phelps and Washington counties are considered deficient by MoDOT standards. Much of the problems with local bridges are due to age and obsolete design.

The high cost associated with bridge replacement keeps communities from addressing many bridges. Even the cost to repair bridges is high when using conventional technologies. Maintaining and upgrading transportation infrastructure is a challenge for rural regions because of the sparse density of residents and number of roads and bridges running throughout the area. The low Average Daily Traffic (ADT) on most rural bridges seems to make the cost for bridge replacement ineffective. Low-volume bridges make it difficult for rural areas to compete for grant funding to assist with bridge replacements because rural areas are in competition with larger metropolitan areas. Rural areas are at a disadvantage because more populated areas can incorporate additional aspects of transportation, such as public transit and major economic impact, in grant proposals.

1.3. Description of the Project

Fiber-reinforced polymer (FRP) materials have recently emerged as a practical alternative for construction and renovation of bridges. Advantages of FRP materials are that they resist corrosion, long outlive conventional materials, and have high strength-to-weight ratio. Placement of FRP material is in two forms, near-surface mounted bars and externally-bonded laminates, and the materials are applied on the underside of bridges. UMR has been working with FRP technology on projects around the state and in the Meramec Region. Projects have included strengthening of bridges in Boone County, Phelps County, and St. Louis. Bridges constructed with FRP materials were installed in the city of St. James, MO. FRP strengthening of bridges has had significant cost and time savings over conventional methods.

MRPC is working with local elected officials, UMR and MoDOT to identify and develop 31 bridge strengthening projects in the four-county area of Crawford, Dent, Phelps and Washington. Counties provide MRPC a list of bridge needs and MRPC staff reviews the list with UMR and MoDOT representatives to determine bridges that would be prime candidates for FRP strengthening technology. MoDOT will also review the bridges to determine those that have previously been inspected and found to be structurally deficient or require a load posting. MoDOT will also help determine if projects can help the counties earn soft-match credit towards larger projects using Bridge Replacement Off-system (BRO) funds. MRPC will then determine the economic development impact each bridge has on the region and prioritize projects based on this ranking. The University will prepare design specifications for applying FRP material to each bridge. Contractors will be competitively procured to install the FRP material and those contractors will be required to have or receive certification from UMR for FRP technology training. The University will monitor the application of FRP material to each bridge. Each county may use a third party engineering firm to seal the design and monitor the contractor's activity to ensure that the results of the FRP technology are accurate and valid. Bridges may be tested for load posting before and after the strengthening process to determine the effect of the activity on the strength of each bridge. It is anticipated that strengthening will allow for the load postings to be removed or significantly raised for the structures subjected to such limitations.

1.4. Complementing Existing Regional Plans

Through MRPC, each county completed a Strategic Plan in 2000-2001 to identify current needs and develop a plan of action. This information became part of the region's Comprehensive Economic Development Strategy. Transportation infrastructure was a common need found in all counties. A top priority for economic development was determined to be the need for a better transportation system. Each county identified an objective to improve existing infrastructure. Activities proposed to address the transportation system included encouraging transportation development to enhance economic growth. Most counties found that tourism is directly related to the transportation system and if the tourism industry is to be promoted in the region, the transportation system must be addressed. Counties determined that activities must include improvements to local roads and bridges as well as state routes.

Each community will be required to cover 30 percent of the cost to reinforce each bridge addressed in their jurisdiction. Communities are also responsible for using a third party engineering firm to seal the University's design work and inspect the work of contractor(s) hired to apply the FRP reinforcement. The bridges to be addressed are not deficient due to poor maintenance, but to age and structural obsolescence. Once strengthened, the bridges will have an increased life by removing or upgrading the current load postings. Each community budgets for road and bridge maintenance and this will not change with the proposed project. Strengthening is the only alternative to replacement, and should not require additional maintenance from the community's road crews.

An improved transportation system is a severe need all across the state, including these four Delta counties of the Meramec Region. The transportation system, bridges in particular, was found to be a top priority in the strategic plans for each county as part of the Comprehensive Economic Development Strategy developed for the region. Transportation was directly related to economic development in each county and for the region. The transportation infrastructure of the region has a direct impact on economic development by providing the means necessary to transport raw materials and products, employees to/from work and consumers to/from business centers.

1.5. Impact of the Project

Strengthening bridges will allow for communities to open bridges to more traffic and facilitate the movement of freight, farm equipment and products, and commuter traffic. Counties will add new strength to bridges that otherwise would need to be replaced or closed due to posting limits. Major employment centers are located in each of the four counties. The industries are dependent upon moving their goods and, in the Meramec Region, goods move only via the road system. Major employment centers rely on the local transportation system to allow access for employees and connecting with larger transportation systems for moving materials and products. Such industries include Doe Run Inc., Salem Memorial District Hospital and US Food Service in Dent County, Dana Brake Parts Inc., Meramec Industries Inc., and Missouri Baptist Hospital in Crawford County, Briggs & Stratton Corp., Boys & Girls Town of Missouri and Wal-Mart Distribution Center in Phelps County and Red Wing Shoe Co., Georgian Gardens Nursing Home and YMCA of the Ozarks in Washington County.

Up to 31 county bridges may be strengthened using the FRP technology. Strengthening will remove load postings or significantly increase postings so that bridges will be open to more traffic. These bridges will allow for more access from county roads to major routes running through the area, directly impacting the economic development potential of the region.

2. INTRODUCTION

This report summarizes the procedures used for the upgrade of the Bridge No. 3855006 (see Figure 2.1), located in Phelps County (Route 3855), MO. The bridge is not actually load posted.

Figure 2.1. Bridge No. 3855006

The total length of the bridge is $7874\ mm\ (25\ ft\ 10\ in)$ and the total width of the deck is $6756\ mm\ (22\ ft\ 2\ in)$. The structure is a 2-span continuous beam and each span consists of three reinforced concrete (RC) girders monolithically cast with a $190\ mm\ (7.5\ in)$ deep deck.

2.1. Objectives

The primary objectives of this document are to analyze the bridge superstructure and to provide the design calculations for its strengthening using a Mechanically Fastened Fiber-Reinforced Polymer system (MF-FRP). The advantage system consists of pre-cured FRP laminates bolted onto the concrete surface in order to provide the necessary flexural reinforcement to the girders and deck. The strength of the technique is in the fact that it does not require any surface preparation prior to the installation of the FRP.

2.2. Bridge Conditions

Prior to the strengthening of the bridge, a detailed investigation was required to determine the initial conditions of the bridge and the properties of the constituent materials. The details of the bridge reinforcement and material properties were unknown due to the unavailability of the bridge plans. As a consequence, at the onset of the project, these properties were determined in-situ, based on visual and Non Destructive Testing (NDT) evaluation.

From visual observations, some concrete spalling along the longitudinal edges of the bridge was observed. The girders and deck showed traces of steel rebar corrosion (see Figure 2.2-a). As a consequence of the insufficient amount of longitudinal reinforcement, all the girders were visibly cracked at mid-span (see Figure 2.2-b). In addition, some bars on the side and at the bottom of the girders were completely exposed with clear signs of corrosion (see Figure 2.3). The abutments appeared in good conditions except for some vertical cracks running down from the edges of the girders across the entire height of the abutments (see Figure 2.4).

a) Girders and Deck

b) Bending Cracks in the Girders

Figure 2.2. Condition of the Superstructure

Furthermore, it was observed that the two central girders are misaligned (see Figure 2.9). The real location of the steel reinforcement in the deck and girders was accurately determined by using a rebar locator. Figure 2.5 shows the layout of the longitudinal reinforcement. For most of the girders it was not possible to detect steel reinforcement at the bottom of the section. In addition, shear reinforcement was not found.

a) Exposed Bar in the Lateral Side b) Exposed Bar in the Bottom Side

Figure 2.3. Condition of the Girders

Figure 2.4. Condition of the Abutments

In order to determine the exact position and amount of longitudinal reinforcement for the girders, concrete was chipped off at different locations.

The longitudinal reinforcement at the mid-span for the central girder for each span is presented in Figure 2.6. It can be stated that the bridge was originally strengthened with four bars $\#4$ $(12.7\ mm\ (0.5\ in)$ diameter). The position of the reinforcement was quite different in the two cases.

a) Lateral Girder b) Central Girder

Figure 2.5. Layout of the Longitudinal Reinforcement in the Girders

At the mid-span section of the central girder of Span S1 (Girder G1.2 in Figure 2.6-a), there were two distinguished layers: the first one had a $25.4\ mm\ (1\ in)$-cover and the second one was at $216\ mm\ (8\frac{1}{2}\ in)$ from the bottom side. At the mid-span section of the central girder of Span S2 (Girder G2.2 in Figure 2.6-b), the bars were regrouped with the centroid at $214\ mm\ (8\frac{7}{16}\ in)$ from the bottom side of the girder; the closest bar to the bottom of the section was located at $159\ mm\ (6\frac{1}{4}\ in)$.

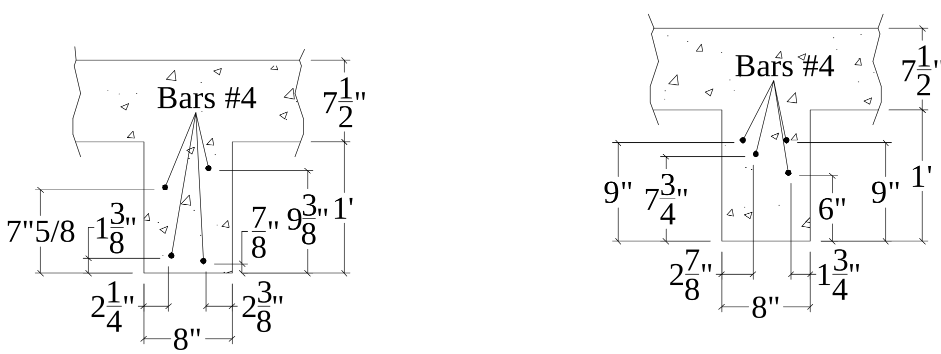

a) Mid-span Section 1 (Girder G1.2) b) Mid-span Section 2 (Girder G2.2)

Figure 2.6. Details of the Sections Chipped Off to Find Longitudinal Reinforcement

In order to determine the amount of shear reinforcement, $76.2\ mm\ (3\ in)$ deep, $254\ mm\ (10\ in)$ long cuts were made along the girders close to the abutments at $127\ mm\ (5\ in)$ from the bottom of the section (see Figure 2.7). No shear reinforcement was found in any of the girders.

The geometry of the bridge is summarized in Table 2.1. Figure 2.8 and Figure 2.9 show the longitudinal and plan view of the bridge. Figure 2.9 also shows the position from where the concrete cores where extracted and the longitudinal and transverse steel reinforcement of the deck. Cross sections for the two spans are summarized in Figure 2.10.

a) Central Girder b) Lateral Girder

Figure 2.7. Concrete Chipped Off to Find Shear Reinforcement

Table 2.1. Geometry of the Bridge

Span	S1	S2
Clear Span	$l_c = 3696\ mm\ (12\ ft\ 1\frac{1}{2}\ in)$	$l_c = 3581\ mm\ (11\ ft\ 9\ in)$
Design Length	$l_d = 3899\ mm\ (12\ ft\ 9\frac{1}{2}\ in)$	$l_d = 3785\ mm\ (12\ ft\ 5\ in)$
Deck Height	$H_d = 190\ mm\ (7.5\ in)$	$H_d = 190\ mm\ (7.5\ in)$
Girder Web Height	$H_g = 305\ mm\ (12\ in)$	$H_g = 305\ mm\ (12\ in)$
Girder Width (Average Value)	$W_g = 203\ mm\ (8\ in)$	$W_g = 203\ mm\ (8\ in)$
Max Distance between Girders On Centers	$d_g = 2480\ mm\ (8\ ft\ 1\frac{5}{8}\ in)$	$d_g = 2581\ mm\ (8\ ft\ 5\frac{5}{8}\ in)$
Max Cantilever Arm	$d_c = 743\ mm\ (2\ ft\ 5\frac{1}{4}\ in)$	$d_c = 724\ mm\ (2\ ft\ 4\frac{1}{2}\ in)$
Roadway Width	$W_r = 6756\ mm\ (22\ ft\ 2\ in)$	
Curb-to-Curb Roadway Width	$W_{rc} = 6452\ mm\ (21\ ft\ 2\ in)$	
Overlay Height	$H_o = 0\ mm\ (0\ in)$	

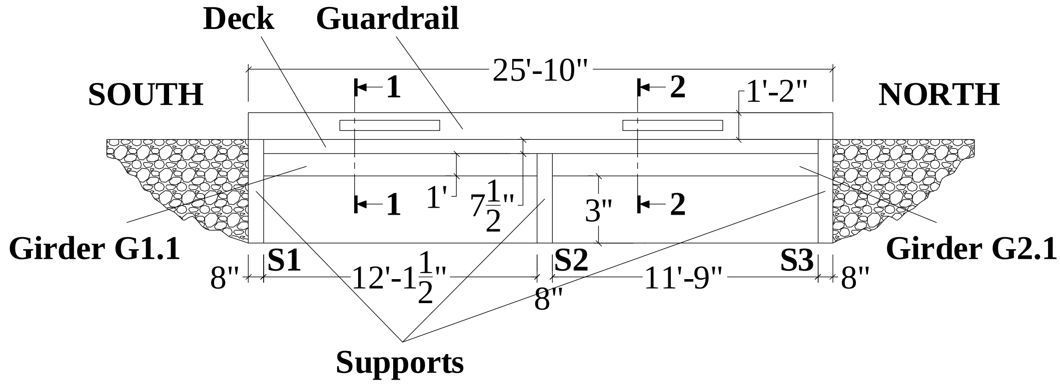

Figure 2.8. Longitudinal View of the Bridge

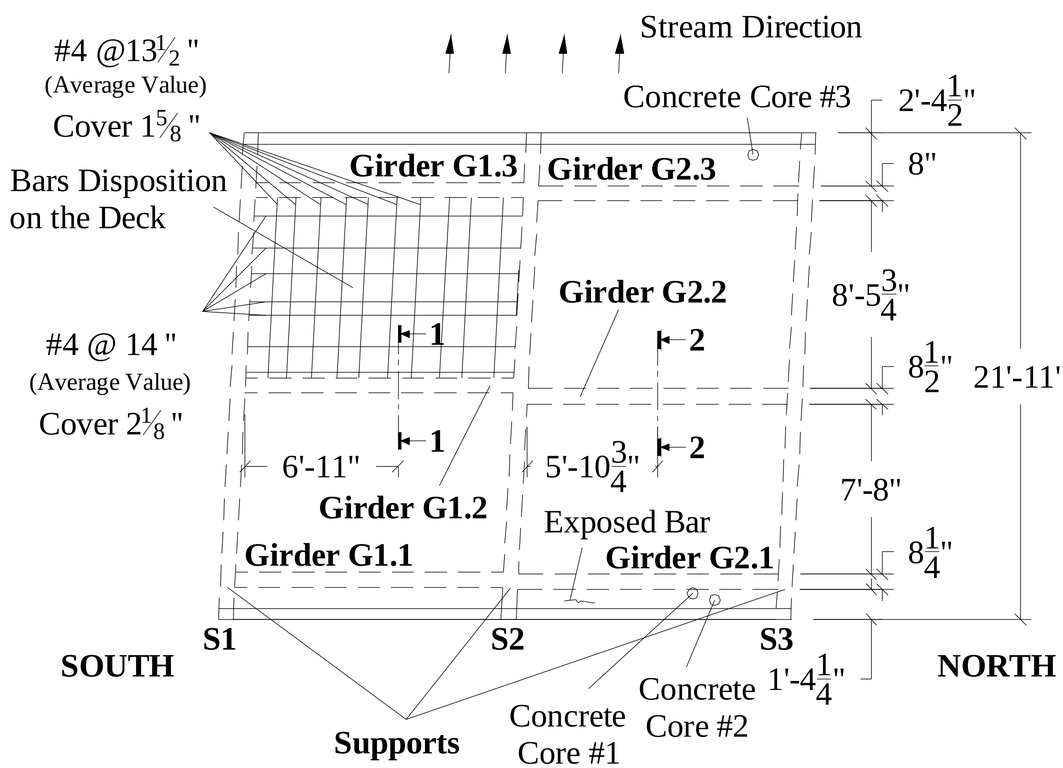

Figure 2.9. Plan View of the Bridge

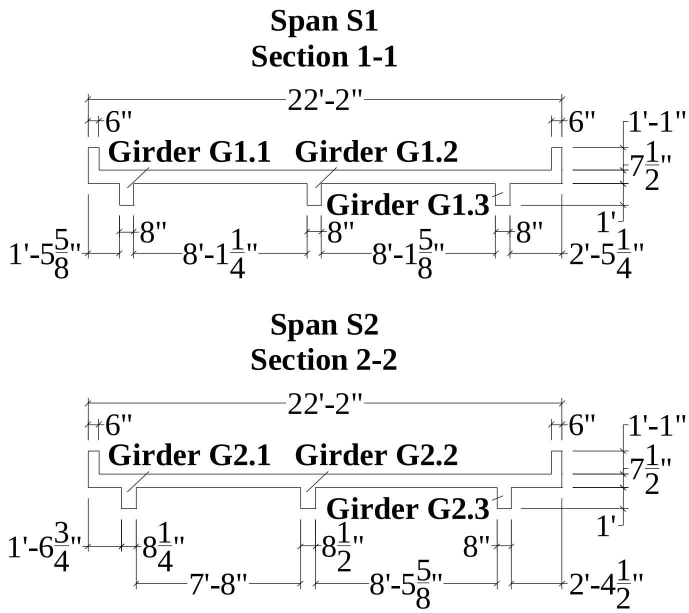

Figure 2.10. Geometry of the Two Spans Section

Two concrete cores were drilled from the deck (see Figure 2.11-a), and they were tested in compliance with ASTM C39/C39M-1 and ASTM C42/C42M-99 (see Figure 2.11-b). The following results were found:

- Average Compression Strength: $f_c^{'} = 45.3\ MPa\ (6575\ psi)$;
- Standard Deviation: $SD_c = 1.5\ MPa\ (219\ psi)$;
- Variance: $c.o.v._c = 100\dfrac{SD_c}{f_c^{'}} = 3.3\%$.

Based on the experimental results, a compression strength of $41.4\ MPa\ (6000\ psi)$ was conservatively assumed for design.

a) Coring b) Compression Tests

Figure 2.11. Material Characterization of the Concrete

Concrete cover and size of longitudinal and transverse steel bars in the deck were determined from the concrete cores (see Figure 2.12-a) as follows:

- Longitudinal Direction

  $\#4$ (12.7 mm $(0.5\ in)$ diameter) steel bars

  average spacing: $355.6\ mm$ $(14\ in)$ on center

  clear concrete cover: $54\ mm$ $(2\,1/8\ in)$;

- Transverse Direction

  $\#4$ (12.7 mm $(0.5\ in)$ diameter) steel bars

  average spacing: $343\ mm$ $(13\,1/2\ in)$ on center

  clear concrete cover: $41.2\ mm$ $(1\,5/8\ in)$.

Concrete cover, number and size of flexural and shear reinforcement for the girders were determined by chipping off concrete at different locations (see Figure 2.12-b). As mentioned before, the longitudinal reinforcement is not the same for each girder and the cover is not constant along the span. Table 2.2 summarized the flexural reinforcement for the section at the mid-span of the girders. There is no shear reinforcement in the girders.

Table 2.2. Flexural Reinforcement in the Mid-span of the Girders

Girder	Number of steel bars #4 (12.7 *mm* (0.5 *in*) diameter)	Clear Concrete Cover [*mm*] ([*in*])
G1.2	2	25.4 (1.0)
	1	193.7 (7⅝)
	1	238.1 (9⅜)
G2.2	1	152.4 (6.0)
	1	196.8 (7¾)
	2	228.6 (9.0)
G1.1 – G1.3 G2.1 – G2.3	2	152.4 (6.0)
	2	228.6 (9.0)

The mechanical properties of the steel reinforcement were determined by testing two specimens cut from an exposed bar found in one of the abutments. They were tested according to ASTM A615 and ASTM A955 (see Figure 2.12-c). The following results were found:

- Average Yield Strength: $f_y = 455.7\ MPa\ (66092\ psi)$;
- Standard Deviation: $SD_y = 10.3\ MPa\ (1497\ psi)$;
- Variance: $c.o.v._y = 100\dfrac{SD_y}{f_y} = 2.3\%$.

Based on the experimental results, a yield value of $455\ MPa\ (66\ ksi)$ was assumed for design.

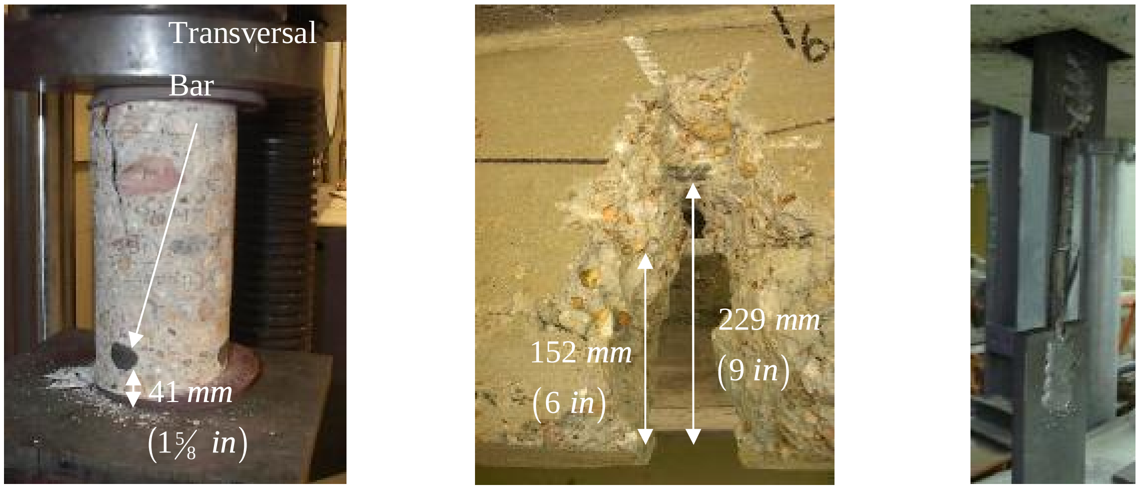

a) Pieces of Bars in a Core b) Broken Section of a Girder c) Tension Test

Figure 2.12. Material Characterization of the Steel Bars

2.3. Conclusions

The layout and amount of longitudinal reinforcement is responsible for the cracking phenomena observed on the girders. Since the girders do not have sufficient longitudinal flexural reinforcement and no shear reinforcement, the bridge can be structurally modeled as a slab supported by the abutments. In addition, since it is not possible to guarantee the flexural continuity across the central abutment, the bridge can be conservatively modeled as two slabs simply-supported over the abutments.

The analysis and design of the bridge presented in the following sections is performed according to the MoDOT Bridge Manual, to the experimental results attained at the University of Wisconsin-Madison (Bank et al., 2002) and at UMR. The assumed load configurations are consistent with the AASHTO Specifications (AASHTO, 2002).

3. STRUCTURAL ANALYSIS

3.1. Load Combinations

For the structural analysis of the bridge, the definitions of design truck and design lane are necessary. This will be addressed in the next section.

Ultimate values of bending moments and shear forces are obtained by multiplying their nominal values with the dead and live load factors and by the impact factor according to AASHTO (2002) as shown in equation (3.1):

$$w_u = g\left[b_d D + b_L (1+I) L\right] \tag{3.1}$$

where

D	is the dead load;
L	is the live load;
g , b_d , b_L	are coefficients as per AASHTO (2002) Table 3.22.1A:
	ultimate conditions $\Rightarrow g = 1.3$, $b_d = 1.0$, $b_L = 1.67$;
	service conditions $\Rightarrow g = 1.0$, $b_d = 1.0$, $b_L = 1.00$;
I	is the live load impact calculated as follows:

$$I = \frac{50}{l_d + 125} = \frac{50}{12.792 + 125} = 0.36 \le 0.30 \tag{3.2}$$

and $l_d = 12\ ft\ 9\frac{1}{2}\ in = 12.792\ ft$ $(3899\ mm)$ represents the span length from center to center of support. The impact factor should not be larger than 0.30, and therefore the latter value is assumed for the design.

3.2. Design Truck and Design Lanes

Prior to the design of the strengthening, the analysis of the bridge was conducted by considering a H15-44 truck load (which represents the design truck load as per AASHTO, 2002 Section 3.7.4) having geometrical characteristics and weight properties shown in Figure 3.1.

According to AASHTO Section 3.6.3 (2002), roadway widths between 6096 and $7315\ mm$ $\left(20 \text{ and } 24\ ft\right)$ shall have two design lanes, each one equal to one-half of the roadway width. However, in this case, the low value of the Annual Daily Traffic ($ADT = 100$) of the bridge allows to deal just with one design lane. To be noted that the centerline of the wheels of the rear axle shown in Figure 3.1 is located $305.0\ mm$ $\left(1.0\ ft\right)$ away from the curb as specified in AASHTO (2002) for slab design.

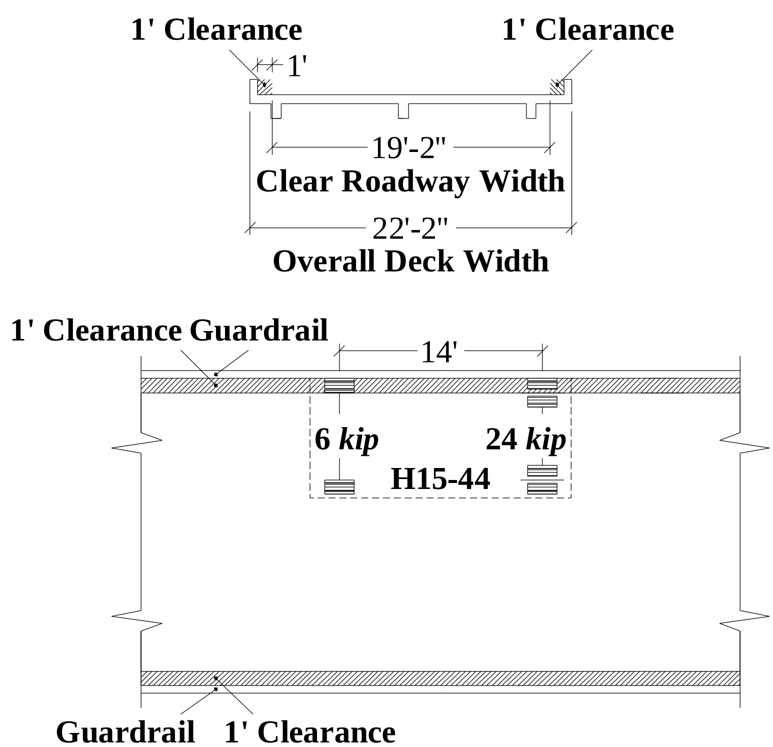

Figure 3.1. Truck Load and Truck Lanes

Two loading conditions are required to be checked as laid out in Figure 3.2.

The H15-44 design truck load (Figure 3.2-a) has a front axle load of $26.7\ kN\ (6.0\ kip)$ and rear axle load located $356\ mm\ (14\ ft)$ behind the drive axle.

The design lane loading condition consists of a load of $2.1\ kN\ (0.48\ kip)$ per linear foot, uniformly distributed in the longitudinal direction with a single concentrated load so placed on the span as to produce maximum stress. The concentrated load and uniform load are considered to be uniformly distributed over a $3048\ mm\ (10.0\ ft)$ width on a line normal to the center of the lane. The intensity of the concentrated load is represented in Figure 3.2-b for both bending moments and shear forces. This load shall be placed in such positions within the design lane as to produce the maximum stress in the member.

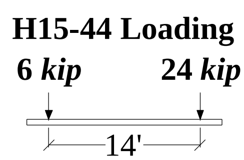

a) Design Truck (H15-44)

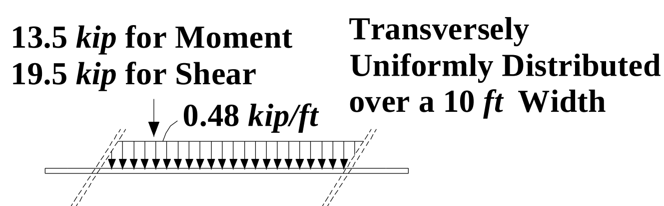

b) Design Lane

Figure 3.2. Loading Conditions

3.3. Slab Analysis

As already mentioned, the flexural reinforcement of the girders was not properly placed and there was no shear reinforcement. Therefore, the analysis was conservatively conducted by neglecting the presence of the girders. In addition, since it was not possible to detect the presence of longitudinal reinforcement in the negative moment region of the deck, the flexural continuity of the deck over the central abutment was conservatively neglected. This led to model the deck as a simply-supported slab between two abutments.

The width used in the analysis and design to distribute the loads was calculated following AASHTO Section 3.24.3.2 (2002) for a one-way slab system. Equations (3.3) and (3.4) give the distribution widths, E_{WL} and E_{LL} respectively for wheel and lane loads, where S represents the spacing of the supports ($[S]=[ft]$).

$$E_{WL} = 4 + 0.06S \leq 7.0\, ft \ \left(2133\, mm\right) \tag{3.3}$$

$$E_{LL} = 2E_{WL} \tag{3.4}$$

Assuming $S = l_d$, it results:

$$\begin{cases} E_{WL} \cong 57\ \mathit{in}\ \left(1448\ mm\right) \\ E_{LL} \cong 114\ \mathit{in}\ \left(2896\ mm\right) \end{cases}.$$

As obtained from the structural analysis, Table 3.1 summarizes the results in terms of unfactored and factored bending moments (M_s and M_u) and shear forces (V_s and V_u). The maximum values, found considering the positions of the load that produces the worst condition (see Figure 3.3) for the structure (i.e., varying the position of the truck along the span of the bridge), are adopted for design. Figure 3.4 and Figure 3.5 show respectively the bending moment M_u and the shear V_u envelopes due to the load obtained, taking for each section (at the distance z from the left support) the maximum value given by the two loading conditions: the worst load condition is that one related to the truck load design.

Table 3.1. Bending Moments and Shear Forces per Foot of Bridge Deck

Loading Condition	*Unfactored Moment*[a)] M_s $\left[\frac{kN \cdot m}{m}\right]$ $\left(\left[\frac{kip \cdot ft}{ft}\right]\right)$	*Factored Moment*[a)] M_u $\left[\frac{kN \cdot m}{m}\right]$ $\left(\left[\frac{kip \cdot ft}{ft}\right]\right)$	*Unfactored Shear*[b)] V_s $\left[\frac{kN}{m}\right]$ $\left(\left[\frac{kip}{ft}\right]\right)$	*Factored Shear*[b)] V_u $\left[\frac{kN}{m}\right]$ $\left(\left[\frac{kip}{ft}\right]\right)$
Dead Load	9.061 (2.037)	11.779 (2.648)	9.296 (0.637)	12.084 (0.828)
H15-44 Load Design Condition *Number of Lanes* = 1				
Truck Design	35.804 (8.049)	101.055 (22.718)	36.733 (2.517)	103.675 (7.104)
Total	44.865 (10.086)	*112.834* (*25.366*)	46.029 (3.154)	*115.759* (*7.932*)
Lane Design	23.751 (5.299)	66.523 (14.955)	32.938 (2.257)	92.963 (6.370)
Total	32.812 (7.336)	*78.302* (*17.603*)	42.234 (2.894)	*42.234* (*7.198*)

a) Computed at a cross-section in the middle of the span.
b) Computed at a cross-section in the middle of the support.

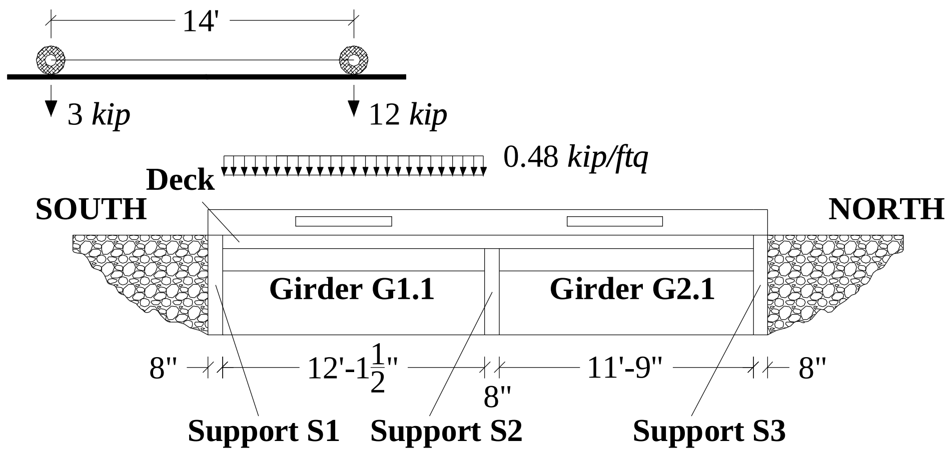

Figure 3.3. Slab Load Conditions

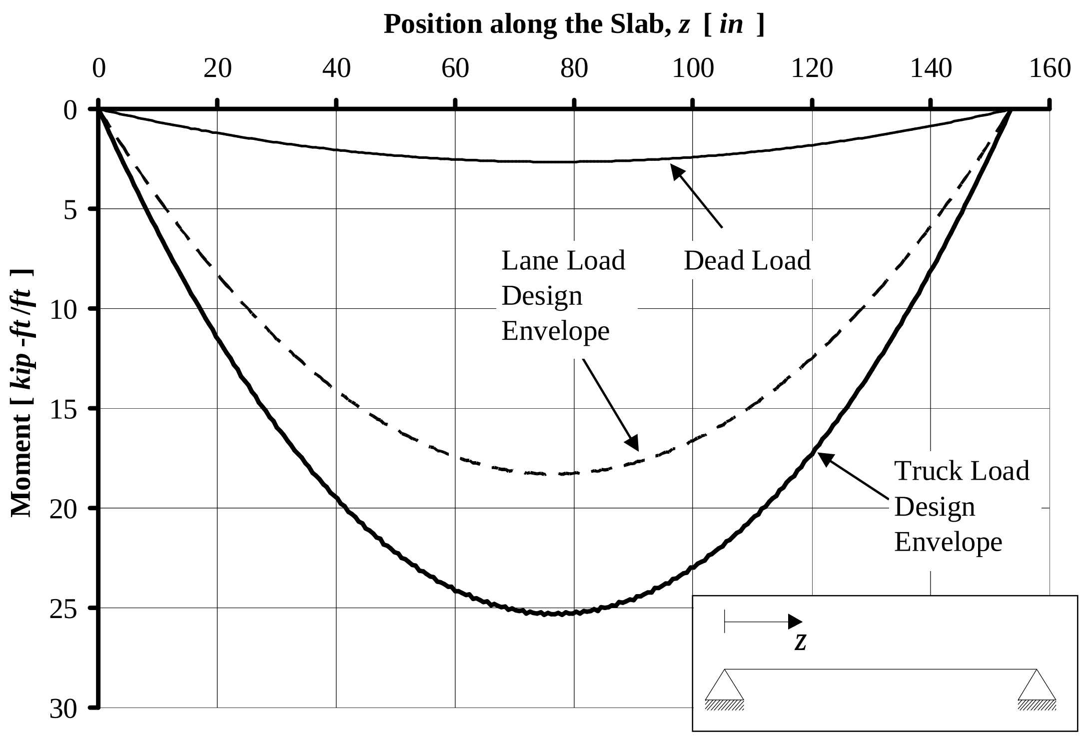

Figure 3.4. Slab Bending Moment Diagrams Envelopes

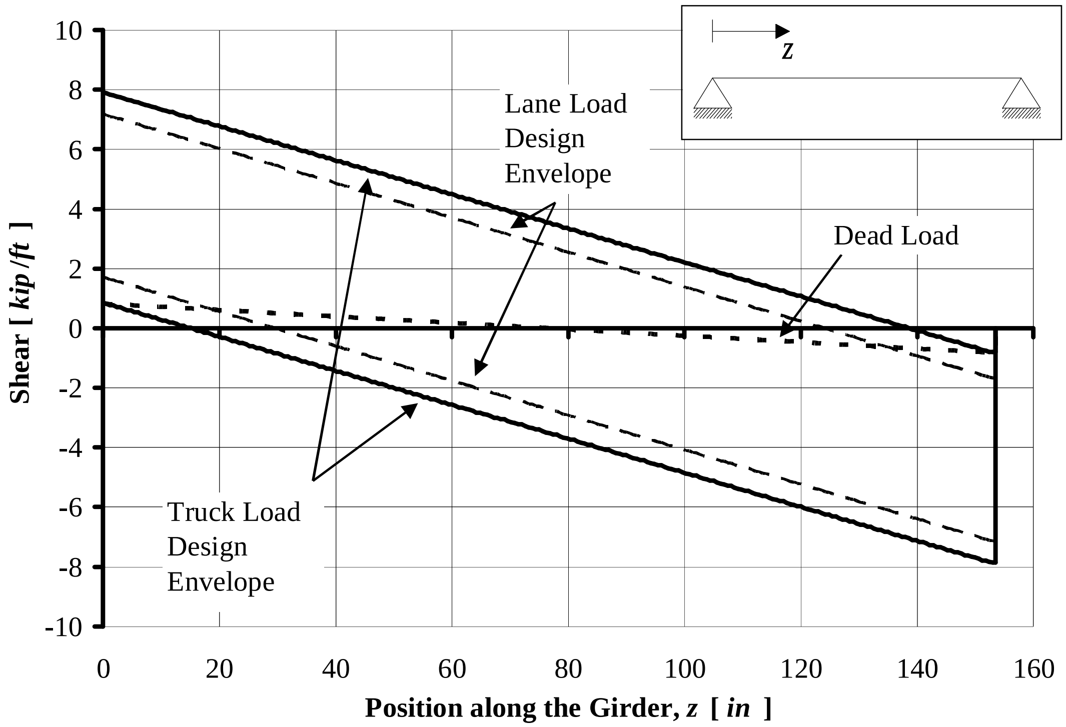

Figure 3.5. Slab Shear Diagrams Envelopes

3.4. Analysis of the Abutments

The abutment can be analyzed as a wall loaded in its plane. According to ACI 318-02 Section 14.5.2, design axial load strength ϕP_n for a wall of solid rectangular cross section with resultant of all factored loads located within the middle third of the overall thickness of the wall is given by

$$\phi P_n = 0.55\phi f_c^{'} A_g \left[1-\left(\frac{kh_c}{32h}\right)^2\right] \cong 2773\ \frac{kN}{m}\ \left(190\ \frac{kip}{ft}\right) \tag{3.5}$$

where

A_g is the gross area of the section;

h is the overall thickness of member;

h_c is the vertical distance between supports;

k is the effective length factor ($k = 2.0$ for walls not braced against lateral translation;

$f = 0.70$ is the strength reduction factor.

The worst loading condition comes out by considering two times the maximum shear demand over the central abutment:

$$R_{ab} = 2V_u = 232 \ \frac{kN}{m} \ \left(15.9 \ \frac{kip}{ft}\right).$$

Since $R_{ab} < f P_n$, the abutments do not need further analysis.

4. DESIGN

4.1. Assumptions

Mechanically-Fastened FRP laminate design is carried out according to the principles of ACI 440.2R-02 (ACI 440 in the following). The properties of concrete, steel and FRP laminates used in the design are summarized in Table 4.1. The concrete and steel properties are obtained by testing of samples while the FRP properties are guaranteed values.

The f factors used to convert nominal values to design capacities are obtained as specified in AASHTO (2002) for the as-built and from ACI 440 for the strengthened members.

Table 4.1. Material Properties

Concrete	*Steel*		*FRP - SAFSTRIP*			
Compressive Strength $f_c^{'}$ $[MPa]$ $([psi])$	Yield Strength f_y $[MPa]$ $([ksi])$	Modulus of Elasticity E_s $[GPa]$ $([ksi])$	Tensile Strength f_{fu}^{*} $[MPa]$ $([ksi])$	Modulus of Elasticity E_f $[GPa]$ $([ksi])$	Thickness t_f $[mm]$ $([in])$	Width w_f $[mm]$ $([in])$
41.4 (6000)	455.0 (66)	200.0 (29000)	588.8 (85.4)	60.7 (8800)	3.175 (0.125)	101.6 (4.00)

Material properties of the FRP reinforcement reported by manufacturers, such as the ultimate tensile strength, typically do not consider long-term exposure to environmental conditions, and should be considered as initial properties. FRP properties to be used in all design equations are given as follows (ACI 440):

$$\begin{aligned} f_{fu} &= C_E f_{fu}^{*} \\ e_{fu} &= C_E e_{fu}^{*} \end{aligned} \tag{4.1}$$

where f_{fu} and e_{fu} are the FRP design tensile strength and ultimate strain considering the environmental reduction factor C_E as given in Table 7.1 (ACI 440), and f_{fu}^{*} and e_{fu}^{*} represent the FRP guaranteed tensile strength and ultimate strain as reported by the manufacturer (see Table 4.1).

The maximum strength that the MF-FRP strengthening can develop depends on the capacity of the connection bolt-strip and, therefore, on the number of fasteners used.

In order to mechanically fasten the FRP laminate to the concrete, the optimal solution in terms of mechanical behavior of the connection was found as a result of an experimental program conducted at UMR. The chosen fastening system consisted of:

- Concrete wedge anchor (diameter $9.525\ mm\ \left(3/8\ in\right)$ and total length $57.15\ mm\ \left(2\,1/4\ in\right)$ - Figure 4.1). The shear capacity T_c of the anchor embedded in the concrete depends upon the embedment depth h_b and the strength of the concrete $f_c^{'}$. The shear strength of the anchor, T_b, becomes equal to T_c with a value of $26.7\ kN\ \left(6.0\ kip\right)$ when $f_c^{'} = 41.4 MPa\ \left(6000\ psi\right)$ and $h_b = 38.1\ mm$ $\left(1\,1/2\ in\right)$;
- Steel washer (inner diameter $11.112\ mm\ \left(7/16\ in\right)$, outer diameter $25.4\ mm\ \left(1\ in\right)$ and thickness $1.587\ mm\ \left(1/16\ in\right)$ - Figure 4.1);
- Epoxy between the washer and the FRP and throughout the hole on the FRP.

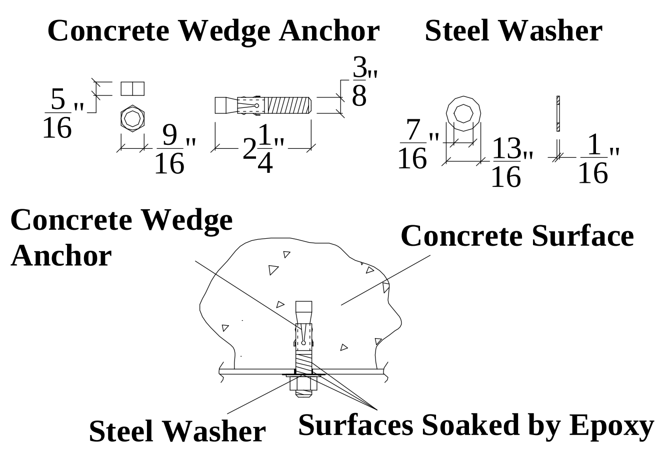

Figure 4.1. Details of the Connection Concrete-FRP

Bond tests on the connection FRP-fastener showed that at the ultimate conditions, the applied load is uniformly distributed between all the fasteners. In addition, it was observed that for concrete having an $f_c^{'} \geq 27.6\ MPa\ \left(4000\ psi\right)$, the failure mode of the connection is due to the bearing of the FRP. The experimental ultimate load supported by this connection was found to be $14.0\ kN\ \left(3.15\ kip\right)$. For design purposes a safety factor equal to 1.25 was assumed and therefore the design capacity of the connection is $R_b = 11.1\ kN\ \left(2.5\ kip\right)$.

Under these assumptions, the minimum number of fasteners $n_{b,\min}$ to anchor each FRP strip so that failure of the FRP controls, is given by:

$$n_{b,\min} = \frac{F_{FRP}}{R_b} \tag{4.2}$$

where F_{FRP} is the maximum load that the FRP strip experiences at ultimate conditions. Assuming $C_E = 0.85$ (i.e., carbon plate exposed in exterior aggressive ambient) and taking into account the net area of the strip (i.e., subtraction of the area lost to insert the bolt), from equation (4.2) the minimum number of bolts to reach the ultimate capacity of the FRP strip is 26. If fewer bolts are used, the failure would occur at the connection (i.e. bearing of the FRP strip).

4.2. Superstructure Design

4.2.1. Assumptions

The geometrical properties and the internal steel flexural reinforcement of the design cross section are summarized in Figure 4.2 and Table 4.2.

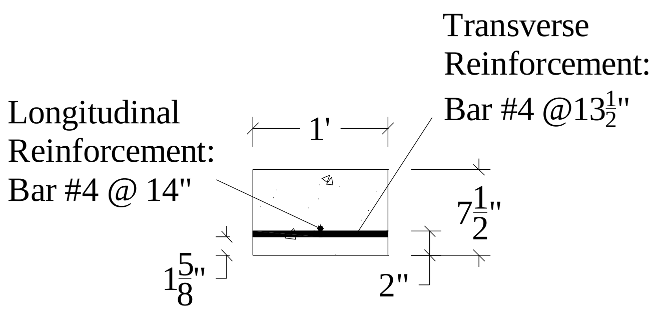

Figure 4.2. Slab Un-strengthened Section

Table 4.2. Geometrical Properties and Internal Steel Reinforcement

Slab Thickness	Slab Longitudinal Tensile Steel Area	Effective Depth	Slab Transverse Tensile Steel Area	Effective Depth
H_d $[mm]$ $([in])$	$A_{s,slab\ long.}$ $[mm^2]$ $([in^2])$	$d_{slab\ long.}$ $[mm]$ $([in])$	$A_{s,slab\ transv.}$ $[mm^2/m]$ $([in^2/ft])$	$d_{slab\ transv.}$ $[mm]$ $([in])$
190 (7½)	108 (0.168)	130 (5⅛)	53 (0.174)	143 (5⅝)

4.2.2. Flexural Strengthening

Table 4.3 summarizes the strengthening recommendations for the superstructure of the bridge. Figure 4.3 and Figure 4.4 detail the longitudinal flexural strengthening. Finally, the pattern of the bolts for longitudinal and transversal reinforcement is shown in Figure 4.5.

Table 4.3. Strengthening Summary

Section	*Strengthening Scheme*	*Design Capacity* fM_n $[kN \cdot m/m]$ $([kip \cdot ft/ft])$		*Moment Demand* M_u $[kN \cdot m/m]$ $([kip \cdot ft/ft])$
		Un-strengthened	*Strengthened*	
Longitudinal Direction	*Deck:* 1 Plate @ 203 *mm* (8 *in*) o/c	18.7 (4.2)	114.8 (25.8)	113.0 (25.4)

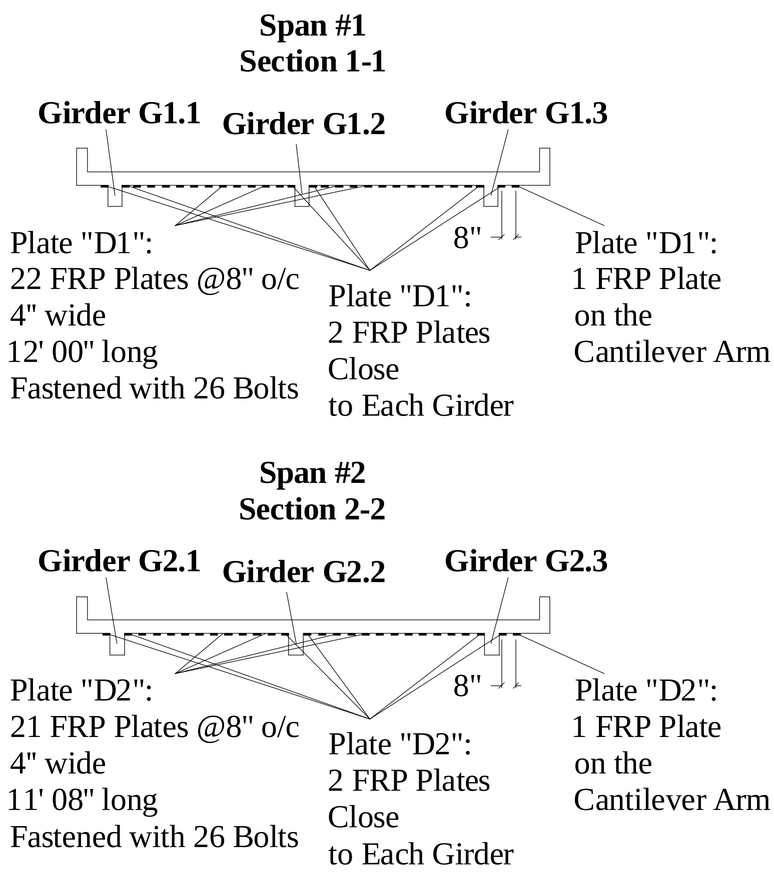

Figure 4.3. Strengthening of the Deck: Sections

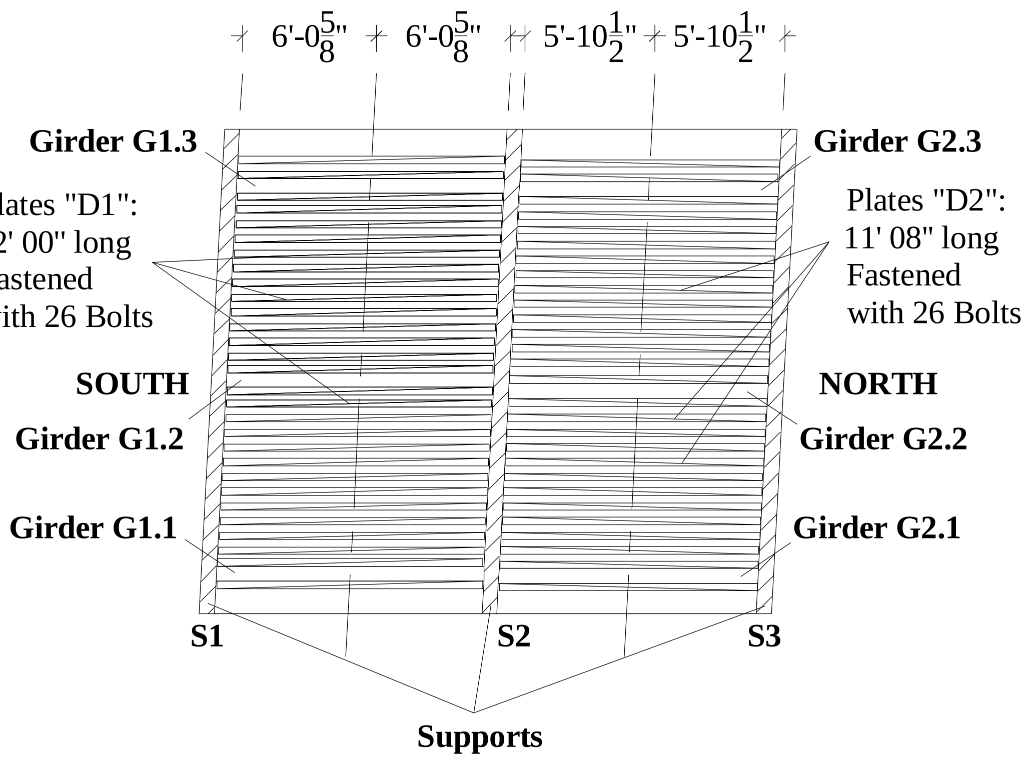

Figure 4.4. Strengthening of the Deck: Plan View

The bolt pattern was verified at the ultimate condition in order to avoid having any section in which the moment demand is greater than the moment capacity. During this step, the position of the bolts is optimized. Figure 4.6 details the moment capacity of the beam along its length for the chosen bolt pattern. Appendix C contains some pictures of the FRP strengthening installation.

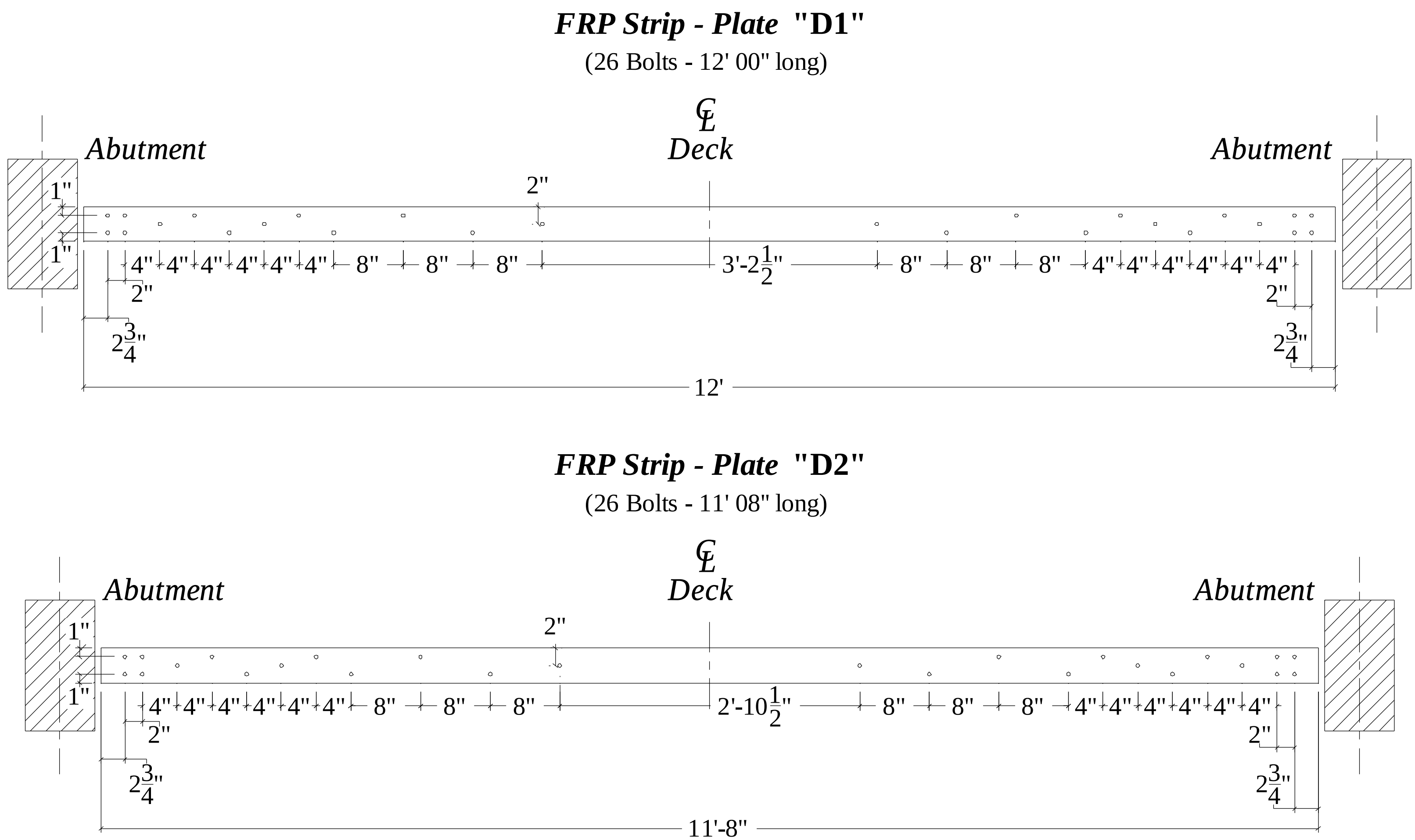

Figure 4.5. Pattern of the Bolts

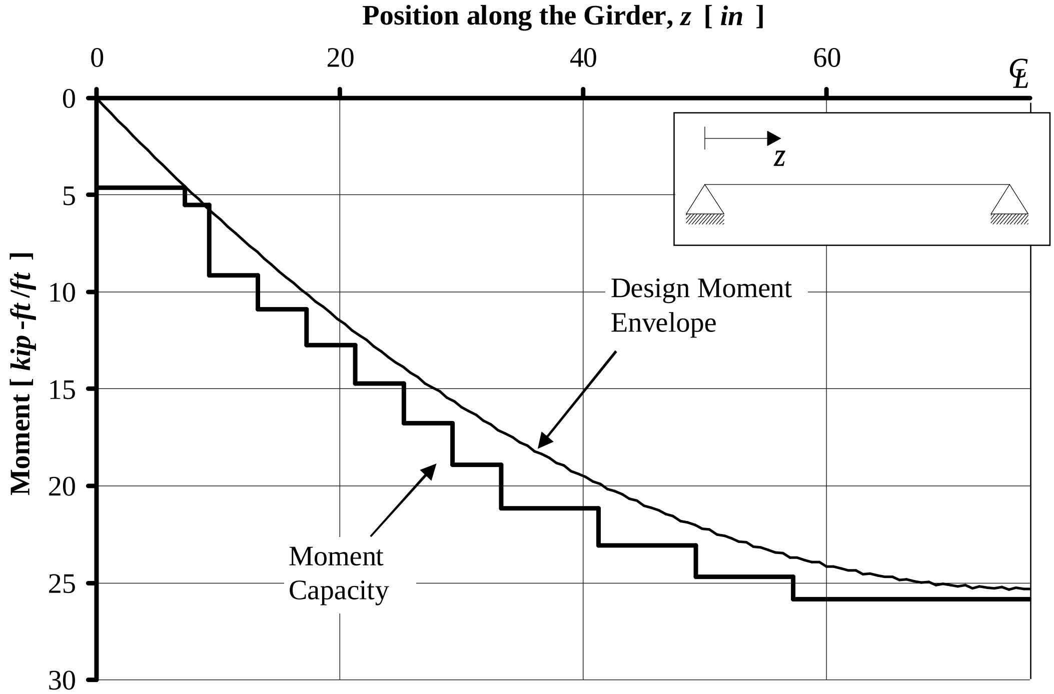

Figure 4.6. Diagram of the Capacity of the Deck at the Ultimate Load Conditions

4.2.3. Shear Check

The concrete contribution to the shear capacity was calculated based on equation (11-5) of ACI 318-02 as follows:

$$\begin{cases} V_c = \left(1.9\sqrt{f_c^{'}} + 2500\, r_w \dfrac{V_u d}{M_u}\right) b_w d \le 3.5\sqrt{f_c^{'}}\, b_w d \\ \left[\, f_c^{'} \right] = [\, psi\,] \end{cases} \tag{4.3}$$

The as-built shear capacity is then computed by adding the concrete contribution to the one due to the shear reinforcement. Table 4.4 summarizes the findings for the superstructure. Since the capacity is higher than the demand, it can be concluded that no shear reinforcement is required.

Table 4.4. Superstructure Shear Capacity

Element	*Shear Capacity* fV_n	*Shear Demand* V_u
Slab $\left[\dfrac{kN}{m}\right]\left(\left[\dfrac{kip}{ft}\right]\right)$	116.7 (8.0)	115.3 (7.9)

4.2.4. Punching Shear Check

The deck must also be checked for punching shear. This check was based on ACI 318-02 requirements. ACI 318-02 Sec. 11.12.2.1 prescribes that for non-prestressed slabs and footings, V_c shall be the smallest of the following expressions:

$$\begin{cases} V_{c,1} = \left(2 + \dfrac{4}{b_c}\right)\sqrt{f_c^{'}}\, b_0 d \\ V_{c,2} = \left(\dfrac{a_s d}{b_0} + 2\right)\sqrt{f_c^{'}}\, b_0 d \qquad \text{with } \left[\, f_c^{'} \right] = [\, psi\,] \\ V_{c,3} = 4\sqrt{f_c^{'}}\, b_0 d \end{cases} \tag{4.4}$$

where:

b_0 is the perimeter of critical section;

d is the distance from the extreme compression fiber to centroid of tension reinforcement;

a_s is 40 for interior load, 30 for edge load and 20 for corner load;

b_c is the ratio of long side to short side of the area over which the load is distributed.

By using a tire contact area as given by AASHTO (2002):

$$\begin{cases} l_{tire} = 254\ mm\ \ (10\ in) \\ w_{tire} = 508\ mm\ \ (20\ in) \\ A_{tire} = l_{tire} w_{tire} = 129032\ mm^2\ \ (200\ in^2) \end{cases} \tag{4.5}$$

the following shear capacity can be found:

$$f_{punch} V_c = f_{punch} \min\left(V_{c,01}, V_{c,02}, V_{c,03}\right) \cong 0.85\left(462\ kN\right) \cong 392\ kN\ \ \left(89.0\ kip\right)$$

which is smaller than the ultimate punching shear capacity given by:

$$g b_L \left(1 + I\right) P_{H15-44} \cong 151.2\ kN\ \ \left(34.0\ kip\right).$$

5. FIELD EVALUATION

5.1. Introduction

Although in-situ bridge load testing is recommended by the AASHTO (2002) Specification as an "effective means of evaluating the structural performance of a bridge", no guidelines currently exist for bridge load test protocols. In each case, the load test objectives, load configuration, instrumentation type and placement, and analysis techniques are to be determined by the organization conducting the test.

In order to validate the behavior of the bridge after strengthening, a static load test was performed with a H15 legal truck (see Figure 5.1), in June 2004 about two months after the strengthening. Figure 5.2 shows the distribution of the load between the axles of the truck and the loading configurations maximizing the stresses and deflections at mid-span of deck panels under a total of six passes, two central and four laterals. For each pass, two stops were executed centering the truck rear axle over the marks on the deck. During each stop, the truck was stationary for at least two minutes before proceeding to the next location in order to allow stable readings.

Figure 5.1. Load Tests after Strengthening on Bridge No. 3855006

Displacements in the longitudinal and transverse directions were measured using Linear Variable Differential Transducers (LVDTs). Strains in the strengthening material were monitored by means of strain gages. Figure 5.3 shows the details of the instrumentation whose layout was designed to gain the maximum amount of information about the structure.

Figure 5.4 reports the displacement relative to Pass #4 corresponding to the rear axle of the truck at the middle of the span S1 (Stop #2) and S2 (Stop #1). It is interesting to note that the deck deflected like a continuous slab over two spans while for design purposes the continuity of the superstructure over the central pier was conservatively neglected. In addition, the bridge performed well in terms of overall deflection. In fact, the maximum deflection measured during the load test is below the allowable deflection prescribed by AASHTO, 2002 Section 8.9.3 ($d_{\max} \leq l_d / 800 = 4.620\ mm\ \left(0.182\ in\right)$).

Figure 5.5 reports the reading of the strain gages applied to the FRP laminates, relative to Pass #5. The strain readings (between 75 and 90 me) for the most loaded part of the slab indicate a satisfactory performance of the FRP laminates. The distribution of strains is approximately symmetric as it could be expected from a symmetric load condition. For some loading conditions, it was found that some of the laminates were less engaged. This kind of behavior is typical of the non-bond critical strengthening systems where the strengthening needs relatively large deformations of the structure before being completely engaged.

Results for the other load configurations are summarized in Appendix A together with the theoretical values obtained with the Finite Element Method (FEM) model described in the following section.

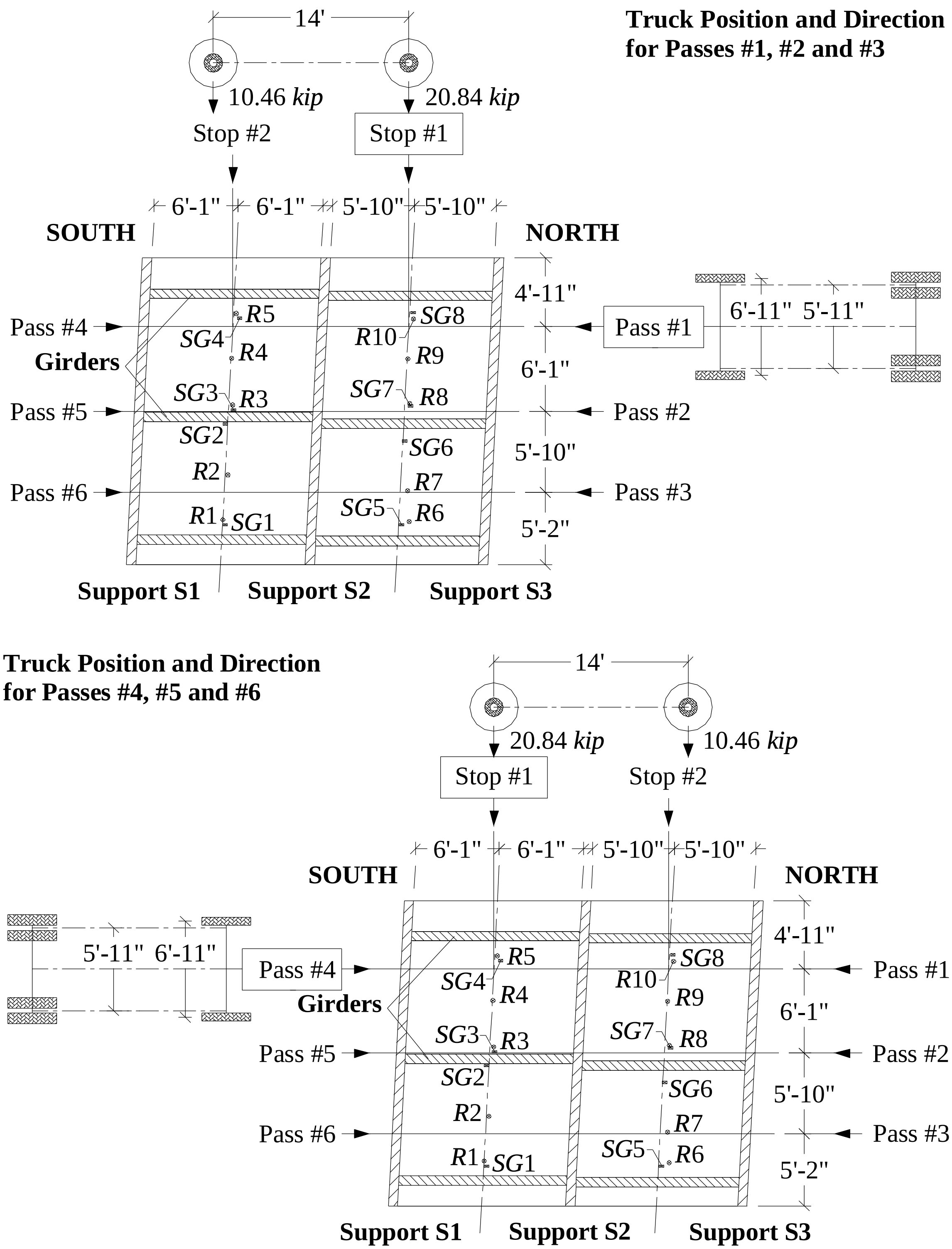

Figure 5.2. Legal Truck Used in the Load Test after Strengthening

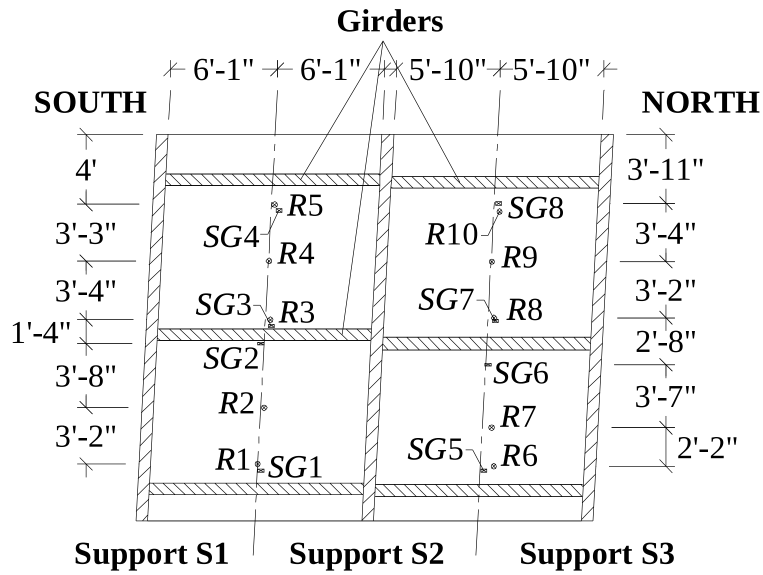

Figure 5.3. LVDT and Strain Gage Positions in the Load Test after Strengthening

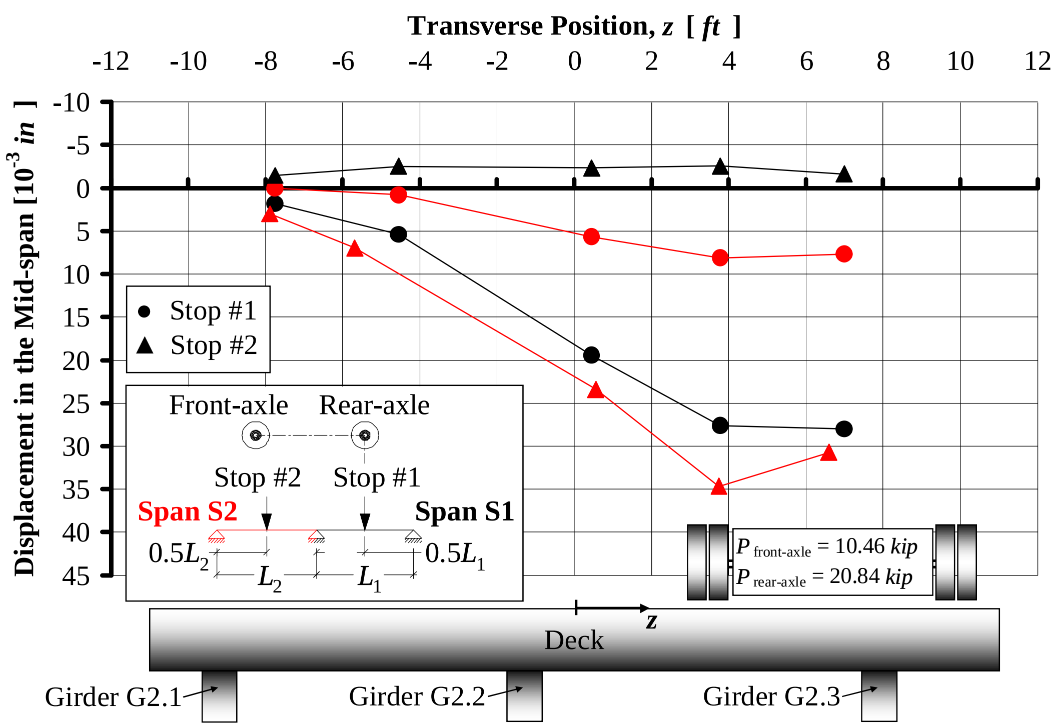

Figure 5.4. Mid-span Displacement, Pass #4

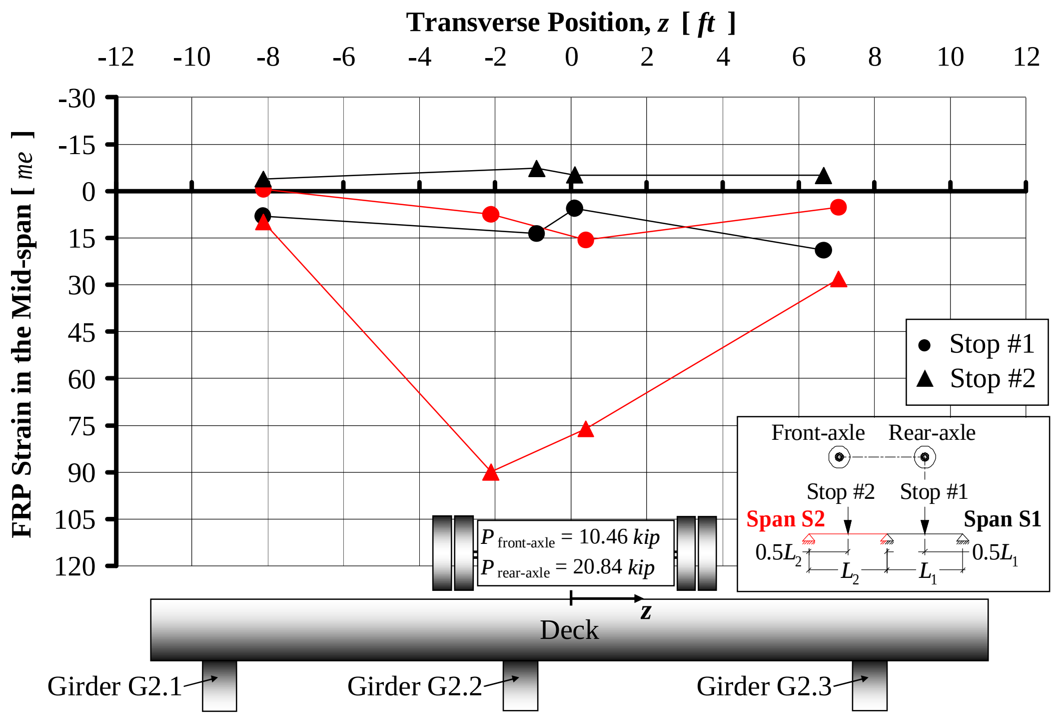

Figure 5.5. Mid-span Strain in the FRP Laminates, Pass #5

5.2. Additional Load Test

A dynamic test was conducted on the strengthened bridge to determine the impact factor by moving the truck on Pass #2 and Pass #5 at speeds equal to 4.5, 8.9 and 13.4 m/s (10, 20 and 30 MPH). The dynamic test was performed acquiring the data at a frequency of 20 Hz. The live load impact factor I was computed as the ratio between the difference between the maximum dynamic and static displacements to the maximum static deflection (i.e. Pass #2 and Pass #5). As an example, Figure 5.6 shows the dynamic deflections as a function of time at a 13.4 m/s (30 MPH) speed. Figure 5.7 plots the live load impact factor I for displacements and strains for different truck speeds (the truck speed is considered positive if the truck ran from North to South). It can be noticed that the impact factor decreases for speeds higher than 8.9 m/s $(20\ MPH)$. This is due to the fact that by increasing the speed, the time of application of the load on the bridge is reduced and, consequently, the corresponding deflection is reduced due to bridge hysteretic behavior.

From Figure 5.7 it is possible to extrapolate two values for the maximum impact factor $I_{experimental,\ Pass\ \#2}$, 0.86 and 2.09 according to the reading of the LVDTs and the strain gauges, respectively. Both values are higher than the one used for design ($I = 0.30$ according to AASHTO (2002)). The higher value of impact factors derived from the displacements readings are related to LVDTs positioned at the sides of the decks (i.e. R1, R5, R6 and R10), while the impact factors determined considering the rest of the LVDTs were found to be less than 0.30. This implies that, in reality, the portions of the slab interested by the higher impact load factor would still experience a load below the design value. On the other hand, the strain in some FRP laminates under dynamic loads was three times ($I_{experimental,\ Pass\ \#2} = 2.09$) the static one. This can be considered just a local effect since a crack ran through the width of the deck right over where the strain gauges were placed.

Appendix B reports all the results obtained at different truck speeds.

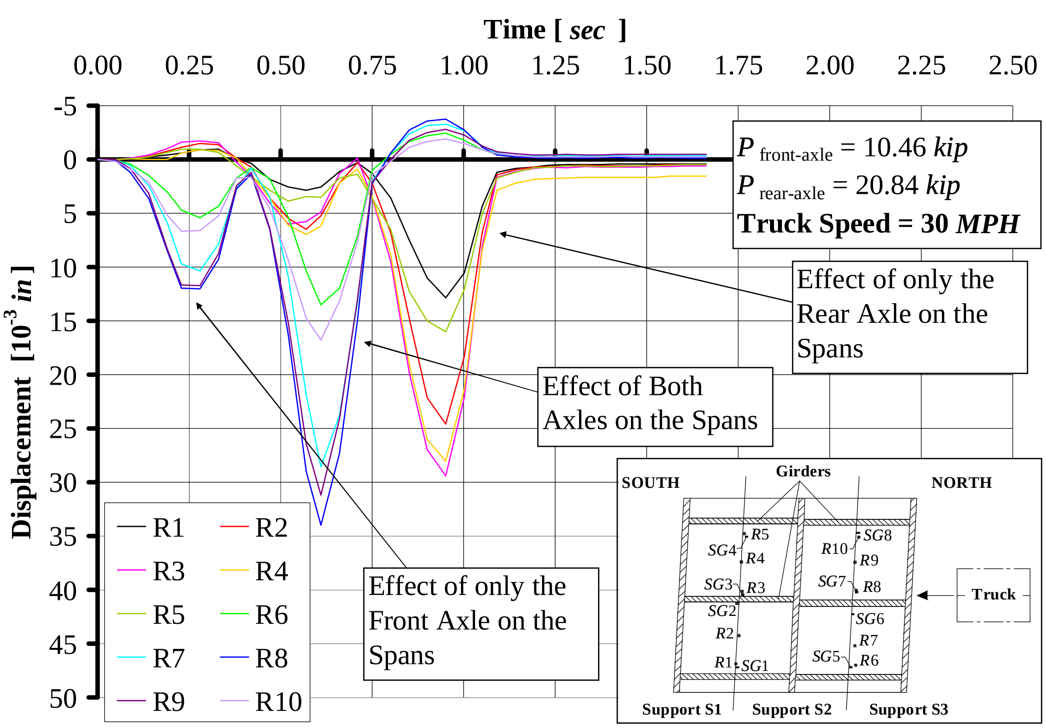

Figure 5.6. After Strengthening Displacements at 13.4 m/s (30 MPH)

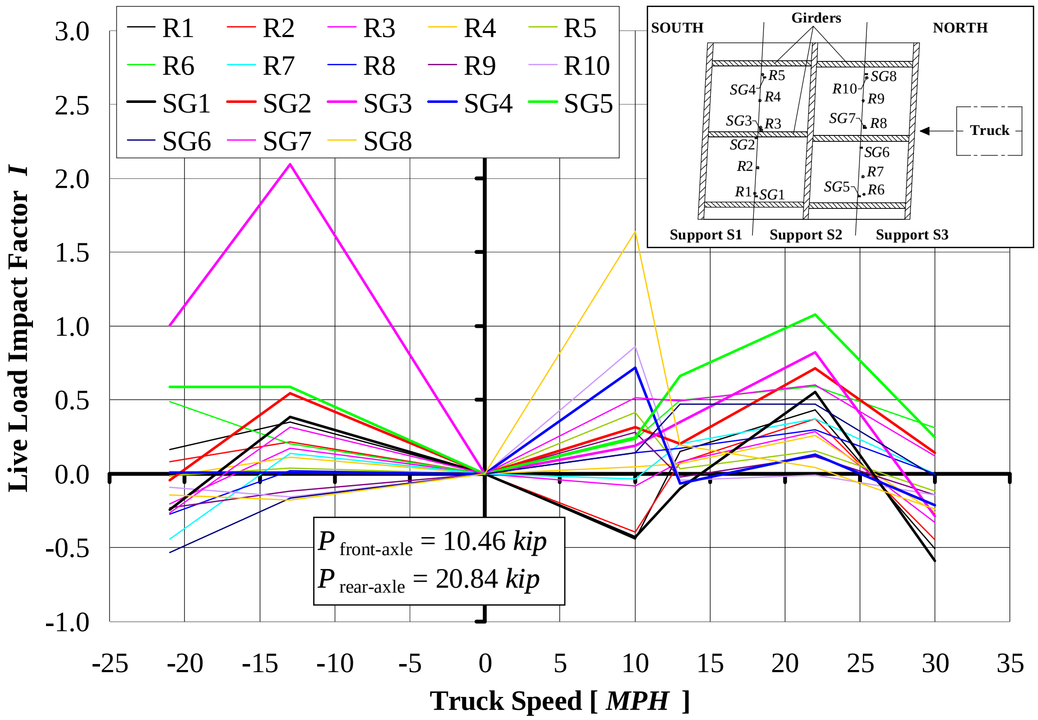

Figure 5.7. Live Load Impact Factor I versus Truck Speed

5.3. FEM Analysis

In this section, a FEM analysis model is described. This model was developed in order to interpret the experimental data collected during the test after the strengthening. For this purpose, a commercially available finite element program ANSYS 7.1 was used. Details of the geometry can be found in Figure 5.8 and Figure 5.9.

The element SOLID65 was chosen to model the concrete and the FRP laminates. SOLID65 is used for the three-dimensional modeling of solids with or without reinforcing bars. The solid is capable of cracking in tension and crushing in compression. In addition, up to three different rebar specifications may be defined. The element is defined by eight nodes having three degrees of freedom at each node: translations in the nodal x, y and z directions. SOLID65 is subject to the following assumption and restrictions:

- cracking is permitted in three orthogonal directions at each integration point;

- if cracking occurs at an integration point, the cracking is modeled through an adjustment of material properties which effectively treats the cracking as a “smeared band” of cracks, rather than discrete cracks;
- the concrete material is assumed to be initially isotropic;
- whenever the reinforcement capability of the element is used, the reinforcement is assumed to be “smeared” throughout the element;
- in addition to cracking and crushing, the concrete may also undergo plasticity, with the Drucker-Prager failure surface being most commonly used. In this case, the plasticity is done before the cracking and crushing checks.

For this project, the material properties of concrete were assumed to be isotropic and linear elastic, since the applied load was relatively low with respect to the ultimate load condition. The modulus of elasticity of the concrete was based on the measured compressive strength of the cores obtained from the slab according to the standard equation ACI 318-02 Section 8.5.1:

$$E_c = 57000\sqrt{f_c^{'}}\ psi = 57000\sqrt{6575}\ psi \approx\ 32.2\ GPa\ \left(4672\ ksi\right) \text{ with } \left[f_c^{'}\right] = \left[psi\right].$$

In order to take into account the presence of the cracks in the deck and the deterioration of the concrete of girders and curbs, as a result of a parametric analysis, the modulus of elasticity was reduced to $5.2\ GPa\ \left(750\ ksi\right)$ and $17.2\ GPa\ \left(2500\ ksi\right)$ in the elements corresponding to the cracks and girders in the span S1, and girders in the span S2, respectively, as shown in Figure 5.8b. The depth of the cracks was chosen according to the data collected during the in-situ inspection while the width was assumed to be equal to the elements dimensions. The concrete Poisson’s ratio was set to 0.19. Different elements were used to optimize the model and decrease the computation time. The chosen shape and size in the longitudinal and transverse cross sections allowed to locate more accurately the steel rebars (see Figure 5.9a), to properly connect the FRP laminates to the surface of the concrete (see Figure 5.9b) and to reduce the number of the elements in the “secondary” parts of the model, such as the curbs (see Figure 5.9a). Due to the uneven spacing of the steel rebars in the transverse and longitudinal direction, it was preferred to smear the steel reinforcement across the entire length and width of the slab, respectively. The modulus of the elasticity and the Poisson’s ratio for the steel reinforcement were assumed as $200.0\ GPa\ \left(29000\ ksi\right)$ and 0.3, respectively.

The connections between the FRP laminates and the concrete surface were modeled as rigid, neglecting any form of non-linearity due to a potential initial non-perfect engagement of the strengthening. Modulus of the elasticity and the Poisson's ratio for the FRP laminates were assumed to be $60.6\ GPa\ (8800\ ksi)$ and 0.3, respectively.

The bridge was vertically and transversally restrained in correspondence to the three supports, while the longitudinal displacement was fixed to zero at the central abutment only (see Figure 5.9). The loads were assumed as uniformly distributed over $508\times254\ mm\ (20\times10\ in)$ areas as specified in AASHTO (2002) Section 4.3.30. Such loads were applied at the top of the deck simulating, in such way, the truck wheel prints (see Figure 5.8a). The uniform load was concentrated at the nodes corresponding to the truck wheel print and each force was determined by dividing the total load for the number of nodes.

Figure 5.10 reports the experimental and analytical mid-span displacements, relative to Pass #4. The graph shows a good match in deflections between experimental and analytical results.

Figure 5.11 compares experimental and analytical strains on the FRP, relative to Pass #4. The graph shows a good match in strains between experimental and analytical results for the strips fastened beneath the deck of span S2. The mismatch for the laminates in the middle of span S1 can be explained with the incomplete engagement of the FRP laminates to the concrete.

Appendix A reports all the analysis developed for the bridge after the strengthening.

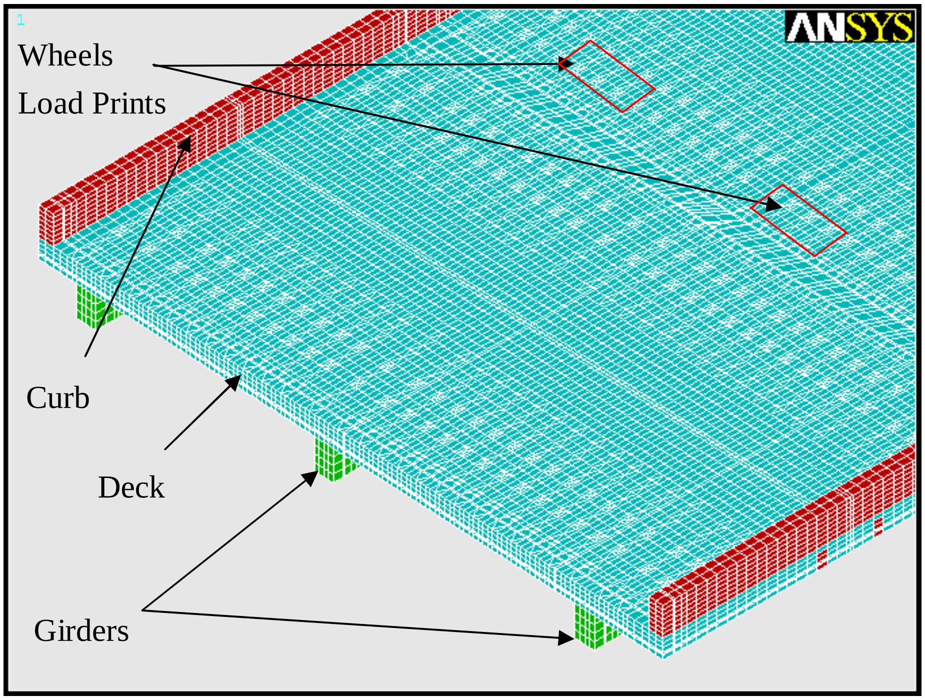

a) Global View of the Model

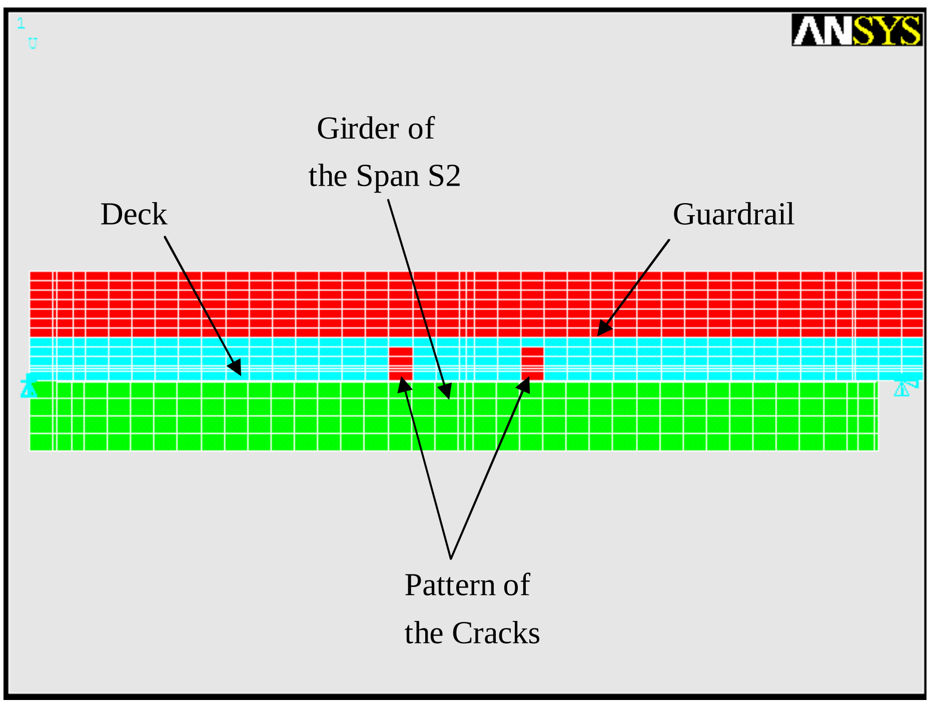

b) Details of the Cracks Modeling

Figure 5.8. FEM Model Geometry (I)

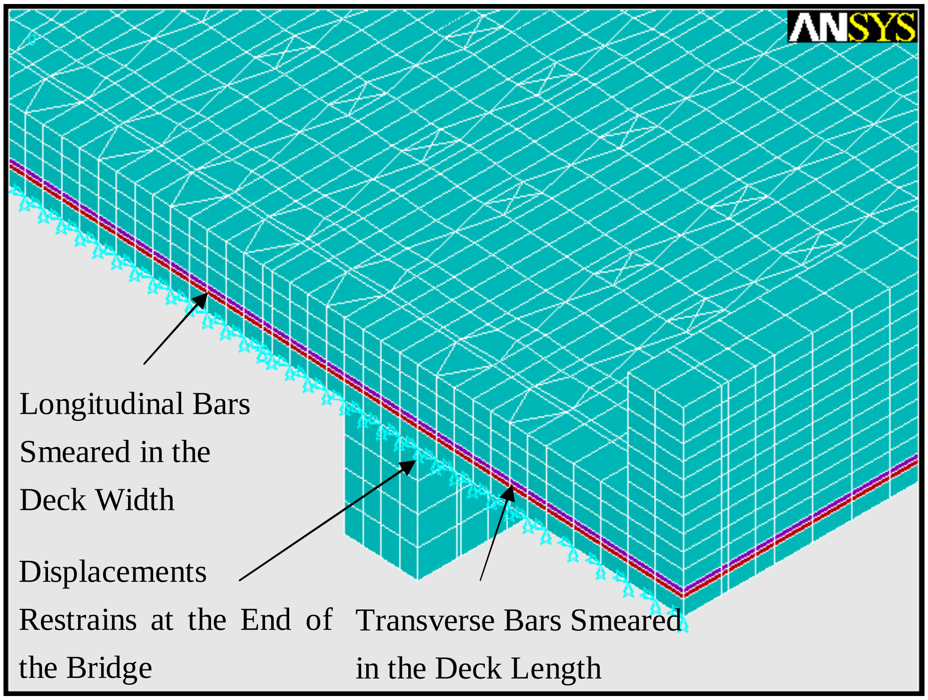

a) Details of the Steel Reinforcement and Boundary Conditions

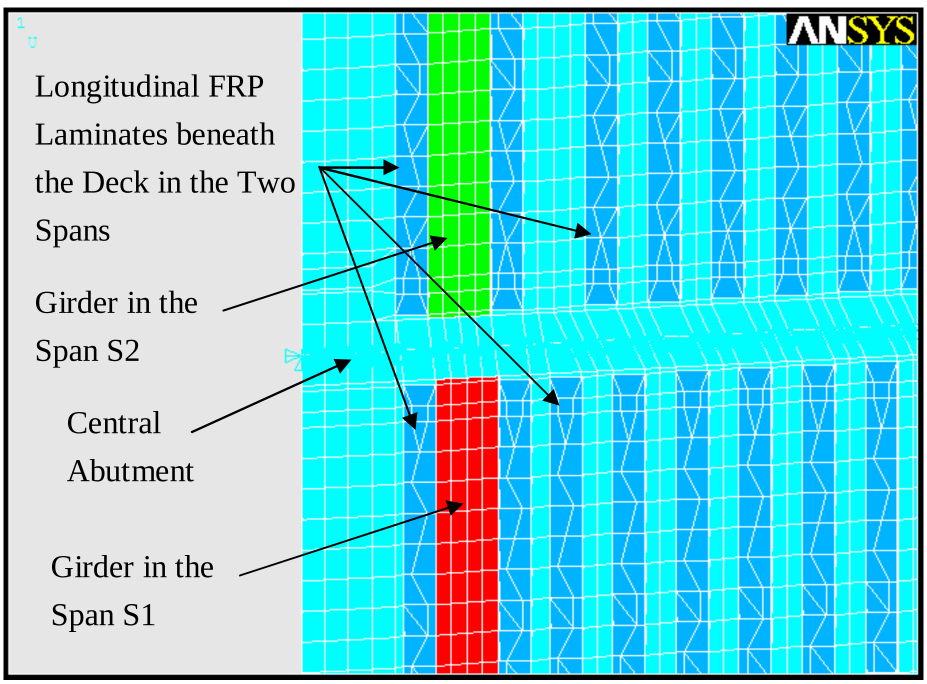

b) Details of the FRP Strenghtening (Bottom View)

Figure 5.9. FEM Model Geometry (II)

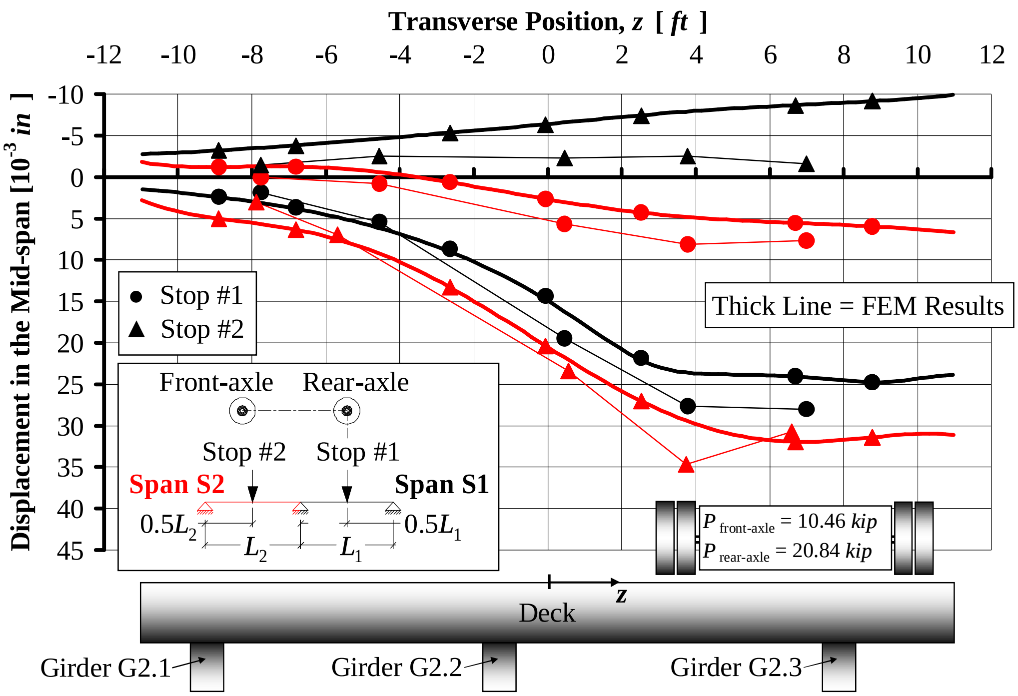

Figure 5.10. Comparison of Experimental and Analytical Results for Mid-span Displacement, Pass #4

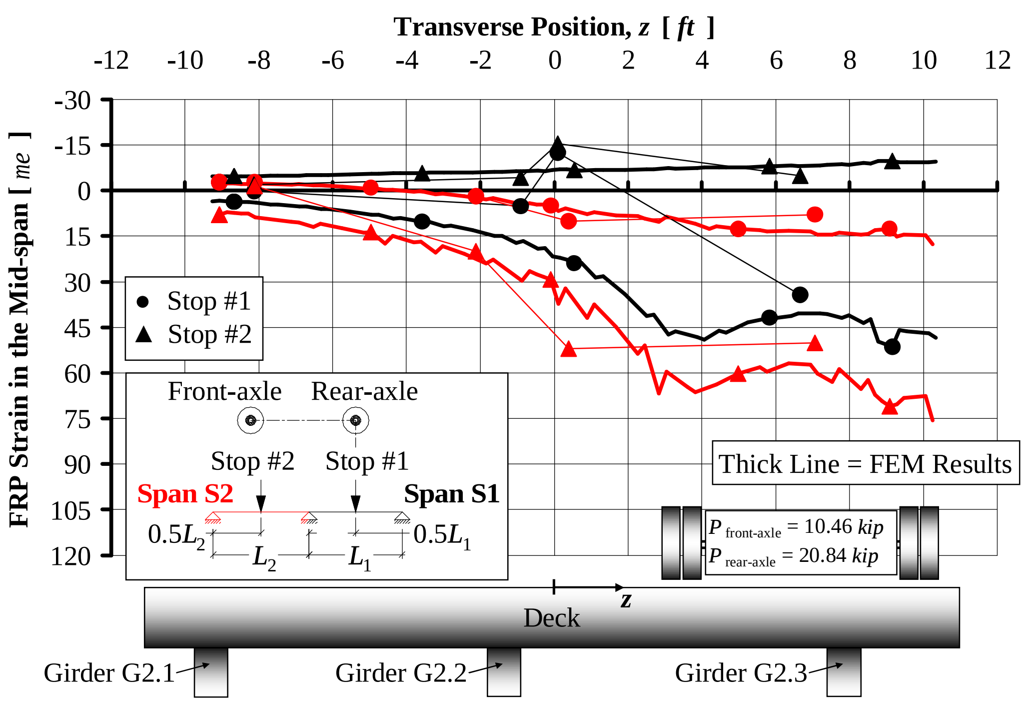

Figure 5.11. Comparison of Experimental and Analytical Results for Strain in the FRP Fastened on the Deck at Mid-span, Pass #4

6. LOAD RATING

Bridge load rating calculations provide a basis for determining the safe load capacity of a bridge. According to the Missouri Department of Transportation (MoDOT), anytime a bridge is built, rehabilitated, or reevaluated for any reason, inventory and operating ratings are required using the Load Factor rating. All bridges should be rated at two load levels, the maximum load level called the Operating Rating and a lower load level called the Inventory Rating. The Operating Rating is the maximum permissible load that should be allowed on the bridge. Exceeding this level could damage the bridge. The Inventory Rating is the load level the bridge can carry on a daily basis without damaging the bridge.

In Missouri, for the Load Factor Method the Operating Rating is based on the appropriate ultimate capacity using current AASHTO specifications (AASHTO, 1996). The vehicle used for the live load calculations in the Load Factor Method is the HS20 truck. If the stress levels produced by this vehicle configuration are exceeded, load posting may be required.

The method for determining the rating factor is that outlined by AASHTO in the Manual for Condition Evaluation of Bridges (AASHTO, 2002). Equation (6.1) was used:

$$RF = \frac{C - A_1 D}{A_2 L(1 + I)} \tag{6.1}$$

where:

RF is the Rating Factor;

C is the capacity of the member;

D is the dead load effect on the member;

L is the live load effect on the member;

I is the impact factor to be used with the live load effect;

A_1 is the factor for dead loads;

A_2 is the factor for live loads.

Since the load factor method is being used, A_1 is taken as 1.3 and A_2 varies depending on the desired rating level. For Inventory Rating, $A_2 = 2.17$, and for Operating Rating, $A_2 = 1.3$.

To determine the rating RT of the bridge, equation (6.2) was used:

$$RT = RF \cdot W \tag{6.2}$$

where W is the weight of the nominal truck used to determine the live load effect.

For the bridge No. 3855006, the Load Rating was calculated for a number of different trucks, HS20, H20, 3S2 and MO5. Ratings are required at the inventory and operating levels by the load factor method on each bridge for the HS20 truck. The H20 legal vehicle is used to model the load for single unit vehicles. The 3S2 vehicle is used as a model for all other vehicles. The MO5 is used to model the commercial zone loadings.

For each of the different loading conditions, the maximum shear and maximum moment were calculated. Impact factors are also taken into account for Load Ratings. This value is 30% for the bridge No. 3855006. The shear and moment values for the deck are shown in Table 6.1.

Table 6.1. Maximum Shear and Moment due to Live Load for the Deck

Truck	Maximum Shear $[kN]$ $([kip])$	Maximum Moment $[kN \cdot m]$ $([kip \cdot ft])$	Maximum Shear with Impact $[kN]$ $([kip])$	Maximum Moment with Impact $[kN \cdot m]$ $([kip \cdot ft])$
HS20	14.86 (3.34)	14.55 (10.73)	19.35 (4.35)	18.91 (13.95)
MO5	15.75 (3.54)	13.15 (9.70)	20.46 (4.60)	17.10 (12.61)
H20	12.68 (2.85)	10.56 (7.79)	16.46 (3.70)	13.72 (10.12)
3S2	12.72 (2.86)	10.56 (7.79)	16.55 (3.72)	13.72 (10.12)

Table 6.2 and Table 6.3 give the results of the Load Rating pertaining to moment and shear respectively for the deck.

Table 6.2. Rating Factor for the Deck (Bending Moment)

Truck	Rating Factor *RF*	Rating *RT* ton_{SI} $([ton])$	Rating Type
HS20	1.293	42.2 (46.6)	Operating
HS20	0.775	25.3 (27.9)	Inventory
MO5	1.430	46.7 (51.5)	Operating
H20	1.533	27.8 (30.7)	Posting
3S2	1.533	50.9 (56.2)	Posting

Table 6.3. Rating Factor for the Deck (Shear)

Truck	Rating Factor *RF*	Rating *RT* ton_{SI} $([ton])$	Rating Type
HS20	47.9	43.5 (47.9)	Operating
HS20	28.7	26.0 (28.7)	Inventory
MO5	46.1	41.8 (46.1)	Operating
H20	26.9	24.4 (26.9)	Posting
3S2	49.1	44.5 (49.1)	Posting

According to Table 6.3, the bridge should be posted at $24.4\ ton_{SI}$ $(26.9\ ton)$. Therefore, since the legal loads established for Missouri are defined as $20.9\ ton_{SI}$ $23.0\ ton$ for single unit vehicles and $36.3\ ton_{SI}$ $(40.0\ ton)$ for all others, the existing load posting can be removed.

7. Conclusions

Conclusions based on the retrofitting of the bridge utilizing FRP materials can be summarized as follows:

- The mechanically Fastened (MF) FRP system showed to be a feasible solution for the strengthening of the bridge;
- In-situ load testing has proven to be useful and convincing;
- The FEM analysis has shown good match with experimental results demonstrating the effectiveness of the strengthening technique;
- As a result of FRP strengthening, the load posting of the bridge can be removed.

8. REFERENCES

AASHTO (1996). "LRFD bridge design specifications." Second Edition, Published by the American Association of State Highway and Transportation Officials, Washington D.C.

AASHTO (2002). "Standard specifications for highway bridges." 17th Edition, Published by the American Association of State Highway and Transportation Officials, Washington D.C.

ACI Committee 318 (1999). "Building code requirements for structural concrete and commentary." ACI 318R-99, Published by the American Concrete Institute, Farmington Hills, MI.

ACI Committee 318 (2002). "Building code requirements for structural concrete and commentary." ACI 318R-02, Published by the American Concrete Institute, Farmington Hills, MI.

ACI Committee 440 (1996). "State-of-the-art report on FRP for concrete structures." ACI 440R-96, Manual of Concrete Practice, ACI, Farmington Hills, MI, 68 pp.

ACI Committee 440 (2002). "Guide for the design and construction of externally bonded FRP systems for strengthening concrete structures." ACI 440.2R-02, Published by the American Concrete Institute, Farmington Hills, MI.

Alkhrdaji, T., Nanni, A., Chen, G., and Barker, M. (1999). "Upgrading the transportation infrastructure: solid RC decks strengthened with FRP." Concrete International, American Concrete Institute, Vol. 21, No. 10, October, pp. 37-41.

ANSYS User's Manual for Revision 6.1 (2000). Volume I Procedure and Volume III Elements, Swanson Analysis Systems, Inc.

Arora, D. (2003). "Rapid strengthening of reinforced concrete bridge with mechanically fastened fiber-reinforced polymer strips." M.Sc. Thesis, University of Wisconsin – Madison.

Bank, L. C., Lamanna A. J., Ray, J. C., and Velásquez G. I. (2002). "Rapid strengthening of reinforced concrete beams with mechanically fastened, fiber-reinforced polymeric composite materials." US Army Corps of Engineers, Washington D.C.

Bank, L. C., Borowicz D. T., Lamanna A. J., Ray J. C., and Velásquez G. I. (2002). "Rapid strengthening of full-sized concrete beams with powder-actuated fastening systems and Fiber-Reinforced Polymer (FRP) composite materials." US Army Corps of Engineers, Washington D.C.

Borowicz, D. T. (2002). "Rapid strengthening of concrete beams with powder-actuated fastening systems and Fiber-Reinforced Polymer (FRP) composite materials." M.Sc. Thesis, University of Wisconsin – Madison.

Lamanna, A.J. (2002). "Flexural strengthening of reinforced concrete beams with mechanically fastened fiber reinforced polymer strips." PhD Thesis, University of Wisconsin – Madison.

APPENDICES

APPENDIX

A. After Strengthening Test Results

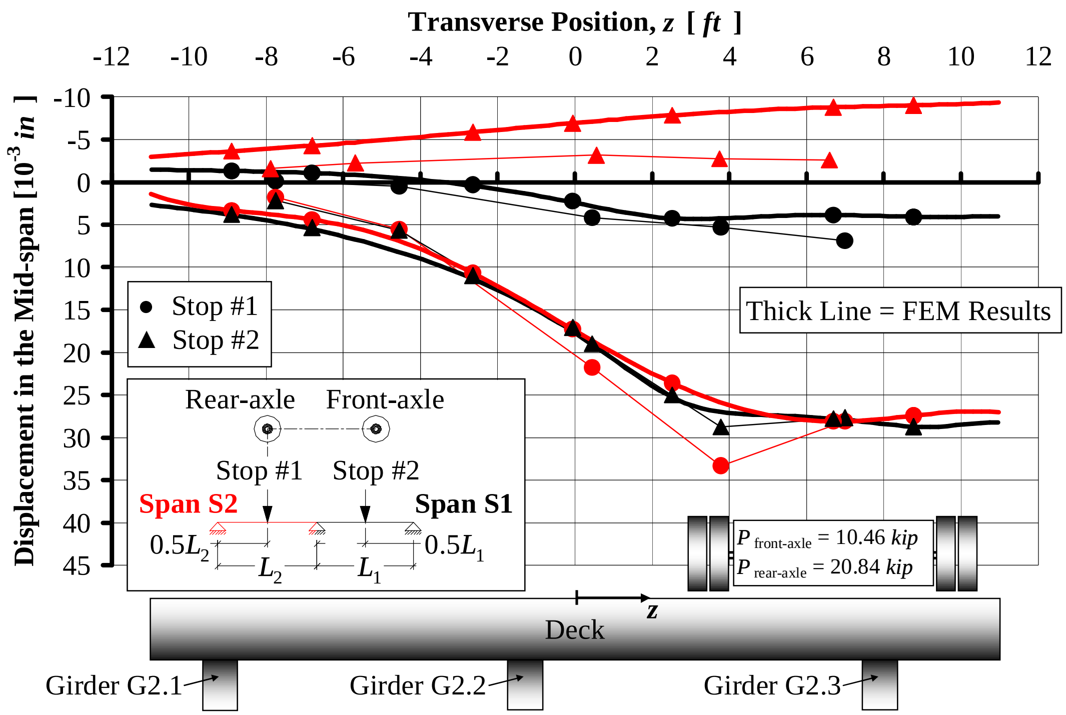

Figure A. 1. After Strengthening Mid-span Displacement, Pass #1

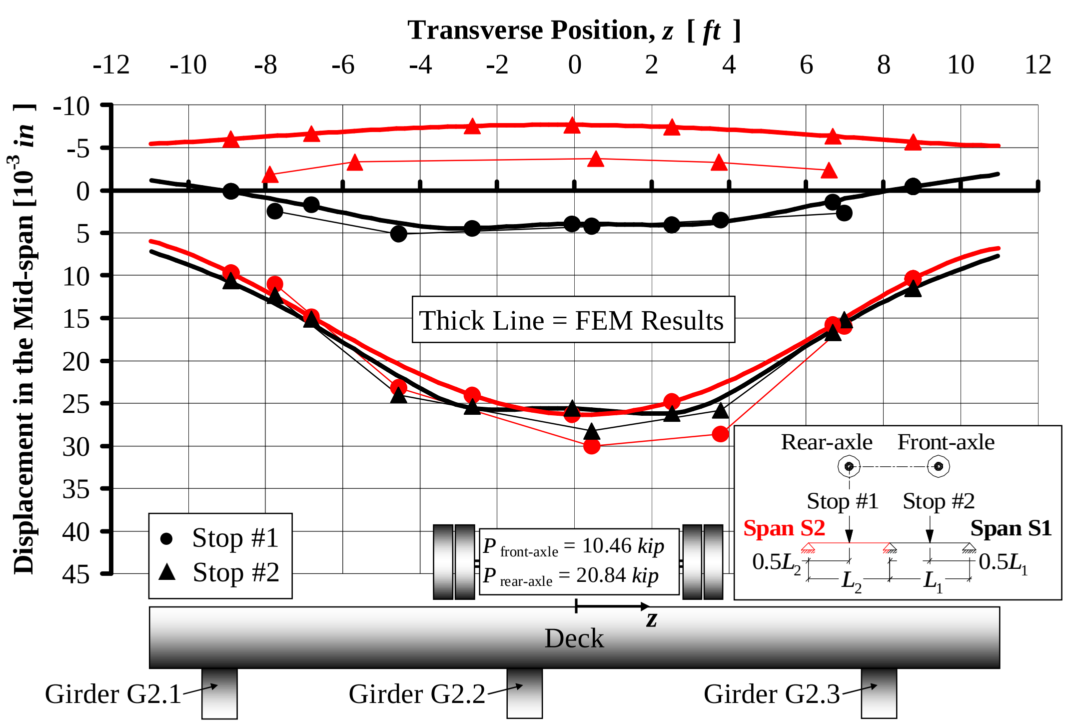

Figure A. 2. After Strengthening Mid-span Displacement, Pass #2

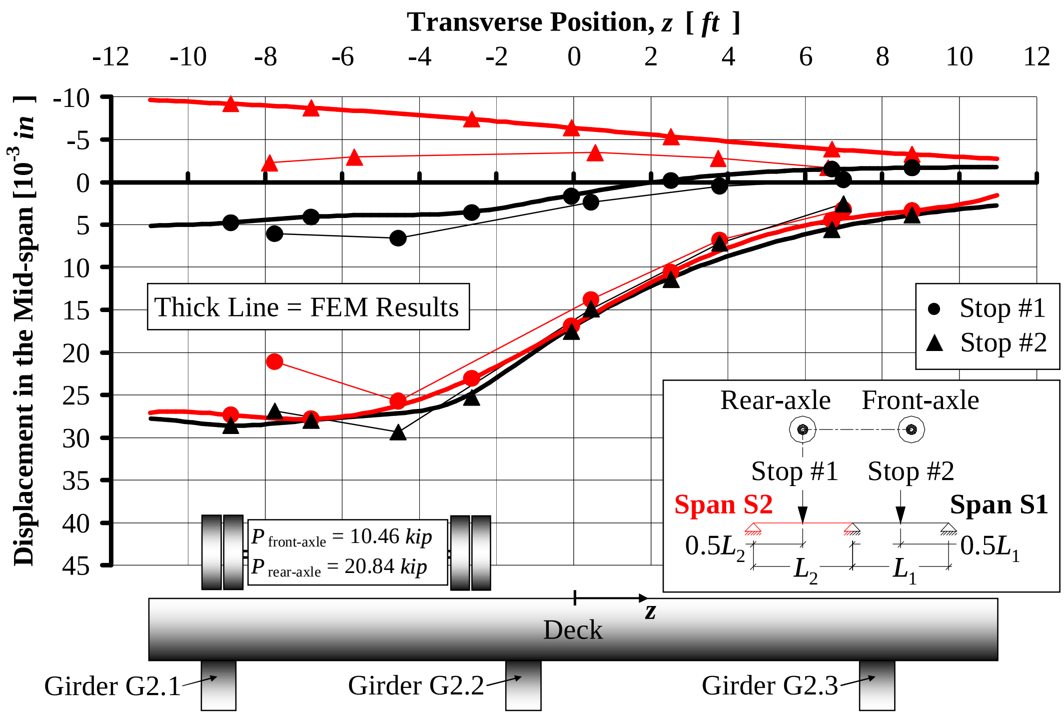

Figure A. 3. After Strengthening Mid-span Displacement, Pass #3

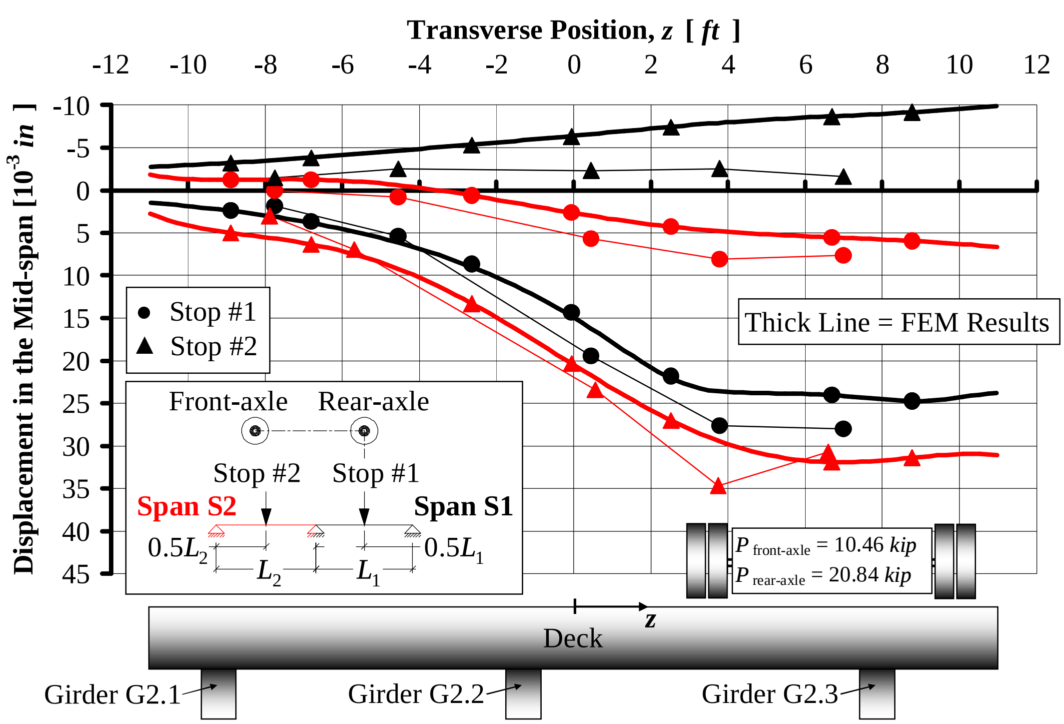

Figure A. 4. After Strengthening Mid-span Displacement, Pass #4

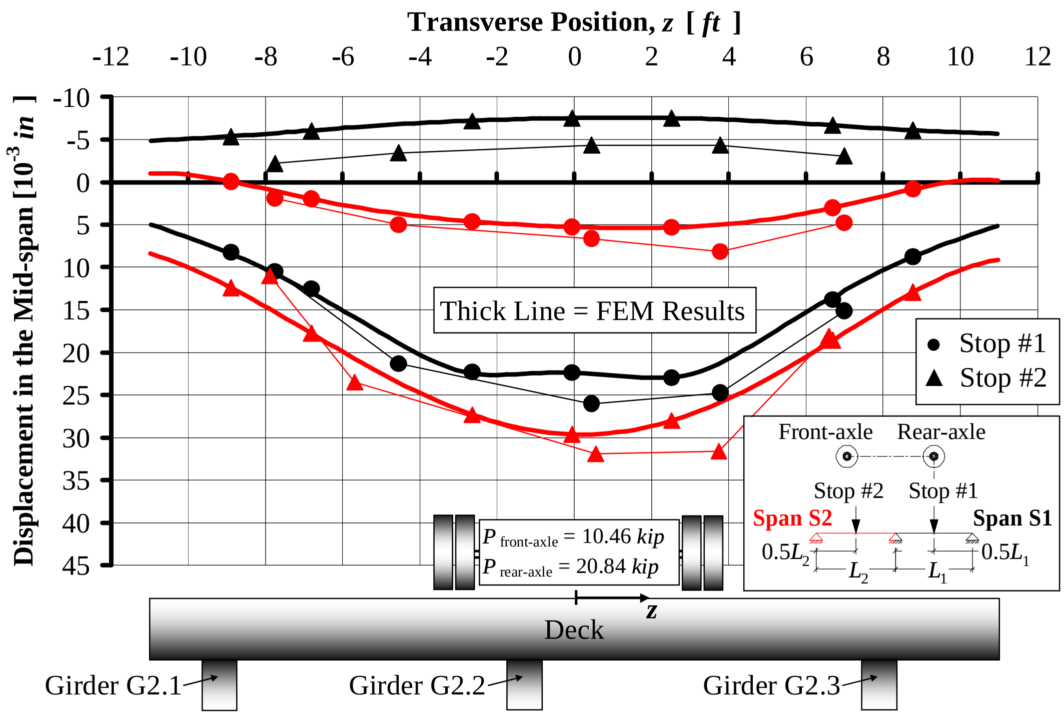

Figure A. 5. After Strengthening Mid-span Displacement, Pass #5

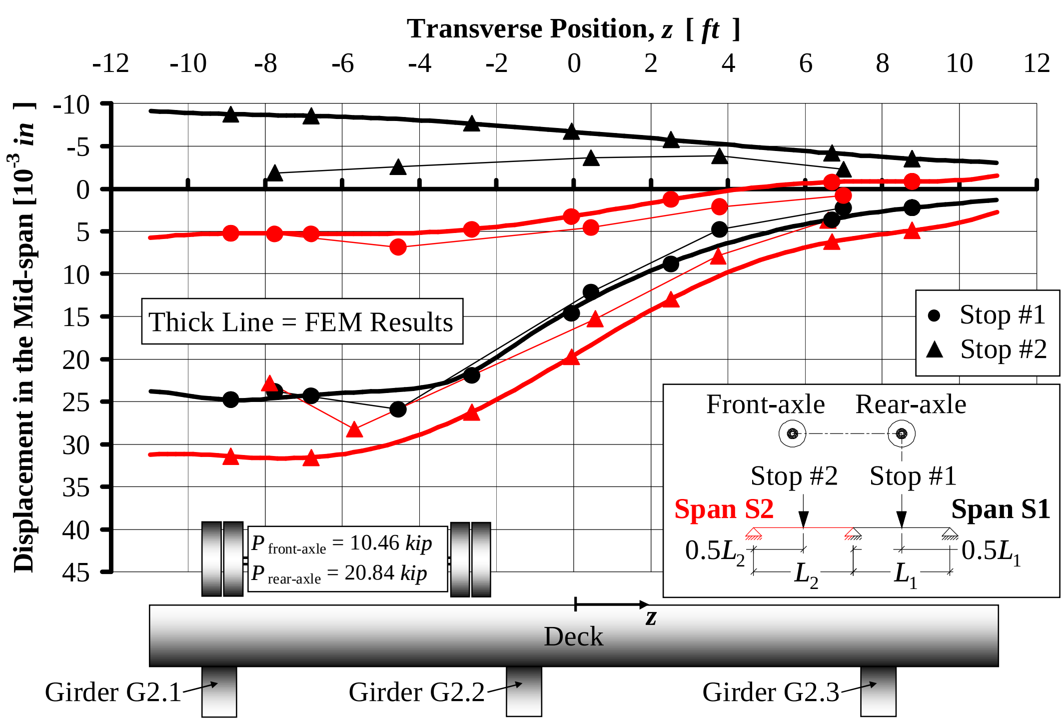

Figure A. 6. After Strengthening Mid-span Displacement, Pass #6

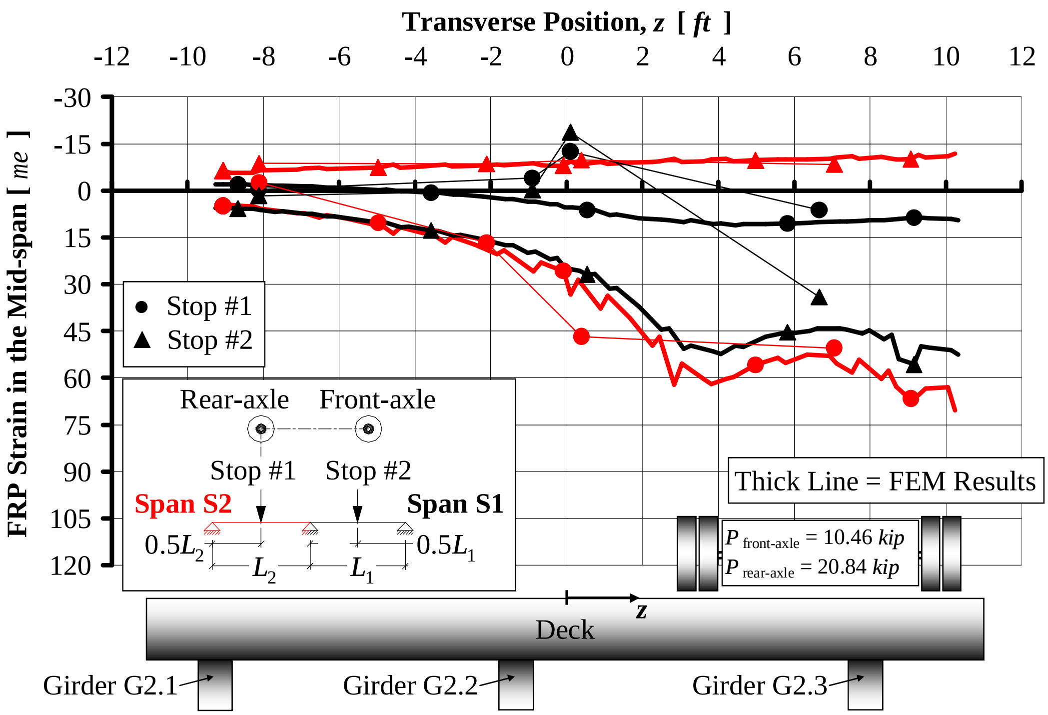

Figure A. 7. Strain in the FRP Strengthening on the Deck at Mid-span, Pass #1

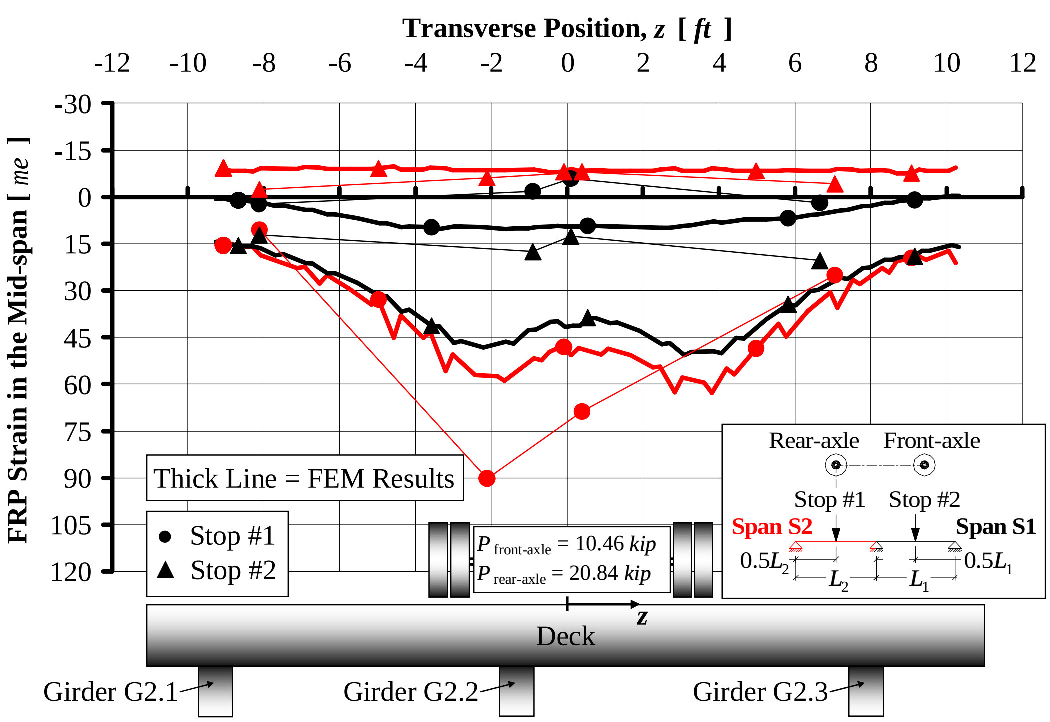

Figure A. 8. Strain in the FRP Strengthening on the Deck at Mid-span, Pass #2

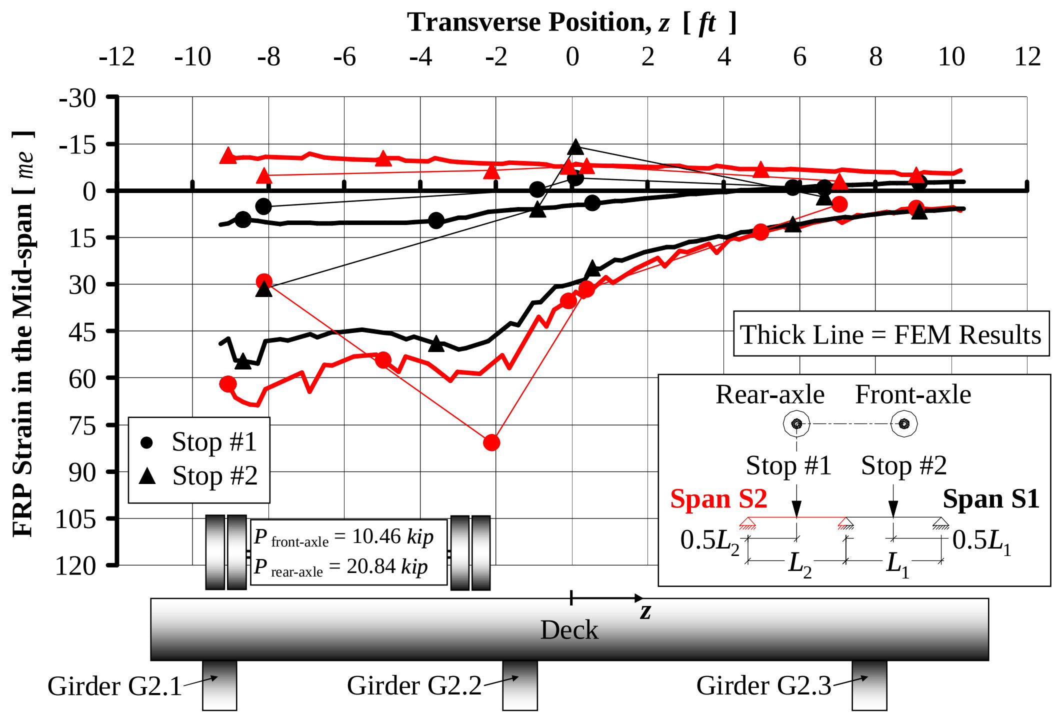

Figure A. 9. Strain in the FRP Strengthening on the Deck at Mid-span, Pass #3

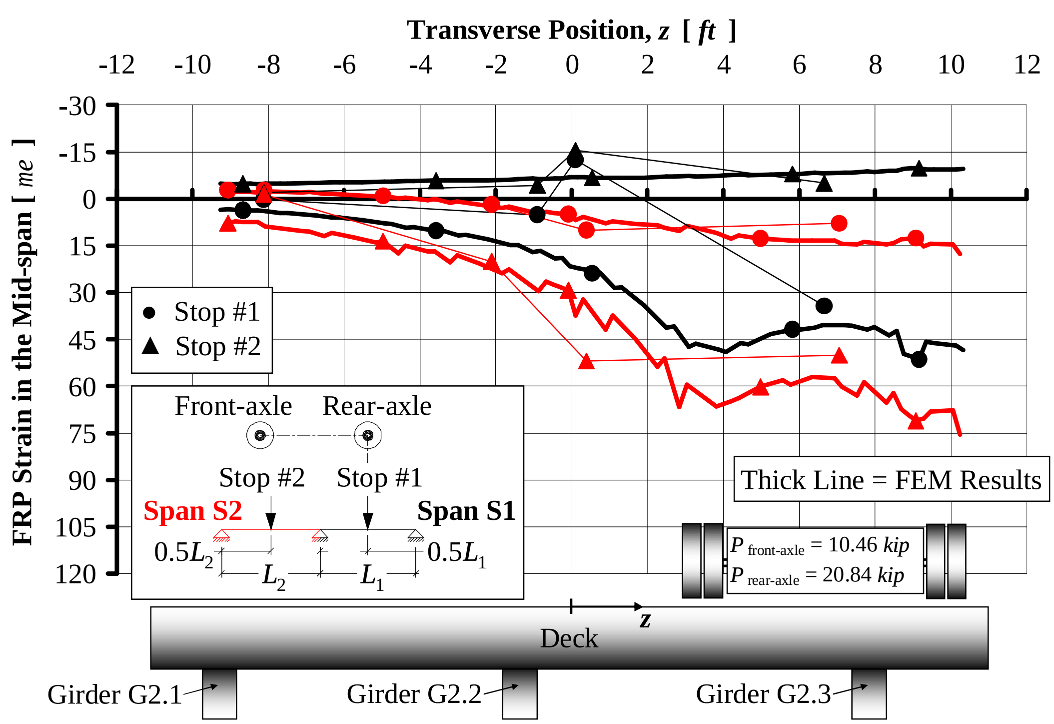

Figure A. 10. Strain in the FRP Strengthening on the Deck at Mid-span, Pass #4

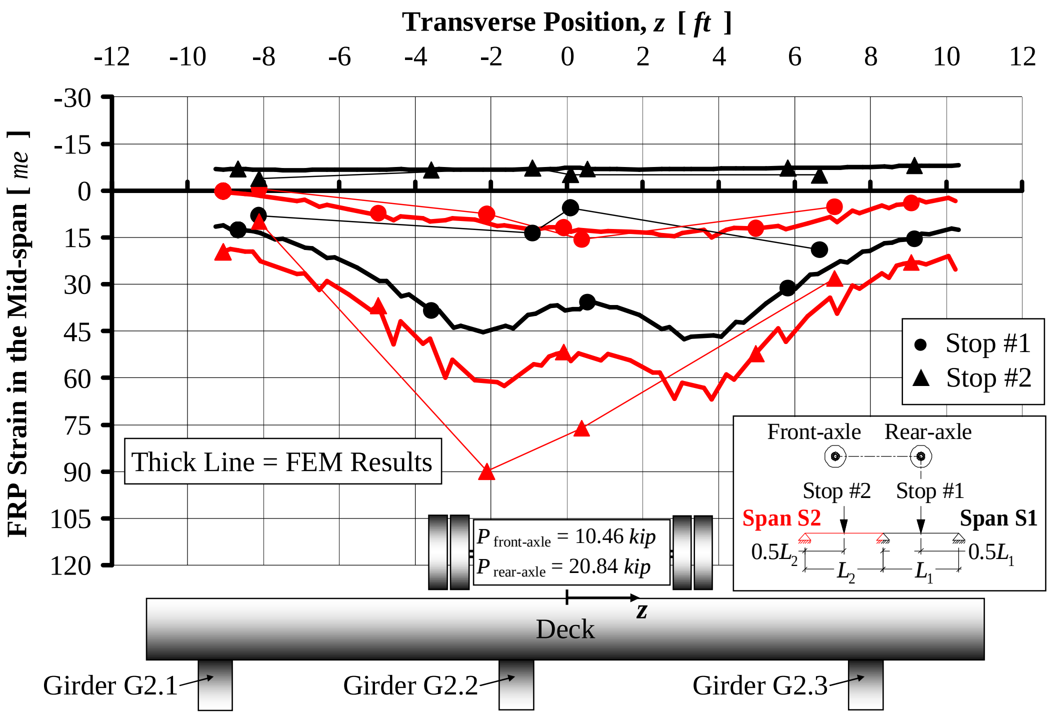

Figure A. 11. Strain in the FRP Strengthening on the Deck at Mid-span, Pass #5

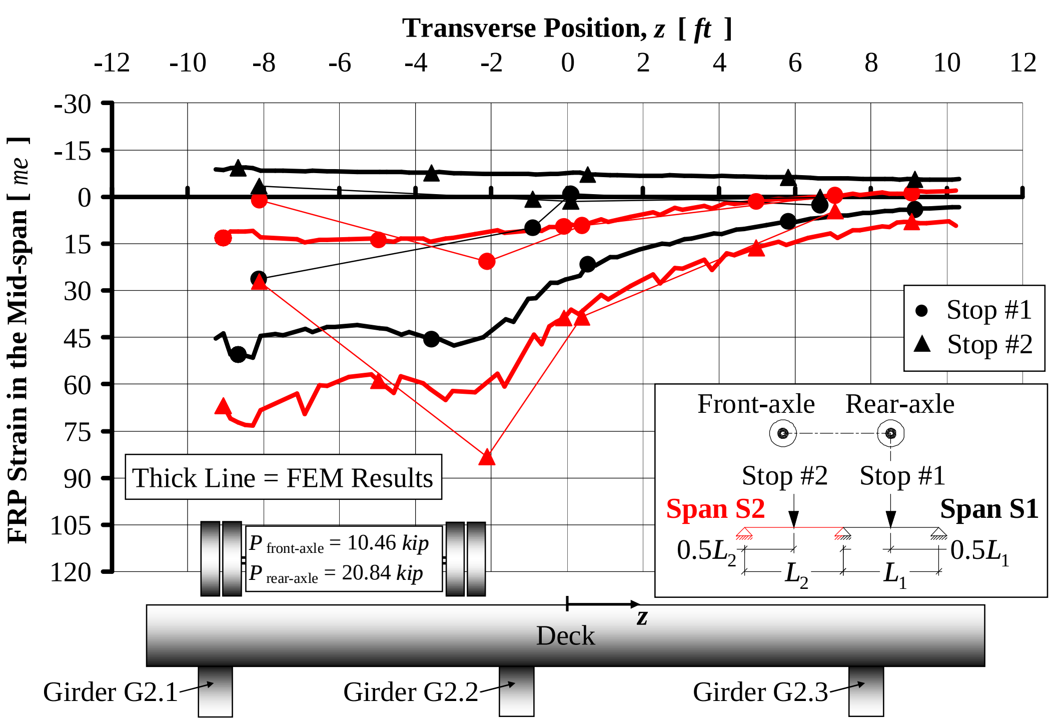

Figure A. 12. Strain in the FRP Strengthening on the Deck at Mid-span, Pass #6

APPENDIX

B. Dynamic Test Results

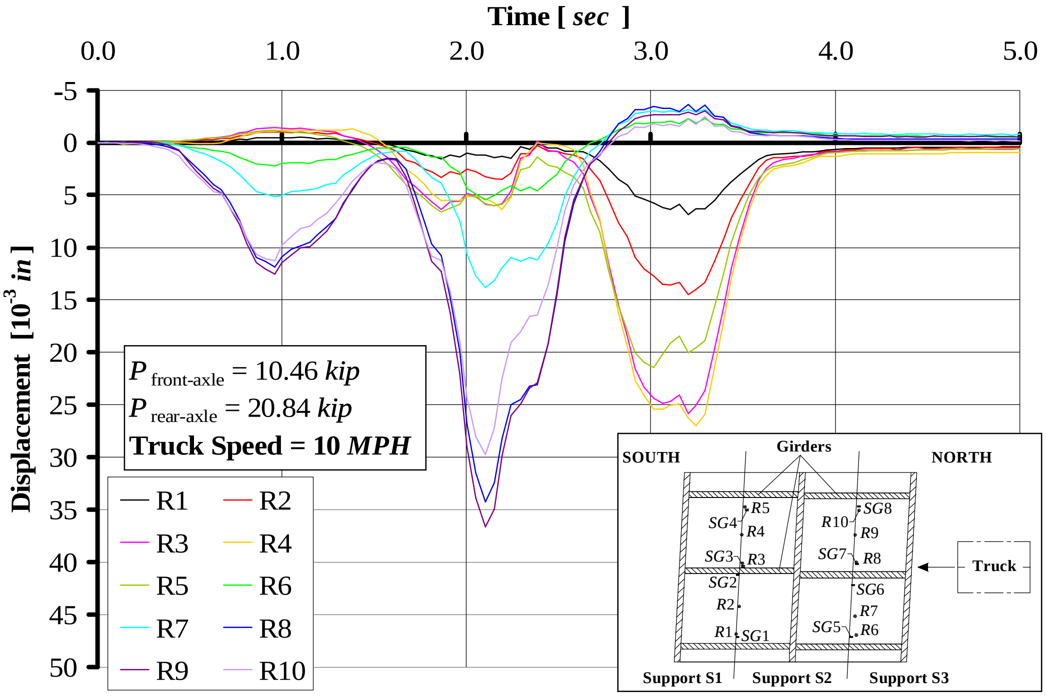

Figure B. 1. After Strengthening Displacements at 4.5 m/s $(10\ MPH)$

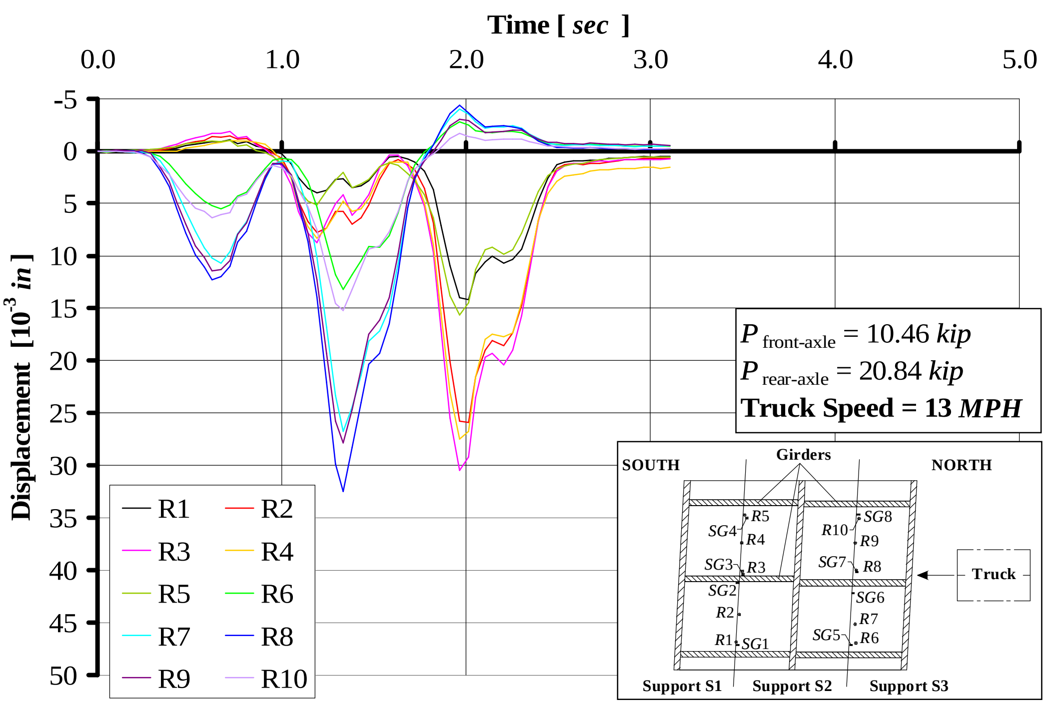

Figure B. 2. After Strengthening Displacements at 5.8 m/s $(13\ MPH)$ (I)

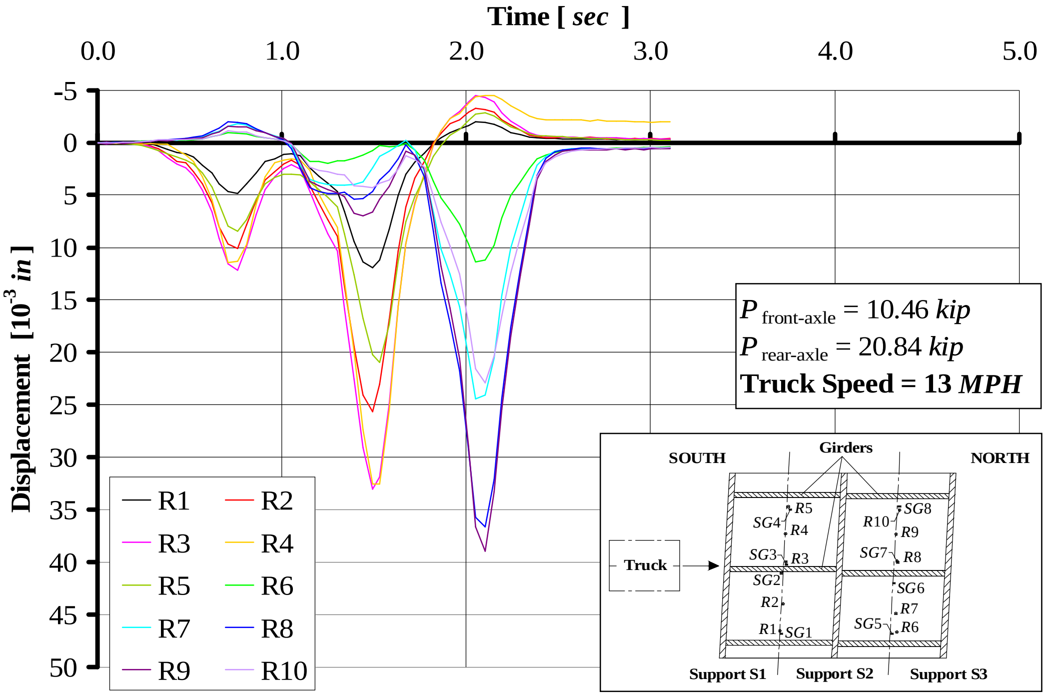

Figure B. 3. After Strengthening Displacements at 5.8 m/s $(13\ MPH)$ (II)

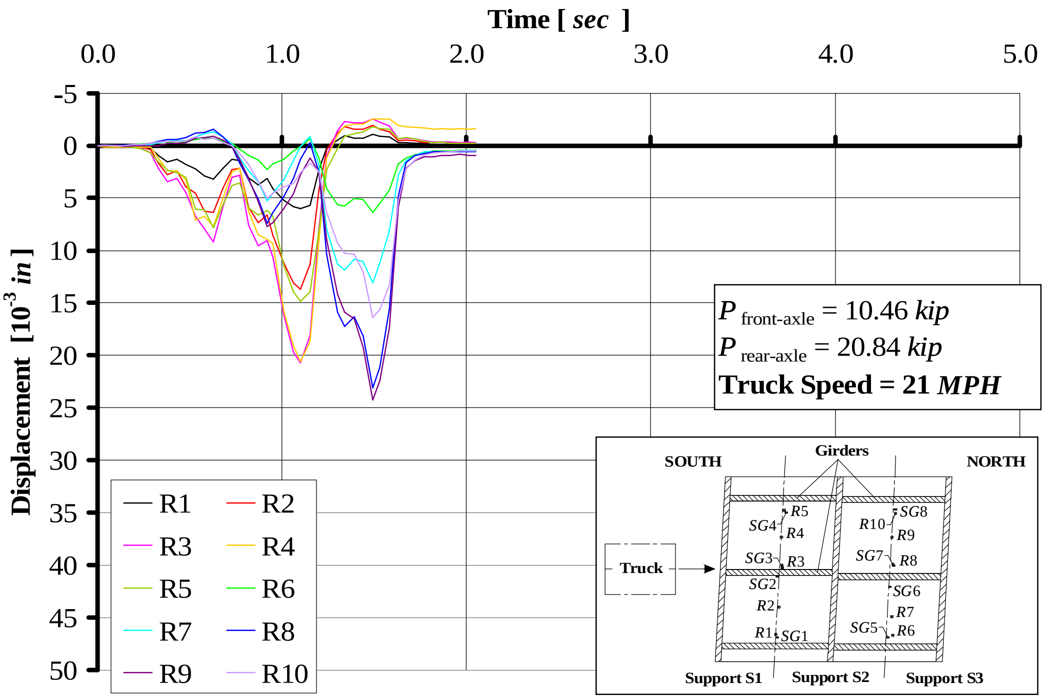

Figure B. 4. After Strengthening Displacements at 9.4 m/s $(21\ MPH)$

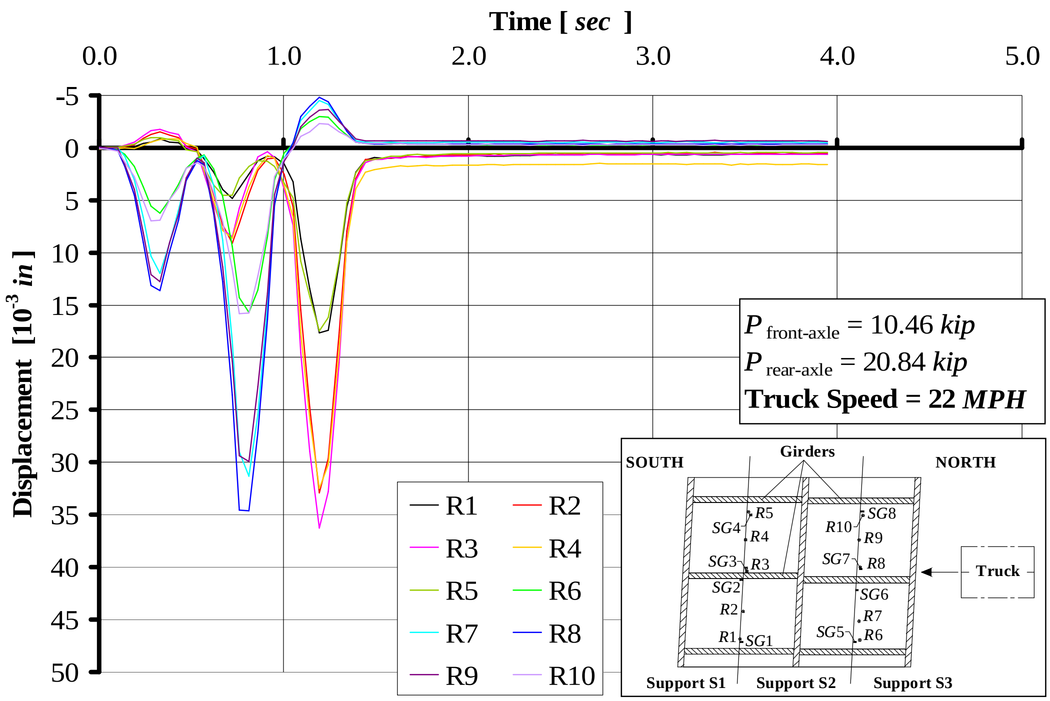

Figure B. 5. After Strengthening Displacements at 9.8 m/s $(22\ MPH)$

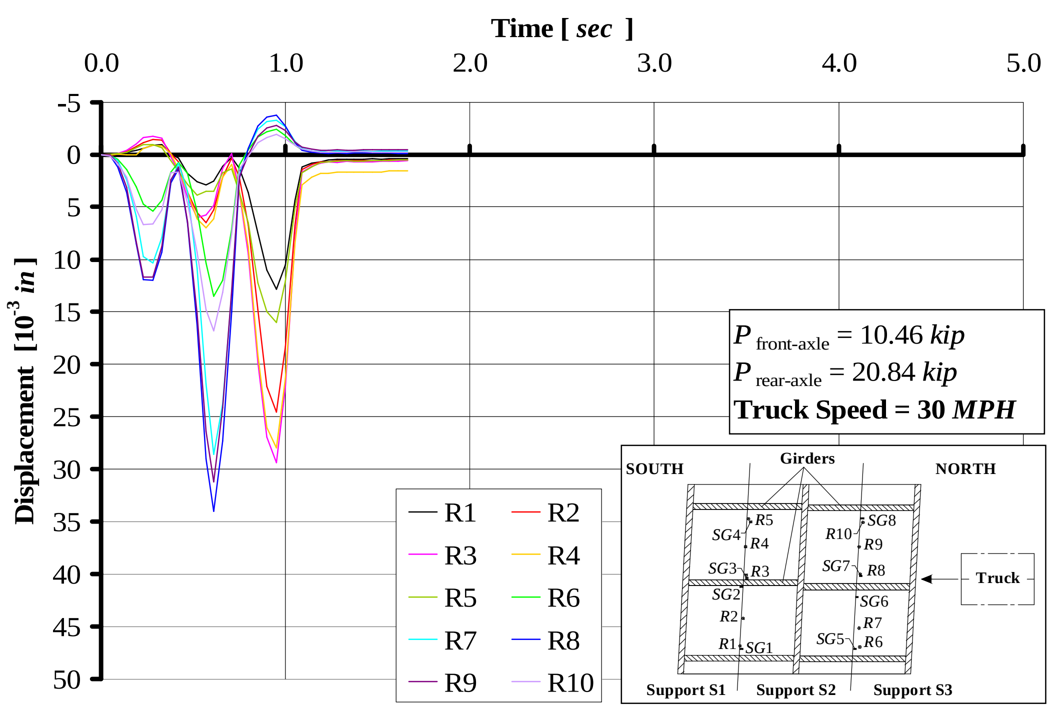

Figure B. 6. After Strengthening Displacements at 13.4 m/s $(30\ MPH)$

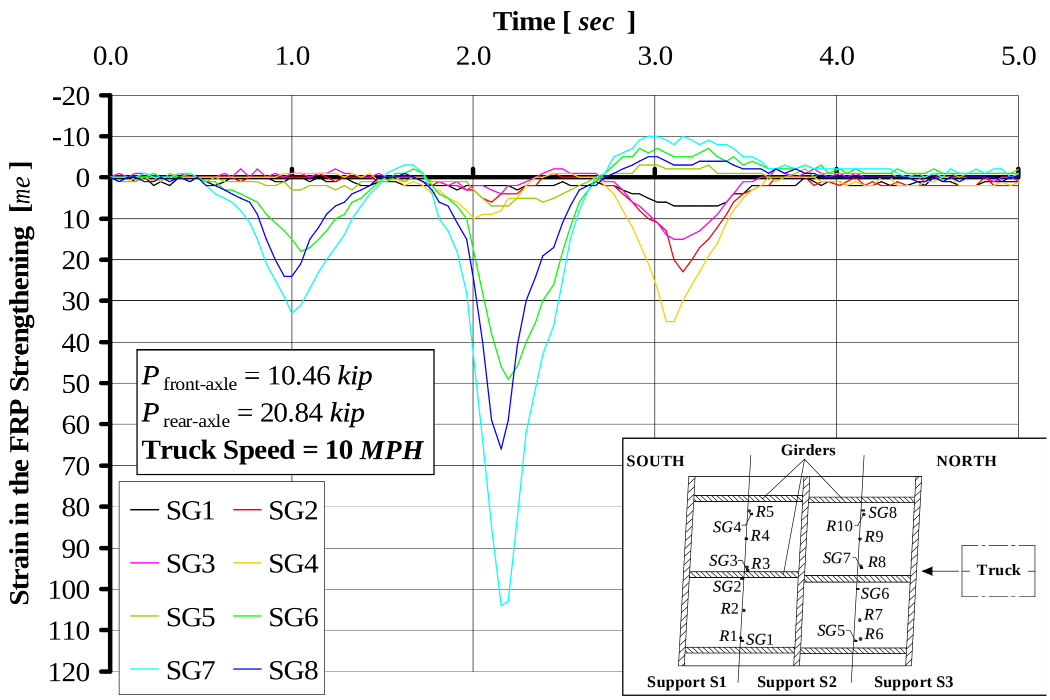

Figure B. 7. After Strengthening Strain in the FRP Laminates at $4.5\ m/s\ \left(10\ MPH\right)$

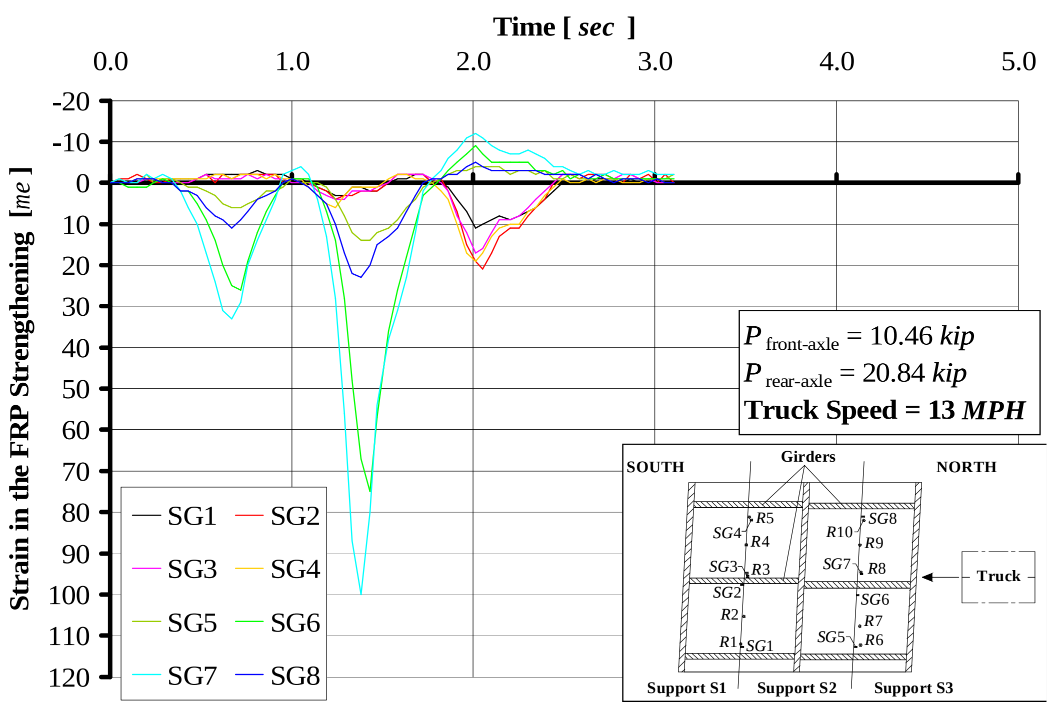

Figure B. 8. After Strengthening Strain in the FRP Laminates at $5.8\ m/s\ \left(13\ MPH\right)$ (I)

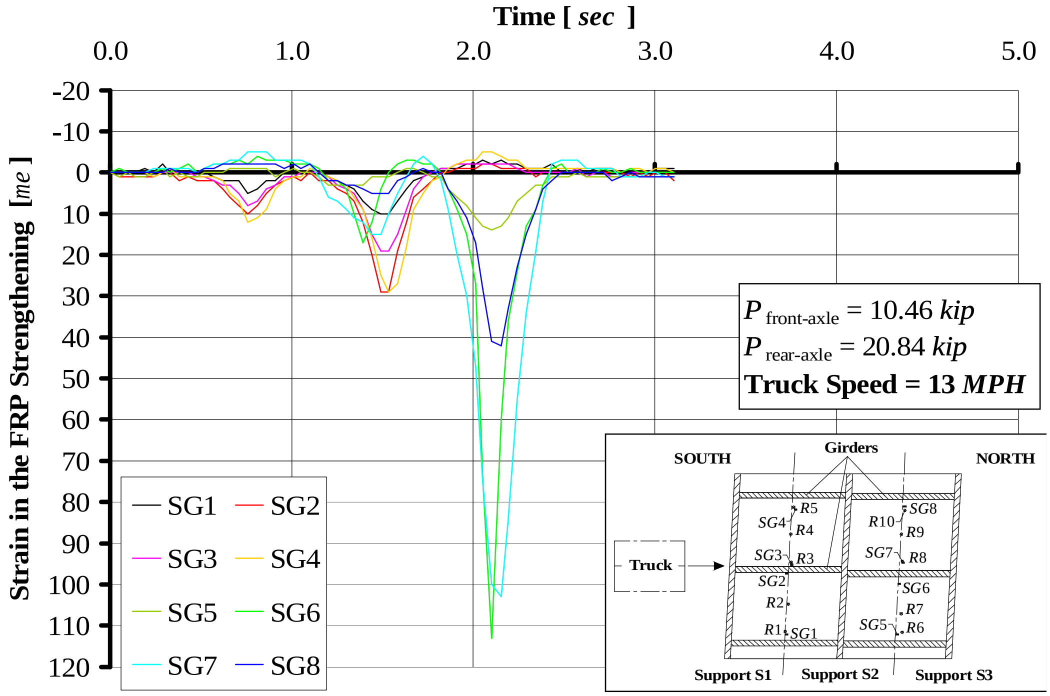

Figure B. 9. After Strengthening Strain in the FRP Laminates at 5.8 m/s $(13\ MPH)$ (II)

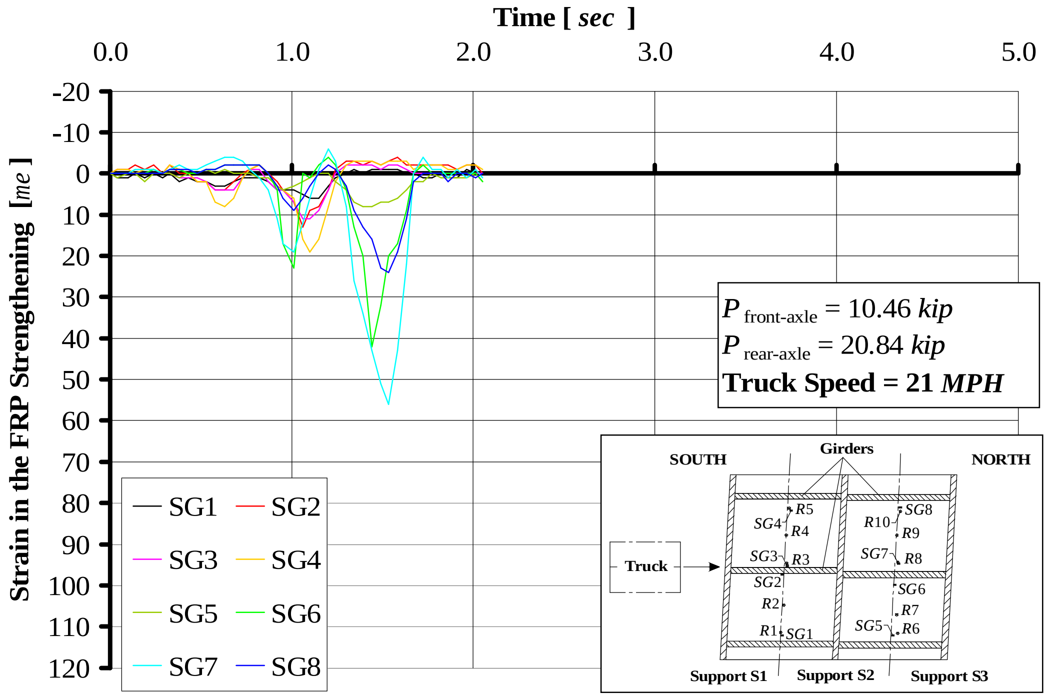

Figure B. 10. After Strengthening Strain in the FRP Laminates at 9.4 m/s $(21\ MPH)$

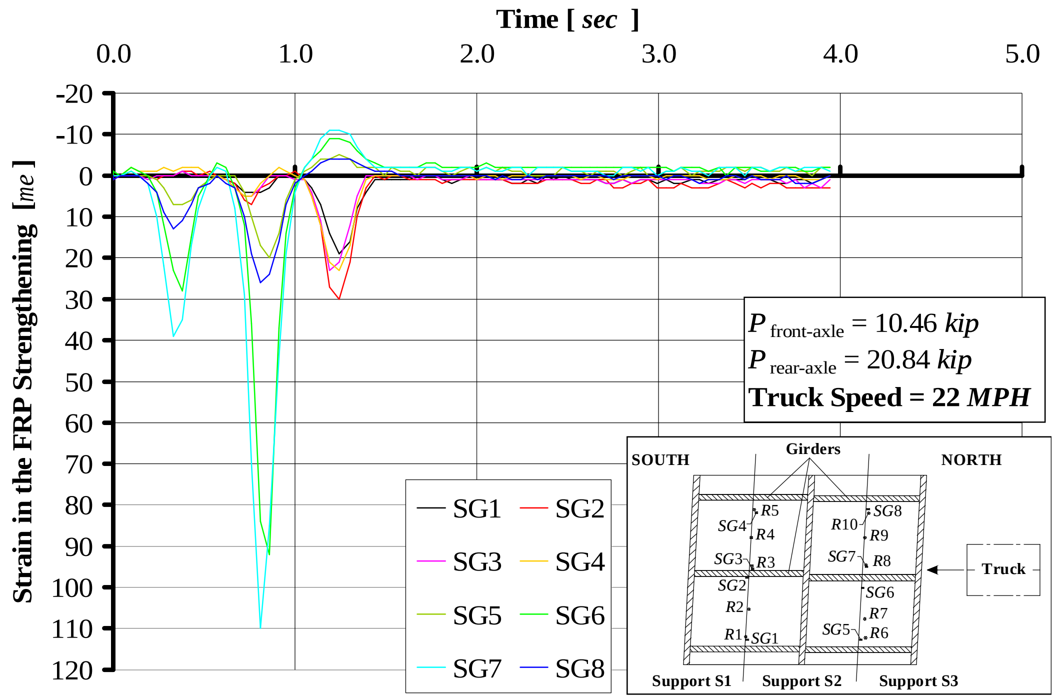

Figure B. 11. After Strengthening Strain in the FRP Laminates at 9.8 m/s $(22\ MPH)$

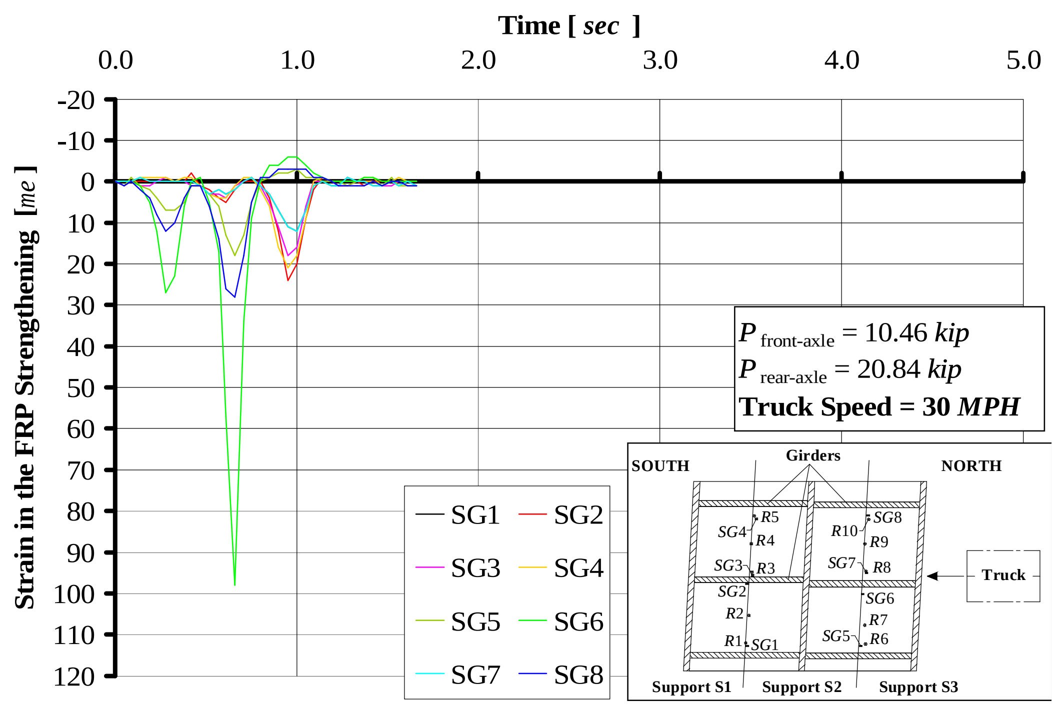

Figure B. 12. After Strengthening Strain in the FRP Laminates at 13.4 m/s $(30\ MPH)$

APPENDIX

C. Installation of the MF-FRP Strengthening System

Figure C. 1. Drilling of the Pre-cured FRP Laminates

a) Removal of Surface Unevenness   b) Temporary Attachment of the Laminates

Figure C. 2. Positioning of the Pre-cured FRP Laminates

Figure C. 3. Drilling of the Holes in the Concrete

a) Hole Filling with Epoxy b) Bolt Hammering c) Torque Control Clamping

Figure C. 4. Fastening Procedure

Figure C. 5. Bridge No. 3855006 after Strengthening

RESEARCH INVESTIGATION

DESIGN AND IN-SITU LOAD TESTING OF BRIDGE No. 2210010

COUNTY ROAD 6210 – PHELPS COUNTY, MO

PREPARED FOR THE

MISSOURI DEPARTMENT OF TRANSPORTATION

IN COOPERATION WITH THE

UNIVERSITY TRANSPORTATION CENTER

Written By:

Andrea Rizzo, MS Candidate

Nestore Galati, Research Engineer

Antonio Nanni, V. & M. Jones Professor of Civil Engineering

CENTER FOR INFRASTRUCTURE ENGINEERING STUDIES

UNIVERSITY OF MISSOURI – ROLLA

Submitted

February 2005

DESIGN AND IN-SITU LOAD TESTING OF BRIDGE No. 2210010

COUNTY ROAD 6210 – PHELPS COUNTY, MO

Executive Summary

This report presents the use of Mechanically Fastened - Fiber Reinforced Polymers (MF-FRP) pre-cured laminates for the flexural strengthening of a concrete bridge. The advantage system consists of pre-cured FRP laminates bolted onto the concrete surface in order to provide the necessary flexural reinforcement to girders and deck. The strength of the technique is in the fact that it does not require any surface preparation prior to the installation of the FRP.

The bridge selected for this project is a 3-span deck: one span is simply-supported while the other two are continuous. In the design, each span of the structure was assumed simply-supported by the abutments. The bridge is located on County Road 6210 in Phelps County, MO. The bridge analysis was performed for maximum loads determined in accordance to AASHTO 17th edition. The strengthening scheme was designed in compliance with the ACI 440.2R-02 design guide and on previous research work on this new type of strengthening MF-FRP system.

The retrofitting of the structure was executed in spring 2004. The MF-FRP strengthening technique was easily implemented and showed satisfactory performance. A load test after the strengthening was performed and a Finite Element Method (FEM) analysis was undertaken. The numerical model was able to represent the behavior of the bridge and demonstrated, in such way, that the posting limit can be removed.

ACKNOWLEDGMENTS

The project was made possible with the financial support received from the UMR - University Transportation Center on Advanced Materials, Center for Infrastructure Engineering Studies at the University of Missouri-Rolla and Meramec Regional Planning Commission (MRPC). Master Contractors installed the FRP systems. Strongwell provided the FRP materials.

The authors would like to acknowledge Rick Pilcher, District Liaison Engineer at MoDOT, and Lesley Bennish, Community Development Specialist from Meramec Regional Planning Commission, for their assistance in this project.

TABLE OF CONTENTS

Page

LIST OF ILLUSTRATIONS

LIST OF TABLES

NOMENCLATURE

ADT	Annual Daily Traffic
A_g	Gross Area of a Section
A_s	Area of the Generic Tensile Non-Prestressed Steel Reinforcement
$A_{s,slab\ long.}$	Area of the Longitudinal Tensile Non-Prestressed Steel Reinforcement of the Deck
$A_{s,slab\ transv.}$	Area of the Transverse Tensile Non-Prestressed Steel Reinforcement of the Deck
A_{tire}	Area of the Print of a Wheel according to AASHTO (2002): $A_{tire} = l_{tire} w_{tire}$
A_1	Factor for Dead Loads
A_2	Factor for Live Loads
b_0	Perimeter of Critical Section
$c.o.v._c$	Coefficient of Variation for the Compressive Strength $f_c^{'}$ of Concrete: $c.o.v._c = \frac{f_c^{'}}{SD_c}$
$c.o.v._y$	Coefficient of Variation for the Specified Yield Strength f_y of Non-prestressed Steel Reinforcement: $c.o.v._y = \frac{f_y}{SD_y}$
C	Capacity of the Member
C_E	Environmental Reduction Factor according to ACI 440 Table 7.1: for Carbon Plate Exposed in Exterior Aggressive Ambient $C_E = 0.85$
CC	Concrete Core
d	Effective Depth of the Steel Reinforcement for a Generic Section
$d_{slab\ long.}$	Effective Depth of the Longitudinal Tensile Non-Prestressed Steel Reinforcement of the Deck

$d_{slab\ transv.}$	Effective Depth of the Transverse Tensile Non-Prestressed Steel Reinforcement of the Deck
Di	Deck No. with $i = 1, 2$ or 3
D	Dead Load of the Bridge
E_c	Modulus of Elasticity of Concrete according ACI 318-02 Section 8.5.1: $E_c = 57000\sqrt{f_c^{'}}\ psi$ with $\left[f_c^{'}\right] = [psi]$
E_f	Modulus of Elasticity of the Pre-Cured FRP Laminate
E_s	Modulus of Elasticity of Non-Prestressed Steel Reinforcement
E_{LL}	Lane Loads according to AASHTO Section 3.24.3.2 (2002): $E_{LL} = 2E_{WL}$
$f_c^{'}$	Specified Compressive Strength of Concrete
f_{fu}	Design Tensile Strength of the Pre-Cured FRP Laminate: $f_{fu} = C_E f_{fu}^{*}$
f_{fu}^{*}	Guaranteed Tensile Strength of the Pre-Cured FRP Laminate as Reported by the Manufacturer
f_y	Specified Yield Strength of Non-Prestressed Steel Reinforcement
f_{FRP}	Stress in the Pre-Cured FRP Laminate at Service Conditions
f_{steel}	Stress in the Non-Prestressed Steel Reinforcement at Service Conditions
F_{FRP}	Maximum Axial Load that the Pre-Cured FRP Laminate Experiences at Ultimate Conditions
h	Overall Thickness of Member
h_a	Maximum Distance from the Abutment of the Live Load
h_b	Embedment Depth of the Anchor
h_c	Vertical Distance between Supports of the Wall
H_c	Vertical Clearance
H_d	Height of the Deck
H_o	Height of the Deck Overlay

i	Subscript for the Two Different Load Conditions: $i = HS20-44$ for the Truck Load and $i = tm$ for the Tandem Load
I	Live Load Impact Factor: $I = \frac{50}{l_d + 125} \leq 0.30$ where $[l_d] = [ft]$
$I_{experimental,\, i}$	Live Load Impact Factor Measured during the Load Test after Strengthening in the Pass No. i with $i = Pass\ \#1, Pass\ \#2, Pass\ \#3$
k	Effective Length Factor according to ACI 318-02 Section 14.5.2: $k = 2.0$ for Walls Not Braced against Lateral Translation
k_a	Active Earth Pressure Coefficient from Coulomb Analysis according to AASHTO (2002) Figure 5.5.2A
k_s	Coefficient of Earth Pressure due to Surcharge
l_c	Clear Span of the Slab
l_d	Design Length of the Slab
l_{tire}	Size of the Print of a Wheel in the Longitudinal Direction according to AASHTO (2002)
L	Live Load Applied on the Bridge. The Same Symbol is Used in Some Figures to Indicate the Design Span of the Bridge
M_d	Flexural Capacity of the Element Calculated in Absence of Axial Load
M_n	Nominal Moment Strength at Section
M_s	Unfactored Moment due to the Most Demanding Load Condition for a Structural Element
$M_{sx,Si}$	Unfactored Moment due to the Demanding Load Condition x for the Support Si ($x = a$ or b)
$M_{s,slab}$	Unfactored Moment due to the Most Demanding Load Condition for the Slab
$M_{s,Si}$	Unfactored Moment due to the Most Demanding Load Condition for the Support Si

M_u	Ultimate (Factored) Moment due to the Most Demanding Load Condition for a Structural Element
$M_{ux,Si}$	Ultimate (Factored) Moment due to the Demanding Load Condition x for the Support Si ($x = a$ or b)
$M_{u,slab}$	Ultimate (Factored) Moment due to the Most Demanding Load Condition for the Slab
$M_{u,Si}$	Ultimate (Factored) Moment due to the Most Demanding Load Condition for the Support Si
$n_{b,\min}$	Minimum Number of Fastener to Anchor a Pre-Cured FRP Laminate so that Failure in Tension Controls: $n_{b,\min} = \frac{F_{FRP}}{R_b}$
p_E	Horizontal Component of the Active Earth Pressure
p_{LL}	Horizontal Earth Pressure
$p_{TL,i}$	Horizontal Pressure Distribution
P	Generic Concentrated Load Applied to a Structure
P_d	Axial Capacity in Compression of the Element Calculated in Absence of Flexure
$P_{Front-Axle}$	Total Load corresponding to the Truck Front Axle
$P_{Rear-Axle}$	Total Load corresponding to the Truck Rear Axles
$P_{sx,Si}$	Unfactored Axial Demand under the Load Condition x for the Support Si ($x = a$ or b)
$P_{HS20-44}$	Weight of a Rear Axle Wheel of the $HS20-44$ Truck
P_n	Nominal Axial Capacity of the Concrete Walls for Unit of Length
$P_{ux,Si}$	Factored Axial Demand under the Load Condition x for the Support Si ($x = a$ or b)
q_s	Uniform Surcharge Applied to the Upper Surface of the Active Earth Wedge

r	Radial Distance from Point of Load Application to a Point on the Wall
R_{ab}	Ultimate (Factored) Axial Load due to the Most Demanding Load Condition for the Two Abutments
R_b	Design Shear Capacity of the Connection
Ri	LVDT No. i with $i=1,2..10$
RF	Rating Factor
R_{pier}	Maximum Axial Load in the Piers
RT	Rating of the Bridge: $RT = RF \cdot W$
S	Spacing of the Supports
Si	Span No. i with $i=1,2$ or 3. The Same Symbol is Used to Indicate the Support No. i with $i=1,2..4$
SD_c	Standard Deviation for the Specified Compressive Strength $f_c^{'}$ of Concrete
SD_y	Standard Deviation for the Specified Yield Strength f_y of Non-prestressed Steel Reinforcement
SGi	Strain Gauge No. i with $i=1,2..8$
t_f	Thickness of the Pre-cured FRP Laminate
T_b	Shear Capacity of the Connection
T_c	Shear Capacity of the Anchor Embedded in Concrete
V_c	Concrete Contribution to the Shear Capacity
V_n	Nominal Shear Strength at Section
$V_{c,i}$	Nominal Shear Strength at Section for Punching Shear Check: $i=1,2,3$
V_s	Unfactored Shear due to the Most Demanding Load Condition for a Structural Element
$V_{s,slab}$	Unfactored Shear due to the Most Demanding Load Condition for the Slab

$V_{s,Si}$ — Unfactored Shear due to the Most Demanding Load Condition for the Support Si

V_u — Ultimate (Factored) Shear due to the Most Demanding Load Condition for a Structural Element

$V_{u,slab}$ — Ultimate (Factored) Shear due to the Most Demanding Load Condition for the Slab

$V_{u,Si}$ — Ultimate (Factored) Shear due to the Most Demanding Load Condition for the Support Si

w_f — Width of the Pre-Cured FRP Laminate

w_s — Walls and Abutments Width

w_{tire} — Size of the Print of a Wheel in the Transverse Direction according to AASHTO (2002)

W — Weight of the Nominal Truck Used to Determine the Live Load Effect

W_r — Width of the Roadway

W_{rc} — Width of the Roadway between Curbs

x — Generic Position of the Truck in the Transverse Direction of the Bridge or the Horizontal Distance from Back of Wall to Point of Load Application

z — Distance from the Left Support of the Generic Section. Sometimes is the Direction of the Axis of the Wall

a — Skew of the Bridge

a_s — Coefficient Used in the Punching Shear Check according to ACI 318-02: $a_s = 40$ for Interior Load; $a_s = 30$ for Edge Load; $a_s = 20$ for Corner Load

b — Slope Angle of the Soil

b_c — Ratio of Long Side to Short Side of the Area over Which the Load is Distributed for Punching Shear Check

b_d — Coefficient as per AASHTO (2002) Table 3.22.1A: $b_d = 1.0$ for Ultimate Conditions and $b_d = 1.0$ for Service Conditions

b_L Coefficient as per AASHTO (2002) Table 3.22.1A: $b_L = 1.67$ for Ultimate Conditions and $b_L = 1.00$ for Service Conditions

g Coefficient as per AASHTO (2002) Table 3.22.1A: $g = 1.3$ for Ultimate Conditions and $g = 1.0$ for Service Conditions. The Same Symbol is also Used to Indicate the Effective Soil Unit Weight

d Angle of Wall Friction according to AASHTO (2002) Table 5.5.2B

$d_{\max}$ Maximum Displacement Experienced during Load Tests

e_{fu} Design Tensile Strain of the Pre-cured FRP Laminate: $e_{fu} = C_E e^*_{fu}$

e^*_{fu} Guaranteed Tensile Strain of the Pre-cured FRP Laminate as Reported by the Manufacturer

f Strength Reduction Factor according to ACI 318-02 Section 9.3: $f = 0.70$ for Axial Load and Axial Load with Flexure for Member without Spiral Reinforcement conforming to ACI 318-02 Section 10.9.3. The Same Symbol is Applied to Indicate the Factors Used to Convert Nominal Values to Design Capacities of Member

f_{punch} Strength Reduction Factor for Punching Shear Check according to ACI 318-02 Section 9.3: $f_{punch} = 0.85$

j Effective Angle of Internal Friction

n Poisson’s Ratio

q Angle of Backfill of Wall to the Vertical

r_w Ratio of Tensile Non-Prestressed Steel Reinforcement: $r_w = \dfrac{A_s}{b_w d}$

w_u Ultimate Value of Stresses due to Moments and Shear Forces

CONVERSION OF UNITS

1 Inch (in) = $8.333 \cdot 10^{-2}$ Feet (ft)

1 Inch (in) = $2.54 \cdot 10^{-2}$ Meters (m)

1 Foot (ft) = 12 Inches (in)

1 Foot (ft) = $3.048 \cdot 10^{-1}$ Meters (m)

1 Kip (kip) = 4.448222 Kilonewton (kN)

1 Kip (kip) = $4.448222 \cdot 10^{3}$ Newton (N)

1 Kip (kip) = 10^{3} Pounds-Force (lbf)

1 Kip per Square Inch (ksi) = 6.894757 Mega Pascal (MPa)

1 Kip per Square Inch (ksi) = $6.894757 \cdot 10^{6}$ Pascal (Pa)

1 Mile per Hour (MPH) = 4.470 Meter per Second (m/s)

1 Pound-Force (lbf) = 4.448222 Newton (N)

1 Pound-Force (lbf) = $4.448222 \cdot 10^{-3}$ Newton (kN)

1 Pound-Force per Square Inch (psi) = $6.894757 \cdot 10^{-3}$ Megapascal (MPa)

1 Pound-Force per Square Inch (psi) = $6.894757 \cdot 10^{3}$ Pascal (Pa)

1 SI Ton (ton_{SI}) = 0.90720 Ton (ton)

1 Ton-Force (ton) = $2 \cdot 10^{3}$ Pounds-Force (lbf)

1 Ton-Force (ton) = 2 Kips (kip)

1. BACKGROUND

1.1. Delta Regional Authority Program Project

In December 2002, as a result of its partnership with University of Missouri, Rolla – University Transportation Center (UMR-UTC), the Meramec Regional Planning Commission (MRPC) received a $193895 grant award from the Delta Regional Authority for bridge improvement projects in Crawford, Dent, Phelps, and Washington Counties.

1.2. Need for the Proposed Project

Transportation infrastructure is one of the major economic development needs for the Meramec Region. Local roads and bridges affect the economic welfare of the region by providing links to the major routes. Local roads and bridges are the collector systems into the larger state highway system for the transport of manufactured products and agricultural goods, accessing employment centers, and bringing travelers and tourists to the region. While many residents are engaged in agriculture and use the roads for farm-to-market routes, a growing number of people are working in cities and living in unincorporated areas relying on rural roads to commute to work. Aging bridges prohibit growth in much of the region because they severely limit access to many communities.

According to the National Bridge Inventory in 1995, 29 percent of county bridges do not meet minimum tolerable conditions to be left as-is. Nationwide, 40 percent of rural bridges are posted as to weight or other travel restrictions. Load postings are defined as the safe loads to cross a bridge. Loads over the posted limit cause damage to the structure and shorten the life of the bridge. Examples of vehicles affected would be school buses, fire trucks and ambulances, commercial truck traffic and large farm equipment. Dump trucks are affected by all load postings according to the Missouri Department of Transportation (MoDOT) and emergency vehicles are affected by most postings. The Federal Highway Administration (FHWA) classifies 32 percent of rural bridges as structurally deficient. Over one-third of the rural bridges in Crawford, Dent, Phelps and Washington counties are considered deficient by MoDOT standards. Much of the problems with local bridges are due to age and obsolete design.

The high cost associated with bridge replacement keeps communities from addressing many bridges. Even the cost to repair bridges is high when using conventional technologies. Maintaining and upgrading transportation infrastructure is a challenge for rural regions because of the sparse density of residents and number of roads and bridges running throughout the area. The low Average Daily Traffic (ADT) on most rural bridges seems to make the cost for bridge replacement ineffective. Low-volume bridges make it difficult for rural areas to compete for grant funding to assist with bridge replacements because rural areas are in competition with larger metropolitan areas. Rural areas are at a disadvantage because more populated areas can incorporate additional aspects of transportation, such as public transit and major economic impact, in grant proposals.

1.3. Description of the Project

Fiber-reinforced polymer (FRP) materials have recently emerged as a practical alternative for construction and renovation of bridges. Advantages of FRP materials are that they resist corrosion, long outlive conventional materials, and have high strength-to-weight ratio. Placement of FRP material is in two forms, near-surface mounted bars and externally-bonded laminates, and the materials are applied on the underside of bridges. UMR has been working with FRP technology on projects around the state and in the Meramec Region. Projects have included strengthening of bridges in Boone County, Phelps County, and St. Louis. Bridges constructed with FRP materials were installed in the city of St. James, MO. FRP strengthening of bridges has had significant cost and time savings over conventional methods.

MRPC is working with local elected officials, UMR and MoDOT to identify and develop 31 bridge strengthening projects in the four-county area of Crawford, Dent, Phelps and Washington. Counties provide MRPC a list of bridge needs and MRPC staff reviews the list with UMR and MoDOT representatives to determine bridges that would be prime candidates for FRP strengthening technology. MoDOT will also review the bridges to determine those that have previously been inspected and found to be structurally deficient or require a load posting. MoDOT will also help determine if projects can help the counties earn soft-match credit towards larger projects using Bridge Replacement Off-system (BRO) funds. MRPC will then determine the economic development impact each bridge has on the region and prioritize projects based on this ranking. The University will prepare design specifications for applying FRP material to each bridge. Contractors will be competitively procured to install the FRP material and those contractors will be required to have or receive certification from UMR for FRP technology training. The University will monitor the application of FRP material to each bridge. Each county may use a third party engineering firm to seal the design and monitor the contractor's activity to ensure that the results of the FRP technology are accurate and valid. Bridges may be tested for load posting before and after the strengthening process to determine the effect of the activity on the strength of each bridge. It is anticipated that strengthening will allow for the load postings to be removed or significantly raised for the structures subjected to such limitations.

1.4. Complementing Existing Regional Plans

Through MRPC, each county completed a Strategic Plan in 2000-2001 to identify current needs and develop a plan of action. This information became part of the region's Comprehensive Economic Development Strategy. Transportation infrastructure was a common need found in all counties. A top priority for economic development was determined to be the need for a better transportation system. Each county identified an objective to improve existing infrastructure. Activities proposed to address the transportation system included encouraging transportation development to enhance economic growth. Most counties found that tourism is directly related to the transportation system and if the tourism industry is to be promoted in the region, the transportation system must be addressed. Counties determined that activities must include improvements to local roads and bridges as well as state routes.

Each community will be required to cover 30 percent of the cost to reinforce each bridge addressed in their jurisdiction. Communities are also responsible for using a third party engineering firm to seal the University's design work and inspect the work of contractor(s) hired to apply the FRP reinforcement. The bridges to be addressed are not deficient due to poor maintenance, but to age and structural obsolescence. Once strengthened, the bridges will have an increased life by removing or upgrading the current load postings. Each community budgets for road and bridge maintenance and this will not change with the proposed project. Strengthening is the only alternative to replacement, and should not require additional maintenance from the community's road crews.

An improved transportation system is a severe need all across the state, including these four Delta counties of the Meramec Region. The transportation system, bridges in particular, was found to be a top priority in the strategic plans for each county as part of the Comprehensive Economic Development Strategy developed for the region. Transportation was directly related to economic development in each county and for the region. The transportation infrastructure of the region has a direct impact on economic development by providing the means necessary to transport raw materials and products, employees to/from work and consumers to/from business centers.

1.5. Impact of the Project

Strengthening bridges will allow for communities to open bridges to more traffic and facilitate the movement of freight, farm equipment and products, and commuter traffic. Counties will add new strength to bridges that otherwise would need to be replaced or closed due to posting limits. Major employment centers are located in each of the four counties. The industries are dependent upon moving their goods and, in the Meramec Region, goods move only via the road system. Major employment centers rely on the local transportation system to allow access for employees and connecting with larger transportation systems for moving materials and products. Such industries include Doe Run Inc., Salem Memorial District Hospital and US Food Service in Dent County, Dana Brake Parts Inc., Meramec Industries Inc., and Missouri Baptist Hospital in Crawford County, Briggs & Stratton Corp., Boys & Girls Town of Missouri and Wal-Mart Distribution Center in Phelps County and Red Wing Shoe Co., Georgian Gardens Nursing Home and YMCA of the Ozarks in Washington County.

Up to 31 county bridges may be strengthened using the FRP technology. Strengthening will remove load postings or significantly increase postings so that bridges will be open to more traffic. These bridges will allow for more access from county roads to major routes running through the area, directly impacting the economic development potential of the region.

2. INTRODUCTION

This report summarizes the procedures used for the upgrade of the Bridge No. 2210010 (see Figure 2.1), located in Phelps County (County Road 6210), MO. The bridge is actually load posted to a maximum weight of 10.9 ton_{SI} $(12\ ton)$.

Figure 2.1. Bridge No. 2210010

The total length of the bridge is $9754\ mm\ (32\ ft)$ and the total width of the deck is $6325\ mm\ (20\ ft\ 9\ in)$. The structure is a 3-span $229\ mm\ (9\ in)$ deep deck: one span is simply-supported while the other two are continuous.

2.1. Objectives

The primary objectives of this document are to analyze the bridge superstructure and to provide the design calculations for its strengthening using a Mechanically Fastened Fiber-Reinforced Polymer system (MF-FRP). The advantage system consists of pre-cured FRP laminates bolted onto the concrete surface in order to provide the necessary flexural reinforcement to deck and abutments. The strength of the technique is in the fact that it does not require any surface preparation prior to the installation of the FRP.

2.2. Bridge Conditions

Prior to the strengthening of the bridge, a detailed investigation was required to determine the initial conditions of the bridge and the properties of the constituent materials. The details of the bridge reinforcement and material properties were unknown due to the unavailability of the bridge plans. As a consequence, at the onset of the project, these properties were determined in-situ, based on visual and Non Destructive Testing (NDT) evaluation.

From visual observations, some concrete spalling along the longitudinal edges of the bridge was observed. The deck showed traces of steel rebar corrosion (see Figure 2.2-a) and erosion (see Figure 2.2-b). In addition, some bars on the corners of the deck were completely exposed with clear signs of corrosion (see Figure 2.2-c). Some cracks ran parallel and normal to the traffic direction along the two continuous spans (see Figure 2.2-d).

a) Steel Rebar Corrosion on the Deck

b) Erosion on the Deck

c) Exposed Bar in the Lateral Side

d) Crack Parallel and Normal to the Traffic Direction

Figure 2.2. Condition of the Superstructure

The concrete walls appeared to be in good condition except for some vertical cracks running down across their entire height (see Figure 2.3-a). Some bars on the corner were completely exposed with clear corrosion signs (see Figure 2.3-b). A horizontal crack was found across the retaining abutment downhill (see Figure 2.4-a) while the soil is not in perfect contact with the surface of the other abutment (see Figure 2.4-b).

a) Vertical Cracks

b) Exposed Bar in the Corner

Figure 2.3. Condition of the Walls

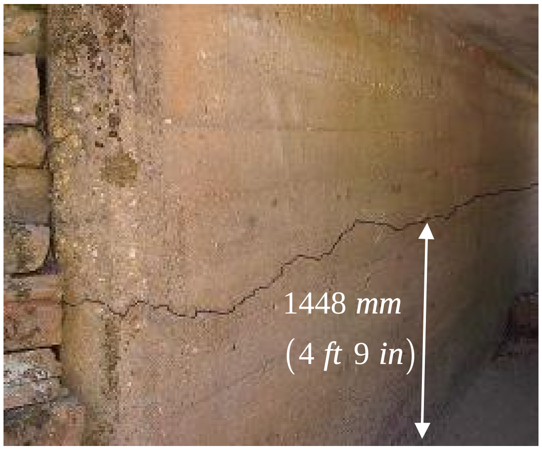

a) Horizontal Crack across the Retaining Abutment Downhill

b) Soil not in Perfect Contact with the Surface of the Abutment

Figure 2.4. Condition of the Abutments

The geometry of the bridge is summarized in Table 2.1. Figure 2.5 and Figure 2.6 show the longitudinal and plan view of the bridge. Figure 2.6 also displays the position from where the concrete cores were extracted and the longitudinal and transverse steel reinforcement of the deck.

Table 2.1. Geometry of the Bridge

Span	S1	S2	S3
Clear Span (Parallel to the Traffic Direction)	$l_c = 3335\ mm$ $(10\ ft\ 11\frac{5}{16}\ in)$	$l_c = 3433\ mm$ $(11\ ft\ 3\frac{5}{32}\ in)$	$l_c = 3285\ mm$ $(10\ ft\ 9\frac{5}{16}\ in)$
Design Length (Parallel to the Traffic Direction)	$l_d = 3505\ mm$ $(11\ ft\ 6\ in)$	$l_d = 3604\ mm$ $(11\ ft\ 9\frac{29}{32}\ in)$	$l_d = 3499\ mm$ $(11\ ft\ 5\frac{6}{8}\ in)$
Deck Height	$H_d = 229\ mm$ $(9\ in)$	$H_d = 229\ mm$ $(9\ in)$	$H_d = 229\ mm$ $(9\ in)$
Vertical Clearance (Measured in the Middle Span)	$H_c = 2118\ mm$ $(6\ ft\ 11\frac{3}{8}\ in)$	$H_c = 2262\ mm$ $(7\ ft\ 5\frac{1}{16}\ in)$	$H_c = 2413\ mm$ $(7\ ft\ 11\ in)$
Walls and Abutments Width	$w_s = 203\ mm\ (8\ in)$		
Skew	$a = 27^o$		

Slope Angle of the Soil (Angle to Fill to the Horizontal)	Abutment S1: $b = 0^o$ Abutment S4: $b = 7^o$
Roadway Width (Orthogonal to the Traffic Direction)	$W_r = 6325\ mm\ (20\ ft\ 9\ in)$
Curb-to-Curb Roadway Width (Orthogonal to the Traffic Direction)	$W_{rc} = 5766\ mm\ (18\ ft\ 11\ in)$
Overlay Height	$H_o = 0\ mm\ (0\ in)$

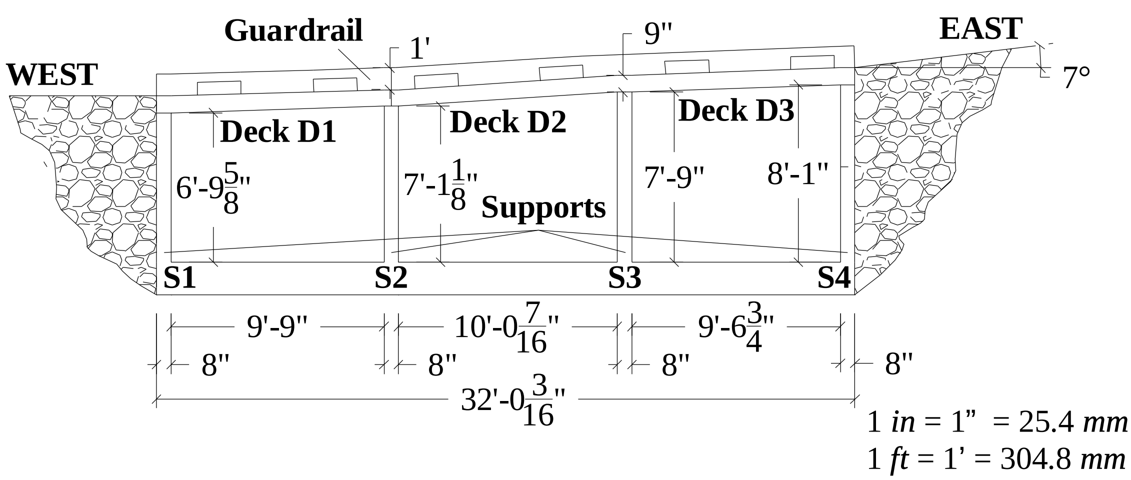

Figure 2.5. Longitudinal View of the Bridge

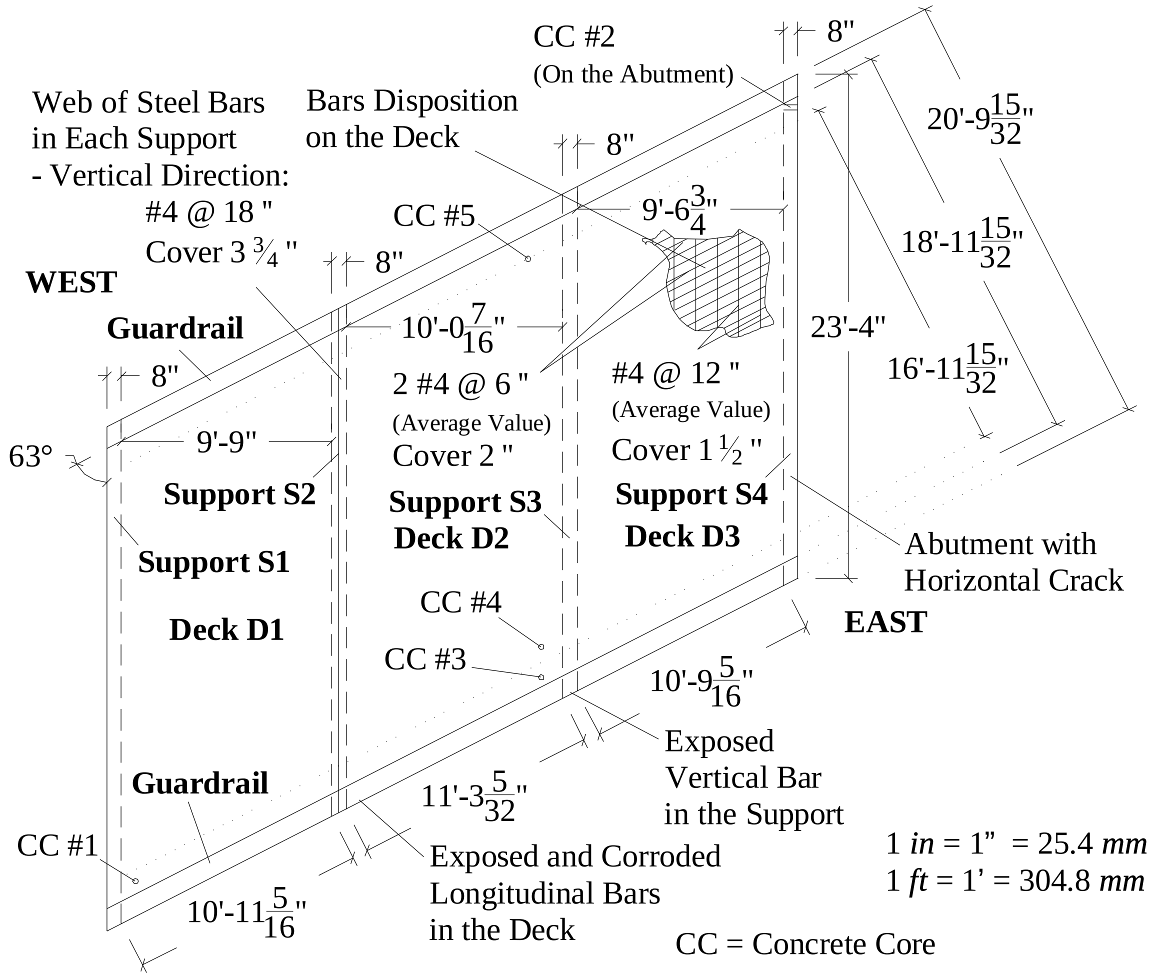

Figure 2.6. Plan View of the Bridge

Four concrete cores were drilled from the deck (see Figure 2.7-a) and one from the support S4, and were tested in compliance with ASTM C39/C39M-1 and ASTM C42/C42M-99 (see Figure 2.7-b). The following results were found:

- Average Compression Strength: $f_c^{'} = 23.2\ MPa\ \left(3365\ psi\right)$;
- Standard Deviation: $SD_c = 2.8\ MPa\ \left(413\ psi\right)$;
- Variance: $c.o.v._c = 100\dfrac{SD_c}{f_c^{'}} = 12.3\%$.

Based on the experimental results, a compression strength of $23.2\ MPa\ \left(3365\ psi\right)$ was assumed for design.

a) Coring b) Compression Tests

Figure 2.7. Material Characterization of the Concrete

The real location of the steel reinforcement in the deck, walls and abutments was accurately determined by using a rebar locator. The size and the cover of the bars were determined by visual inspection of the exposed bars and those found in the concrete cores.

Concrete cover and size of longitudinal (parallel to the traffic direction) and transverse steel bars in the deck were determined by visual inspection (see Figure 2.2-c) and from the concrete cores (see Figure 2.8) as follows:

- Transverse Direction

  $\#4$ ($12.7\ mm$ $(0.5\ in)$ diameter) steel bars

  average spacing: $305\ mm$ $(12\ in)$ on center

  clear concrete cover: $38\ mm$ $(1\frac{1}{2}\ in)$;

- Longitudinal Direction

  $2\#4$ ($12.7\ mm$ $(0.5\ in)$ diameter) steel bars average spacing: 152 mm $(6\ in)$ on center

clear concrete cover: 51 mm $(2\ in)$.

Concrete cover, number and size of flexural and shear reinforcement for the abutments and walls were determined by visual inspection (see Figure 2.3-b). The reinforcement consists of a web of steel bars:

- Vertical Direction

  #4 (12.7 mm $(0.5\ in)$ diameter) steel bars

  average spacing: 457 mm $(18\ in)$ on center

  clear concrete cover: 95 mm $(3\frac{3}{4}\ in)$.

Comparing the bridge with others of the same age and type, a yield value of 344.7 MPa $(50\ ksi)$ was assumed for design.

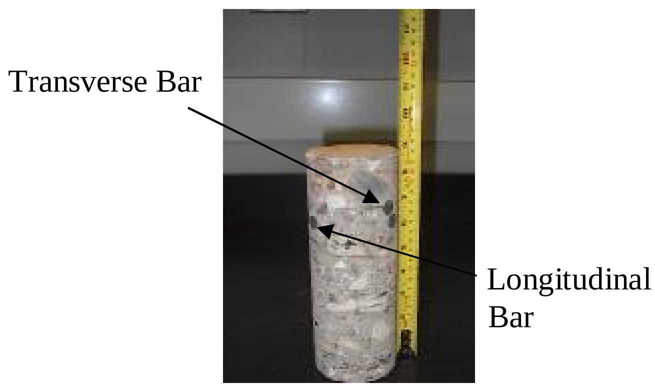

Figure 2.8. Material Characterization of the Steel Bars

2.3. Conclusions

The flexural capacity of the deck can be improved by the use of the MF-FRP system in order to recover the loss of strength due to the corrosion of the bars and eventually remove the load posting. The superstructure of the bridge can be modeled as a slab supported by abutments and walls. In addition, since it is not possible to guarantee the flexural continuity across the central walls, the bridge can be conservatively modeled as three simply-supported slabs.

The mid-height horizontal crack running on the abutment S4 is due to the active pressure of the soil and the surcharge due to the live loads. The actual amount of steel reinforcement is not adequate for the new design load and therefore vertical MF-FRP strips will provide the necessary strengthening. The abutment can be modeled as a beam supported by the deck and the footing. In addition, since it is not possible to easily detect the actual amount of reinforcement in the footing, the abutment can be conservatively modeled as a simply-supported beam.

The analysis and design of the bridge presented in the following sections is performed according to the MoDOT Bridge Manual, to the experimental results attained at the University of Wisconsin-Madison (Bank et al., 2002) and at UMR. The assumed load configurations are consistent with the AASHTO Specifications (AASHTO, 2002).

3. STRUCTURAL ANALYSIS

3.1. Load Combinations

For the structural analysis of the bridge, the definitions of design truck and design lane are necessary. This will be addressed in the next section.

Ultimate values of bending moments and shear forces are obtained by multiplying their nominal values with the dead and live load factors and by the impact factor according to AASHTO (2002) as shown in equation (3.1):

$$w_u = g\left[b_d D + b_L (1+I) L\right] \tag{3.1}$$

where

D	is the dead load;
L	is the live load;
g, b_d, b_L, b_E	are coefficients as per AASHTO (2002) Table 3.22.1A:
	ultimate conditions $\Rightarrow g = 1.3$, $b_d = 1.0$, $b_L = 1.67$, $b_E = 1.5$;
	service conditions $\Rightarrow g = 1.0$, $b_d = 1.0$, $b_L = 1.00$, $b_E = 1.0$;
I	is the live load impact calculated as follows:

$$I = \frac{50}{l_d + 125} = \frac{50}{12.792 + 125} = 0.36 \leq 0.30 \tag{3.2}$$

and $l_d = 11\,ft\ 9\,{}^{29}\!/_{32}\ in = 11.825\,ft\ (3604\ mm)$ represents the span length from center to center of support. The impact factor should not be larger than 0.30, and therefore the latter value is assumed for the design.

3.2. Design Truck and Design Lanes

Prior to the design of the strengthening, the analysis of the bridge was conducted by considering a HS20-44 truck load (which represents the design truck load as per AASHTO, 2002 Section 3.7.4) having geometrical characteristics and weight properties shown in Figure 3.1.

According to AASHTO Section 3.6.3 (2002), just one design lane should be used. The lane load or standard truck shall be assumed to occupy a width of $3048\ mm\ (10\ ft)$ and placed in such positions on the roadway as will produce the maximum stress in the member under consideration. To be noted that the centerline of the wheels of the rear axle shown in Figure 3.1 is located $305.0\ mm\ (1.0\ ft)$ away from the curb as specified in AASHTO (2002) for slab design.

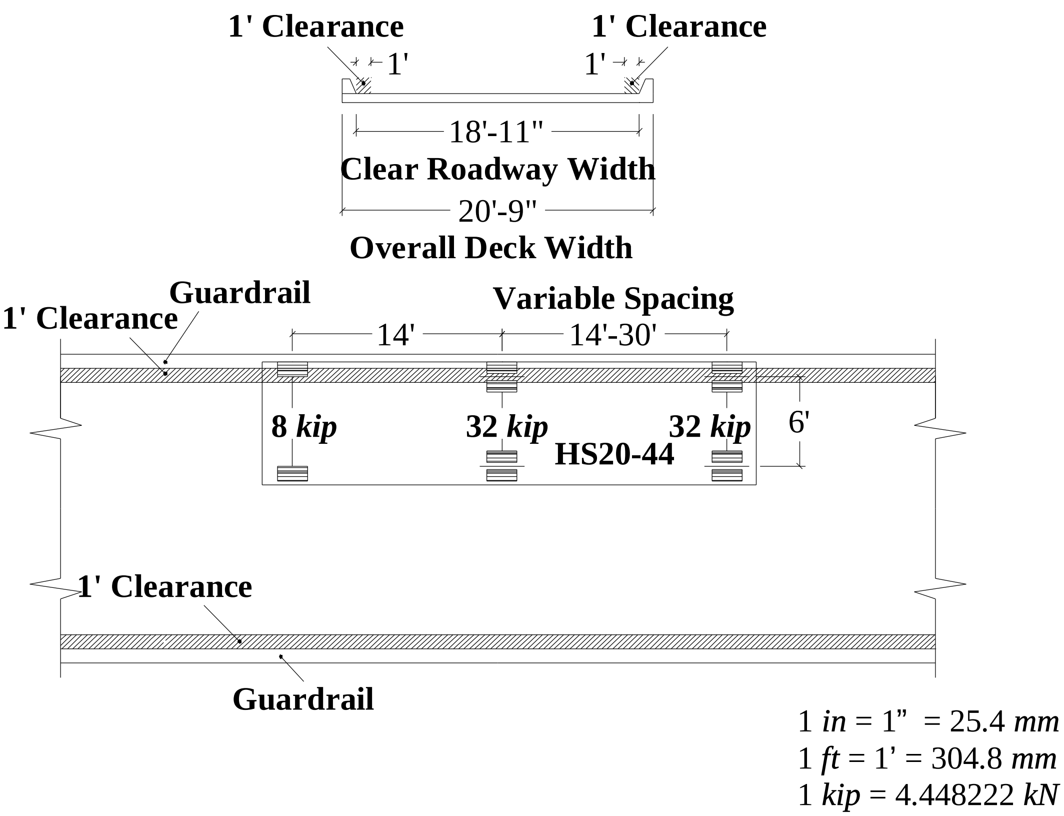

Figure 3.1. Truck Load and Truck Lanes

Two loading conditions are required to be checked as laid out in Figure 3.2.

The HS20-44 design truck load (Figure 3.2-a) has a front axle load of $35.59\ kN\ (8.0\ kip)$, second axle load, located $4267\ mm\ (14\ ft)$ behind the drive axle, of $142.34\ kN\ (32.0\ kip)$ and rear axle load also of $142.34\ kN\ (32.0\ kip)$. The rear axle load is positioned at a variable distance, ranging between $4267\ mm\ (14\ ft)$ and $9144\ mm\ (30.0\ ft)$. Given the specific bridge geometry, the worst loading scenario is obtained for the minimum spacing of $4267\ mm\ (14\ ft)$ between the two rear axles: in particular, since the design span is $l_d = 3604\ mm\ (11.825\ ft)$, only one axle at a time will be on each span.

The design lane loading condition consists of a load of $2.85\ kN\ (0.64\ kip)$ per linear foot, uniformly distributed in the longitudinal direction with a single concentrated load so placed on the span as to produce maximum stress. The concentrated load and uniform load are considered to be uniformly distributed over a $3048\ mm\ (10\ ft)$ width on a line normal to the center lane of the lane. The intensity of the concentrated load is represented in (Figure 3.2-b) for both bending moments and shear forces. This load shall be placed in such positions within the design lane as to produce the maximum stress in the member.

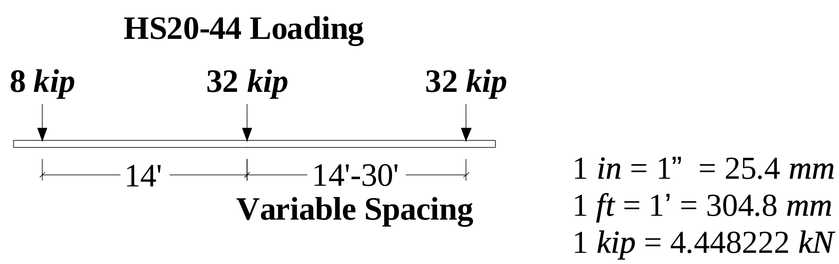

a) Design Truck (HS20-44)

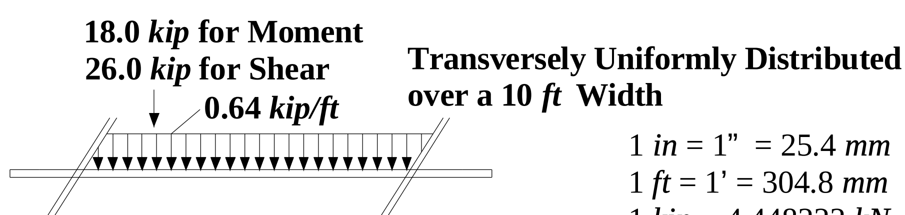

b) Design Lane

Figure 3.2. Loading Conditions

3.3. Slab Analysis

Since it was not possible to detect the presence of longitudinal reinforcement in the negative moment regions, the continuity of the deck over the walls was conservatively neglected. This led to model the deck as a slab simply-supported between two consecutive supports.

Figure 3.3 and Figure 3.4 show the critical loading conditions for the slab between supports S2 and S3. The design value was determined from the truck design when the rear axle wheels are in the position #3 (see Figure 3.3), being this one the most demanding to the structure. The load of each wheel was spread over a surface $508\times254\ mm\ \left(20\times10\ in\right)$ as prescribed in the AASHTO (2002) Section 4.3.30. A commercial Finite Elements Program (SAP 2000) was used to analyze the structure. Along the traffic direction, the ultimate and the service moment ($M_{u,slab}$ and $M_{s,slab}$ respectively) found from this analysis were (see Figure 3.5):

$$M_{u,slab} \cong 111.2\ \frac{kN\cdot m}{m}\left(25.0\ \frac{kip\cdot ft}{ft}\right) \qquad M_{s,slab} \cong 53.8\ \frac{kN\cdot m}{m}\left(12.1\ \frac{kip\cdot ft}{ft}\right)$$

while the ultimate and the service shear ($V_{u,slab}$ and $V_{s,slab}$ respectively) were:

$$V_{u,slab} \cong 102.2\ \frac{kN}{m}\left(7.0\ \frac{kip}{ft}\right) \qquad V_{s,slab} \cong 49.6\ \frac{kN}{m}\left(3.4\ \frac{kip}{ft}\right).$$

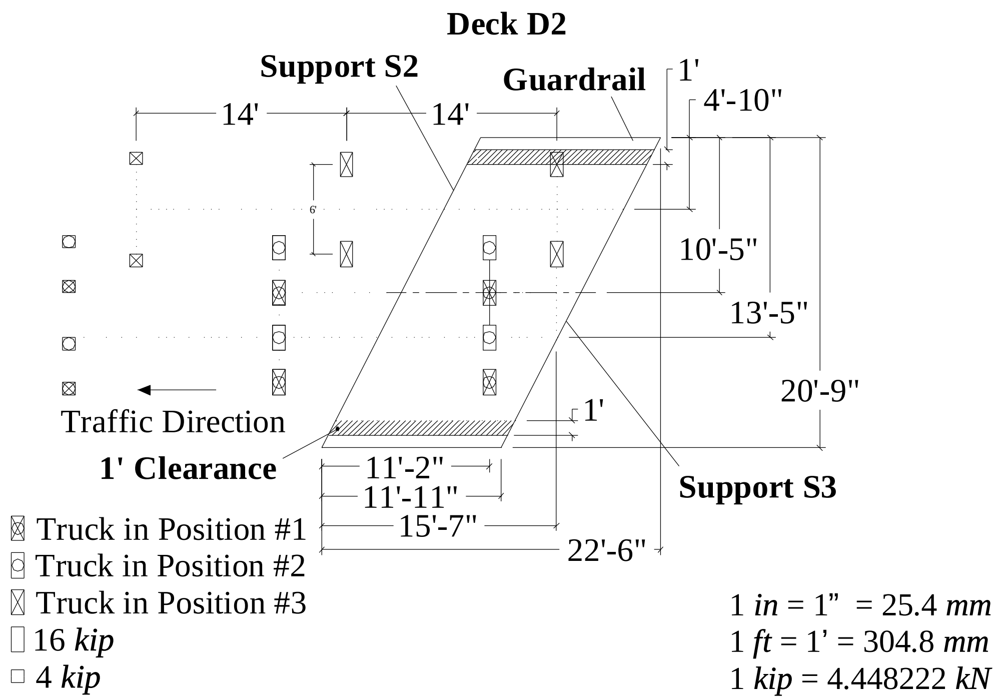

Figure 3.3. Slab Load Conditions: Standard Truck

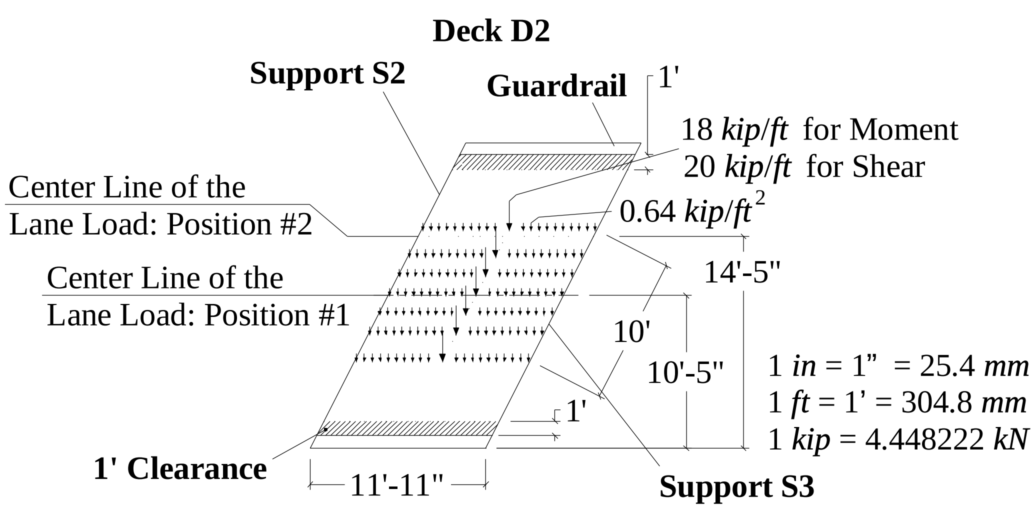

Figure 3.4. Slab Load Conditions: Lane Load

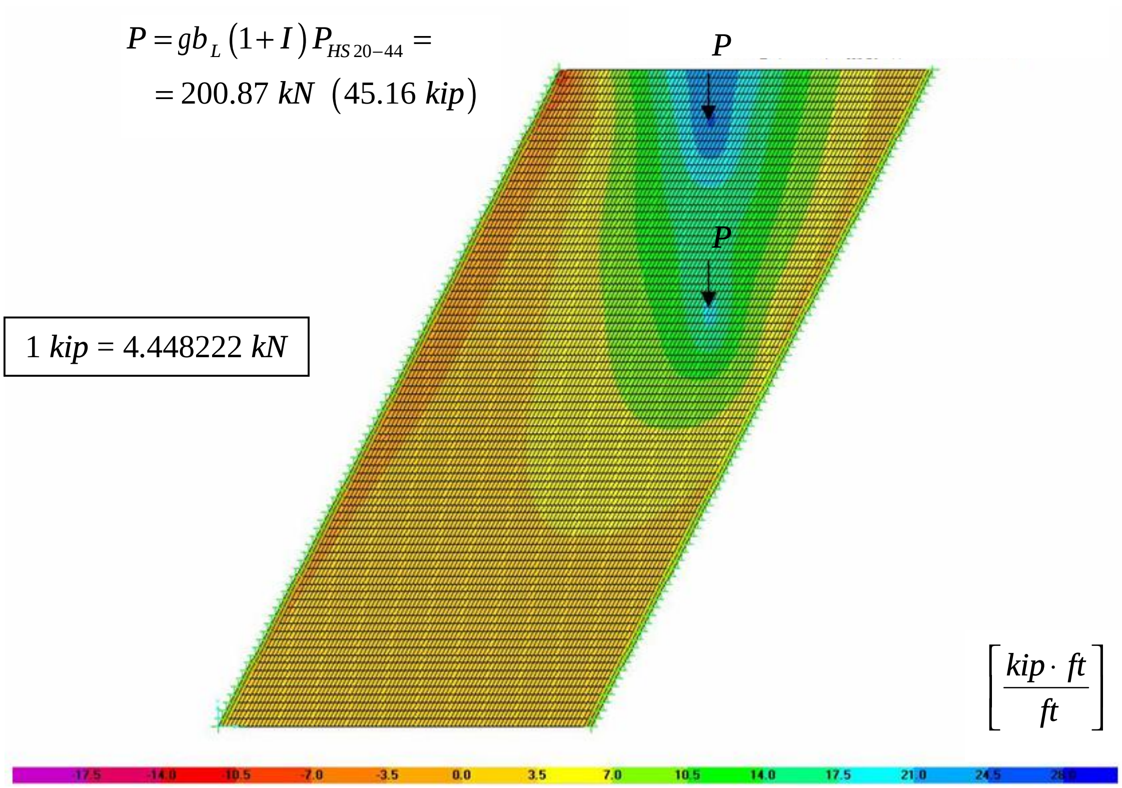

Figure 3.5. Slab Longitudinal Bending Moment Distribution

3.4. Analysis of Walls S2 and S3

The two walls can be analyzed as walls loaded in their plane. According to ACI 318-02 Section 14.5.2, design axial load strength $f P_n$ for a wall of solid rectangular cross section with resultant of all factored loads located within the middle third of the overall thickness of the wall is given by

$$f P_n = 0.55 f f_c^{'} A_g \left[1-\left(\frac{kh_c}{32h}\right)^2\right] \cong 1562 \ \frac{kN}{m} \ \left(107 \ \frac{kip}{ft}\right) \tag{3.3}$$

where

A_g	is the gross area of the section;
h	is the overall thickness of member;
h_c	is the vertical distance between supports ($h_c = 2362 \ mm$ $\left(7 \ ft + 9 \ in\right)$);
k	is the effective length factor (conservatively, $k = 1.0$ as for walls unrestrained against rotation at both ends);
$f = 0.70$	is the strength reduction factor.

The worst loading condition comes out by considering the truck design load: in particular, the maximum axial load is achieved when one wheel of the two rear axles is right over the wall (see Figure 3.6):

$$R_{pier} = \frac{g b_L \left(1+I\right) P_{HS\,20-44}}{w_{tire}} = \frac{45.157 \ kip}{1.\bar{6} \ ft \left(\equiv 20 \ in\right)} \cong 27.1 \ \frac{kip}{ft} \ \left(395.5 \ \frac{kN}{m}\right).$$

Since $R_{pier} < f P_n$, the walls S2 and S3 do not need further analysis.

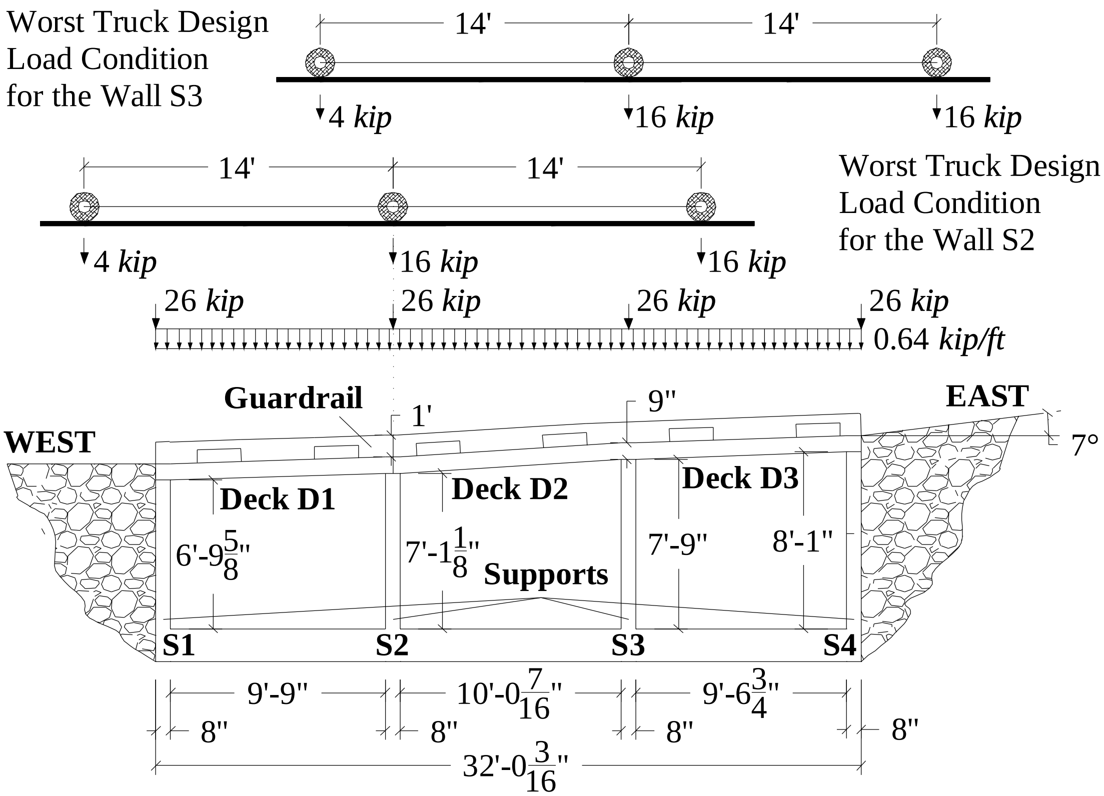

1 *in* = 1" = 25.4 *mm*
1 *ft* = 1' = 304.8 *mm*
1 *kip* = 4.448222 *kN*

Figure 3.6. Walls S2 and S3 Load Conditions

3.5. Analysis of Abutments S1 and S4

The abutments S1 and S4 can be analyzed as walls loaded in and out of their plane by the earth pressure and the surcharge loads. Figure 3.7 shows the loads acting over the abutment S4 and the model used to calculate the stresses in the element.

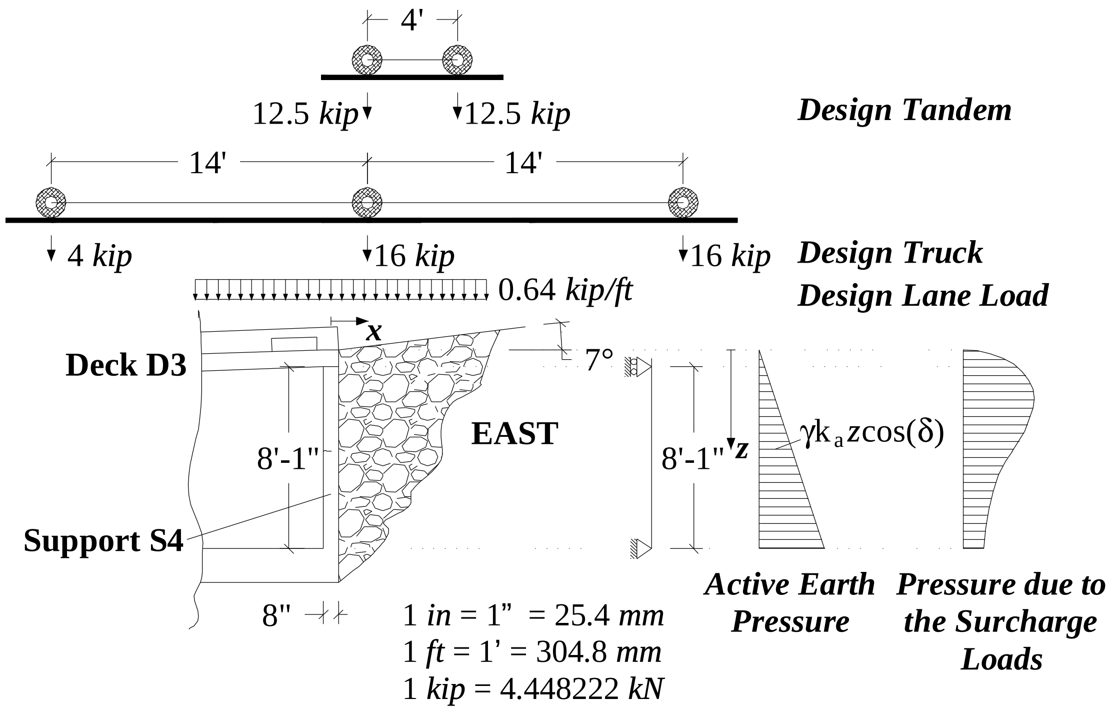

Figure 3.7. Abutment S4 Load Conditions

At ultimate condition, it is reasonable to consider just the active pressure of the earth since the ultimate condition implies relative movement bigger than the values of Table C3.11.1-1 (AASHTO, 1998). In addition, a live load surcharge shall be applied where a vehicular load is expected to act on the surface of the backfill within a distance equal to the wall height behind the back face of the wall. According to AASHTO (1998) Section 3.6.1.3.1, different conditions must be computed in order to evaluate:

1) the effect of one HS20-44 design truck combined with the effect of the design lane load;

2) the effect of the design tandem combined with the effect of the design lane. The design tandem consists of a pair of $111.21\,kN\ (25.0\,kip)$ axle spaced $1219\ mm\ (4.0\,ft)$ apart.

According to AASHTO (1998) Section 3.11.6, the surcharge load in the case of truck or tandem design can be conservatively modeled as a point load. On the other hand, the surcharge load in the case of lane design can be assumed to act on the entire surface of the backfill until a distance equal to the wall height behind the back face of the wall.

Varying the position x of the concentrated loads (see Figure 3.7), it was possible to find the design envelope of the compression, moment and shear per unit width of the wall along the $z-$axis.

3.5.1. Active Earth Pressure

The horizontal component p_E of the active earth pressure is given by:

$$\begin{cases} p_E = g\,k_a \cos(d)\,z \\ k_a = \dfrac{\sin(q+j)^2}{\sin(q)^2 \sin(q-d)\left(1+\sqrt{\dfrac{\sin(j+d)\sin(j-b)}{\sin(q-d)\sin(q+b)}}\right)^2} \end{cases} \tag{3.4}$$

where

g is the effective soil unit weight for compacted sand, silt or clay according to AASHTO (1998) Table 3.5.1-1 ($g = 18.85\ \dfrac{kN}{m^3}\left(120\ \dfrac{lbf}{ft^3}\right)$).

The water pressure can be neglected since the structure is provided for the thorough drainage of the backfilling material by means of crushed rock and gravel drains;

k_a is the active earth pressure coefficient from Coulomb analysis according to AASHTO (2002) Figure 5.5.2A;

d is the angle of wall friction: conservatively, $d = 17^o$ according to AASHTO (2002) Table 5.5.2B;

z the depth below effective top of wall ($[z]=[m]$ or $[ft]$);

q is the angle of backfill of wall to the vertical: $q = 90^o$;

j is the effective angle of internal friction. For drained soils, it varies between $\left[30^o, 40^o\right]$: conservatively, $j = 30^o$;

b is the slope angle of the soil: $b = 0^o$ for the abutment S1;
$b = 7^o$ for the abutment S4.

Therefore, for the unit width of the wall it results:

$$\begin{cases} p_E = 1.645z \left[\dfrac{kN}{m}\right] \left(34.363z \left[\dfrac{lbf}{ft}\right]\right) \\ k_a = 0.299 \end{cases} \qquad \text{for the abutment S1;}$$

$$\begin{cases} p_E = 1.797 \left[\dfrac{kN}{m}\right] \left(37.524z \left[\dfrac{lbf}{ft}\right]\right) \\ k_a = 0.327 \end{cases} \qquad \text{for the abutment S4.}$$

3.5.2. Surcharge Loads

The design lane load was modeled as uniform surcharge acting on the entire surface of the backfill until a distance equal to the wall height behind the back face of the wall. According to AASHTO (1998) Section 3.11.6.1, a constant horizontal p_{LL} earth pressure shall be added to the basic earth pressure. This constant pressure may be taken as:

$$p_{LL} = k_s q_s \tag{3.5}$$

where

k_s is the coefficient of earth pressure due to surcharge: in this case, $k_s = k_a = 0.327$;

q_s is the uniform surcharge applied to the upper surface of the active earth wedge: $q_s = 9.34 \cdot 10^{-3}\ \dfrac{kip}{ft}\ \left(0.64\ \dfrac{kip}{ft}\right)$.

Therefore, for the unit width of both walls S1 and S4 it results:

$$p_{LL} = 0.305\ \frac{kN}{m}\ \left(20.927\ \left[\frac{lbf}{ft}\right]\right).$$

The truck and tandem lane load were modeled as point loads moving between the interval $x = 0\ m\ (0\ ft)$ and $x = h_a$ ($h_a = 2073\ mm\ (6\ ft + 9\tfrac{5}{8}\ in)$ for the abutment S1 and $h_a = 2464\ mm\ (8\ ft + 1\ in)$ for the abutment S4: see Figure 3.7). According to AASHTO (1998) Section 3.11.6.1, the horizontal pressure distribution $p_{TL,i}$ may be taken as:

$$p_{TL,i} = \frac{P}{p\,r^2}\left[\frac{3zx^2}{r^3} - \frac{r(1-2n)}{r+z}\right] \tag{3.6}$$

where

i	is the subscript for the two different load conditions: $i = HS20-44$ for the truck load and $i = tm$ for the tandem load;
P	is the load: $P = 71.17\ kN\ (16\ kip)$ for $i = HS20-44$ and $P = 55.60\ kN$ $(12.5\ kip)$ for $i = tm$;
z	is the position at which the pressure is calculated ($[m]$ or $[ft]$);
x	is the horizontal distance from back of wall to point of load application: $x \in [0\ m\ (ft),\ h_a]$;
r	is the radial distance from point of load application to a point on the wall: conservatively, it was assumed $r = \sqrt{x^2 + z^2}$;
n	is the Poisson's ratio: conservatively, it was assumed $n = 0.5$.

Therefore, for the unit width of both walls S1 and S4 it results:

$$p_{TL,HS20-44} = 0.021\frac{zx^2}{(x^2+z^2)^{5/2}}\ \left[\frac{kN}{m}\right]\ \left(15.279\frac{zx^2}{(x^2+z^2)^{5/2}}\ \left[\frac{lbf}{ft}\right]\right)$$

$$p_{TL,tm} = 0.016\frac{zx^2}{(x^2+z^2)^{5/2}}\ \left[\frac{kN}{m}\right]\ \left(11.937\frac{zx^2}{(x^2+z^2)^{5/2}}\ \left[\frac{lbf}{ft}\right]\right).$$

3.5.3. Design Stresses for the Abutment S1

Figure 3.8 shows the earth pressure distribution along the height of the wall S1 for the different type of loads analyzed in the previous sections. Figure 3.9 and Figure 3.10 plot, respectively, the ultimate moment and shear envelope diagrams.

The ultimate ($M_{u,S1}$ and $V_{u,S1}$) and the service ($M_{s,S1}$ and $V_{s,S1}$) stresses were the following (the design shear stresses were computed at a distance $0.5H_d + w_s$):

$$M_{u,S1} \cong 28.47\ \frac{kN\cdot m}{m}\left(6.4\ \frac{kip\cdot ft}{ft}\right) \qquad M_{s,S1} \cong 13.34\ \frac{kN\cdot m}{m}\left(3.0\ \frac{kip\cdot ft}{ft}\right).$$

$$V_{u,S1} \cong 45.24\ \frac{kN}{m}\left(3.1\ \frac{kip}{ft}\right) \qquad V_{s,S1} \cong 21.89\ \frac{kN}{m}\left(1.5\ \frac{kip}{ft}\right)$$

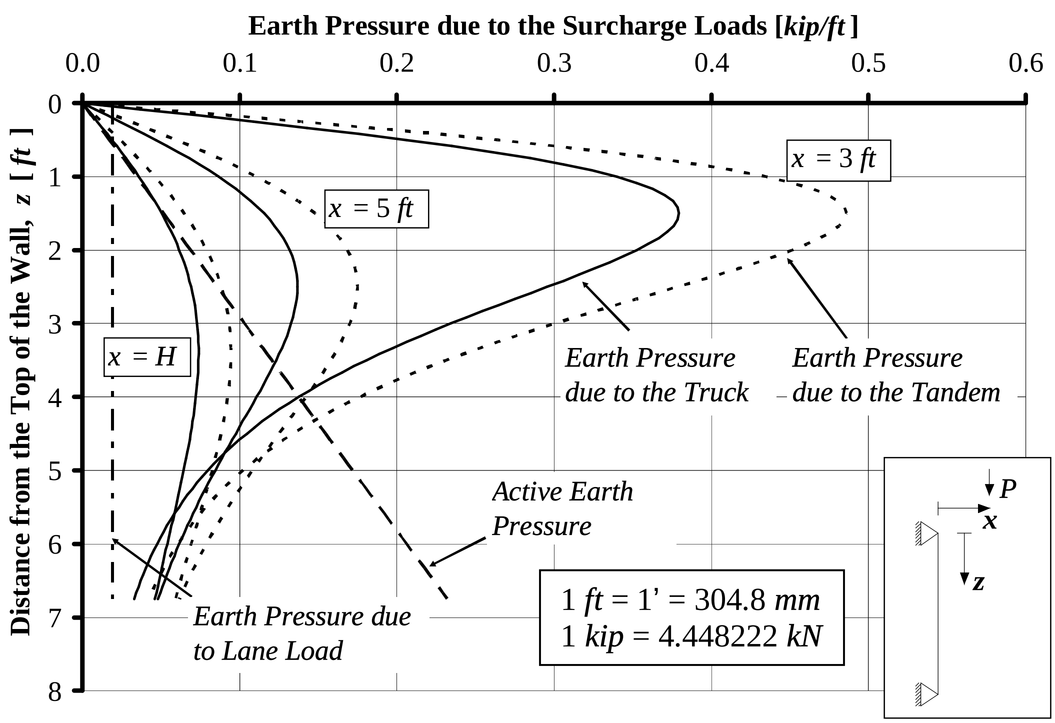

Figure 3.8. Earth Pressure along the Height for the Abutment S1

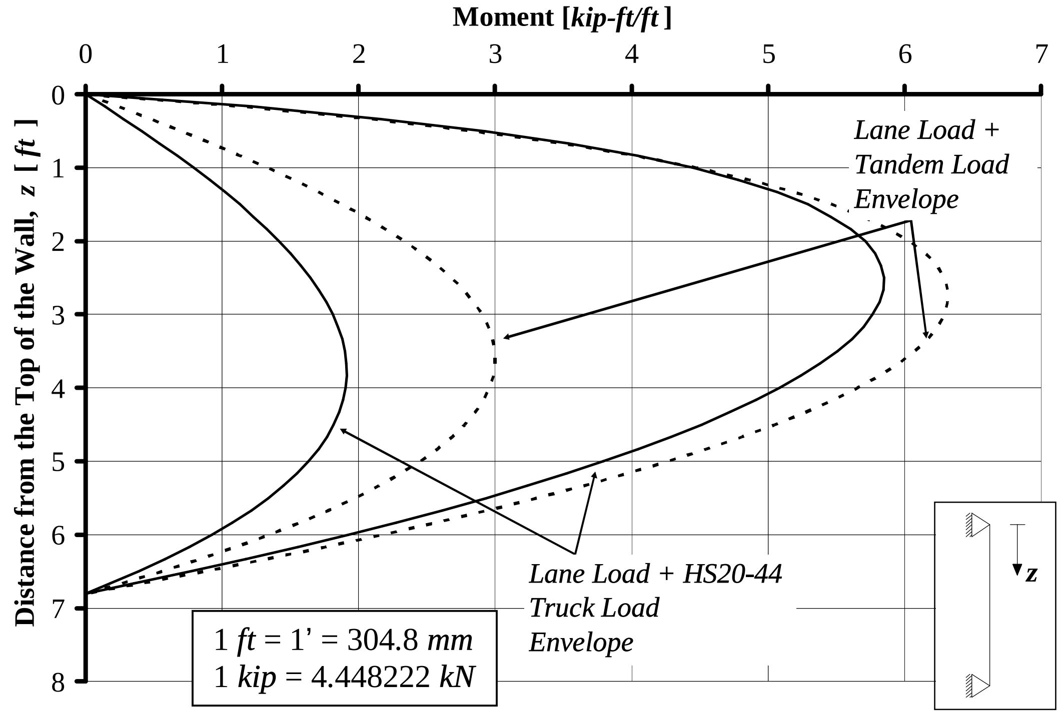

Figure 3.9. Ultimate Moment Envelope Diagram for the Abutment S1

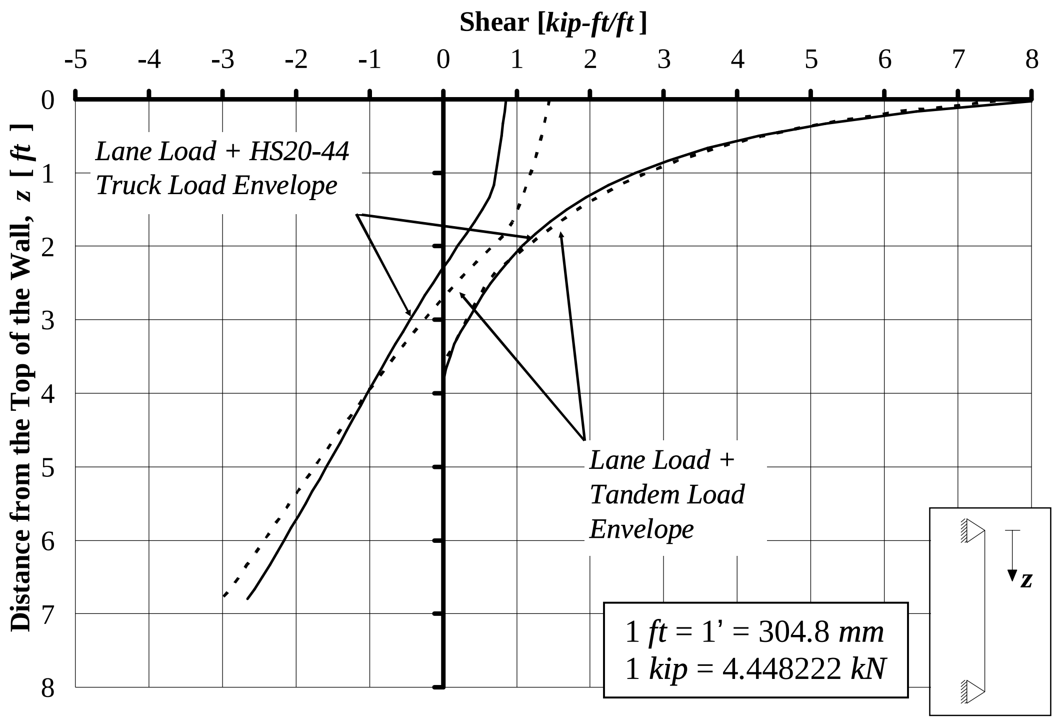

Figure 3.10. Ultimate Shear Envelope Diagram for the Abutment S1

In order to calculate the worst combination of axial load and bending moment, the two load conditions depicted in Figure 3.11 were analyzed.

In the load condition A (see Figure 3.11-a), the rear axle wheel of the HS20-44 design truck is right over the abutment S4 and the lane design uniform load is distributed on the deck D1 and on the backfill earth.

In the load condition B (see Figure 3.11-b), the rear axle wheel of the tandem load is right over the abutment S4 and the lane design uniform load is on the deck D1 and on the backfill earth.

According to AASHTO (2002) Section 3.24.3.2, for lane loads, the distribution width E_{LL} over the deck shall be

$$E_{LL} = 2\min\left(1219 + 0.06S, 2134\ mm\right) \quad \text{or} \quad E_{LL} = 2\min\left(4 + 0.06S, 7\ ft\right) \qquad (3.7)$$

where S is the effective span length ($[S] = mm$ or ft): it is $S = 3505\ mm$ $(11.50\ ft)$ and therefore it results $E_{LL} = 2859\ mm\ (9.38\ ft)$.

For the load condition A, the ultimate ($M_{ua,S1}$ and $P_{ua,S1}$) and the service ($M_{sa,S1}$ and $P_{sa,S1}$) stresses are:

$$M_{ua,S1} \cong 8.90\ \frac{kN \cdot m}{m}\ \left(2.0\ \frac{kip \cdot ft}{ft}\right) \qquad M_{sa,S1} \cong 4.45\ \frac{kN \cdot m}{m}\ \left(1.0\ \frac{kip \cdot ft}{ft}\right)$$

$$P_{ua,S1} \cong 607.11\ \frac{kN}{m}\ \left(41.6\ \frac{kip}{ft}\right) \qquad P_{sa,S1} \cong 280.20\ \frac{kN}{m}\ \left(19.2\ \frac{kip}{ft}\right)$$

while for the load condition B, the ultimate ($M_{ub,S1}$ and $P_{ub,S1}$) and the service ($M_{sb,S1}$ and $P_{sb,S1}$) stresses are:

$$M_{ub,S1} \cong 18.24\ \frac{kN \cdot m}{m}\ \left(4.1\ \frac{kip \cdot ft}{ft}\right) \qquad M_{sb,S1} \cong 8.90\ \frac{kN \cdot m}{m}\ \left(2.0\ \frac{kip \cdot ft}{ft}\right).$$

$$P_{ub,S1} \cong 477.22\ \frac{kN}{m}\ \left(32.7\ \frac{kip}{ft}\right) \qquad P_{sb,S1} \cong 220.40\ \frac{kN}{m}\ \left(15.1\ \frac{kip}{ft}\right)$$

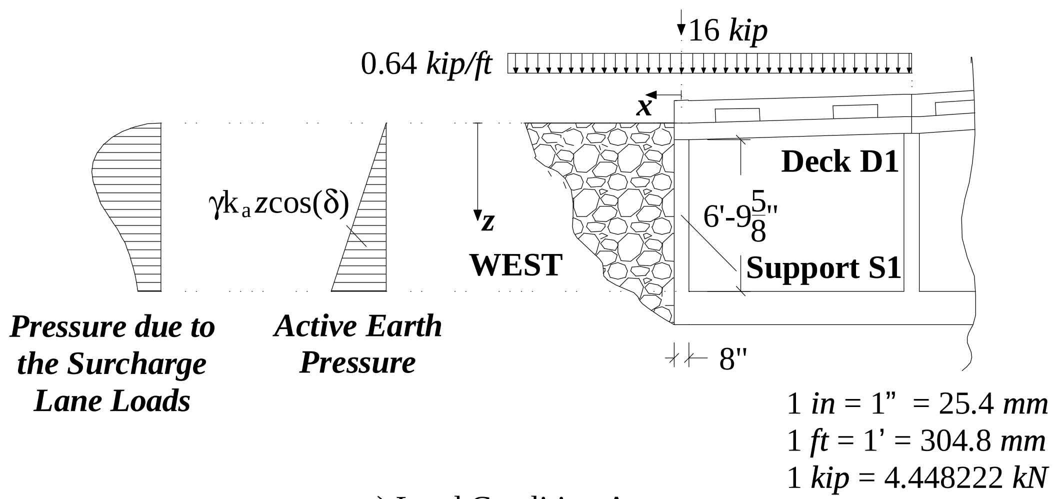

a) Load Condition A

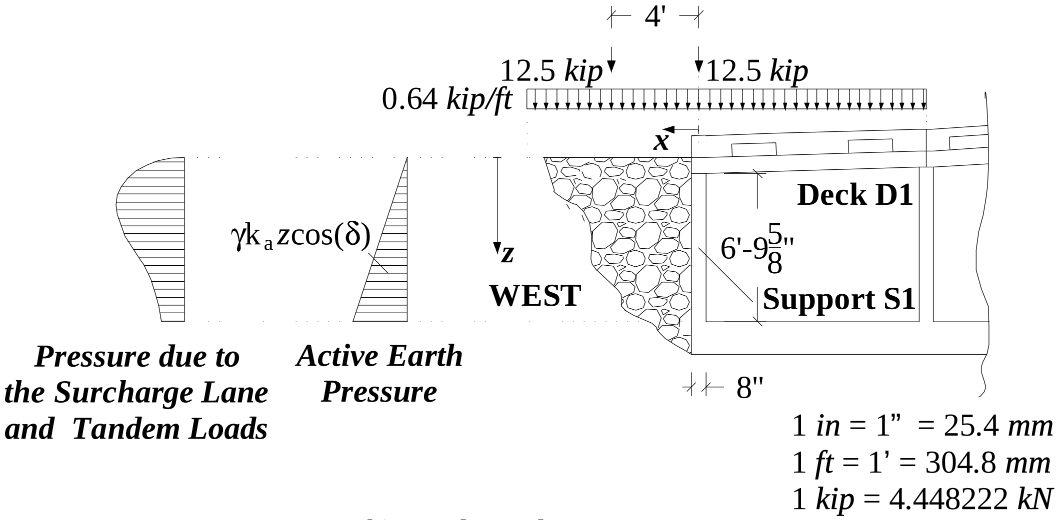

b) Load Condition B

Figure 3.11. Load Conditions for Maximum Compression Stresses in the Abutment S1

3.5.4. Design Stresses for the Abutment S4

Figure 3.12 shows the earth pressure distribution along the height of the wall S4 for the different type of loads analyzed in the previous sections. Figure 3.13 and Figure 3.14 plot, respectively, the ultimate moment and shear envelope diagrams.

Therefore, the design moment is located at about 1524 mm $(5\ ft)$ from the ground (the position located theoretically has a value very close to the actual position of the crack in the wall). The design shear stress was computed at a distance $0.5H_d + w_s$. The ultimate ($M_{u,S4}$ and $V_{u,S4}$) and the service ($M_{s,S4}$ and $V_{s,S4}$) stresses were the following:

$$M_{u,S4} \cong 36.92\ \frac{kN \cdot m}{m} \left(8.3\ \frac{kip \cdot ft}{ft}\right) \qquad M_{s,S4} \cong 17.79\ \frac{kN \cdot m}{m} \left(4.0\ \frac{kip \cdot ft}{ft}\right).$$

$$V_{u,S4} \cong 61.29\ \frac{kN}{m} \left(4.2\ \frac{kip}{ft}\right) \qquad V_{s,S4} \cong 29.19\ \frac{kN}{m} \left(2.0\ \frac{kip}{ft}\right)$$

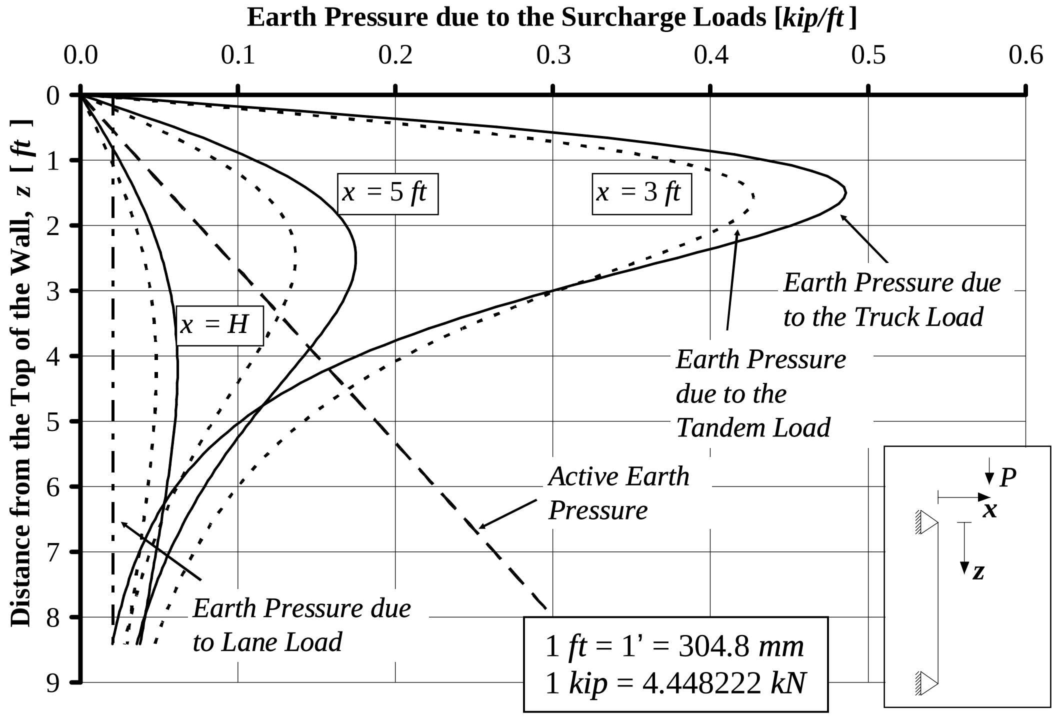

Figure 3.12. Earth Pressure along the Height for the Abutment S4

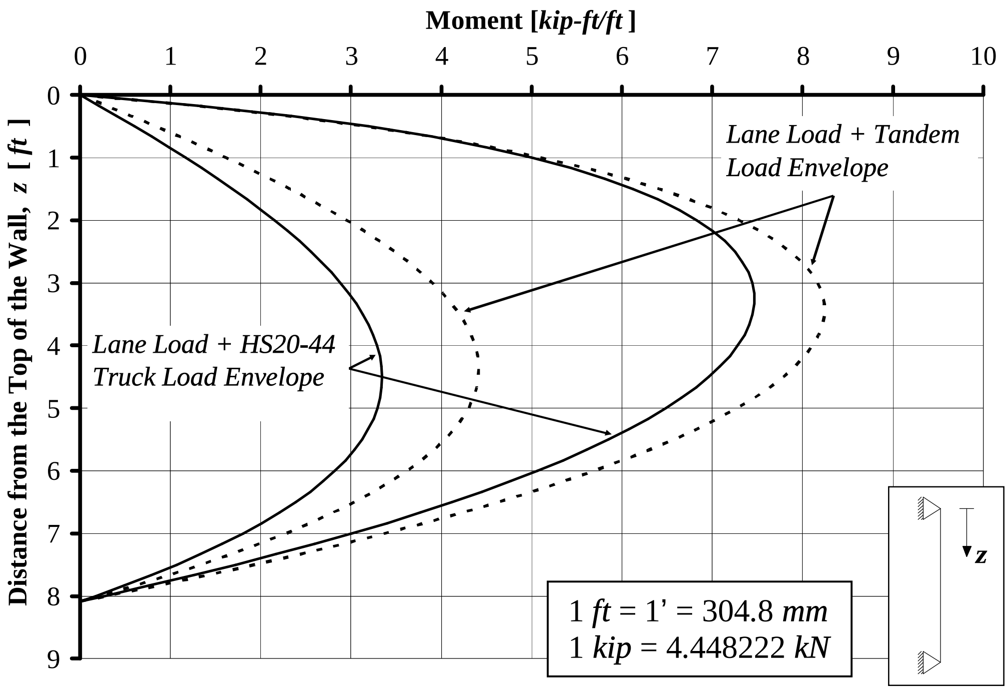

Figure 3.13. Ultimate Moment Envelope Diagram for the Abutment S4

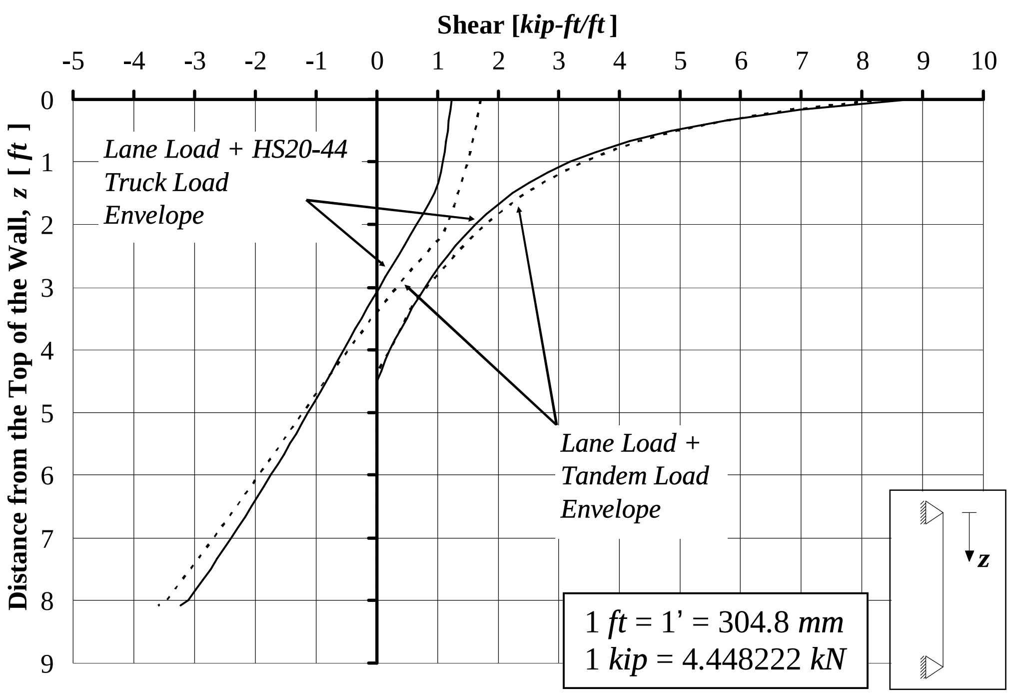

Figure 3.14. Ultimate Shear Envelope Diagram for the Abutment S4

In order to calculate the worst combination of axial load and bending moment, the two load conditions depicted in Figure 3.15 were considered.

In the load condition A (see Figure 3.15-a), the rear axle wheel of the HS20-44 design truck is right over the abutment S4 and the lane design uniform load is distributed on the deck D3 and on the backfill earth.

In the load condition B (see Figure 3.15-b), the rear axle wheel of the tandem load is right over the abutment S4 and the lane design uniform load is on the deck D3 and on the backfill earth.

According to AASHTO (2002) Section 3.24.3.2, for lane loads, the distribution width E_{LL} over the deck shall be

$$E_{LL} = 2\min\left(1219 + 0.06S, 2134\ mm\right) \quad \text{or} \quad E_{LL} = 2\min\left(4 + 0.06S, 7\ ft\right) \tag{3.8}$$

where S is the effective span length ($[S]=[mm]$ or $[ft]$): it is $S = 3499\ mm\ (11.48\ ft)$ and therefore it results $E_{LL} = 2856\ mm\ (9.37\ ft)$.

For the load condition A, the ultimate ($M_{ua,S4}$ and $P_{ua,S4}$) and the service ($M_{sa,S4}$ and $P_{sa,S4}$) stresses are:

$$M_{ua,S4} \cong 15.12\ \frac{kN \cdot m}{m}\left(3.4\ \frac{kip \cdot ft}{ft}\right) \qquad M_{sa,S4} \cong 7.56\ \frac{kN \cdot m}{m}\left(1.7\ \frac{kip \cdot ft}{ft}\right)$$
$$P_{ua,S4} \cong 607.11\ \frac{kN}{m}\left(41.6\ \frac{kip}{ft}\right) \qquad P_{sa,S4} \cong 280.20\ \frac{kN}{m}\left(19.2\ \frac{kip}{ft}\right)$$

while for the load condition B, the ultimate ($M_{ub,S4}$ and $P_{ub,S4}$) and the service ($M_{sb,S4}$ and $P_{sb,S4}$) stresses are:

$$M_{ub,S4} \cong 26.24\ \frac{kN \cdot m}{m}\left(5.9\ \frac{kip \cdot ft}{ft}\right) \qquad M_{sb,S4} \cong 12.9\ \frac{kN \cdot m}{m}\left(2.9\ \frac{kip \cdot ft}{ft}\right)$$
$$P_{ub,S4} \cong 477.22\ \frac{kN}{m}\left(32.7\ \frac{kip}{ft}\right) \qquad P_{sb,S4} \cong 220.37\ \frac{kN}{m}\left(15.1\ \frac{kip}{ft}\right).$$

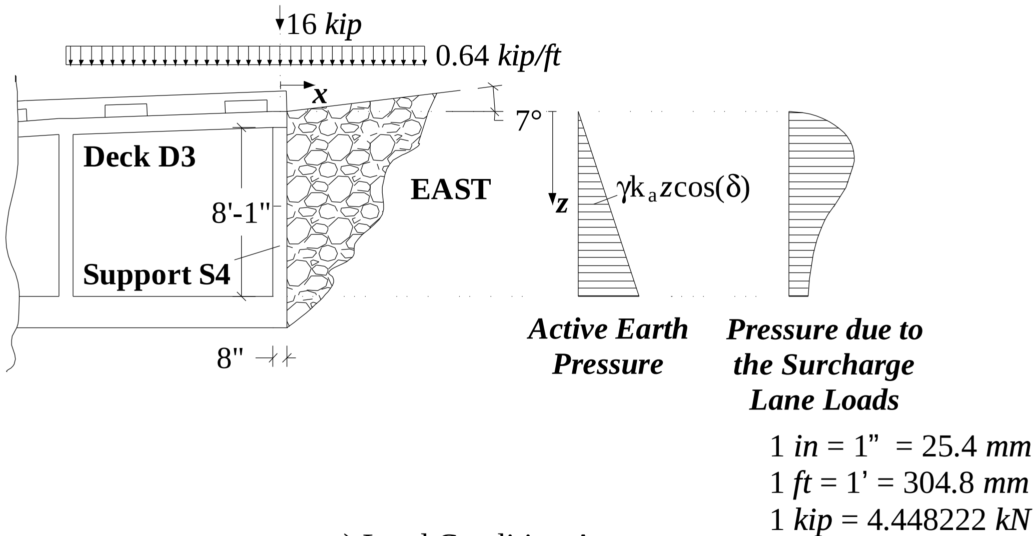

a) Load Condition A

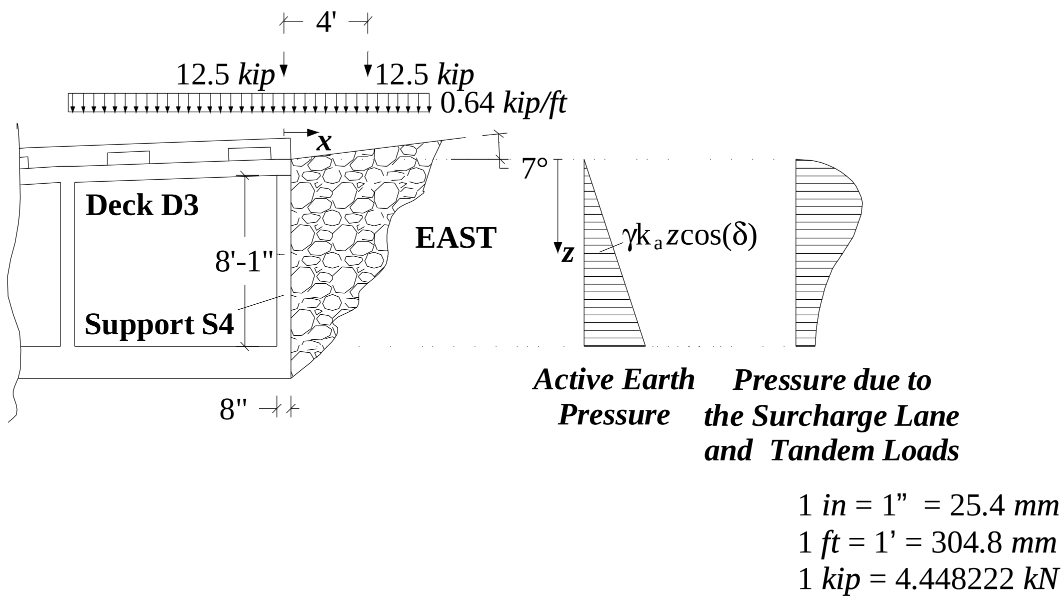

b) Load Condition B

Figure 3.15. Load Conditions for Maximum Compression Stresses in the Abutment S4

4. DESIGN

4.1. Assumptions

Mechanically-Fastened FRP laminate design is carried out according to the principles of ACI 440.2R-02 (ACI 440 in the following). The properties of concrete, steel and FRP laminates used in the design are summarized in Table 4.1. The concrete and steel properties are obtained by testing of samples while the FRP properties are guaranteed values.

The f factors used to convert nominal values to design capacities are obtained as specified in AASHTO (2002) for the as-built and from ACI 440 for the strengthened members.

Table 4.1. Material Properties

Concrete	*Steel*		*FRP - SAFSTRIP*			
Compressive Strength $f_c^{'}$ $[MPa]$ $([psi])$	Yield Strength f_y $[MPa]$ $([ksi])$	Modulus of Elasticity E_s $[GPa]$ $([ksi])$	Tensile Strength f_{fu}^{*} $[MPa]$ $([ksi])$	Modulus of Elasticity E_f $[GPa]$ $([ksi])$	Thickness t_f $[mm]$ $([in])$	Width w_f $[mm]$ $([in])$
23.2 (3365)	344.7 (50)	200.0 (29000)	588.8 (85.4)	60.7 (8800)	3.175 (0.125)	101.6 (4.00)

Material properties of the FRP reinforcement reported by manufacturers, such as the ultimate tensile strength, typically do not consider long-term exposure to environmental conditions, and should be considered as initial properties. FRP properties to be used in all design equations are given as follows (ACI 440):

$$\begin{aligned} f_{fu} &= C_E f_{fu}^{*} \\ e_{fu} &= C_E e_{fu}^{*} \end{aligned} \tag{4.1}$$

where f_{fu} and e_{fu} are the FRP design tensile strength and ultimate strain considering the environmental reduction factor C_E as given in Table 7.1 (ACI 440), and f_{fu}^* and e_{fu}^* represent the FRP guaranteed tensile strength and ultimate strain as reported by the manufacturer (see Table 4.1).

The maximum strength that the MF-FRP strengthening can develop depends on the capacity of the connection bolt-strip and, therefore, on the number of fasteners used.

In order to mechanically fasten the FRP laminate to the concrete, the optimal solution in terms of mechanical behavior of the connection was found as a result of an experimental program conducted at UMR. The chosen fastening system consisted of:

- Concrete wedge anchor (diameter $9.525\ mm\ (3/8\ in)$ and total length $57.15\ mm\ (2\,1/4\ in)$ - Figure 4.1). The shear capacity T_c of the anchor embedded in the concrete depends upon the embedment depth h_b and the strength of the concrete $f_c^{'}$. The shear strength of the anchor, T_b, becomes equal to T_c with a value of $26.7\ kN\ (6.0\ kip)$ when $f_c^{'} = 41.4 MPa\ (6000\ psi)$ and $h_b = 38.1\ mm$ $(1\,1/2\ in)$;
- Steel washer (inner diameter $11.112\ mm\ (7/16\ in)$, outer diameter $25.4\ mm\ (1\ in)$ and thickness $1.587\ mm\ (1/16\ in)$ - Figure 4.1);
- Epoxy between the washer and the FRP and throughout the hole on the FRP.

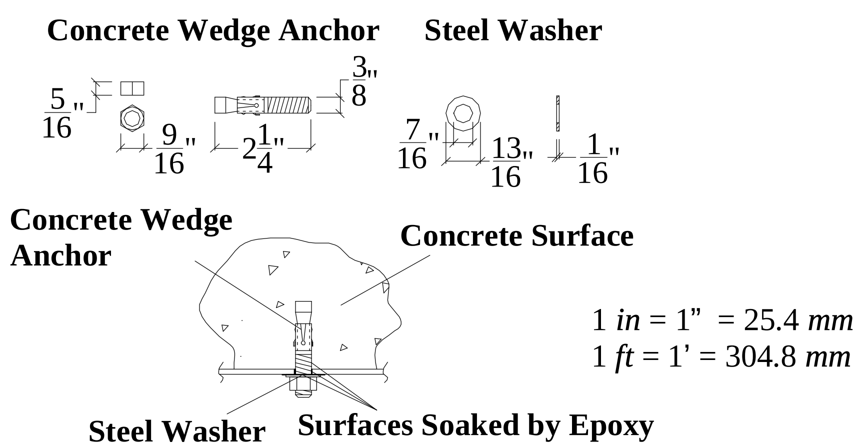

Figure 4.1. Details of the Connection Concrete-FRP

Bond tests on the connection FRP-fastener showed that at the ultimate conditions, the applied load is uniformly distributed between all the fasteners. In addition, it was observed that for concrete having an $f_c^{'} \geq 27.6\ MPa\ (4000\ psi)$, the failure mode of the connection is due to the bearing of the FRP. The experimental ultimate load supported by this connection was found to be $14.0\ kN\ (3.15\ kip)$. For design purposes a safety factor equal to 1.25 was assumed and therefore the design capacity of the connection is $R_b = 11.1\ kN\ (2.5\ kip)$.

Under these assumptions, the minimum number of fasteners $n_{b,\min}$ to anchor each FRP strip so that failure of the FRP controls, is given by:

$$n_{b,\min} = \frac{F_{FRP}}{R_b} \tag{4.2}$$

where F_{FRP} is the maximum load that the FRP strip experiences at ultimate conditions. Assuming $C_E = 0.85$ (i.e., carbon plate exposed in exterior aggressive ambient) and taking into account the net area of the strip (i.e., subtraction of the area lost to insert the bolt), from equation (4.2) the minimum number of bolts to reach the ultimate capacity of the FRP strip is 26. If fewer bolts are used, the failure would occur at the connection (i.e. bearing of the FRP strip).

4.2. Superstructure Design

4.2.1. Assumptions

The geometrical properties and the internal steel flexural reinforcement of the design cross section are summarized in Figure 4.2 and Table 4.2.

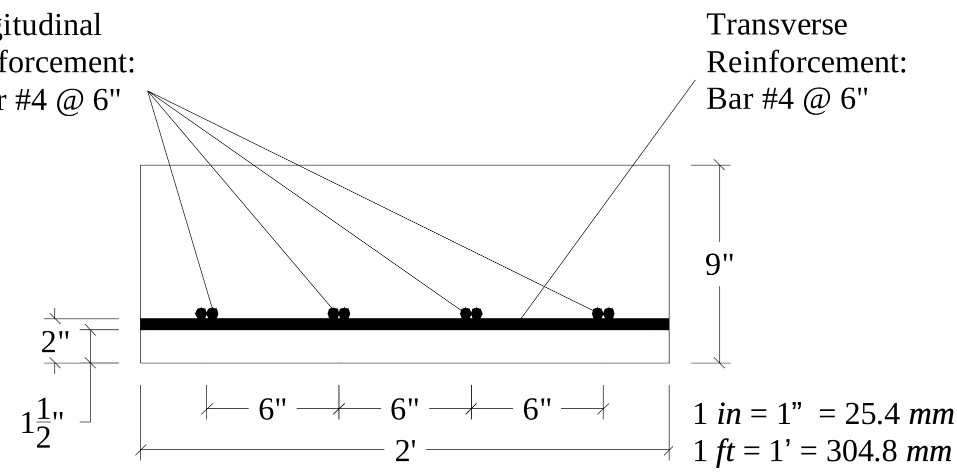

Figure 4.2. Slab Un-Strengthened Section

Table 4.2. Geometrical Properties and Internal Steel Reinforcement

Slab Thickness	Design Width	Slab Longitudinal Tensile Steel Area	Effective Depth	Slab Transverse Tensile Steel Area	Effective Depth
H_d $[mm]$ $([in])$	W $[mm]$ $([in])$	$A_{s,slab\ long.}$ $[mm^2]$ $([in^2])$	$d_{slab\ long.}$ $[mm]$ $([in])$	$A_{s,slab\ transv.}$ $[mm^2/m]$ $([in^2/ft])$	$d_{slab\ transv.}$ $[mm]$ $([in])$
229 (9.0)	610 (24)	1013 (1.570)	197 ($7\frac{3}{4}$)	415 (0.196)	210 ($8\frac{1}{4}$)

4.2.2. Flexural Strengthening

Table 4.3 summarizes the strengthening recommendations for the superstructure of the bridge. Figure 4.3 details the longitudinal flexural strengthening. Finally, the pattern of the bolts is shown in Figure 4.4: to be noted that the spacing of the fasteners in the moment span is related with the moment design and do not take into account the extra fasteners installed to avoid loosing length of laminates. Appendix C contains some pictures of the FRP strengthening installation.

Table 4.3. Deck Strengthening Summary

Section	*Strengthening Scheme*	*Design Capacity* fM_n $[kN \cdot m/m]$ $([kip \cdot ft/ft])$		*Moment Demand* M_u $[kN \cdot m/m]$ $([kip \cdot ft/ft])$
		Un-Strengthened	*Strengthened*	
Longitudinal Direction (Parallel to the Traffic)	*Deck*: 1 Plate @ 610 mm $(24\ in)$ o/c	162.4 (36.5)	233.1 (52.4)	223.0 (50.1)

According to ACI 440.2R-02 (2002) Section 9.4, the stress in the steel must be less than $0.80 f_y$ in service conditions. In addition, in order to avoid creep failure under service loads, the stress in the carbon-FRP has to be limited to the value of $0.55 f_{fu}$ according to ACI 440.2R-02 (2002) Section 9.5. In this case, it results

$$\begin{cases} f_{steel} = 164.8\ MPa\ (23.9\ ksi) < 0.8 f_y = 275.8\ MPa\ (40.0\ ksi) \\ f_{FRP} = 68.9\ MPa\ (10.0\ ksi) < 0.55 f_{fu} = 324.1\ MPa\ (47.0\ ksi) \end{cases}.$$

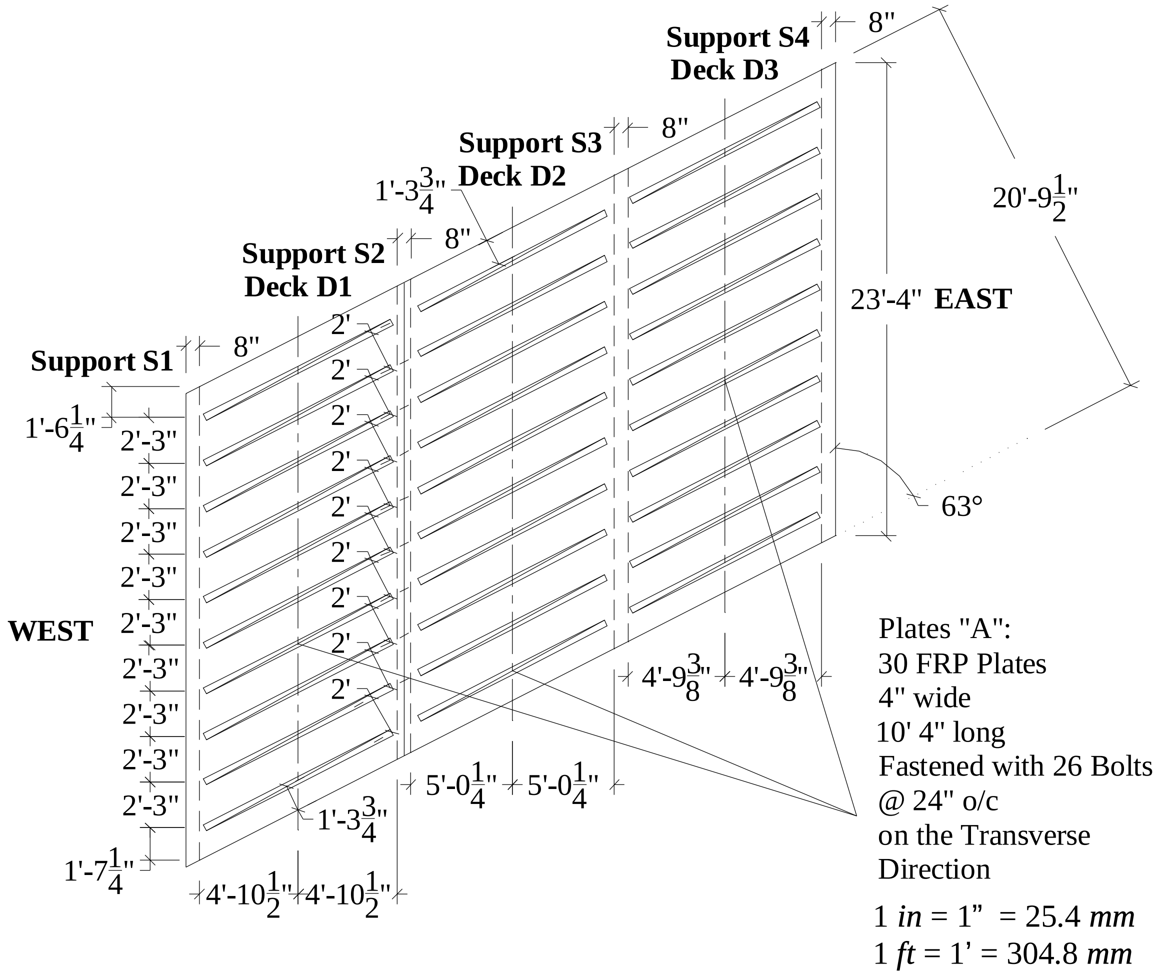

Figure 4.3. Strengthening of the Deck: Plan View

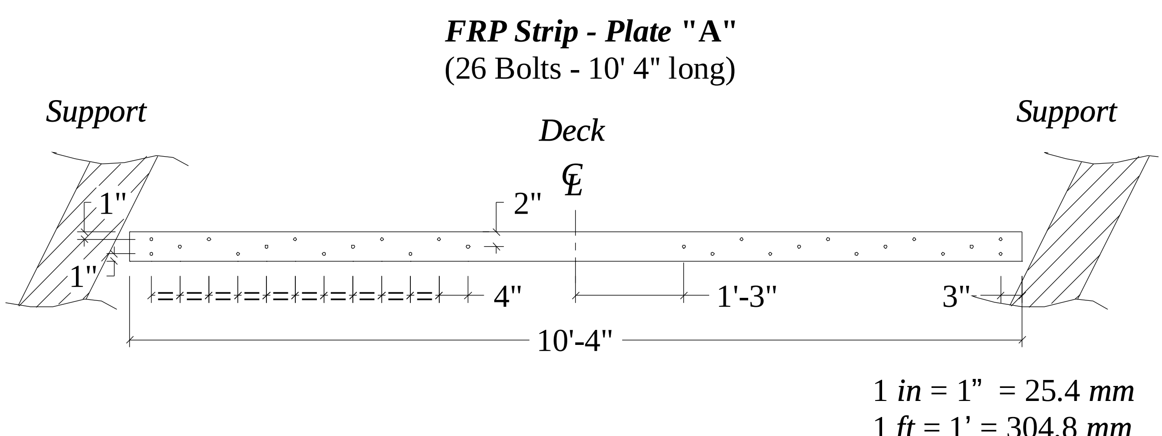

Figure 4.4. Bolts Pattern for Plates "A"

4.2.3. Shear Check

The concrete contribution V_c to the shear capacity was calculated based on equation (8-48) of AASHTO (2002) as follows:

$$\begin{cases} V_c = \left(1.9\sqrt{f_c^{'}} + 2500\, r_w \dfrac{V_u d}{M_u}\right) b_w d \le 3.5\sqrt{f_c^{'}} b_w d \\ \left[f_c^{'} \right] = [psi] \end{cases} \tag{4.3}$$

The as-built shear capacity is then computed by adding the concrete contribution to the one due to the shear reinforcement. In this case, no shear reinforcement is present: Table 4.4 summarizes the findings for the superstructure. Since the capacity is higher than the demand, it can be concluded that no shear reinforcement is required.

Table 4.4. Superstructure Shear Capacity

Element	*Shear Capacity* fV_n	*Shear Demand* V_u
Slab $\left[\dfrac{kN}{m}\right] \left(\left[\dfrac{kip}{ft}\right]\right)$	134.2 (9.2)	102.2 (7.0)

4.2.4. Punching Shear Check

The deck must also be checked for punching shear. This check was based on AASHTO (2002) Article 8.16.6.6 requirements according to which, for non-prestressed slabs and footings, V_c shall be the smallest of the following expressions:

$$\begin{cases} V_{c,1} = \left(2 + \dfrac{4}{b_c}\right)\sqrt{f_c^{'}} b_0 d \\ V_{c,2} = 4\sqrt{f_c^{'}} b_0 d \end{cases} \quad \text{with} \quad \left[f_c^{'} \right] = [psi] \tag{4.4}$$

where:

b_0 is the perimeter of critical section;

d is the distance from the extreme compression fiber to centroid of tension reinforcement;

a_s is 40 for interior load, 30 for edge load and 20 for corner load;

b_c is the ratio of long side to short side of the area over which the load is distributed.

By using a tire contact area as given by AASHTO (2002):

$$\begin{cases} l_{tire} = 254\ mm\ \ (10\ in) \\ w_{tire} = 508\ mm\ \ (20\ in) \\ A_{tire} = l_{tire} w_{tire} = 129032\ mm^2\ \ (200\ in^2) \end{cases} \tag{4.5}$$

the following shear capacity can be found:

$$f_{punch} V_c = f_{punch} \min\left(V_{c,1}, V_{c,2}\right) \cong 0.85\left(412\ kN\right) \cong 351\ kN\ \ \left(78\ kip\right)$$

which is smaller than the ultimate punching shear capacity given by:

$$g b_L \left(1 + I\right) P_{HS20-44} \cong 196.0\ kN\ \ \left(44.0\ kip\right).$$

4.3. Abutments S1 and S4 Design

4.3.1. Assumptions

The geometrical properties and the internal steel flexural reinforcement of the design cross sections are summarized in Figure 4.5 and Table 4.5.

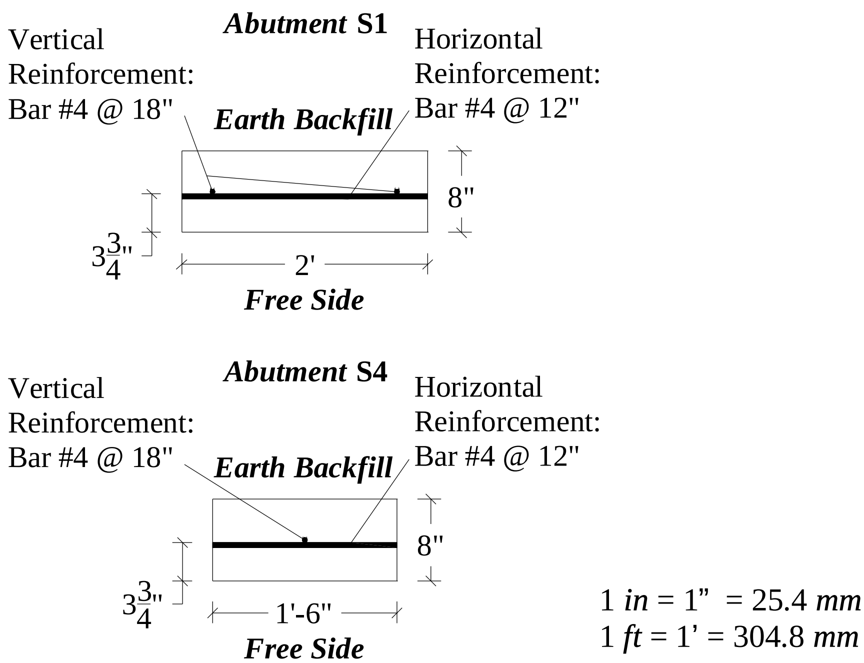

Figure 4.5. Abutments S1 and S4 Un-strengthened Section

Table 4.5. Abutments S1 and S4 Geometrical Properties and Internal Steel Reinforcement

Abutment	Thickness	Width	Vertical Tensile Steel Area	Effective Depth	Horizontal Tensile Steel Area	Effective Depth
	H $[mm]$ $([in])$	W $[mm]$ $([in])$	$A_{s,slab\ long.}$ $[mm^2]$ $([in^2])$	$d_{slab\ long.}$ $[mm]$ $([in])$	$A_{s,slab\ trasv.}$ $[mm^2/m]$ $([in^2/ft])$	$d_{slab\ trasv.}$ $[mm]$ $([in])$
S1	203 (8)	610 (24)	126 (0.196)	102 (4)	414 (0.196)	89 ($3\frac{1}{2}$)
S4	203 (8)	457 (18)	168 (0.261)	102 (4)	414 (0.196)	89 ($3\frac{1}{2}$)

4.3.2. Flexural Strengthening

Table 4.6 summarizes the strengthening recommendations for the superstructure of the bridge. Figure 4.6 and Figure 4.7 detail the longitudinal flexural strengthening, respectively, for the abutments S1 and S4. Finally, the pattern of the bolts is shown in

Figure 4.8 and Figure 4.9: to be noted that the spacing of the fasteners in the moment span is related with the moment design and do not take into account the extra fasteners installed to avoid loosing length of laminates.

Table 4.6. Abutments S1 and S4 Strengthening Summary

Abutment	*Section*	*Strengthening Scheme*	*Design Capacity* fM_n		*Moment Demand* M_u
			$\left[\frac{kN \cdot m}{m}\right]\left(\left[\frac{kip \cdot ft}{ft}\right]\right)$		
			Un-Strengthened	*Strengthened*	
S1	Vertical Direction	1 Plate @ 610 mm (24 in) o/c	16.9 (3.8)	75.1 (16.9)	56.5 (12.7)
S4	Vertical Direction	1 Plate @ 457 mm (18 in) o/c	12.5 (2.8)	70.2 (15.8)	55.6 (12.5)

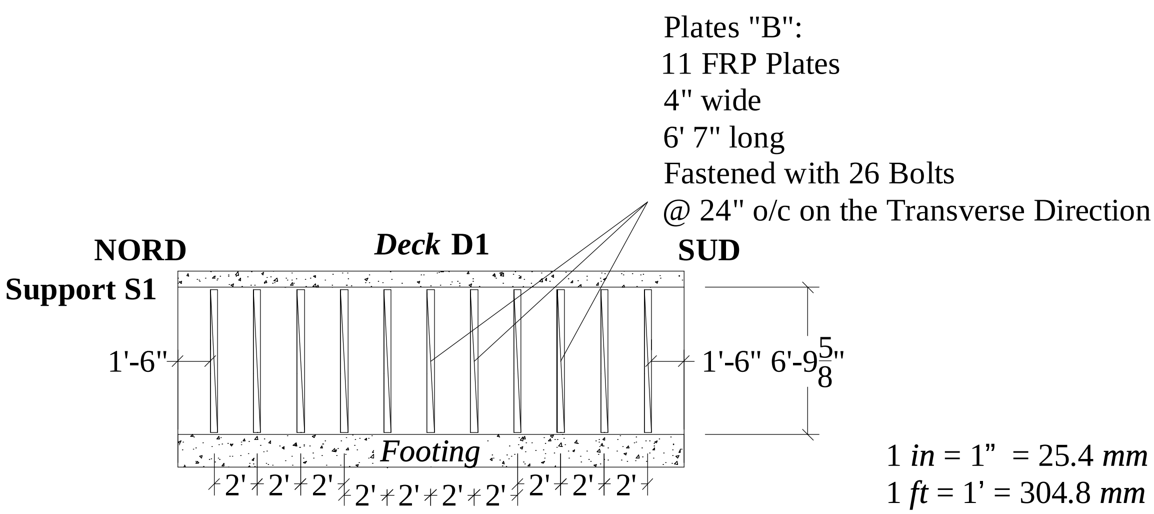

Figure 4.6. Strengthening of the Abutment S1: Plan View

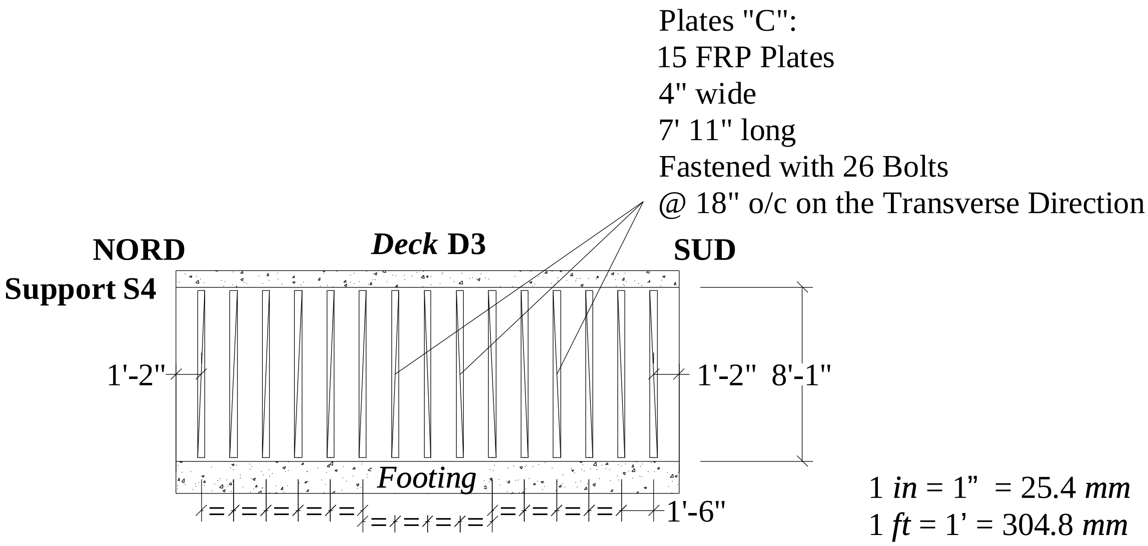

Figure 4.7. Strengthening of the Abutment S4: Plan View

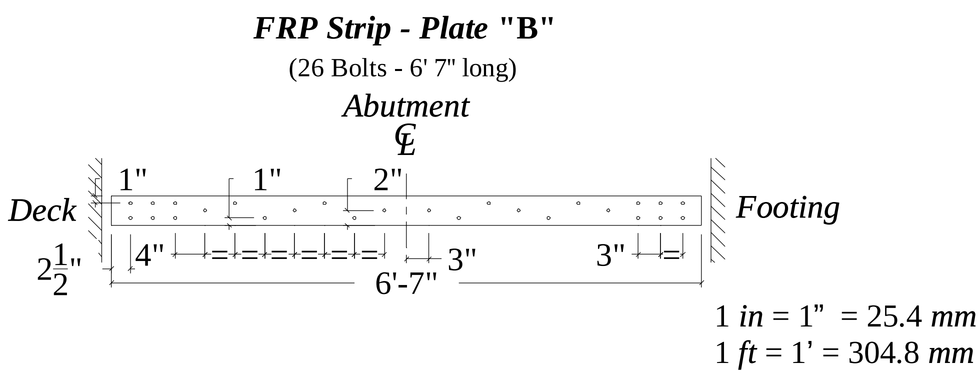

Figure 4.8. Bolts Pattern for Plates "B" for the Abutment S1

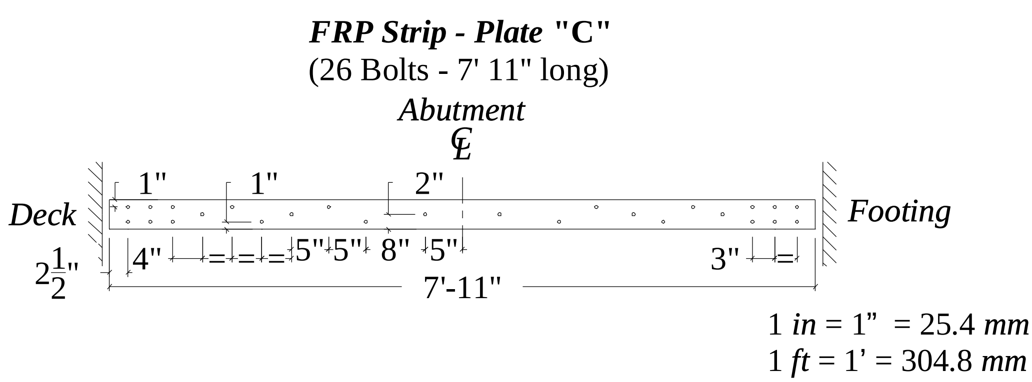

Figure 4.9. Bolts Pattern for Plates "C" for the Abutment S4

The bolts pattern was verified at the ultimate condition in order to avoid having any section in which the moment demand was greater than the moment capacity. During this step, the position of the bolts was optimized. Figure 4.10 and Figure 4.11 detail the moment capacity, respectively, of the abutments S1 and S4 along their height for the chosen bolts pattern: the moment capacity is close enough to the flexure demand in all the load configurations for both elements.

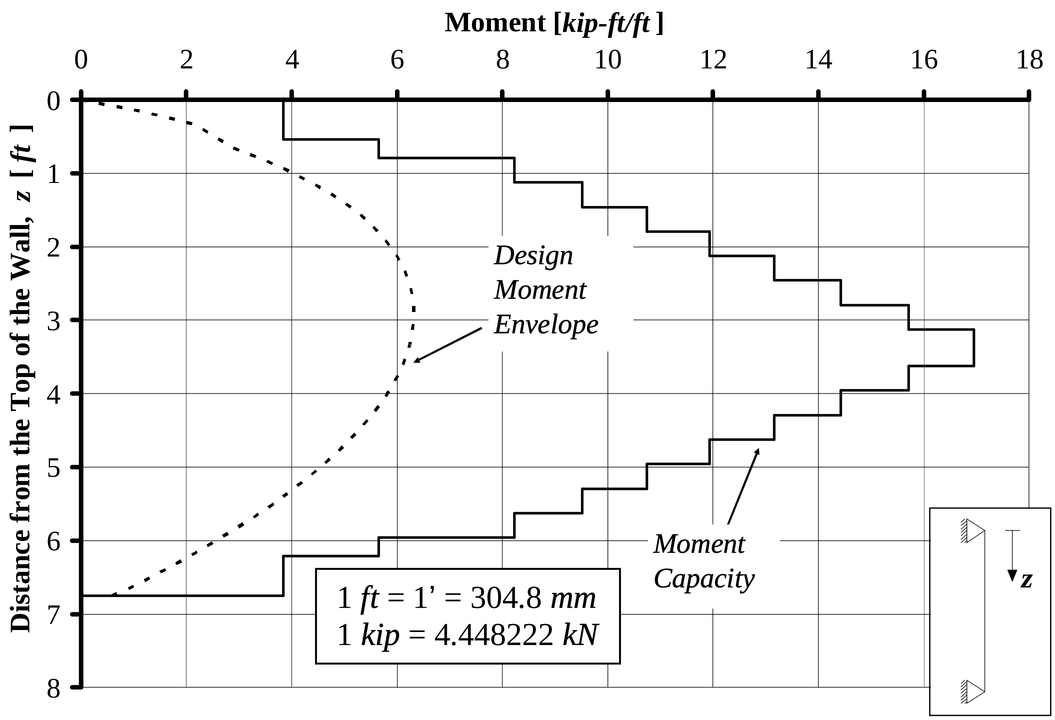

Figure 4.10. Diagram of the Abutment S1 Capacity at Ultimate Load Conditions

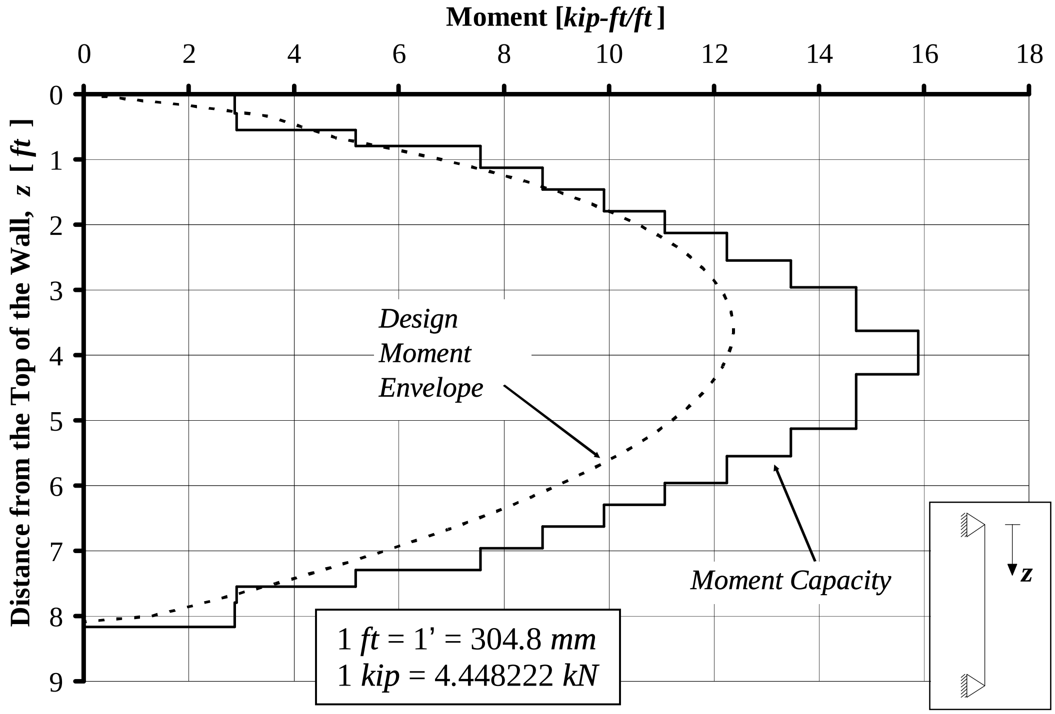

Figure 4.11. Diagram of the Abutment S4 Capacity at Ultimate Load Conditions

According to ACI 440.2R-02 (2002) Section 9.4, the stress in the steel must be less than $0.80 f_y$ in service conditions. In addition, in order to avoid creep failure under service loads, the stress in the carbon-FRP has to be limited to the value of $0.55 f_{fu}$ according to ACI 440.2R-02 (2002) Section 9.5. In this case, it results

$$\begin{cases} f_{steel} = 23.44\ MPa\ (3.4\ ksi) < 0.8 f_y = 275.8\ MPa\ (40.0\ ksi) \\ f_{FRP} = 24.13\ MPa\ (3.5\ ksi) < 0.55 f_{fu} = 324.1\ MPa\ (47.0\ ksi) \end{cases}$$

for the abutment S1 and

$$\begin{cases} f_{steel} = 120.7\ MPa\ (17.5\ ksi) < 0.8 f_y = 275.8\ MPa\ (40.0\ ksi) \\ f_{FRP} = 95.15\ MPa\ (13.8\ ksi) < 0.55 f_{fu} = 324.1\ MPa\ (47.0\ ksi) \end{cases}$$

for the abutment S4.

4.3.3. Shear Check

The concrete contribution V_c to the shear capacity was calculated based on equation (8-48) of AASHTO (2002) as follows:

$$\begin{cases} V_c = \left(1.9\sqrt{f_c^{'}} + 2500\, r_w \dfrac{V_u d}{M_u}\right) b_w d \le 3.5\sqrt{f_c^{'}}\, b_w d \\ \left[f_c^{'} \right] = \left[psi \right] \end{cases} \tag{4.6}$$

The as-built shear capacity is then computed by adding the concrete contribution to the one due to the shear reinforcement.

In this case, no shear reinforcement is present: Table 4.7 summarizes the findings for the abutments S1 and S4. Since the capacity is higher than the demand, it can be concluded that no shear reinforcement is required for both elements.

Table 4.7. Abutments S1 and S4 Shear Capacity

Element	*Shear Capacity* fV_n	*Shear Demand* V_u
Abutment S1 $\left[\frac{kN}{m}\right] \left(\left[\frac{kip}{ft}\right]\right)$	68.6 (4.7)	45.3 (3.1)
Abutment S4 $\left[\frac{kN}{m}\right] \left(\left[\frac{kip}{ft}\right]\right)$	68.6 (4.7)	61.3 (4.2)

4.3.4. Combined Flexure and Axial Load Check

As mentioned before, the abutments S1 and S4 were analyzed as walls loaded in and out of their plane. Conservatively, the combined flexure and axial load check can be done using

$$\frac{P}{P_d}+\frac{M}{M_d}\leq 1 \tag{4.7}$$

where

P and M	are, respectively, the actual compression and flexure loads;
P_d	is the axial capacity in compression calculated in absence of flexure;
M_d	is the flexural capacity calculated in absence of axial load.

According to ACI 318-02 Section 14.5.2, design axial load strength $P_d = f P_n$ for a wall of solid rectangular cross section with resultant of all factored loads located within the middle third of the overall thickness of the wall is given by

$$P_d = f P_n = 0.55 f f_c A_g \left[1-\left(\frac{kh_c}{32h}\right)^2\right] \tag{4.8}$$

where

A_g	is the gross area of the section;
h	is the overall thickness of member;
h_c	is the vertical distance between supports ($h_c = 2073\ mm$ $\left(6\ ft + 9\frac{5}{8}\ in\right)$ for the abutment S1 and $h_c = 2464\ mm$ $\left(8\ ft + 1\ in\right)$ for the abutment S4);
k	is the effective length factor (conservatively, $k = 1.0$ as for walls unrestrained against rotation at both ends);
$f = 0.70$	is the strength reduction factor.

Table 4.8 summarizes the positive findings for the abutments S1 and S4.

Table 4.8. Abutments S1 and S4 Combined Flexure and Axial Load Check

Element	*Design Axial Load Strength* fP_n	*Compression Load* P	*Flexure Load* M	*Check* $\frac{P}{P_d}+\frac{M}{M_d}\leq 1$
	$\frac{kN}{m}\left(\left[\frac{kip}{ft}\right]\right)$	$\frac{kN}{m}\left(\left[\frac{kip}{ft}\right]\right)$	$\left[\frac{kN\cdot m}{m}\right]\left(\left[\frac{kip\cdot ft}{ft}\right]\right)$	
Abutment S1				
Load Condition A	1620 (111)	607 (41.6)	8.9 (2.0)	0.609
Load Condition B	1620 (111)	477 (32.7)	18.2 (4.1)	0.778
Abutment S4				
Load Condition A	1547 (106)	607 (41.6)	15.1 (3.4)	0.713
Load Condition B	1547 (106)	477 (32.7)	26.2 (5.9)	0.867

5. FIELD EVALUATION

5.1. Introduction

Although in-situ bridge load testing is recommended by the AASHTO (2002) Specification as an “effective means of evaluating the structural performance of a bridge”, no guidelines currently exist for bridge load test protocols. In each case, the load test objectives, load configuration, instrumentation type and placement, and analysis techniques are to be determined by the organization conducting the test.

In order to validate the behavior of the bridge after strengthening, a static load test was performed with a H25 legal truck (see Figure 5.1), in June 2004 about two months after the strengthening. Figure 5.2 shows the distribution of the load between the axles of the truck and the loading configurations maximizing the stresses and deflections at mid-span of deck panels under a total of three passes, one central and two laterals. For each pass, ten stops were executed centering the truck rear axle over the marks on the deck. During each stop, the truck was stationary for at least two minutes before proceeding to the next location in order to allow stable readings.

Figure 5.1. Load Tests after Strengthening on Bridge No. 2210010

Displacements in the longitudinal and transverse directions were measured using Linear

Variable Differential Transducers (LVDTs). Strains in the strengthening material of the span S3 were monitored by means of strain gages. Figure 5.3 shows the details of the instrumentation whose layout was designed to gain the maximum amount of information about the structure.

Figure 5.4 reports the displacement relative to Pass #1 Stop #2 corresponding to the rear axle of the truck at the middle of the span S3. It is interesting to note that the deck deflected like a continuous slab over the spans S2 and S3 while for design purposes the continuity of the superstructure over the central abutments was conservatively neglected. In addition, the bridge performed well in terms of overall deflection. In fact, the maximum deflection measured during the load test is below the allowable deflection prescribed by AASHTO, 2002 Section 8.9.3 ($d_{\max} \le l_d / 800 = 3.826\ mm\ (0.150\ in)$).

Figure 5.5 reports the reading of the strain gages applied to the FRP laminates, relative to Pass #1 Stop #8. The maximum strain readings (between 25 and 40 me) for the most loaded part of the slab indicate a satisfactory performance of the FRP laminates under service conditions.

Results for other load configurations are summarized in Appendix A together with the theoretical values obtained with the Finite Element Method (FEM) model described in the following section.

It is important to mention that strain gages and LVDTs were placed to monitor horizontal displacements and deformations in the abutment S4. The strain gages were attached on the FRP strips corresponding to the height of the horizontal crack. For the service loads used in the test, no horizontal displacement was detected while the maximum reading of the strain gages was about 30 me . Thus, those deformations in the FRP strips were ascribed to the local buckling of the FRP plates due to the closing of the crack rather than to the flexural deformation of the concrete walls. Therefore, no further analysis was performed on those data.

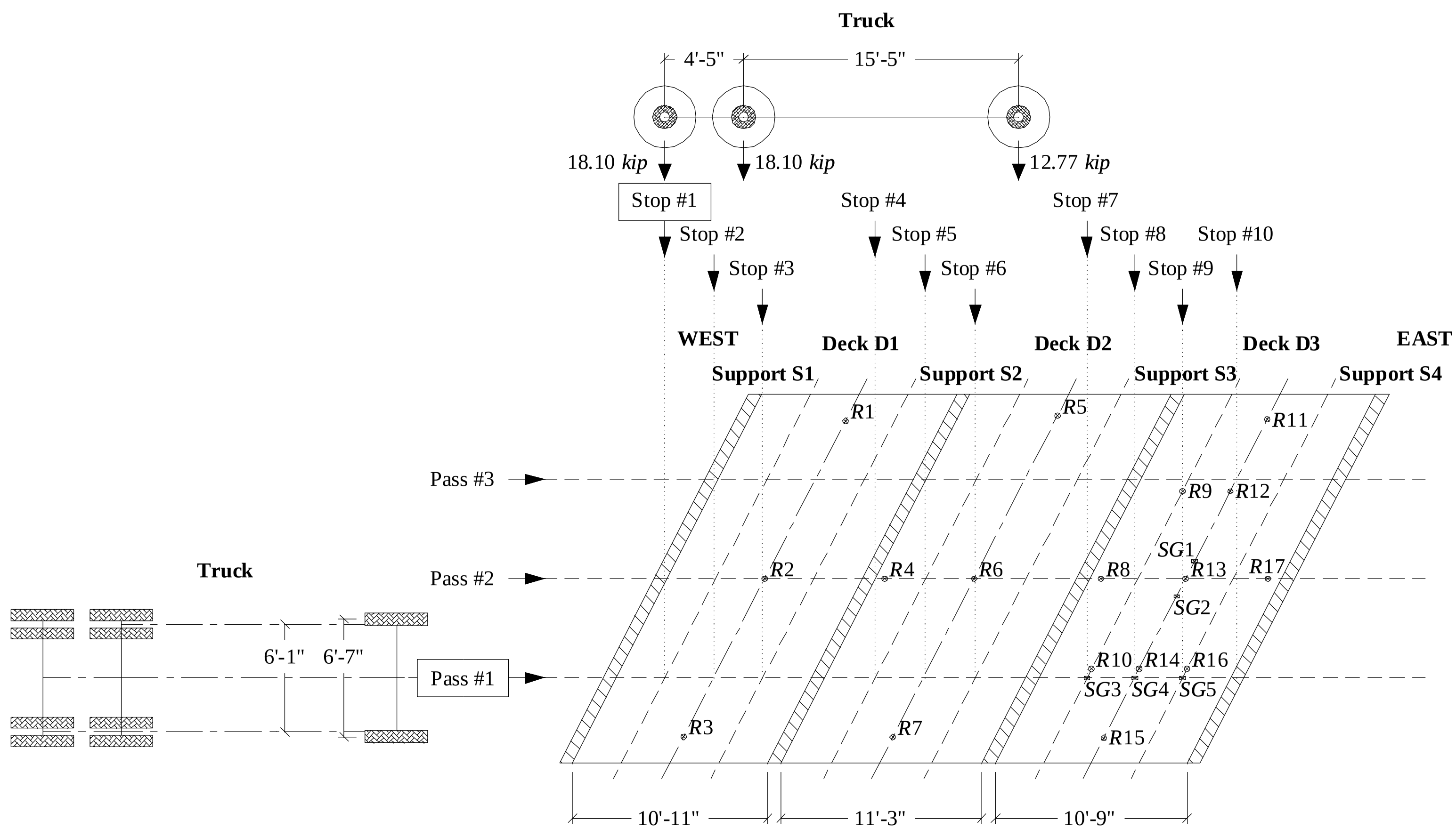

Figure 5.2. Legal Truck Used in the Load Test after Strengthening

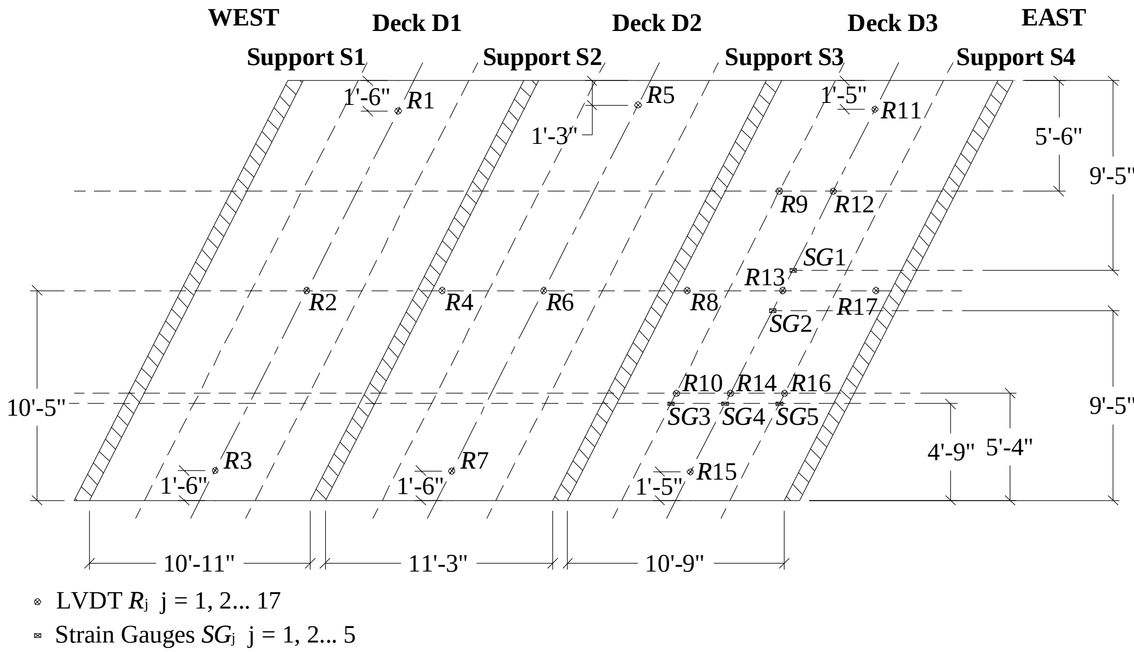

Figure 5.3. LVDT and Strain Gage Positions in the Load Test after Strengthening

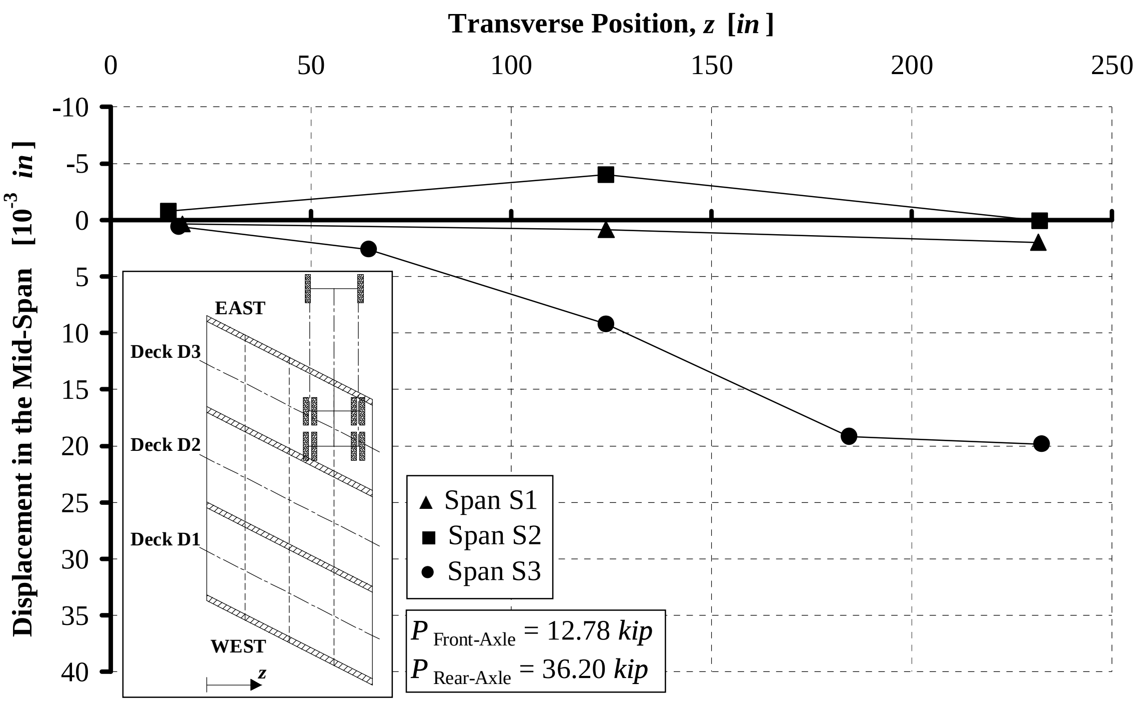

Figure 5.4. Mid-Span Displacement, Pass #1 Stop #2

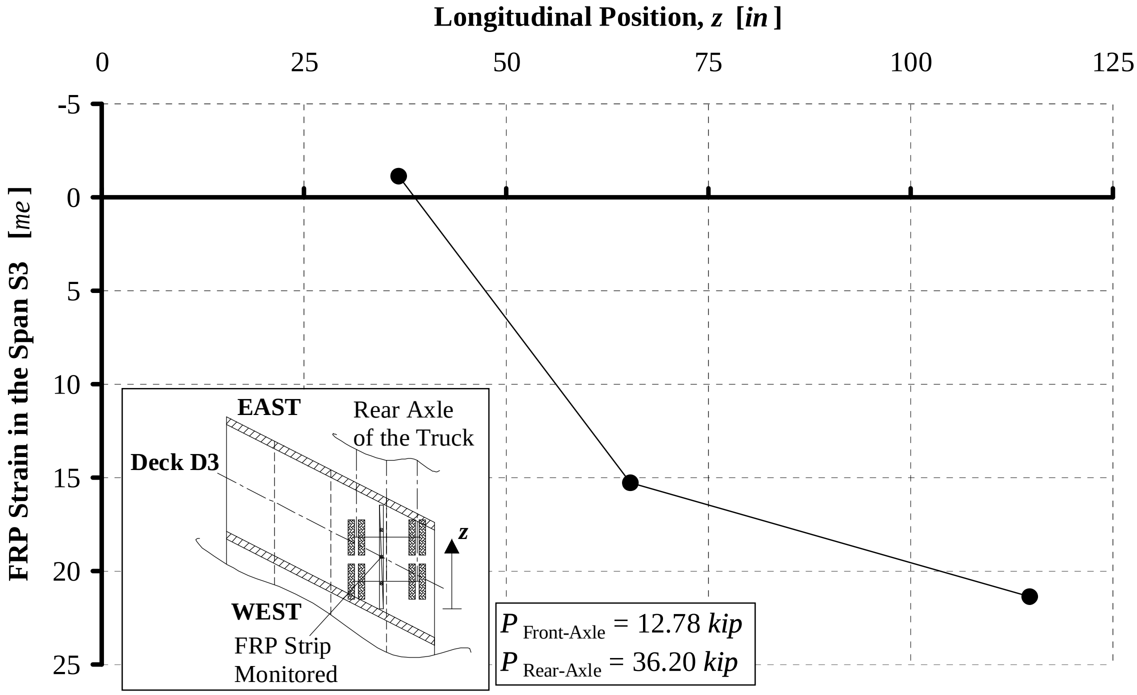

Figure 5.5. Mid-Span Strain in the FRP Laminates, Pass #1 Stop #8

5.2. Additional Load Test

A dynamic test was conducted on the strengthened bridge to determine the impact factor by moving the truck on Pass #2 at speeds equal to 1.1, 2.2, 4.5 and 8.9 m/s (2.5, 5.0, 10.0 and 20.0 MPH). The dynamic test was performed acquiring the data at a frequency of 20 Hz. The live load impact factor I was computed as the ratio between the difference between the maximum dynamic and static displacements to the maximum static deflection (i.e. Pass #2 and Stop #2, #5 and #8 for the span S1, S2 and S3, respectively). As an example, Figure 5.6 shows the dynamic deflections as a function of time at a 2.2 m/s (5 MPH) speed.

Appendix B reports all the results obtained at different truck speeds for displacements and strains. From such curves it is possible to extrapolate two values for the maximum impact factor $I_{experimental}$, 1.10 and 1.56 according to the reading of the LVDTs and the strain gauges, respectively. Both values are higher than the one used for design ($I = 0.30$

according to AASHTO (2002)), but some important considerations must be done taking into account the position of the measurement devices. The higher value of impact factors derived from the displacements readings are related to LVDTs and strain gages positioned at the sides of the decks (i.e. R1, R5, R11…), while the impact factors determined considering the rest of the LVDTs are less than 1.0. This implies that, in reality, the portions of the slab interested by the higher impact load factor would still experience a load below the design value.

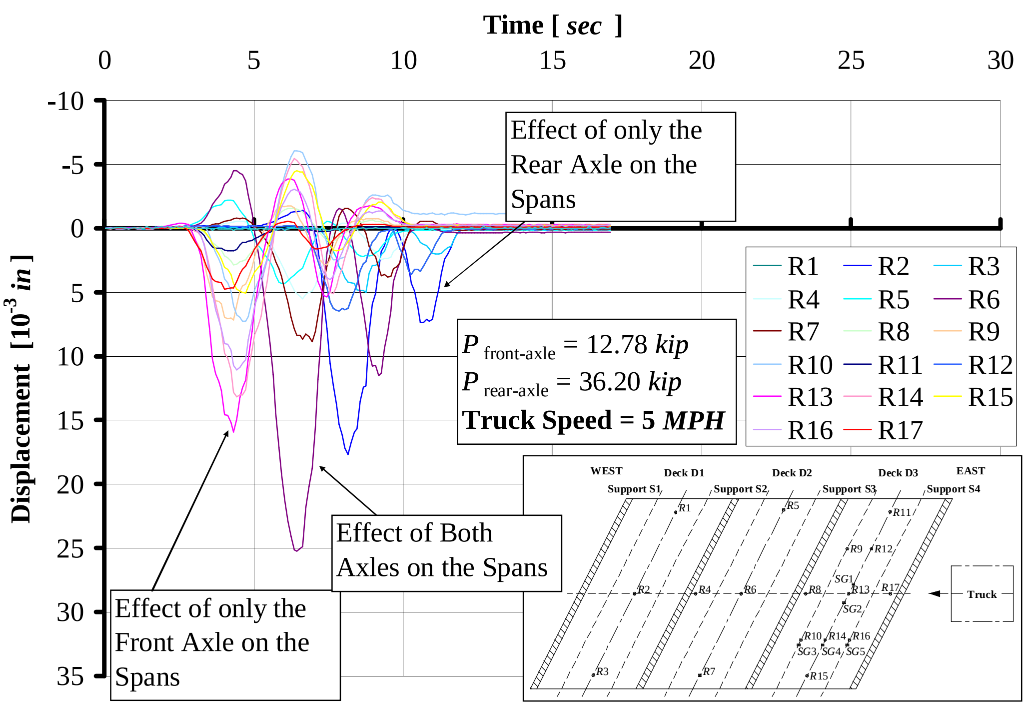

Figure 5.6. After Strengthening Displacements at $2.2\ m/s$ ($5\ MPH$)

5.3. FEM Analysis

In this section, a FEM analysis model is described. This model was developed in order to interpret the experimental data collected during the test after the strengthening. For this purpose, a commercially available finite element program ANSYS 7.1 was used. Details of the geometry can be found in Figure 5.7 and Figure 5.8.

The element SOLID65 was chosen to model the concrete and the FRP laminates. SOLID65 is used for the three-dimensional modeling of solids with or without reinforcing bars. The solid is capable of cracking in tension and crushing in compression. In addition, up to three different rebar specifications may be defined. The element is defined by eight nodes having three degrees of freedom at each node: translations in the nodal x, y and z directions. SOLID65 is subject to the following assumption and restrictions:

- cracking is permitted in three orthogonal directions at each integration point;
- if cracking occurs at an integration point, the cracking is modeled through an adjustment of material properties which effectively treats the cracking as a “smeared band” of cracks, rather than discrete cracks;
- the concrete material is assumed to be initially isotropic;
- whenever the reinforcement capability of the element is used, the reinforcement is assumed to be “smeared” throughout the element;
- in addition to cracking and crushing, the concrete may also undergo plasticity, with the Drucker-Prager failure surface being most commonly used. In this case, the plasticity is done before the cracking and crushing checks.

For this project, the material properties of concrete were assumed to be isotropic and linear elastic, since the applied load was relatively low with respect to the ultimate load condition. The modulus of elasticity of the concrete was based on the measured compressive strength of the cores obtained from the slab according to the standard equation ACI 318-02 Section 8.5.1:

$$E_c = 57000\sqrt{f_c^{'}}\ psi = 57000\sqrt{3365}\ psi \approx\ 23.0\ GPa\ \left(3342\ ksi\right)\ \text{with}\ \left[\,f_c^{'}\right] = \left[psi\right].$$

In order to take into account the presence of the cracks in the deck and the deterioration of the concrete on the sides of the slabs, as a result of a parametric analysis, the modulus of elasticity was reduced to $0.7\ GPa\ \left(100\ ksi\right)$ and $6.9\ GPa\ \left(1000\ ksi\right)$ in the elements corresponding to the longitudinal and transverse cracks, and the damaged concrete areas, respectively, as shown in Figure 5.7b. The depth of the cracks was chosen according to the data collected during the in-situ inspection while the width was assumed to be equal to the elements dimensions; the extension of the damaged concrete areas was determined in the same way. The concrete Poisson's ratio was set to 0.19. Different elements were used to optimize the model and decrease the computation time. The chosen shape and size in the longitudinal and transverse cross sections allowed to locate more accurately the steel rebars (see Figure 5.8a), to properly connect the FRP laminates to the surface of the concrete (see Figure 5.8b) and to reduce the number of the elements in the "secondary" parts of the model, such as the curbs (see Figure 5.8a). Due to the uneven spacing of the steel rebars in the transverse and longitudinal direction, it was preferred to smear the steel reinforcement across the entire length and width of the slab, respectively. The modulus of the elasticity and the Poisson's ratio for the steel reinforcement were assumed as $200.0\ GPa\ (29000\ ksi)$ and 0.3, respectively.

The connections between the FRP laminates and the concrete surface were modeled as rigid, neglecting any form of non-linearity due to a potential initial non-perfect engagement of the strengthening. Modulus of the elasticity and the Poisson's ratio for the FRP laminates were assumed to be $60.6\ GPa\ (8800\ ksi)$ and 0.3, respectively.

The bridge was vertically and transversally restrained in correspondence to the four supports. Two models were built using different longitudinal restrains. In the first, the displacement was fixed to zero at the abutment S2 only (FEM model #1, see Figure 5.8), while, in the second model, the latter condition was set for all the supports (FEM model #2). The loads corresponding to the rear axle were assumed as uniformly distributed over $508 \times 254\ mm\ (20 \times 10\ in)$ areas as specified in AASHTO (2002) Section 4.3.30; the loads corresponding to the front axle were, instead, uniformly distributed over areas proportionally reduced according to the actual geometry of the tires. Such loads were applied at the top of the deck simulating, in such way, the truck wheel prints (see Figure 5.7a).

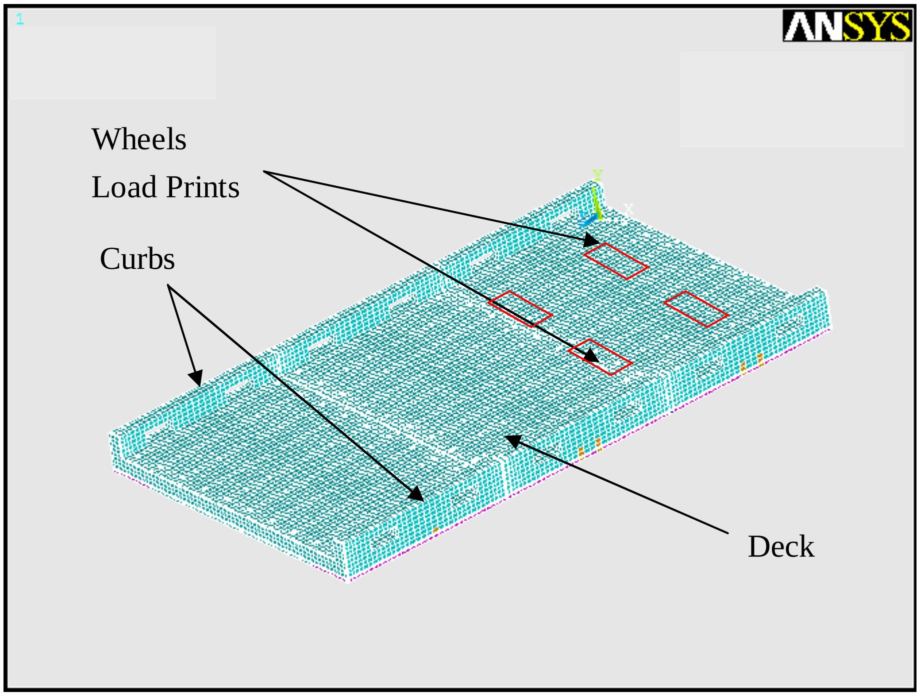

a) Global View of the Model

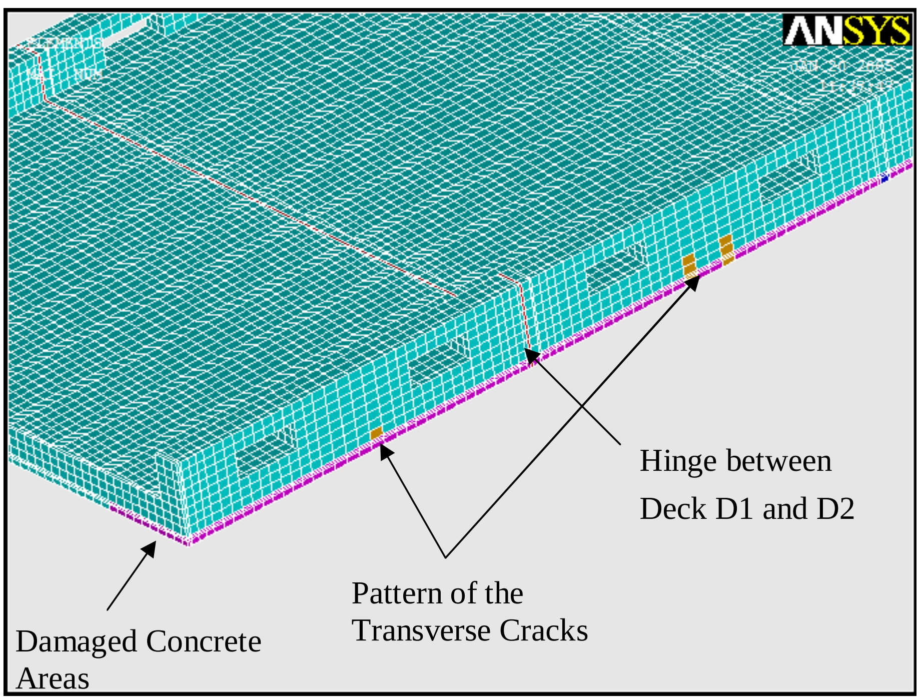

b) Details of the Cracks Modeling

Figure 5.7. FEM Model Geometry (I)

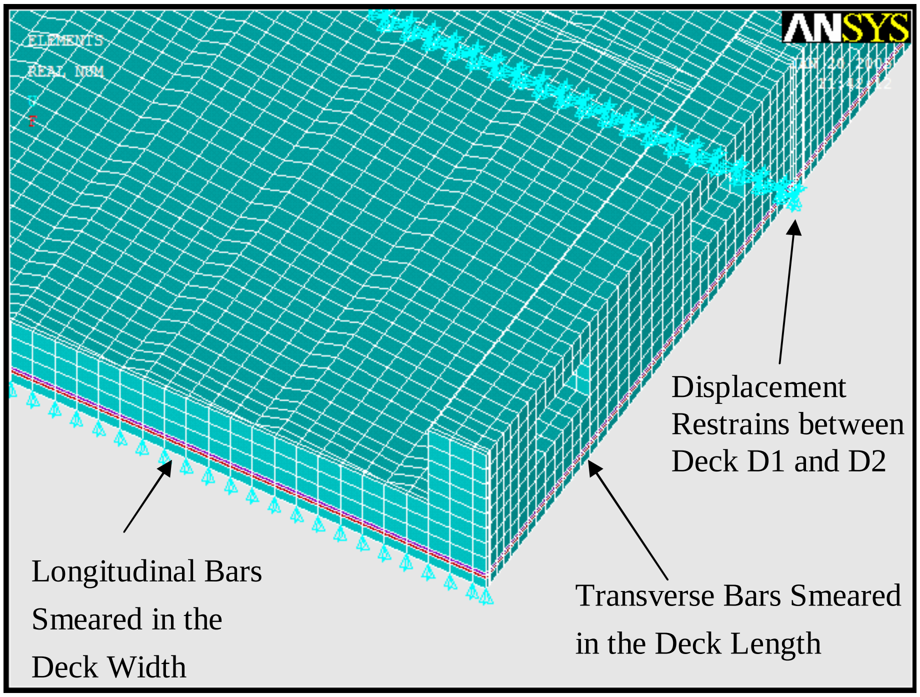

a) Details of the Steel Reinforcement and Boundary Conditions

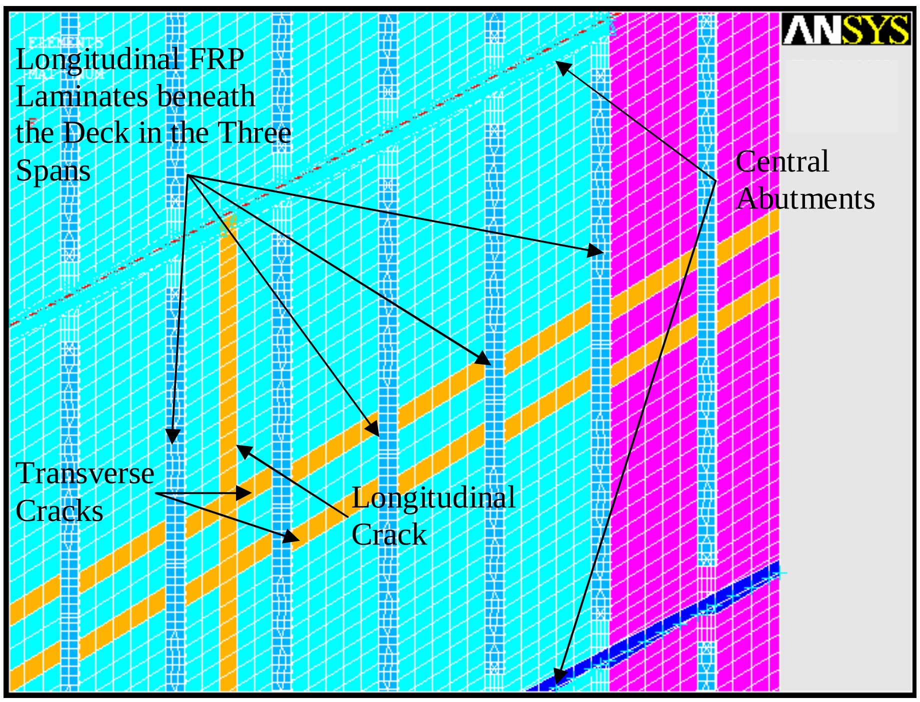

b) Details of the FRP Strenghtening (Bottom View)

Figure 5.8. FEM Model Geometry (II)

Figure 5.9 reports the experimental and analytical mid-span displacements, relative to Pass #3 Stop #7. The graph shows that the experimental deflections are between the analytical results obtained for the two FEM models. The model #1 with longitudinal displacement prevented just on the support S2 is conservative with respect to the overall actual behavior of the structure: on the other hand, the model #1 matches well with the experimental results in the areas where the concrete is damaged.

The same considerations can be made also for the strain gage readings. Figure 5.10 compares experimental and analytical strains on the FRP, relative to Pass #2 Stop #8. The graph shows a good match in strains between experimental and analytical results for the strips fastened beneath the deck of span S3.

Appendix A reports more of the analysis developed for the bridge after the strengthening.

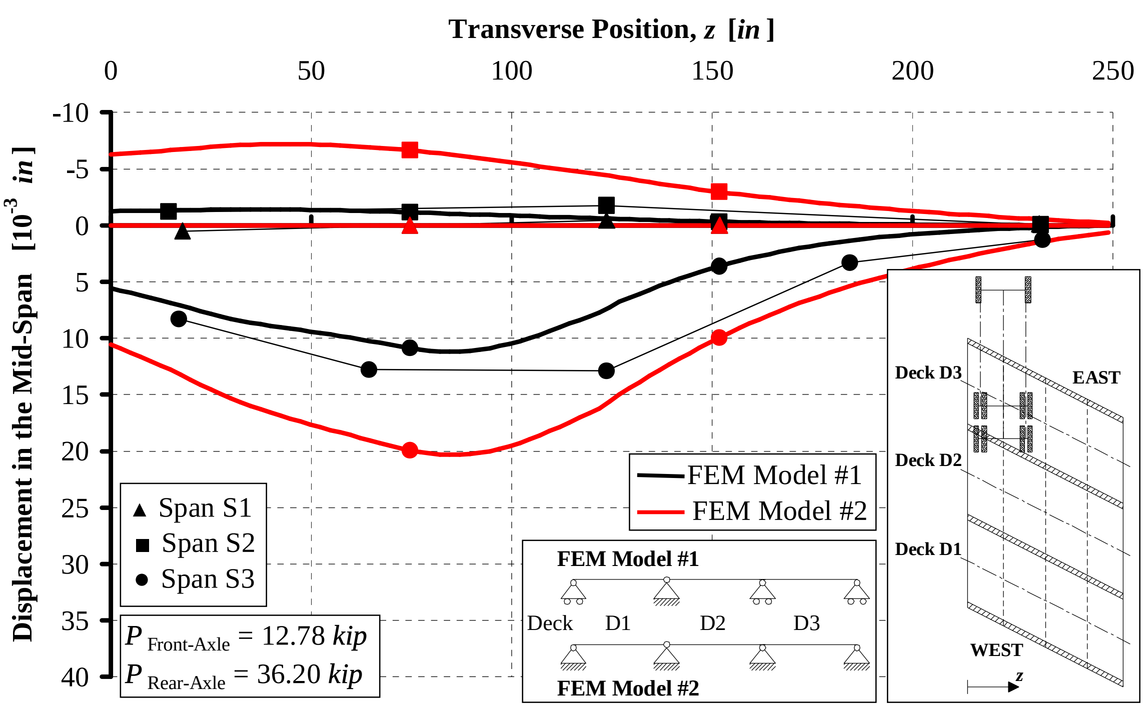

Figure 5.9. Comparison of Experimental and Analytical Results for Mid-Span Displacement, Pass #3 Stop #7

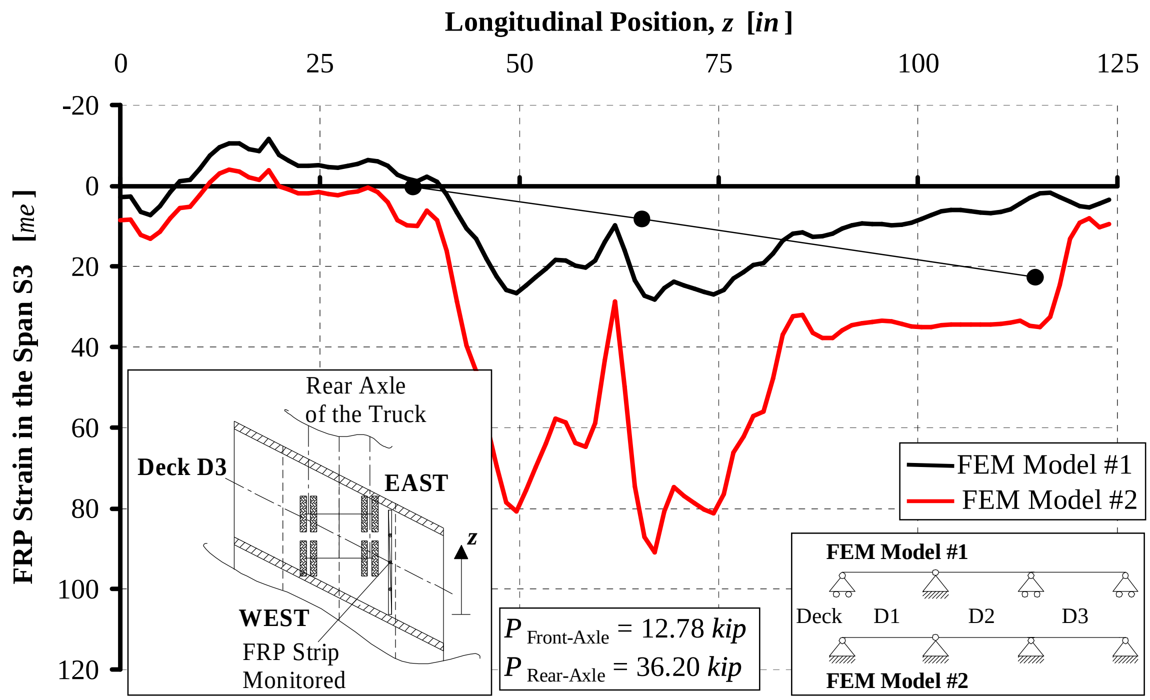

Figure 5.10. Comparison of Experimental and Analytical Results for Strain in the FRP Fastened on the Deck at Mid-Span, Pass #2 Stop #8

6. LOAD RATING

Bridge load rating calculations provide a basis for determining the safe load capacity of a bridge. According to the Missouri Department of Transportation (MoDOT), anytime a bridge is built, rehabilitated, or reevaluated for any reason, inventory and operating ratings are required using the Load Factor rating. All bridges should be rated at two load levels, the maximum load level called the Operating Rating and a lower load level called the Inventory Rating. The Operating Rating is the maximum permissible load that should be allowed on the bridge. Exceeding this level could damage the bridge. The Inventory Rating is the load level the bridge can carry on a daily basis without damaging the bridge.

In Missouri, for the Load Factor Method the Operating Rating is based on the appropriate ultimate capacity using current AASHTO specifications (AASHTO, 1996). The Inventory Rating is taken as 60% of the Operating Rating.

The vehicle used for the live load calculations in the Load Factor Method is the HS20 truck. If the stress levels produced by this vehicle configuration are exceeded, load posting may be required.

The method for determining the rating factor is that outlined by AASHTO in the Manual for Condition Evaluation of Bridges (AASHTO, 2002). Equation (6.1) was used:

$$RF = \frac{C - A_1 D}{A_2 L\left(1 + I\right)} \tag{6.1}$$

where:

RF is the Rating Factor;

C is the capacity of the member;

D is the dead load effect on the member;

L is the live load effect on the member;

I is the impact factor to be used with the live load effect;

A_1 is the factor for dead loads;

A_2 is the factor for live loads.

Since the load factor method is being used, A_1 is taken as 1.3 and A_2 varies depending on the desired rating level. For Inventory Rating, $A_2 = 2.17$, and for Operating Rating, $A_2 = 1.3$.

To determine the rating RT of the bridge, equation (6.2) was used:

$$RT = RF \cdot W \tag{6.2}$$

where W is the weight of the nominal truck used to determine the live load effect.

For the bridge No. 2210010, the Load Rating was calculated for a number of different trucks, HS20, H20, 3S2 and MO5. Ratings are required at the inventory and operating levels by the load factor method on each bridge for the HS20 truck. The H20 legal vehicle is used to model the load for single unit vehicles. The 3S2 vehicle is used as a model for all other vehicles. The MO5 is used to model the commercial zone loadings.

For each of the different loading conditions, the maximum shear and maximum moment were calculated. Impact factors are also taken into account for Load Ratings. This value is 30% for the bridge No. 2210010.

The shear and moment values for the deck are shown in Table 6.1. Table 6.2 and Table 6.3 give the results of the Load Rating pertaining to moment and shear respectively for the deck.

Table 6.1. Maximum Shear and Moment due to Live Load for the Deck

Truck	Maximum Shear $[kN]$ $([kip])$	Maximum Moment $[kN \cdot m]$ $([kip \cdot ft])$	Maximum Shear with Impact $[kN]$ $([kip])$	Maximum Moment with Impact $[kN \cdot m]$ $([kip \cdot ft])$
HS20	19.93 (4.48)	22.17 (16.35)	25.89 (5.82)	28.81 (21.25)
MO5	17.30 (3.89)	14.35 (10.58)	22.46 (5.05)	18.64 (13.75)
H20	17.30 (3.89)	14.35 (10.58)	22.46 (5.05)	18.64 (13.75)
3S2	17.30 (3.89)	14.35 (10.58)	22.46 (5.05)	18.64 (13.75)

Table 6.2. Rating Factor for the Deck (Bending Moment)

Truck	Rating Factor *RF*	Rating *RT* ton_{SI} $([ton])$	Rating Type
HS20	1.754	57.2 (63.1)	Operating
HS20	1.051	34.3 (37.8)	Inventory
MO5	2.711	88.5 (97.6)	Operating
H20	2.332	42.3 (46.6)	Posting
3S2	2.332	77.5 (85.4)	Posting

Table 6.3. Rating Factor for the Deck (Shear)

Truck	Rating Factor *RF*	Rating *RT* ton_{SI} $([ton])$	Rating Type
HS20	2.271	74.2 (81.8)	Operating
HS20	1.361	44.5 (49.0)	Inventory
MO5	2.619	87.0 (95.9)	Operating
H20	2.252	40.8 (45.0)	Posting
3S2	2.252	74.8 (82.5)	Posting

The shear and moment values for the abutment S1 are shown in Table 6.4. Table 6.5 **and** Table 6.6 give the results of the Load Rating pertaining to moment and shear respectively for the abutment S1.

Table 6.4. Maximum Shear and Moment due to Live Load for the Abutment S1

Truck	Maximum Shear $[kN]$ $([kip])$	Maximum Moment $[kN \cdot m]$ $([kip \cdot ft])$	Maximum Shear with Impact $[kN]$ $([kip])$	Maximum Moment with Impact $[kN \cdot m]$ $([kip \cdot ft])$
HS20	9.70 (2.18)	4.38 (3.23)	12.59 (2.83)	5.69 (4.20)
MO5	6.45 (1.45)	3.19 (2.35)	8.41 (1.89)	4.15 (3.06)
H20	6.45 (1.45)	3.19 (2.35)	8.41 (1.89)	4.15 (3.06)
3S2	6.45 (1.45)	3.19 (2.35)	8.41 (1.89)	4.15 (3.06)

Table 6.5. Rating Factor for the Abutment S1 (Bending Moment)

Truck	Rating Factor RF	Rating RT ton_{SI} $([ton])$	Rating Type
HS20	2.703	88.3 (97.3)	Operating
HS20	1.619	52.9 (58.3)	Inventory
MO5	3.712	121.2 (133.6)	Operating
H20	3.193	58.0 (63.9)	Posting
3S2	3.193	106.1 (117.0)	Posting

Table 6.6. Rating Factor for the Abutment S1 (Shear)

Truck	Rating Factor RF	Rating RT ton_{SI} $([ton])$	Rating Type
HS20	2.246	73.3 (80.8)	Operating
HS20	1.345	43.9 (48.4)	Inventory
MO5	3.364	111.8 (123.2)	Operating
H20	2.893	52.5 (57.9)	Posting
3S2	2.893	96.2 (106.0)	Posting

The shear and moment values for the abutment S4 are shown in Table 6.7. Table 6.8 and Table 6.9 give the results of the Load Rating pertaining to moment and shear respectively for the abutment S4.

Table 6.7. Maximum Shear and Moment due to Live Load for the Abutment S4

Truck	Maximum Shear $[kN]$ $([kip])$	Maximum Moment $[kN \cdot m]$ $([kip \cdot ft])$	Maximum Shear with Impact $[kN]$ $([kip])$	Maximum Moment with Impact $[kN \cdot m]$ $([kip \cdot ft])$
HS20	8.01 (1.80)	4.15 (3.06)	10.41 (2.34)	5.38 (3.97)
MO5	5.38 (1.21)	2.81 (2.07)	6.98 (1.57)	3.65 (2.69)
H20	5.38 (1.21)	2.81 (2.07)	6.98 (1.57)	3.65 (2.69)
3S2	5.38 (1.21)	2.81 (2.07)	6.98 (1.57)	3.65 (2.69)

Table 6.8. Rating Factor for the Abutment S4 (Bending Moment)

Truck	Rating Factor RF	Rating RT ton_{SI} $([ton])$	Rating Type
HS20	2.504	81.8 (90.2)	Operating
HS20	1.500	49.0 (54.0)	Inventory
MO5	3.694	120.7 (133.0)	Operating
H20	3.177	57.6 (63.5)	Posting
3S2	3.177	105.6 (116.4)	Posting

Table 6.9. Rating Factor for the Abutment S4 (Shear)

Truck	Rating Factor RF	Rating RT ton_{SI} $([ton])$	Rating Type
HS20	1.865	60.9 (67.1)	Operating
HS20	1.117	36.5 (40.2)	Inventory
MO5	2.777	92.3 (101.7)	Operating
H20	2.388	43.4 (47.8)	Posting
3S2	2.388	79.4 (87.5)	Posting

The axial load values for wall S3 are shown in Table 6.10. Table 6.11 gives the results of the Load Rating pertaining to axial loads for the concrete wall S3.

Table 6.10. Axial Load due to Live Load for the Concrete Wall S3

Truck	Maximum Axial Load $\left[\frac{kN}{m}\right]\left(\left[\frac{kip}{ft}\right]\right)$	Maximum Axial Load with Impact $\left[\frac{kN}{m}\right]\left(\left[\frac{kip}{ft}\right]\right)$
HS20	140.10 (9.60)	182.13 (12.48)
MO5	70.05 (4.80)	91.07 (6.24)
H20	70.05 (4.80)	91.07 (6.24)
3S2	70.05 (4.80)	91.07 (6.24)

Table 6.11. Rating Factor for the Concrete Wall S3 (Axial Load)

Truck	Rating Factor *RF*	Rating *RT* ton_{SI} $([ton])$	Rating Type
HS20	6.534	213.4 (235.2)	Operating
HS20	3.914	127.8 (140.9)	Inventory
MO5	13.067	426.7 (470.4)	Operating
H20	11.238	203.9 (224.8)	Posting
3S2	11.238	373.5 (411.7)	Posting

According to Table 6.3, as a consequence of the FRP strengthening, the maximum live load that can safely utilize the structure for an indefinite period of time is $40.8\ ton_{SI}$ $45.0\ ton$. Therefore, since the legal loads established for Missouri are defined as $20.9\ ton_{SI}$ $23.0\ ton$ for single unit vehicles and $36.3\ ton_{SI}$ $(40.0\ ton)$ for all others, the existing load posting can be removed.

7. CONCLUSIONS

Conclusions based on the retrofitting of the bridge utilizing FRP materials can be summarized as follows:

- the mechanically fastened (MF) FRP system showed to be a feasible solution for the strengthening of the bridge;
- in-situ load testing has proven to be useful and convincing;
- the FEM analysis has shown good match with experimental results demonstrating the effectiveness of the strengthening technique;
- as a result of FRP strengthening, the load posting of the bridge can be removed.

8. REFERENCES

AASHTO (1996). “LRFD bridge design specifications.” Second Edition, Published by the American Association of State Highway and Transportation Officials, Washington D.C.

AASHTO (2002). “Standard specifications for highway bridges.” 17th Edition, Published by the American Association of State Highway and Transportation Officials, Washington D.C.

ACI Committee 318 (1999). “Building code requirements for structural concrete and commentary.” ACI 318R-99, Published by the American Concrete Institute, Farmington Hills, MI.

ACI Committee 318 (2002). “Building code requirements for structural concrete and commentary.” ACI 318R-02, Published by the American Concrete Institute, Farmington Hills, MI.

ACI Committee 440 (1996). "State-of-the-art report on FRP for concrete structures." ACI 440R-96, Manual of Concrete Practice, ACI, Farmington Hills, MI, 68 pp.

ACI Committee 440 (2002). “Guide for the design and construction of externally bonded FRP systems for strengthening concrete structures.” ACI 440.2R-02, Published by the American Concrete Institute, Farmington Hills, MI.

Alkhrdaji, T., Nanni, A., Chen, G., and Barker, M. (1999). “Upgrading the transportation infrastructure: solid RC decks strengthened with FRP.” Concrete International, American Concrete Institute, Vol. 21, No. 10, October, pp. 37-41.

ANSYS User’s Manual for Revision 6.1 (2000). Volume I Procedure and Volume III Elements, Swanson Analysis Systems, Inc.

Arora, D. (2003). “Rapid strengthening of reinforced concrete bridge with mechanically fastened fiber-reinforced polymer strips.” M.Sc. Thesis, University of Wisconsin – Madison.

Bank, L. C., Lamanna A. J., Ray, J. C., and Velásquez G. I. (2002). "Rapid strengthening of reinforced concrete beams with mechanically fastened, fiber-reinforced polymeric composite materials." US Army Corps of Engineers, Washington D.C.

Bank, L. C., Borowicz D. T., Lamanna A. J., Ray J. C., and Velásquez G. I. (2002). "Rapid strengthening of full-sized concrete beams with powder-actuated fastening systems and Fiber-Reinforced Polymer (FRP) composite materials." US Army Corps of Engineers, Washington D.C.

Borowicz, D. T. (2002). "Rapid strengthening of concrete beams with powder-actuated fastening systems and Fiber-Reinforced Polymer (FRP) composite materials." M.Sc. Thesis, University of Wisconsin – Madison.

Lamanna, A.J. (2002). "Flexural strengthening of reinforced concrete beams with mechanically fastened fiber reinforced polymer strips." PhD Thesis, University of Wisconsin – Madison.

APPENDICES

APPENDIX

A. After Strengthening Test Results

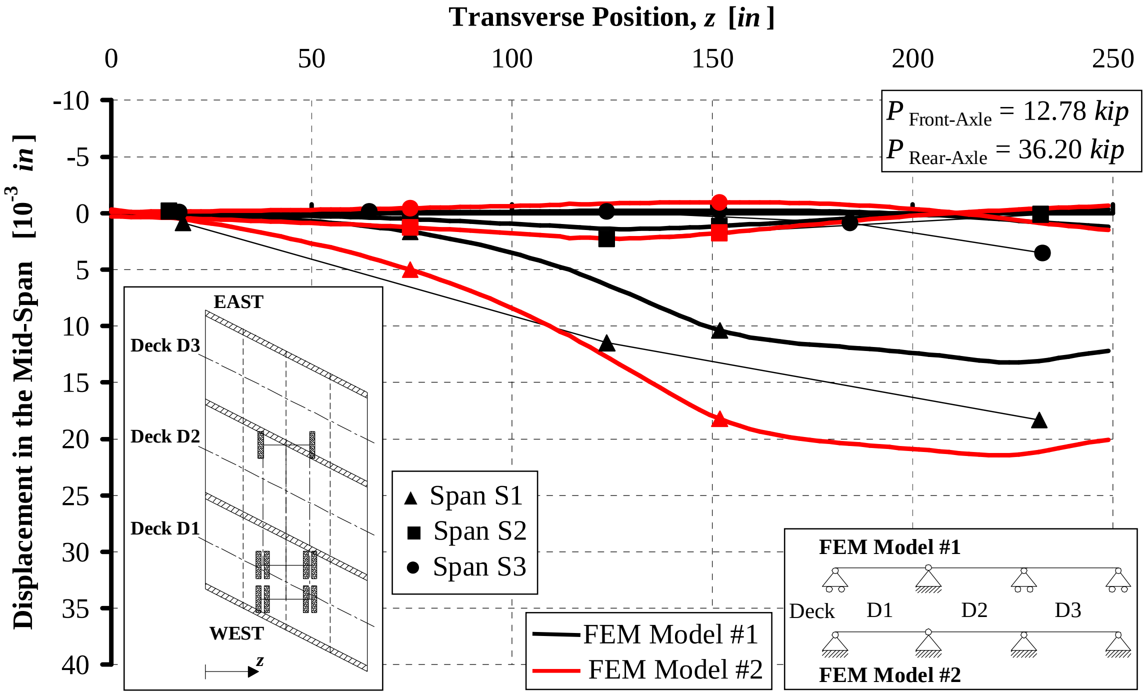

Figure A. 1. After Strengthening Mid-Span Displacement, Pass #1 Stop #2

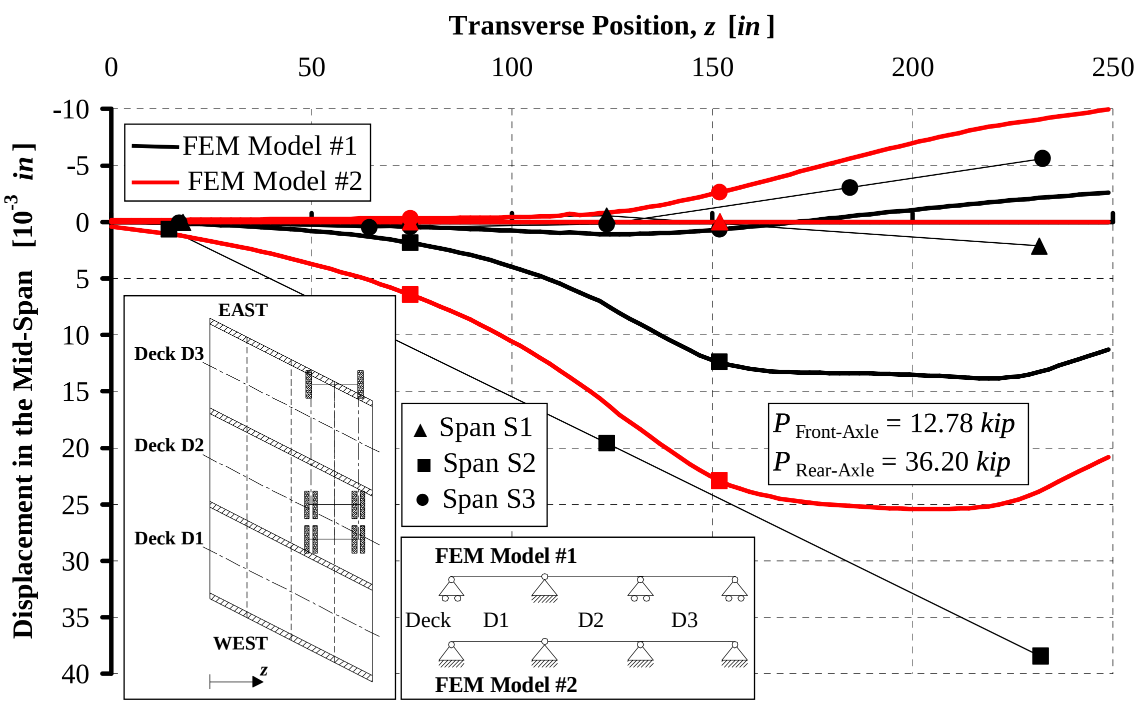

Figure A. 2. After Strengthening Mid-Span Displacement, Pass #1 Stop #5

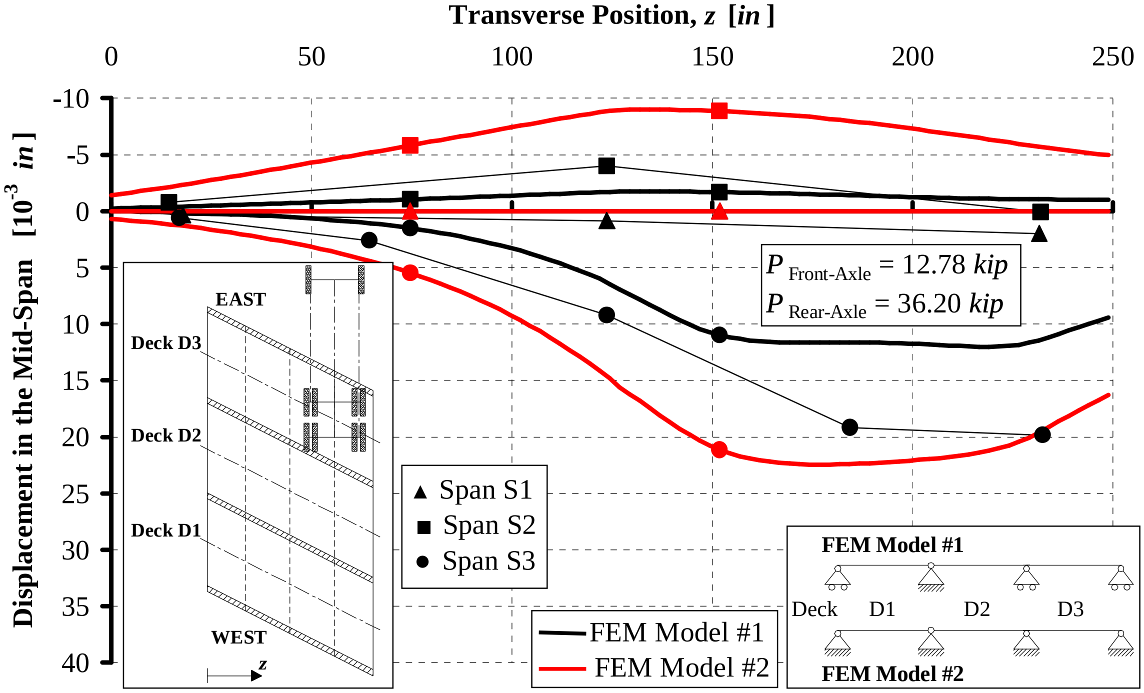

Figure A. 3. After Strengthening Mid-Span Displacement, Pass #1 Stop #8

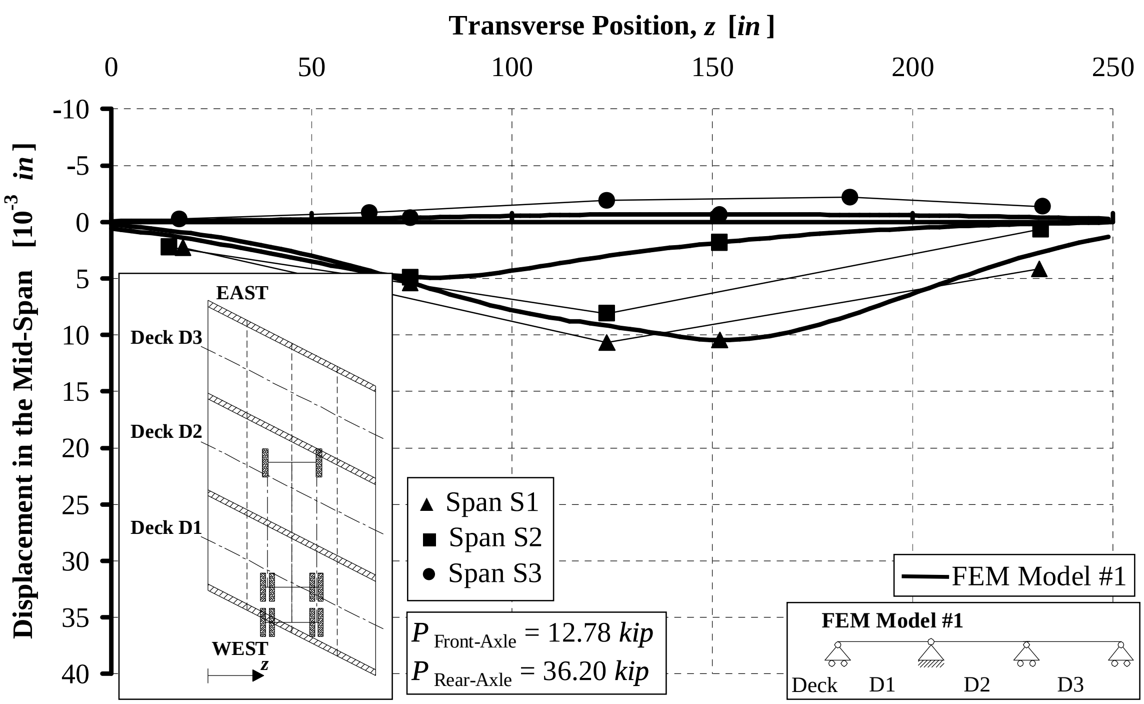

Figure A. 4. After Strengthening Mid-Span Displacement, Pass #2 Stop #1

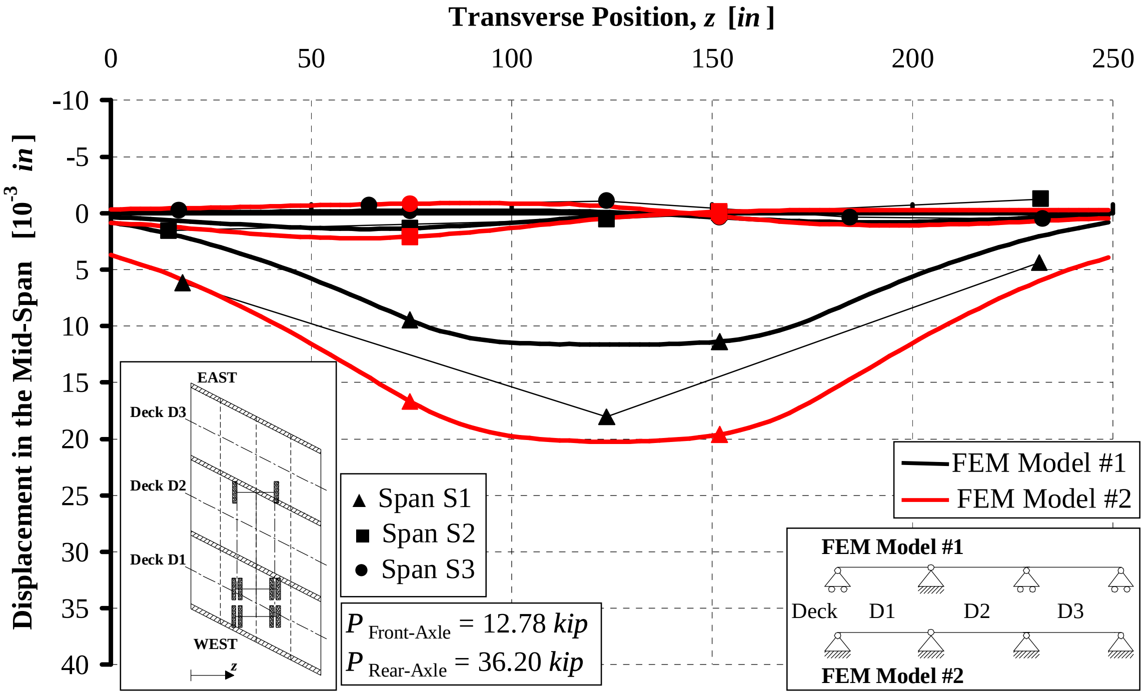

Figure A. 5. After Strengthening Mid-Span Displacement, Pass #2 Stop #2

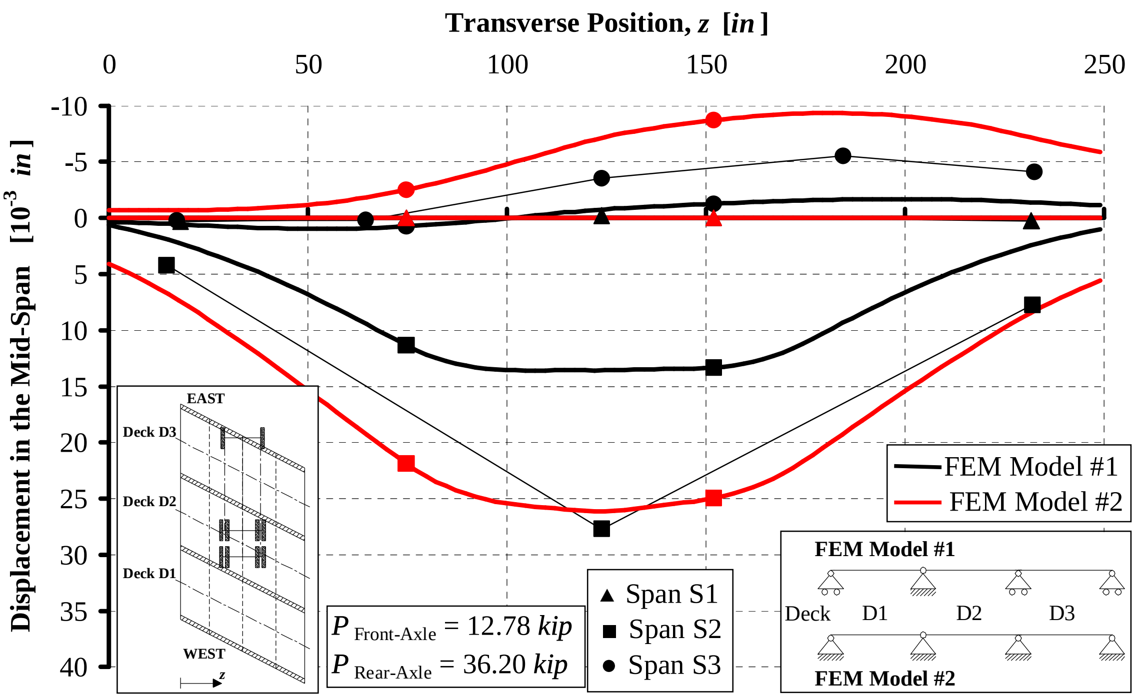

Figure A. 6. After Strengthening Mid-Span Displacement, Pass #2 Stop #5

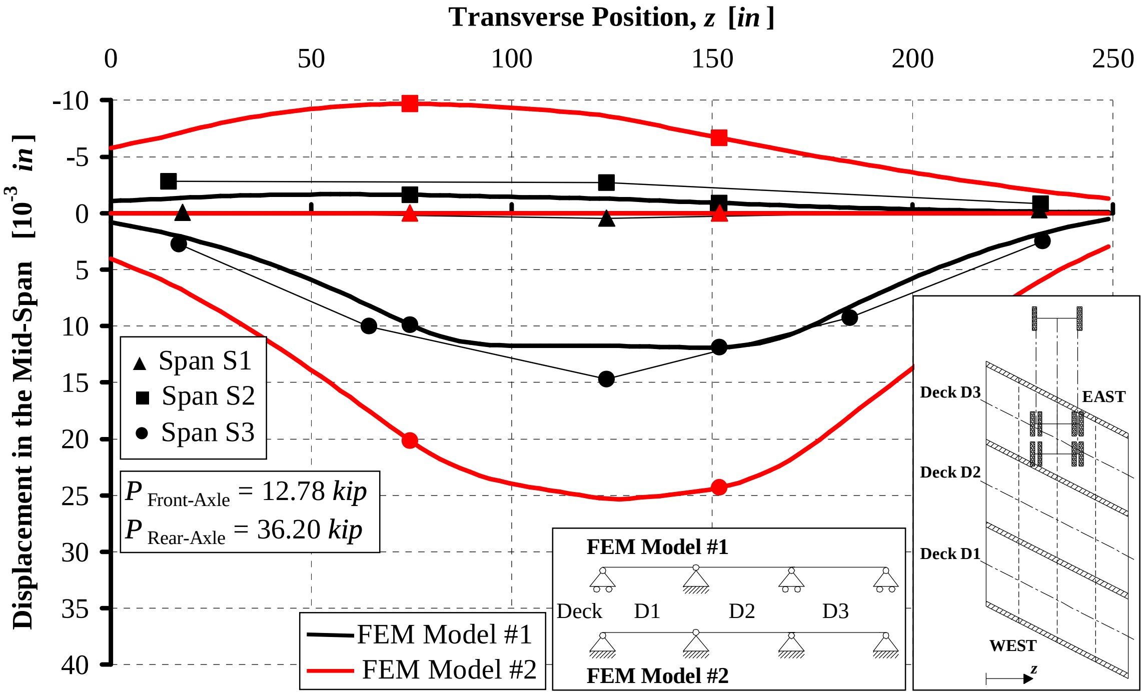

Figure A. 7. After Strengthening Mid-Span Displacement, Pass #2 Stop #8

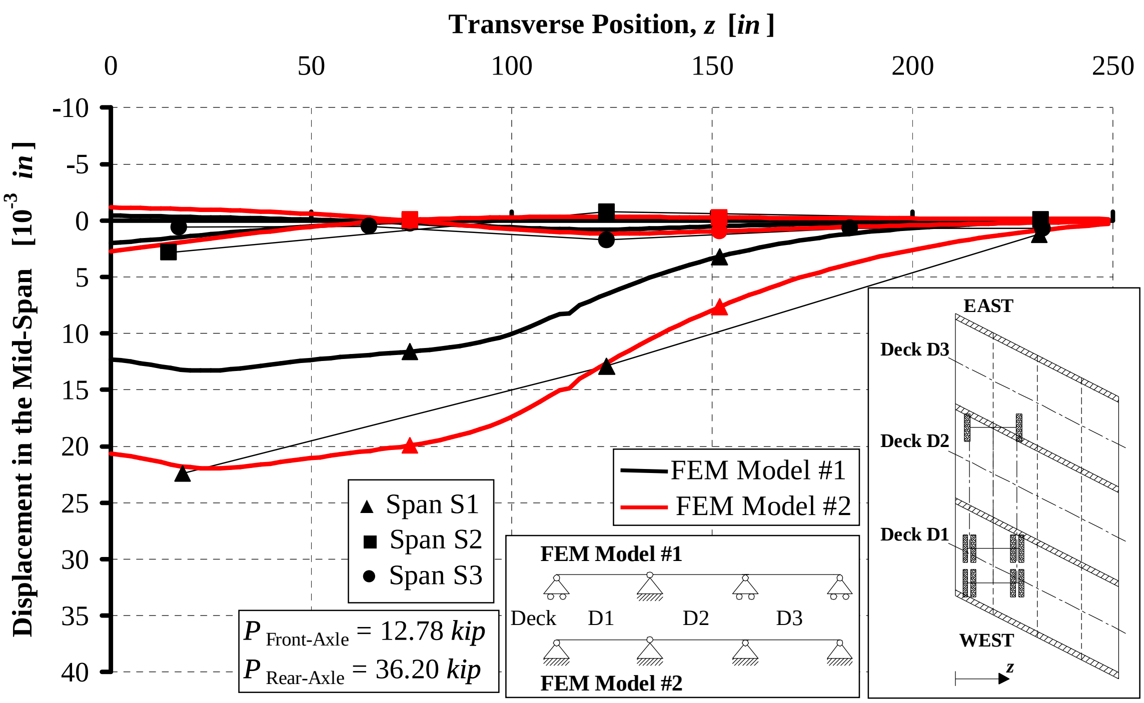

Figure A. 8. After Strengthening Mid-Span Displacement, Pass #3 Stop #2

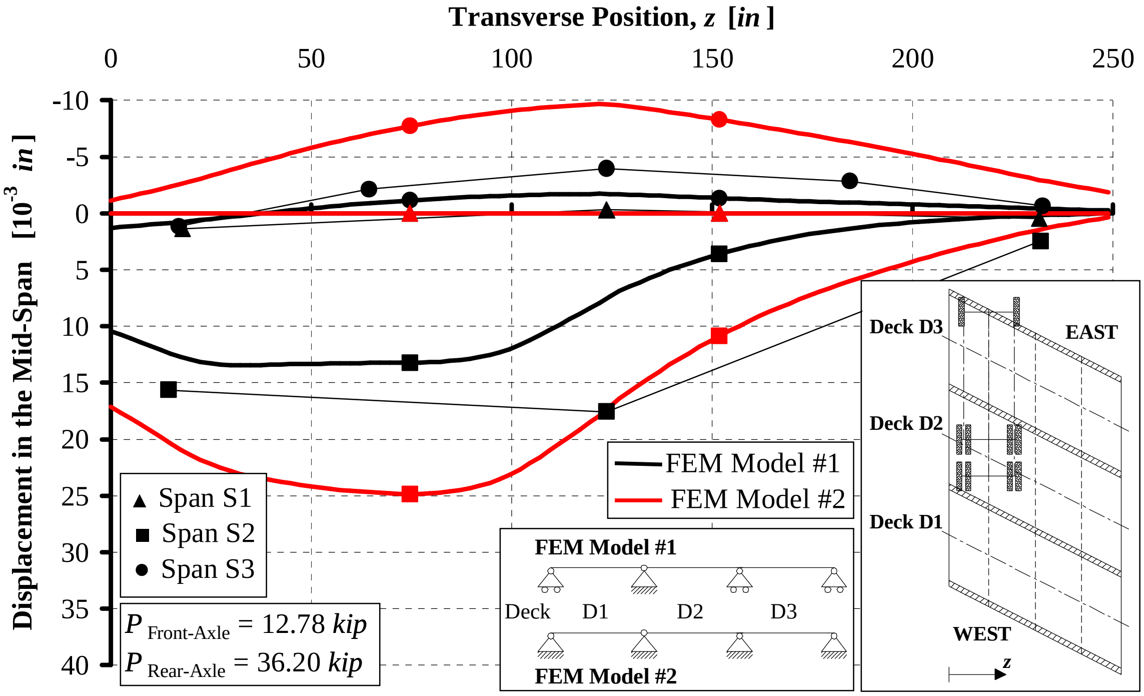

Figure A. 9. After Strengthening Mid-Span Displacement, Pass #3 Stop #5

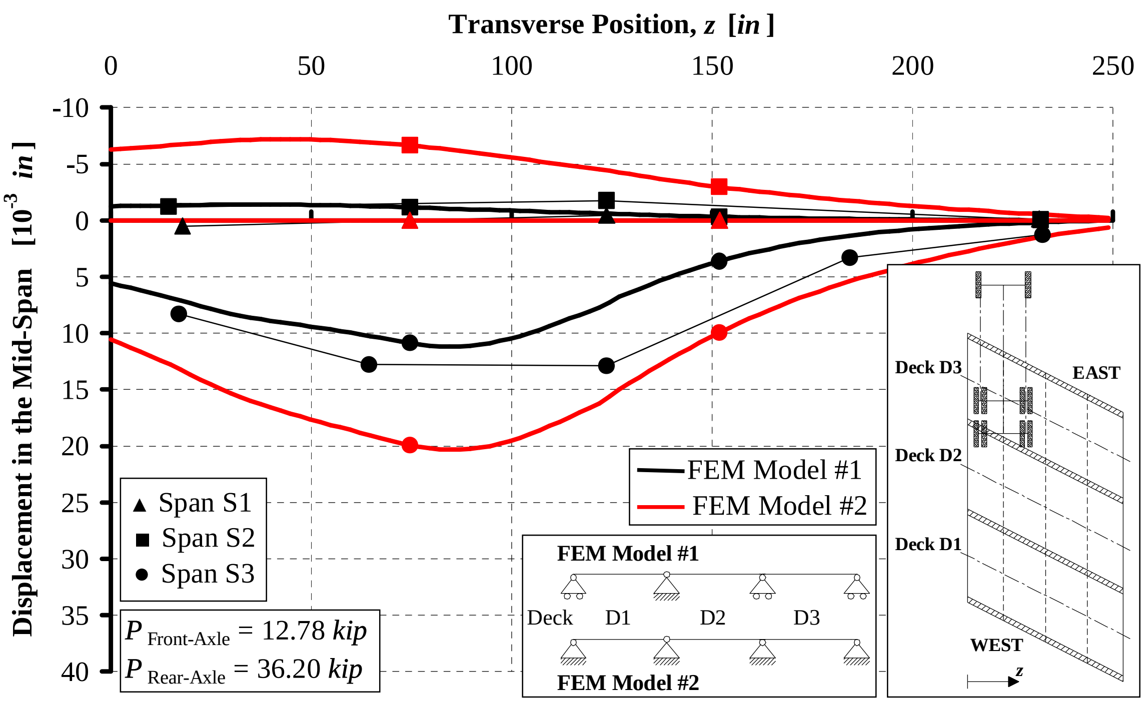

Figure A. 10. After Strengthening Mid-Span Displacement, Pass #3 Stop #7

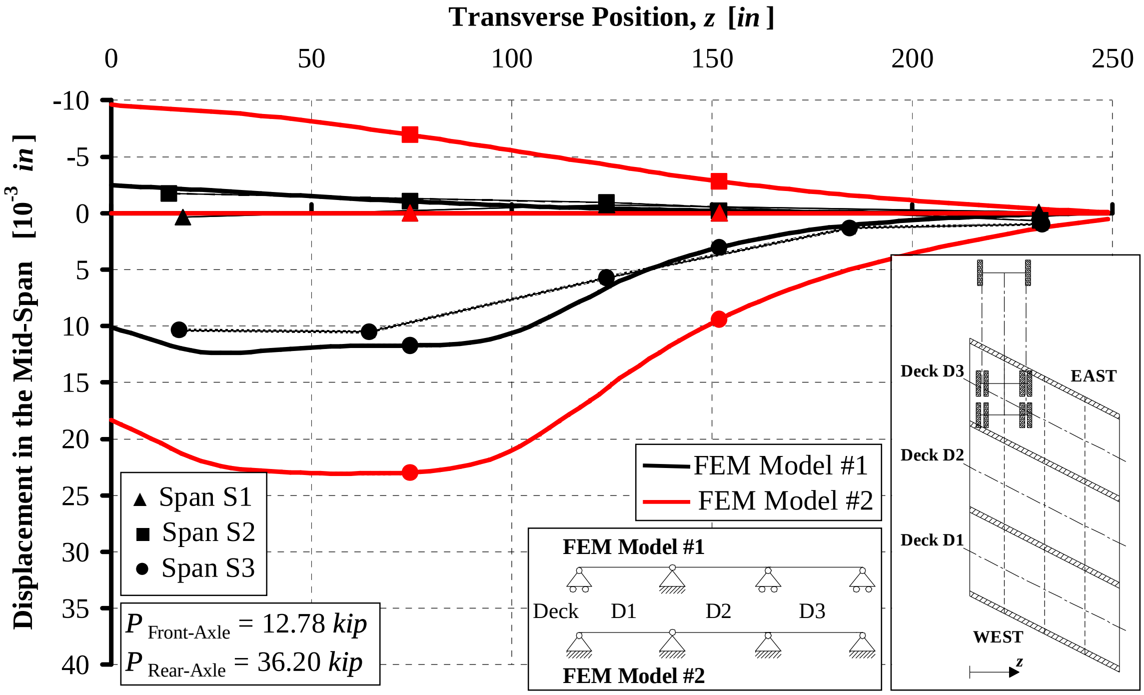

Figure A. 11. After Strengthening Mid-Span Displacement, Pass #3 Stop #8

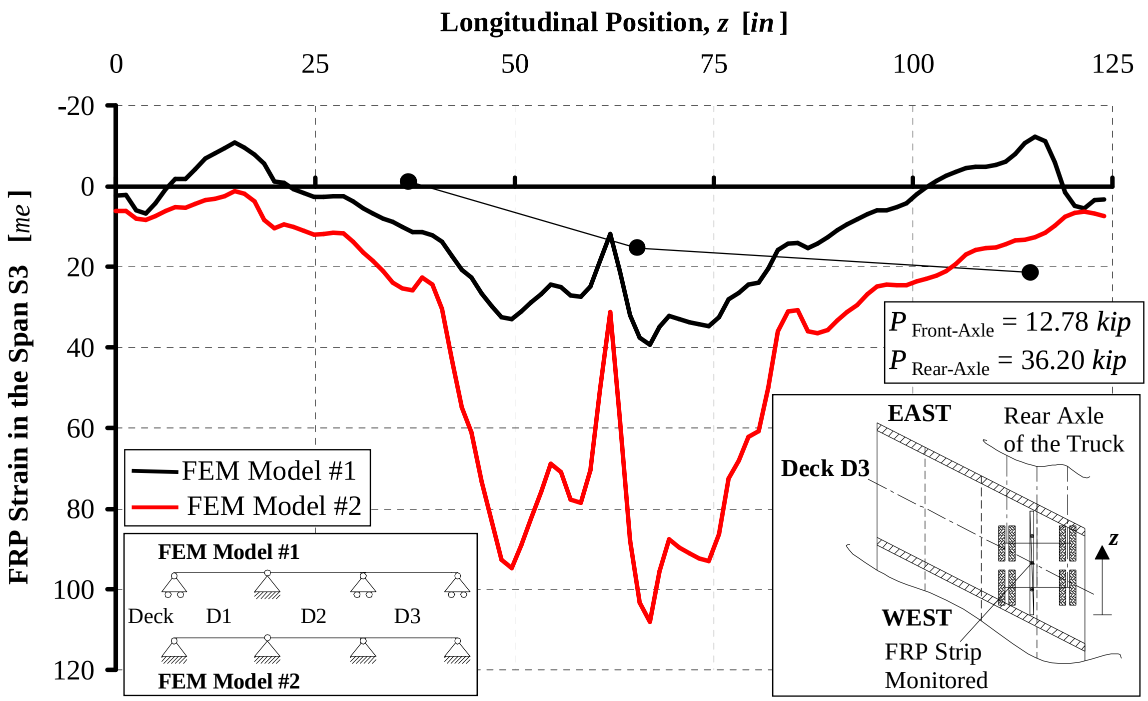

Figure A. 12. Strain in the FRP Strengthening on the Deck D3, Pass #1 Stop #8

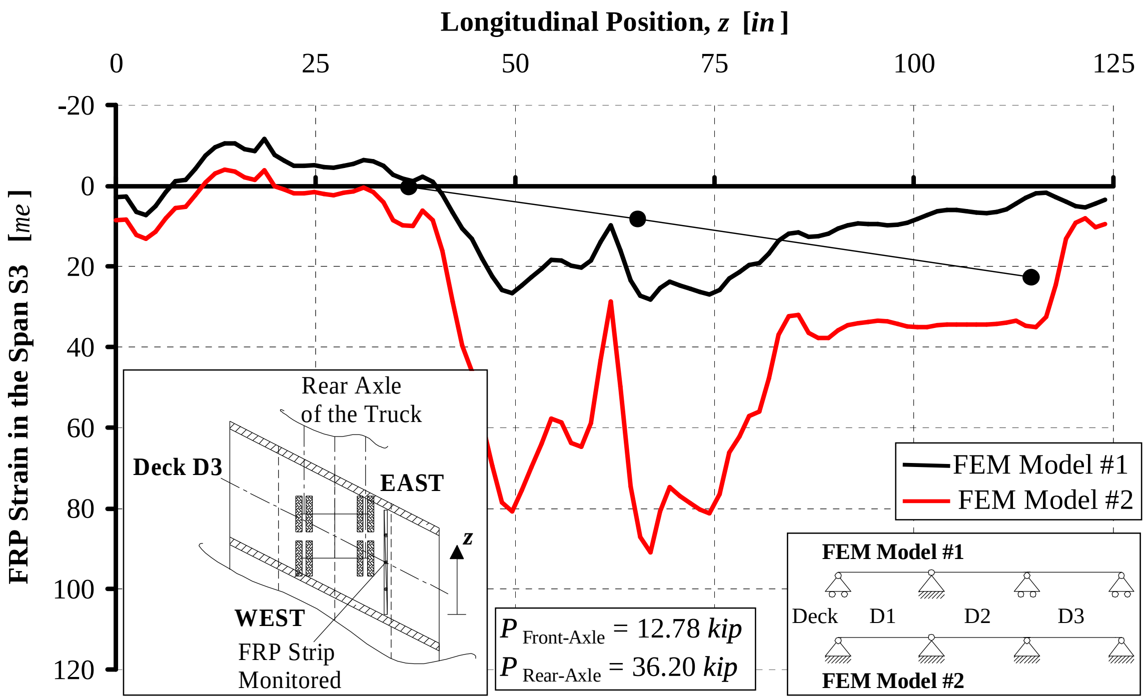

Figure A. 13. Strain in the FRP Strengthening on the Deck D3, Pass #2 Stop #8

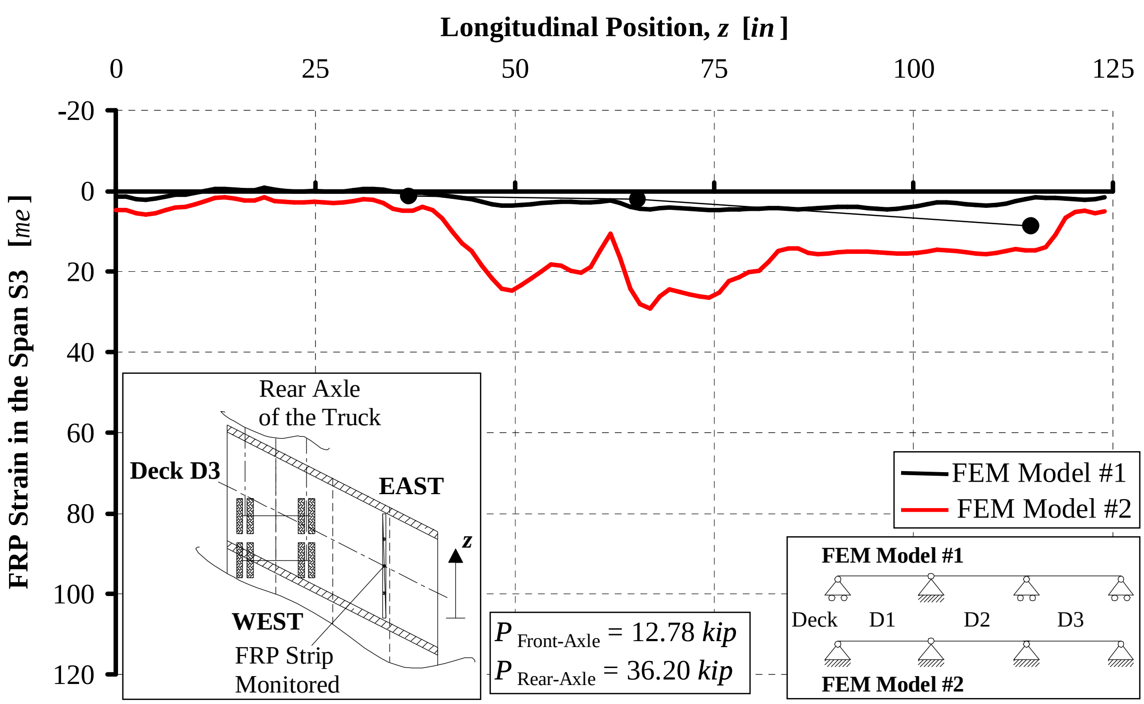

Figure A. 14. Strain in the FRP Strengthening on the Deck D3, Pass #3 Stop #7

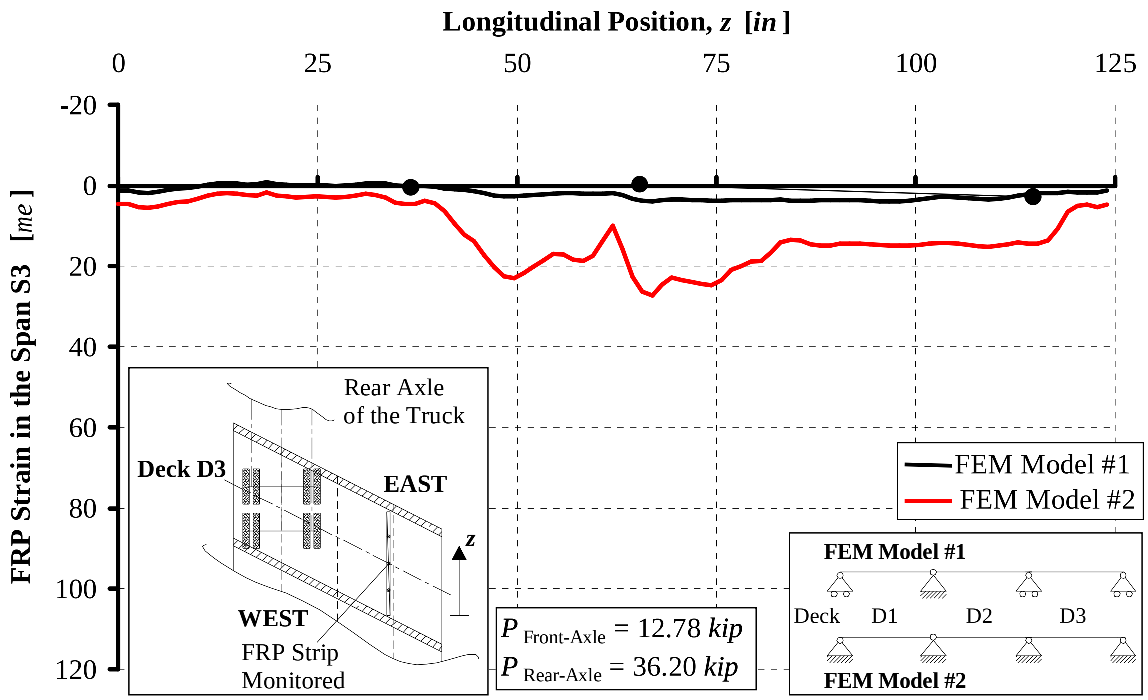

Figure A. 15. Strain in the FRP Strengthening on the Deck D3, Pass #1 Stop #8

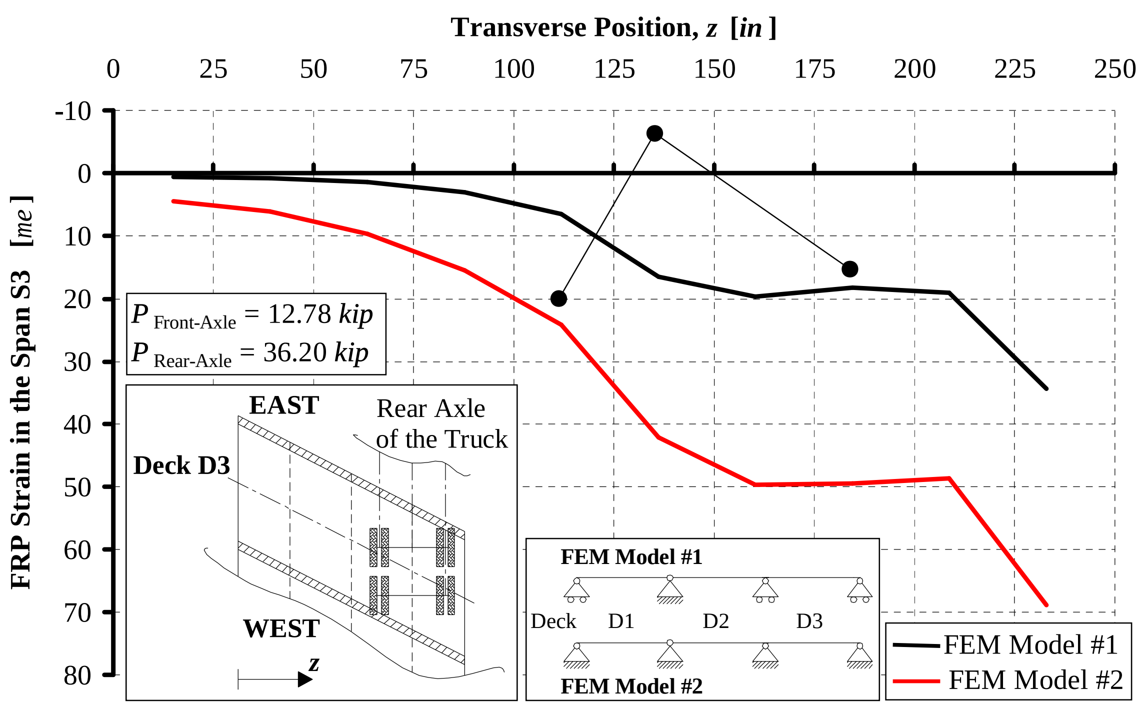

Figure A. 16. Strain in the FRP at the Mid-Span of the Deck D3, Pass #1 Stop #8

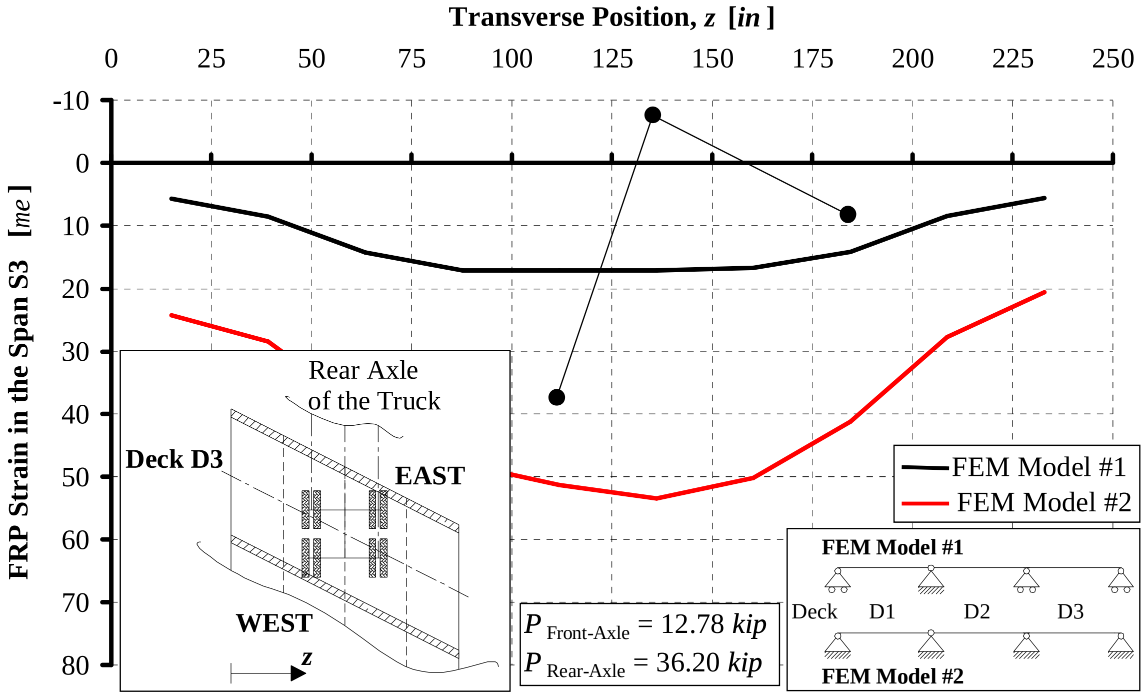

Figure A. 17. Strain in the FRP at the Mid-Span of the Deck D3, Pass #2 Stop #8

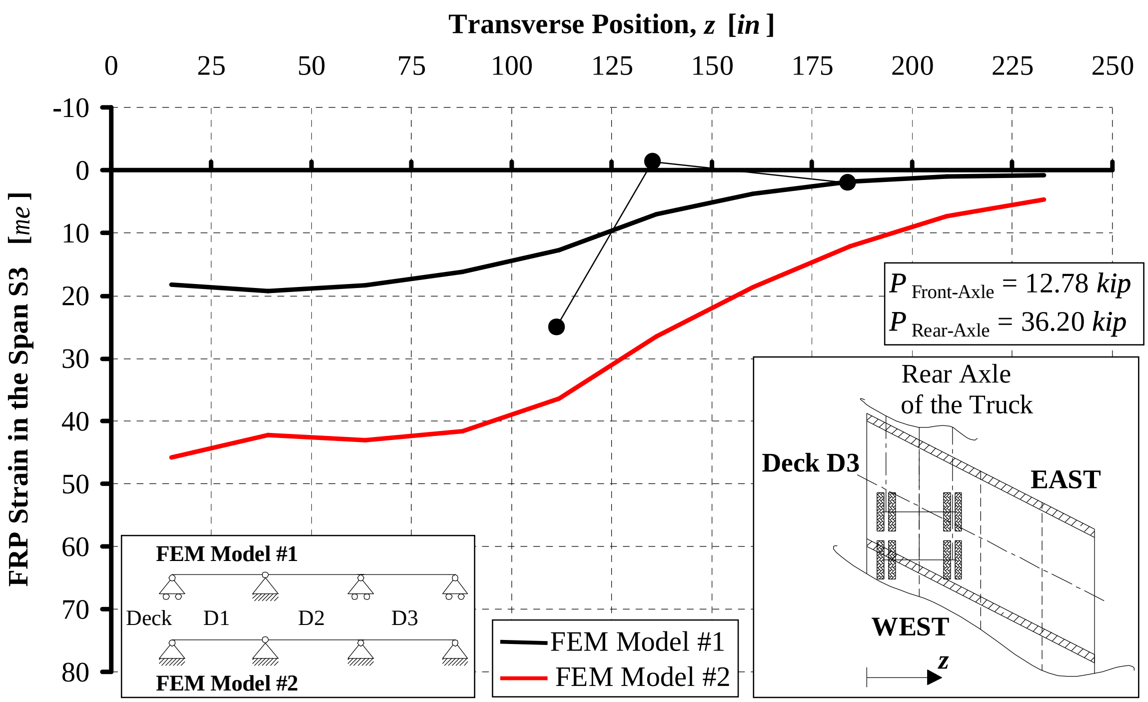

Figure A. 18. Strain in the FRP at the Mid-Span of the Deck D3, Pass #3 Stop #7

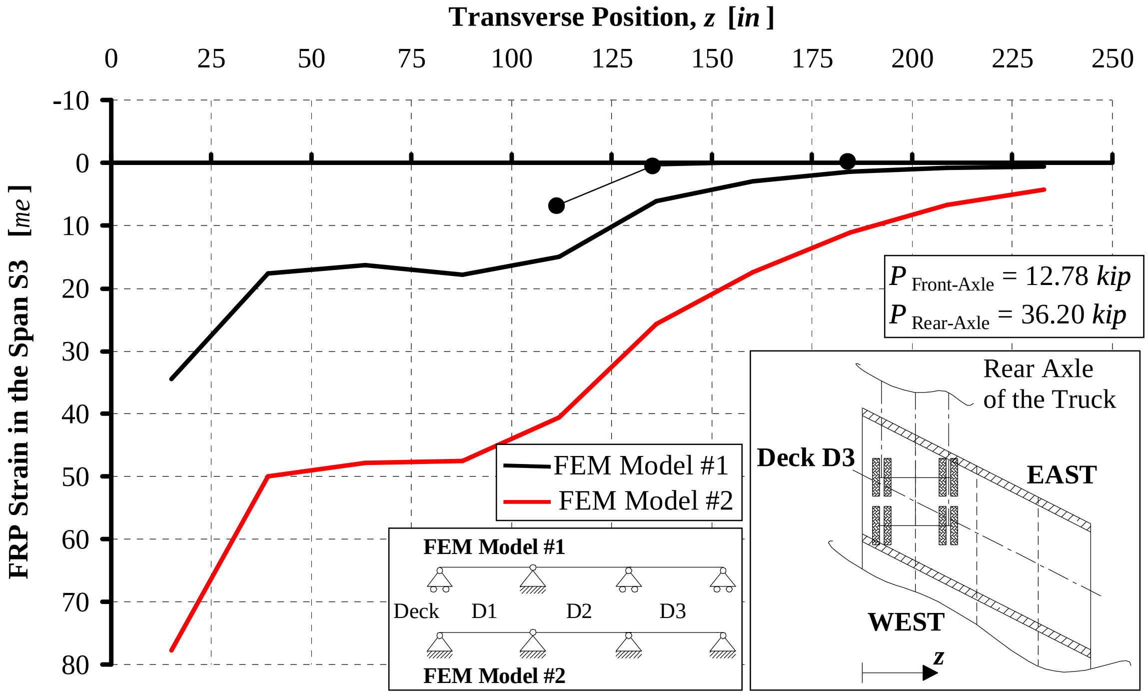

Figure A. 19. Strain in the FRP at the Mid-Span of the Deck D3, Pass #3 Stop #8

APPENDIX

B. Dynamic Test Results

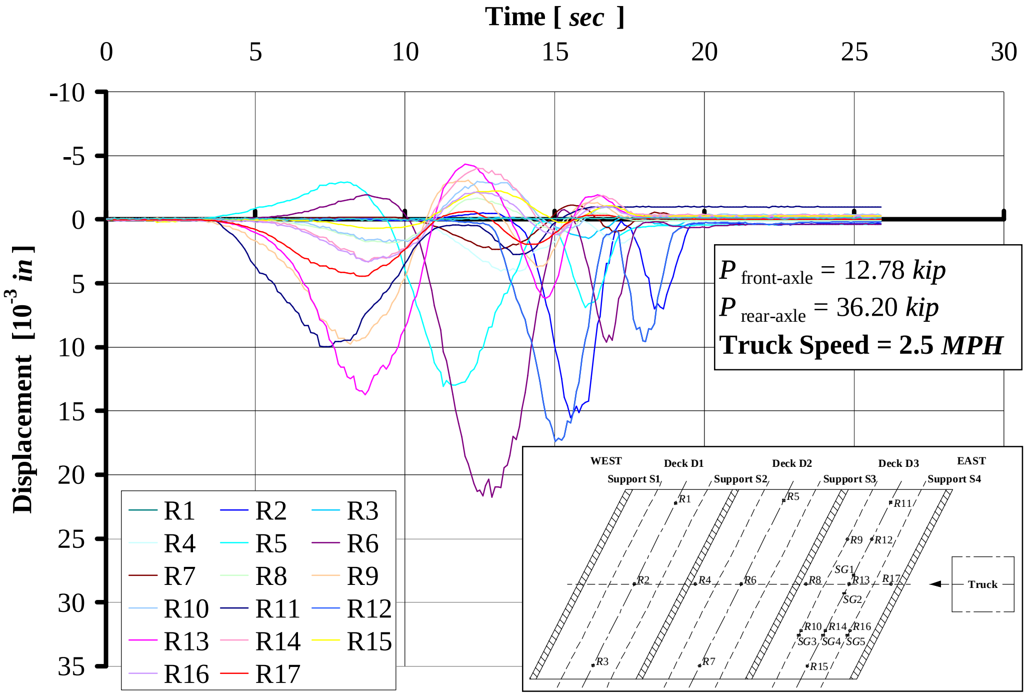

Figure B. 1. After Strengthening Displacements at 1.1 m/s $(2.5\ MPH)$

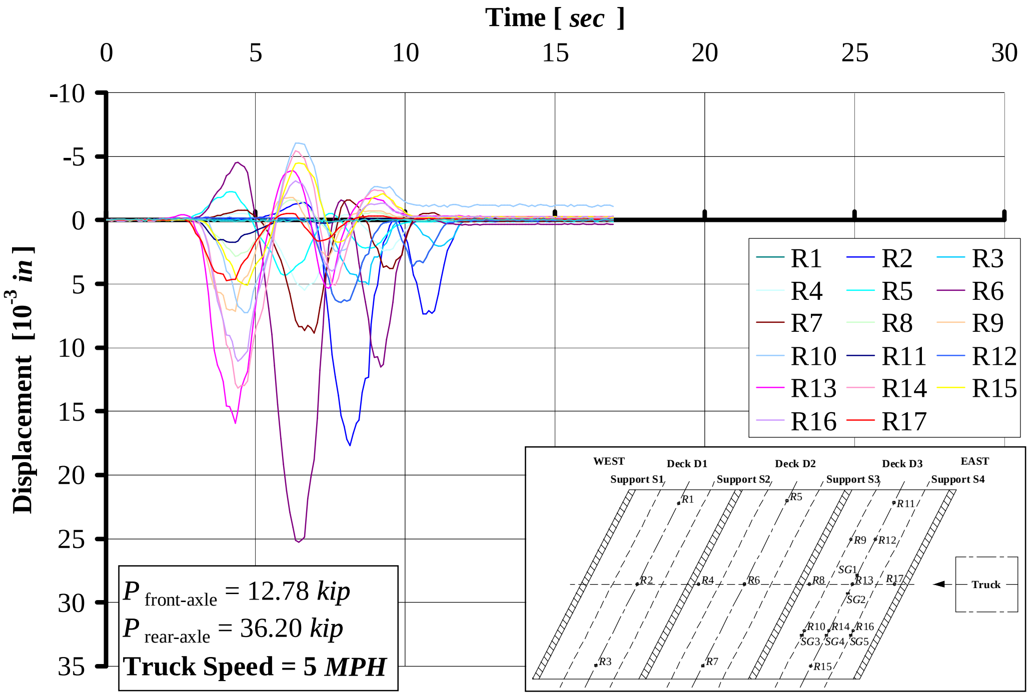

Figure B. 2. After Strengthening Displacements at 2.2 m/s $(5\ MPH)$ (I)

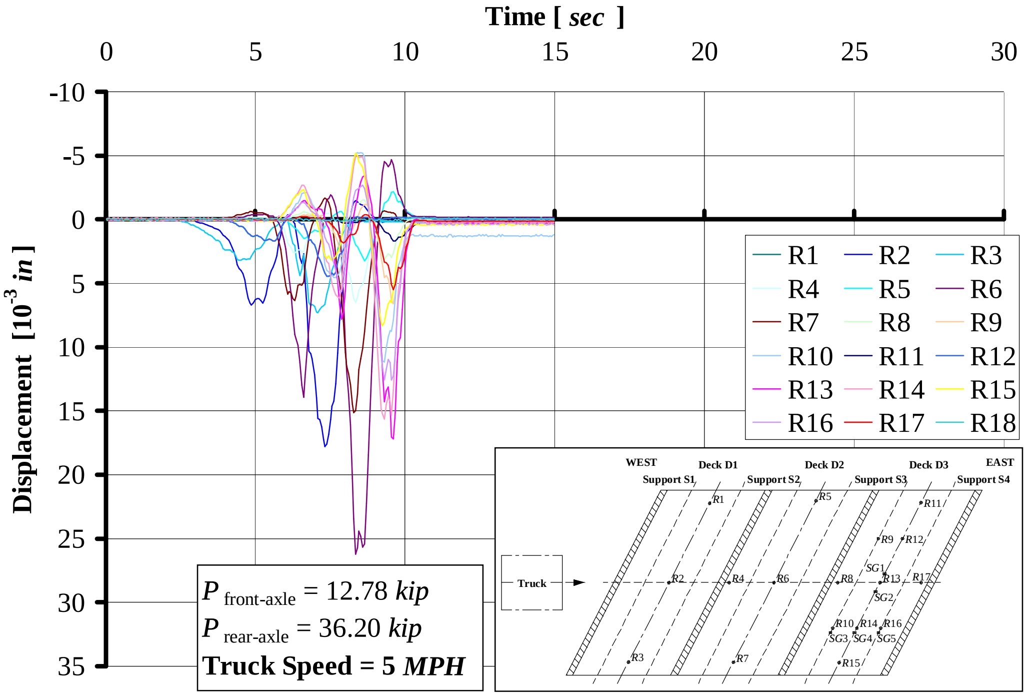

Figure B. 3. After Strengthening Displacements at $2.2\ m/s\ (5\ MPH)$ (II)

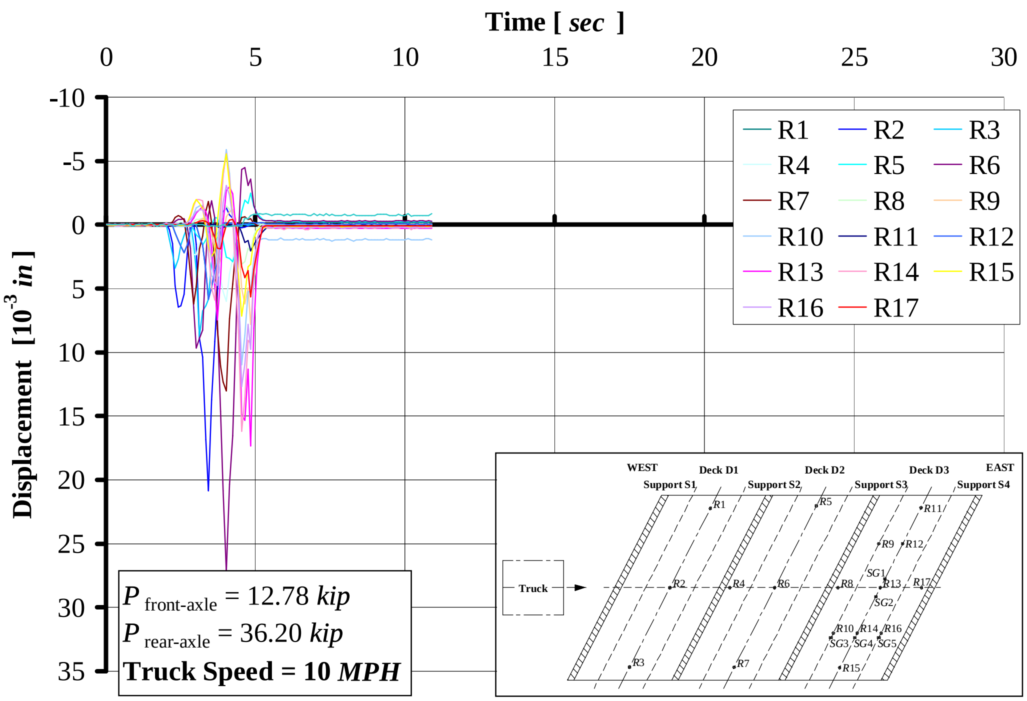

Figure B. 4. After Strengthening Displacements at $4.5\ m/s\ (10\ MPH)$

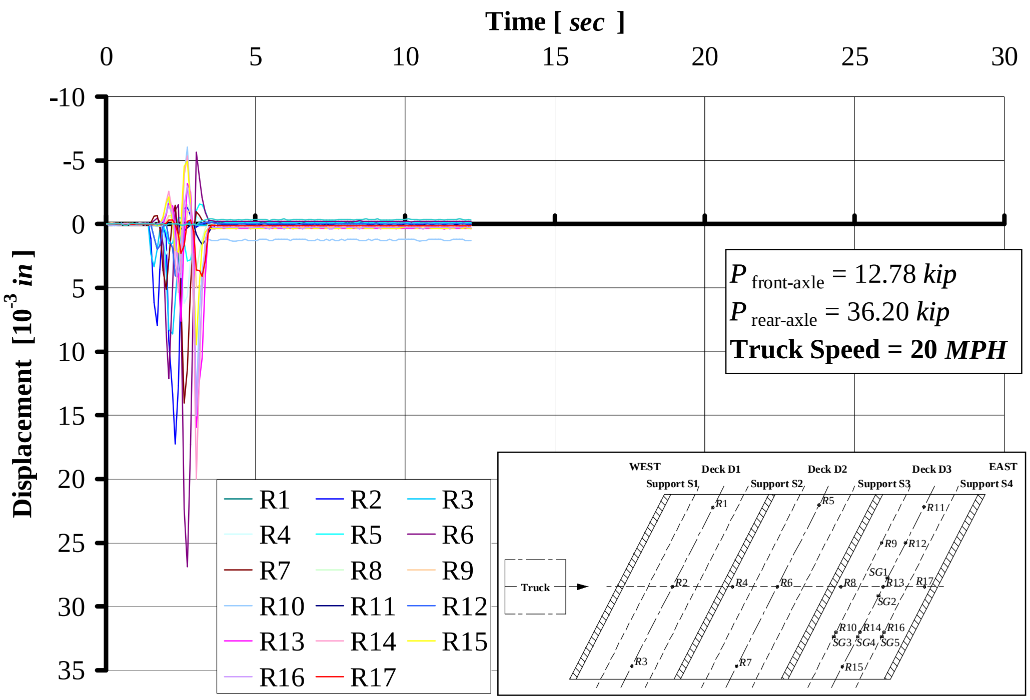

Figure B. 5. After Strengthening Displacements at 8.9 m/s $(20\ MPH)$

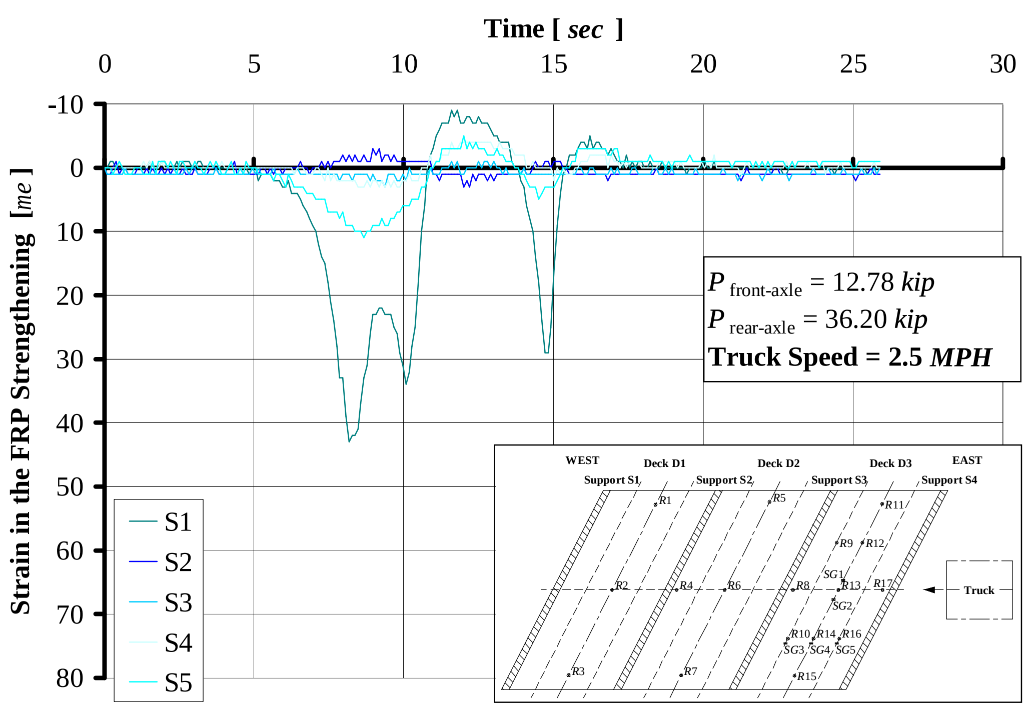

Figure B. 6. After Strengthening Strain in the FRP Laminates at 1.1 m/s $(2.5\ MPH)$

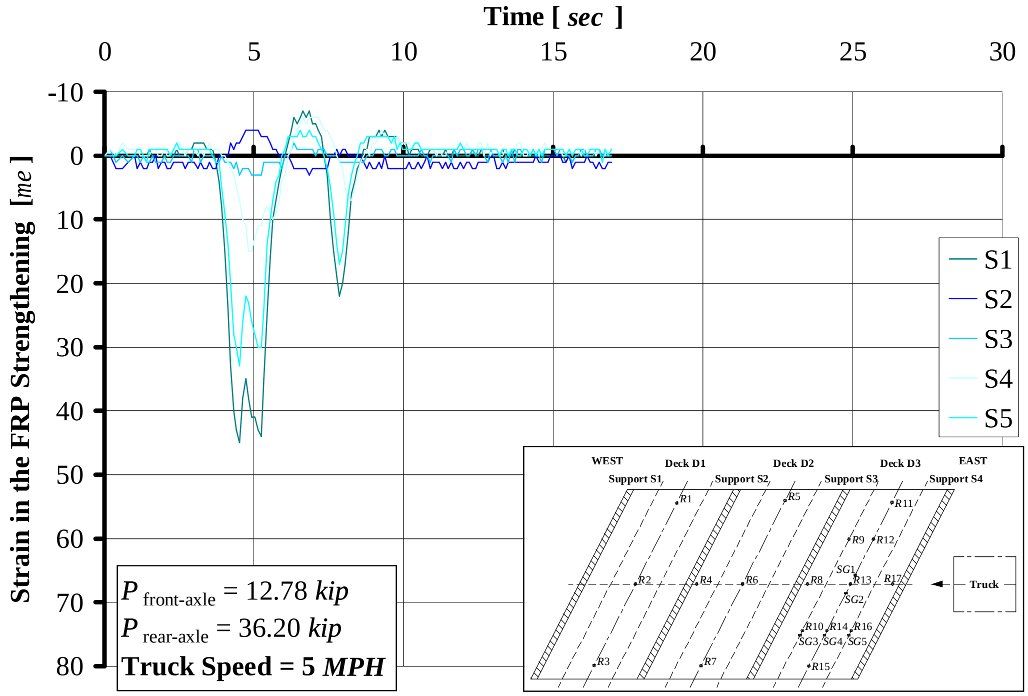

Figure B. 7. After Strengthening Strain in the FRP Laminates at $2.2\ m/s\ (5\ MPH)$ (I)

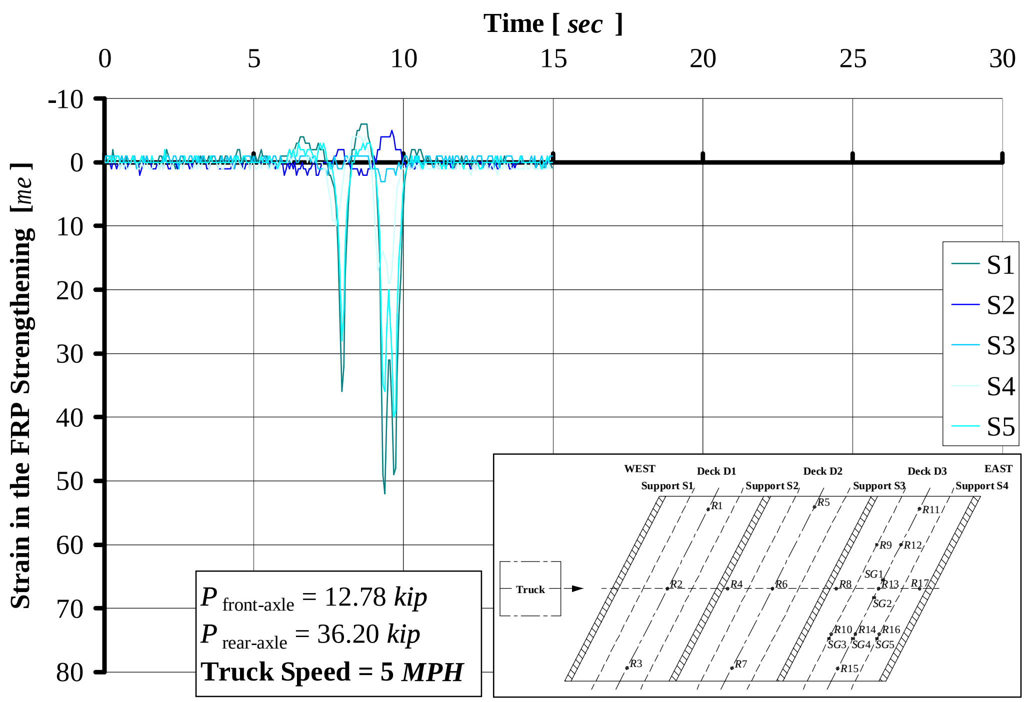

Figure B. 8. After Strengthening Strain in the FRP Laminates at $2.2\ m/s\ (5\ MPH)$ (II)

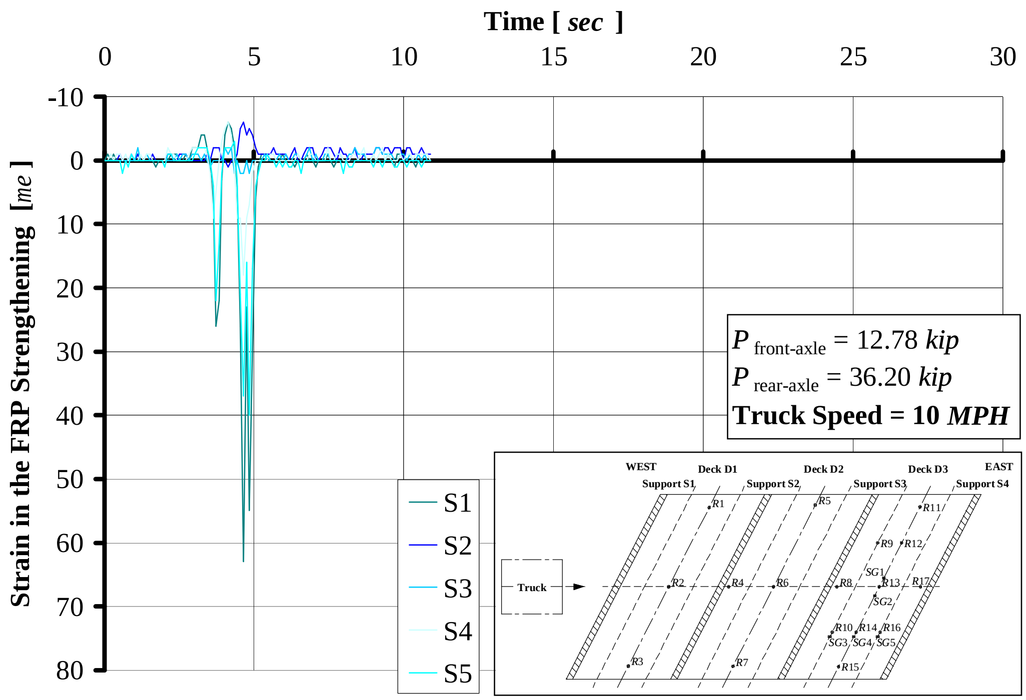

Figure B. 9. After Strengthening Strain in the FRP Laminates at $4.5\ m/s\ (10\ MPH)$

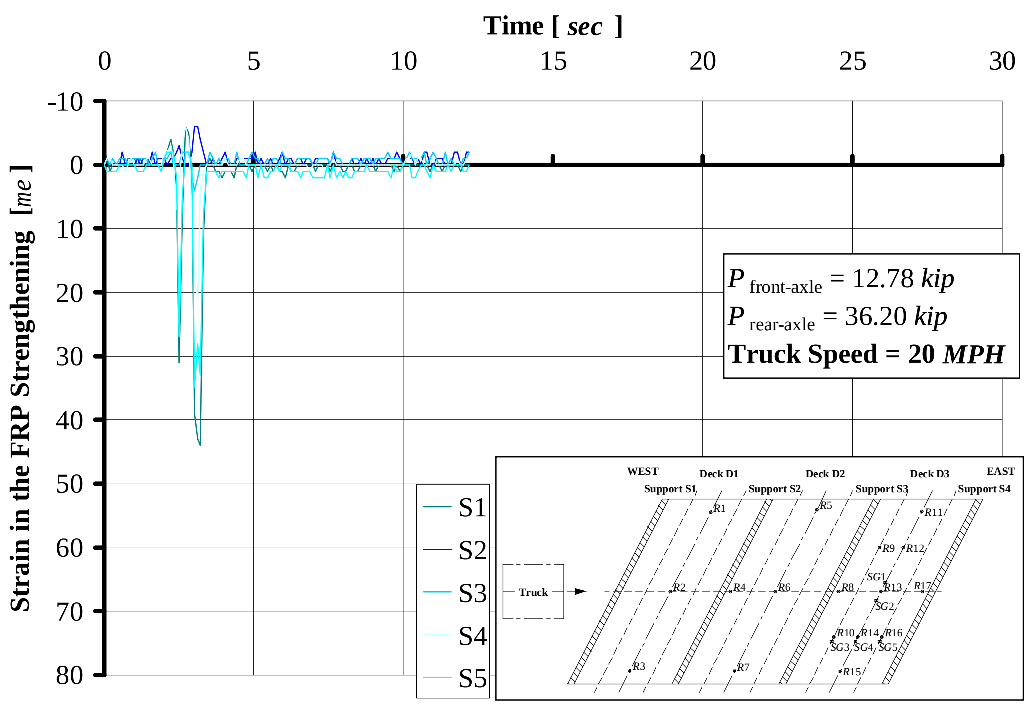

Figure B. 10. After Strengthening Strain in the FRP Laminates at $8.9\ m/s\ (20\ MPH)$

APPENDIX

C. Installation of the MF-FRP Strengthening System

a) Drilling of the Pre-cured FRP Laminates b) Anchors Bolts and Fastening Tools

Figure C. 1. Mechanically Fastening System

a) Scaffolding b) Temporary Attachment of the Laminates

Figure C. 2. Positioning of the Pre-cured FRP Laminates

Figure C. 3. Drilling and Dusting of the Holes in the Concrete

a) Hole Filling with Epoxy b) Bolt Hammering c) Torque Control Clamping

Figure C. 4. Fastening Procedure

Figure C. 5. Bridge No. 2210010 after Strengthening

a) Pre-cured FRP Laminate Fastened beneath a Highly Deteriorated Part of the Deck

b) Bridging of the Crack Running Through the Abutment S4

Figure C. 6. Details of the Strengthening